August 2008

Impact of Mixed Gas Stream on CO_2 Plume Characteristics during and after Carbon Storage Operations in Saline Aquifers

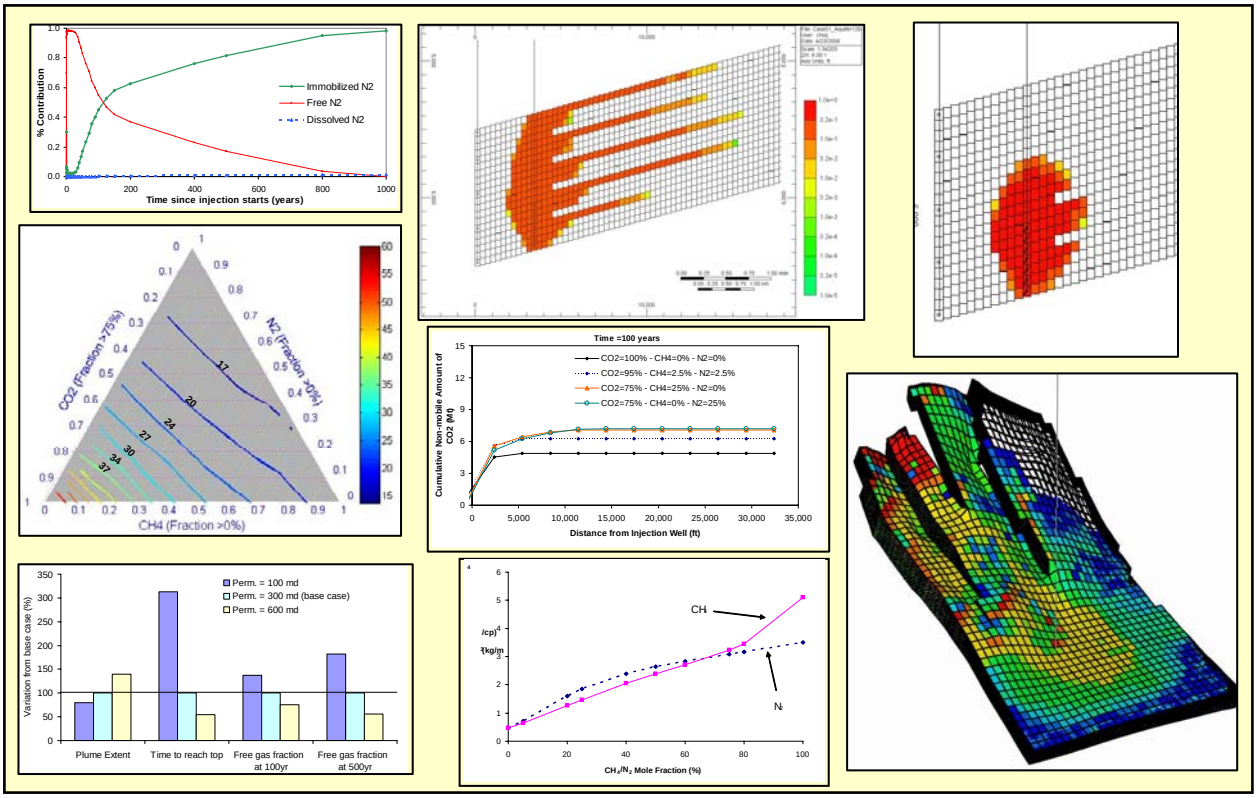

Prepared for:
Chevron Energy Technology Company, Houston, TX

by

Jean-Philippe Nicot, Jong-Won Choi, Yousef Ghomian*, and Ian Duncan
* Department of Petroleum and Geosystems Engineering, UT Austin, now at Chevron Inc.

Bureau of Economic Geology
John A. and Katherine G. Jackson School of Geosciences
The University of Texas at Austin
Austin, Texas 78713-8924

Impact of Mixed Gas Stream on CO_2 Plume Characteristics during and after Carbon Storage Operations in Saline Aquifers

Jean-Philippe Nicot, Jong-Won Choi, Yousef Ghomian*, and Ian Duncan

* Department of Petroleum and Geosystems Engineering, UT Austin, now at Chevron Inc.

Bureau of Economic Geology
John A. and Katherine G. Jackson School of Geosciences
The University of Texas at Austin
Austin, Texas 78713-8924

Summary

The goal of this short study was to explain the effects of CO_2 stream impurities (CH_4 and N_2) on (1) plume spread, (2) rate and extent of major trapping mechanisms, (3) CO_2 storage capacity, and (4) well injectivity. The injection-stream base case consists of a 95% CO_2 stream with 2.5% CH_4 and N_2. We varied the CO_2 fraction from 75% to 100% (on a mole basis), defining three bounding cases: CO_2BC, CH_4BC, and N_2BC containing 100% CO_2, 75% CO_2 and 25% CH_4, and 75% CO_2 and 25% N_2, respectively. In a parametric study of the stream composition, we defined a simple generic reservoir with a uniform permeability of 300 md, a dip of 2°, and porosity of 25%. The model contains 120 300-ft-long cells in the dip direction and also includes four baffles with no permeability parallel to its top and bottom. The gas was injected for 30 years at a depth of about 6,000 ft and at a rate of 26 MMSCFD (equivalent to 0.5 Mt/yr of pure CO_2) in a single well located in the downdip section of the model and perforated in the lower third of the 1,000-ft thickness of the injection formation. Temperature is constant at 135°F. Results are numerically monitored for 1,000 yr after start of injection. The modeling was done using CMG-GEM software, and we used a user-defined set of PVT properties. A sensitivity analysis on important model parameters was also done to assess their importance relative to the parametric-study results.

The study considers only the two trapping mechanisms (residual saturation and brine dissolution) largely impacted by injection-stream composition. Plume spread, or maximum extent, is a strong function of composition. The maximum extent ranges from 10,350 ft for CO_2BC to more than twice the distance for CH_4BC (22,250 ft) and N_2BC (24,250 ft) and varies approximately linearly for intermediate values. Similarly, time for the plume to reach the top of the formation varies from 14 yr (N_2BC) to 18 yr (CH_4BC) to 60 yr (CO_2BC). The main difference between gas components is solubility in brine—CO_2 is approximately 10 times more soluble than CH_4 and N_2 on a mole basis. The buoyant driving force, expressed as the ratio of gas-brine density difference to gas viscosity, is also approximately four times higher in the CH_4BC and N_2BC cases, and the ratio keeps increasing because the fraction of CH_4 and N_2 increases as CO_2 dissolves.

It follows that the CH_4- and/or N_2-rich plume will travel farther and faster than the single-component CO_2 plume. At 1,000 yr after start of injection, all gas in the CH_4BC and N_2BC cases has been immobilized, although only 85% in the CO_2BC case. Riskwise, these results imply that impurities in the injection will help immobilize the plume faster, but the plume will travel farther. In addition, storage capacity analysis also suggests that CH_4/N_2-containing systems trap CO_2 faster. More CO_2 is trapped in these systems even if less of it is injected. It is only between 100 and 200 yr after start of injection that the pure CO_2 system can secure a larger amount of nonmobile CO_2 within a given distance from the injection well. At constant pressure, the total amount injected for a mixture of 75% CO_2 and 25% of either CH_4 or N_2 is approximately 80% of the 100%-CO_2 gas stream. Sensitivity analysis on permeability, porosity, dip, and other parameters suggests that injection-stream composition dominates system behavior. We also used data from an actual field, typical of the Gulf Coast, whose simulation results are similar to those of the generic case, confirming that general behavior of the system is captured by the generic model.

Table of Contents

List of Figures

List of Tables

Acknowledgments

The authors would like to thank the Chevron Energy Technology Company for funding this project and, in particular, the project manager, Vanessa Nuñez-López, who was instrumental in the success of the study.

We are also grateful to the **Computer Modeling Group (CMG)**, Calgary, Canada, for giving us free access to their **GEM** software and to The University of Texas at Austin Petroleum and Geosystems Engineering for facilitating communication between CMG and BEG. The report also benefited from a thorough editing by Lana Dieterich.

Acronyms

BIC	Binary interaction coefficients
CPOR	Rock matrix compressibility
EOS	Equation of state
MMSCFD	Millions of standard cubic feet per day
Mt	Megatons (10^6 metric tons)
PTS	Pressure, temperature, salinity
SCFD	Standard cubic feet per day

Introduction

Geologic sequestration of carbon dioxide (CO_2) is poised to become an important technology for addressing high CO_2 atmospheric concentrations and global warming. However, little work has been done to explain the impact of impurities on subsurface behavior of the CO_2-dominated injection stream. In particular, this report investigates the impact of impurities on two of the trapping mechanisms generally put forward: (1) dissolution of CO_2 into formation brine and (2) immobile residual saturation. The report documents a preliminary study investigating this issue and is limited to injection of CO_2, methane (CH_4), and nitrogen (N_2) into a saline aquifer.

Sparse literature exists on mixed-gas injection, although the industry does deal with these three gases in addition to hydrogen sulfide (H_2S), which is not treated in this study. Injection of CO_2 in saline aquifers is now well documented (e.g., Pruess et al., 2001; Kumar et al., 2004). In addition to many reports investigating the behavior of acid gas (CO_2 and H_2S) injected into a saline aquifer (e.g., Ozah, 2005), Knauss et al. (2005) presented a similar study, also using the Frio site as a realistic example, but with NO_x, SO_x, and H_2S co-contaminants and focusing more on the geochemistry. Vicencio (2007) provided a recent review of N_2 injection in oil and gas fields.

The general approach followed in this report consists of a parametric study and sensitivity analyses of a generic case and of a previously studied site in the Gulf Coast (Ghomian et al., 2008), but modified slightly to meet our objectives. The following sections contain a description of the models used, the software, and a summary of results. Appendix A contains information on development of the user-supplied EOS. Appendix B provides a sample GEM input file. Appendix C displays figures illustrating results from the parametric study and sensitivity analyses of the generic case, whereas Appendix D presents results from the Gulf Coast case. Appendix E presents a noncomprehensive bibliography on behavior of CO_2 and other gases in brines, and Appendix F lists files available on the companion DVDs.

I. Approach

Our general approach consisted of varying the injection-stream composition (from 75 to 100% CO_2 with varying amounts of CH_4 and N_2) and flow and other parameters and in monitoring selected output properties. We performed a sensitivity analysis on the relative importance of gas-stream composition compared with uncertain parameters such as permeability or porosity. We applied the CMG-GEM model to a simple generic case and to a more realistic site in the Texas Gulf Coast (Ghomian et al., 2008). All run results are collected in Appendix C, but a limited number of variables selected as representative of a run (e.g., Kumar, 2008) are discussed in the Results Section:

- Total mobile CO_2 in the aquifer at a given time
- Maximum lateral distance traveled from the injector
- Time the plume takes to reach the top seal

I-1. Software and Routines

Several multiphase flow compositional codes were available for performing required tasks. At least three codes were accessible to us: TOUGH2, developed by Berkeley National Laboratory; Eclipse, currently developed by Schlumberger; and CMG-GEM, developed by the Computer

Modeling Group (CMG). CMG-GEM was eventually chosen for simulations, mostly for convenience, but also because of its immediate availability to us, as well as familiarity with it and its PVT property module by one of us (YG). The module easily handles the partitioning behavior of the four system components (CO_2, CH_4, N_2, and H_2O) between aqueous and gas phases and its impact on flow properties of the system (density, viscosity). Some of the module inputs are presented in Appendix A. Internally, the "oil" phase in GEM is used to model the aqueous phase so that Peng-Robinson Equation of State (PR-EOS) formalism can be used for flash calculations. To take advantage of these compositional features, we defined the aqueous phase as water-rich "oil," and "water" is not modeled. Note that if water had been treated as an individual phase and not a component, thermo-physical interactions between other components present in the model and water as a phase would have been impossible.

The biggest CMG-GEM drawback when dealing with semiregional models, as in this work, is the assumption of an isothermal system. Although CMG can handle temperature variations in a simple way, it does not allow for coupling and flow and heat transport. Because our CMG model is isothermal and H_2O is modeled as a component, temperature and salinity dependence do not appear explicitly. This dependence is included implicitly by making the binary coefficient between CO_2 and H_2O ($BIC_{H2O\text{-}CO2}$) a function of temperature and brine salinity.

Typical run times on a Dell Optiplex 755 (with a 3.0GHz CPU and 3.25 GB of RAM) were 30 min and 3 h from the generic and Gulf Coast models, respectively (both at 1,000 yr). The base-case CMG-GEM input file is listed in Appendix B.

I-2. Reservoir Models

I-2-1 Description of Generic Model

In the spirit of previous similar work (e.g., Kumar, 2004; Ozah, 2005; Kumar, 2008), we used a simple generic model whose geometric characteristics are described in Table 1. Model outputs are monitored for 1,000 yr after start of injection, and the gas stream is injected at a volumetric flow rate of $26 \times 10^{+6}$ SCFD for 30 yr, translating into a yearly mass rate of 0.5 Mt/yr of pure CO_2. The formation modeled consists of a 1,000-ft-thick reservoir consistent, for example, with the Utsira Formation thickness at Sleipner, where 1 Mt/yr is injected and located at an average depth of approximately 6,000 ft. The model box is 2.9 × 6.8 mi (36,000 × 15,300 ft), and the formation is assumed to have a constant dip of 2°. The grid is coarse, with uniform dimensions of 300 × 300 × 50 ft. The sole injection well is located far downdip, next to the downdip boundary (Figure 1). Injection is limited to the lower-third interval. Porosity and permeability are constant at 0.25 and 300 md, respectively. Heterogeneity is handled in a simplistic way by adding four baffles with null porosity parallel to the formation top and bottom just upstream of the injection well and short of a few cells, all the way up to the updip boundary and across the whole width of the model (Figure 1).

Boundaries are closed on five sides of the model grid: top and bottom boundaries are assumed to be bounded by impermeable layers; side boundaries are assumed no-flow, mimicking the possibility of having multiple injection wells in a line source; and the downdip boundary is assumed to be close because, for example, a geopressured zone and sharp decrease in permeability limit water fluxes. The updip boundary is open to flow and is set as a constant pressure boundary by setting five horizontal wells along the y-axis (Figure 1). The updip

boundary is located far enough away not to impact multiphase-flow processes following CO_2 injection in most cases.

Pore space is initially fully saturated with component "water." Initial pressure is hydrostatic and computed by the model assuming a typical hydrostatic gradient of 0.465 psi/ft. PVT properties are user specified (Appendix A) and set for a salinity of 100,000 mg/L.

The only trapping mechanisms available in the model are dissolution and residual-phase mechanisms. Mineral-phase trapping is not generally understood as starting to happen in a meaningful way before hundreds or thousands of years. Structural trapping—that is, CO_2 trapped in the manner of oil and gas accumulations—is not included in the design of the generic model. It helps little in explaining the interplay of all processes and is very site specific.

Table 1. Base-case characteristics of the generic model.

Properties	
Model length	36,000 ft
Model width	15,300 ft
Model thickness	1,000 ft
Number of cells x × y × z	120 × 51 × 20
Cell dimensions	300 × 300 × 50 ft
Dip in x direction	2°
Permeability	300 md
Porosity	0.25
Rock compressibility	5×10^{-6} psi^{-1}
Vertical permeability anisotropy (kv/kh)	0.01
Origin (cell 1,1,1)	Top downdip
Depth at origin center cell	5,500 ft
Hydrostatic pressure gradient	0.465 psi/ft
Initial pressure	Vertical equilibrium ~2,550 psi at origin
Geothermal gradient	15°F/1,000 ft
Temperature	135°F
Injection rate	26 MMSCFD
Injection-stream composition	95% CO_2; 2.5% N_2; 2.5% CH_4
Hysteresis	on
Maximum residual saturation	0.30
Formation water TDS	~100,000 mg/L
Injection period	30 yr
Simulation period	1,000 yr

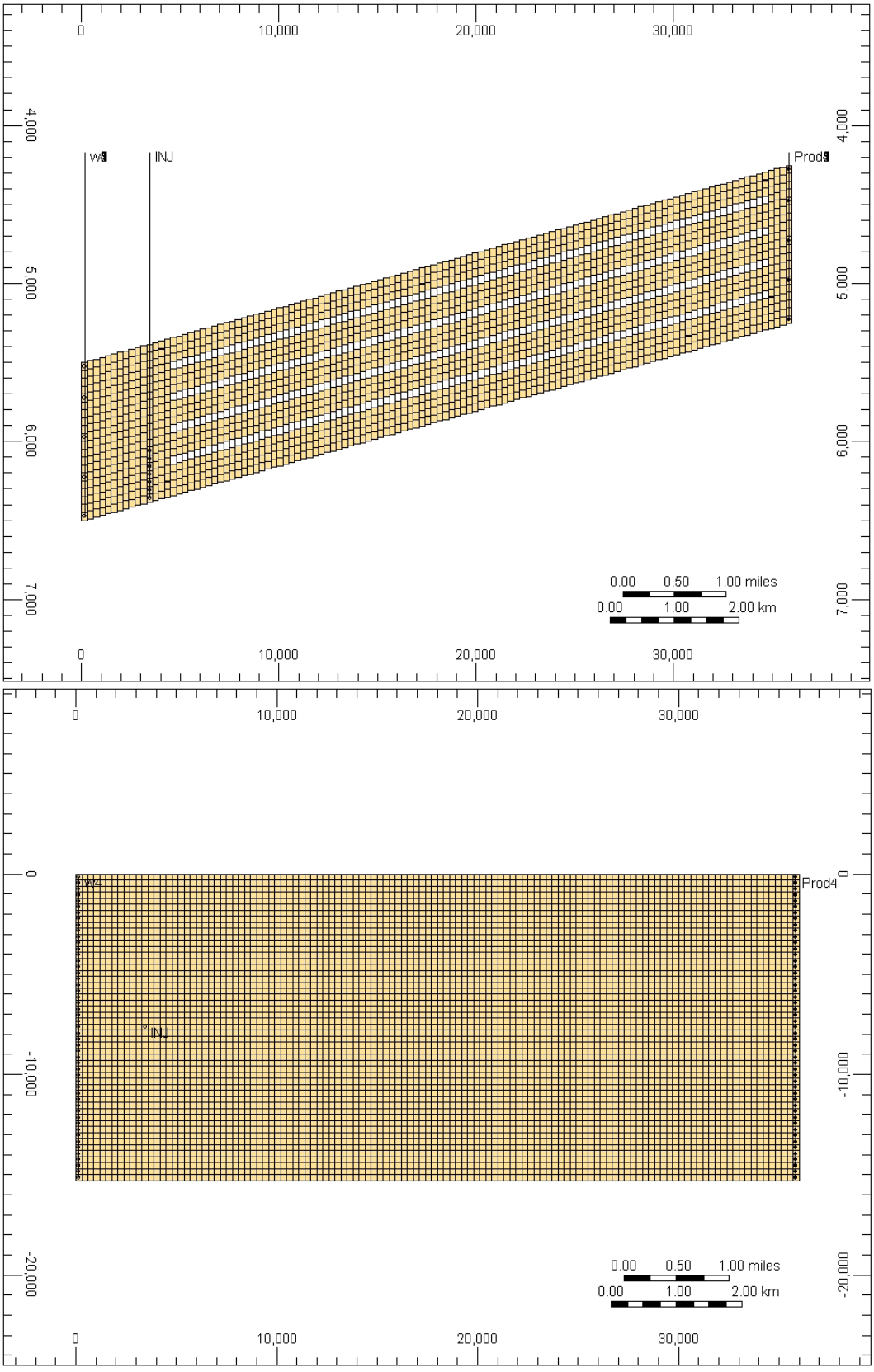

Figure 1. Cross section and map view of the generic model.

I-2-2 Description of Gulf Coast Model

The Texas Gulf Coast model (Figure 2) is taken as described in Ghomian et al. (2008), with the following changes: (1) longer injection and monitoring periods from 12.5 d to 5 yr and from 8+ yr] (3,000 d) to 1,000 yr, respectively; (2) decreased injection rate from 4.73 to 3 MMSCFD; and (3) injection-well location changed to a more downdip location. Please refer to Ghomian et al. (2008) for additional information of this Gulf Coast model. Note that an actual brine experiment (Hovorka et al., 2004, 2006) took place in a similar environment but impacted only a limited area of the domain modeled in this study. Stratigraphy and other properties used in the Ghomian et al. (2008) work and this work were worked out for a much larger domain than that of the brine experiment.

A quick computation shows that, relative to the generic model, the Gulf Coast model total volume is approximately 500 times smaller. To ensure minimal structural trapping at saturation higher than residual, injection rate was decreased from 2.6×10^7 SCFD (generic case) to 3×10^6 SCFD, whereas the injection period was reduced from 30 to 5 yr.

Table 2. Base-case characteristics of the Gulf Coast model (from Table 1 in Ghomian et al., 2008).

Properties	
Model length	3,517 ft
Model width	2,296 ft
Model thickness	100 to 200 ft
Number of cells x × y × z	43 × 28 × 26
Dip	5° - 35°
Average permeability	374 md
Average porosity	0.214
Rock compressibility	5×10^{-6} psi^{-2}
Vertical permeability anisotropy (kv/kh)	0.1
Origin (cell 1,1,1)	Top southernmost cell
Max and min depth	5,323 and 4,406 ft
Hydrostatic pressure gradient	0.465 psi/ft
Initial pressure	2,000 psi
Temperature	135°F
Injection rate	3 MMSCFD
Hysteresis	on
Formation water TDS	~100,000 mg/L
Injection period	5 yr
Simulation period	1,000 yr

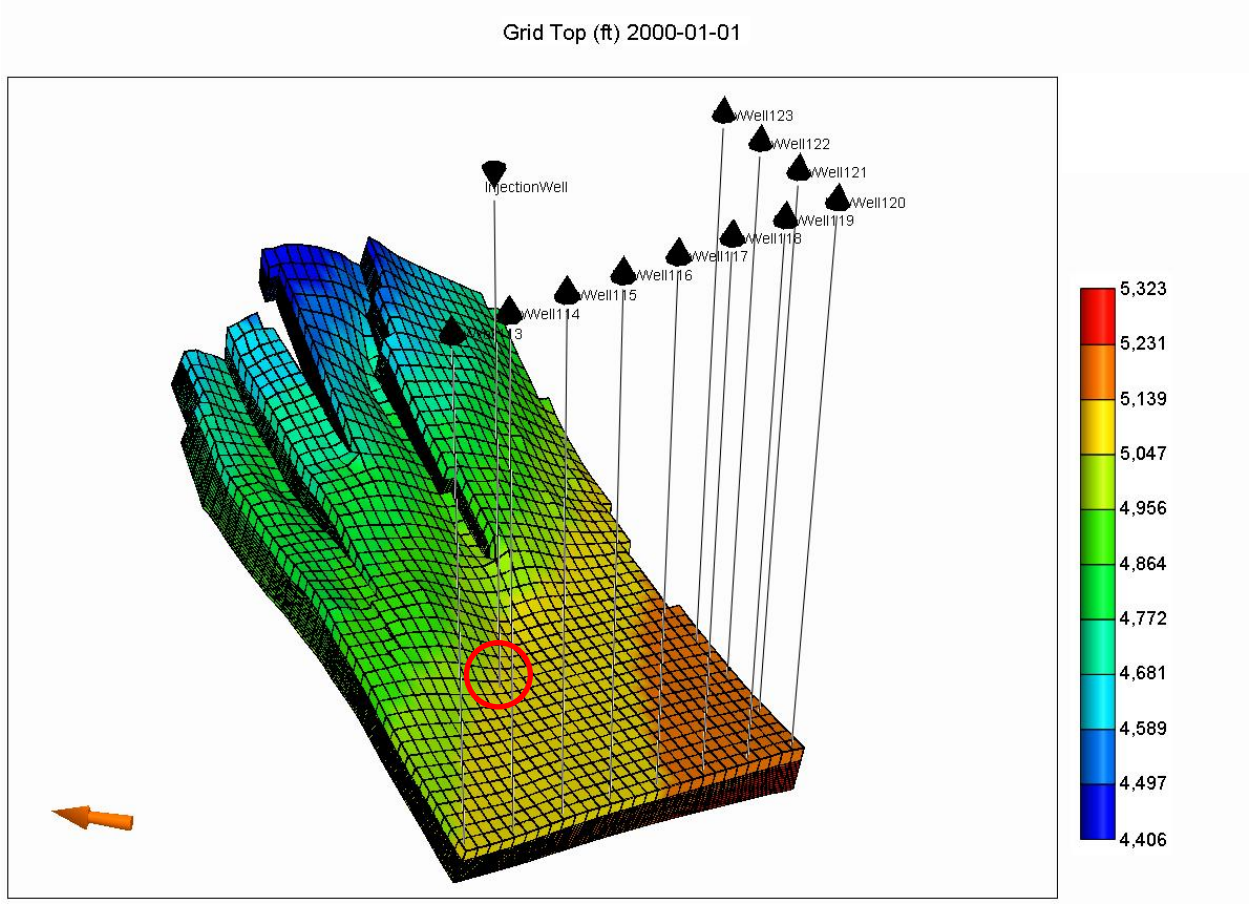

Figure 2. 3D view of the Texas Gulf Coast model showing cell depth and wells on the boundary. Red circle shows approximate location of injection well.

I-3. Reservoir Properties

Relative permeability data used in this study are identical to the set described in Ghomian et al. (2008) and are used in both generic and Gulf Coast models. Relative permeability end points follow relationships established by Holtz (2002) on the Gulf Coast Frio sandstone, and intermediate values follow a Corey model (Figure 3). Holtz (2002), who used published data, suggested that maximum gas residual saturation S_{gr} be a sole function of the porosity ϕ: $S_{gr} = 0.5473 - 0.9696\phi$. It is important to include hysteretic behavior in order to model gas residual saturations accurately. Not including hysteresis will underestimate the amount of gas phase trapped (e.g., Doughty, 2007). Other examples of relative permeability curves are in the public domain (e.g., Bennion and Bachu, 2005) but were not used in this study. In addition, Burton (2008), Kumar (2008), and others showed that it is important to extend relative permeability curves to a gas saturation of 1 (Figure 3) to account for drying effects (residual water partitioning into the gas phase) and subsequent enhanced residual-phase trapping.

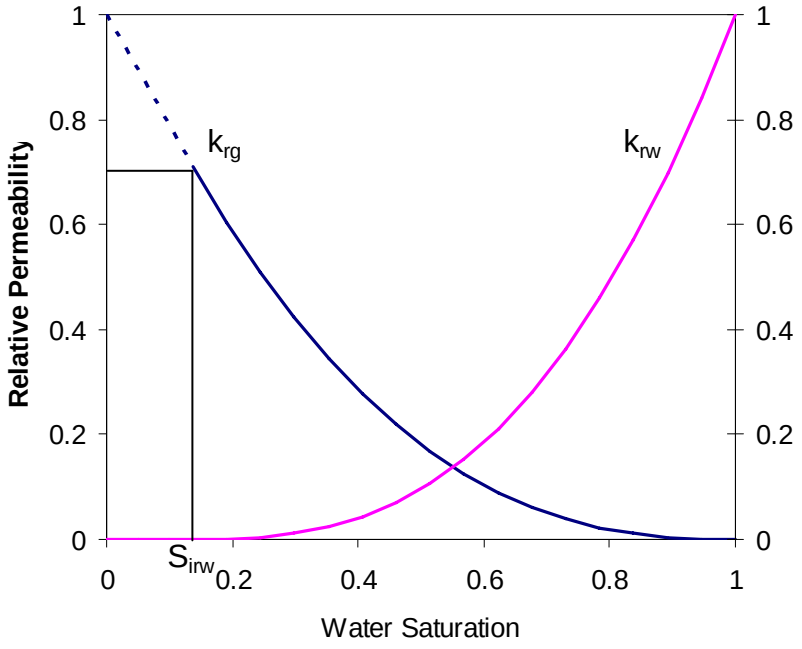

Figure 3. Relative permeability curves used in generic and Gulf Coast models.

I-4. Parametric Study and Sensitivity Analyses

For the generic case, a parametric study was performed on the injection-stream composition (Table 3) and sensitivity analyses on other model inputs (Table 4). Sensitivity analysis on the Gulf Coast case includes only the three cases bounding the variable composition (100% CO_2, 75% CO_2 and 25% N_2, and 75% CO_2 and 25% CH_4). No sensitivity analysis was done on the model parameters of the Gulf Coast model.

Table 3. Listing of injection-stream composition for the parametric study. Reference base case in **bold.**

CO_2	CH_4	N_2	Case#
100	0	0	16
95	5	0	1
	2.5	**2.5**	**3**
	0	5	2
90	10	0	4
	5	5	6
	0	10	5
85	15	0	7
	7.5	7.5	9
	0	15	8
80	20	0	10
	10	10	12
	0	20	11
75	25	0	13
	12.5	12.5	15
	0	25	14

Table 4. Listing of model sensitivity cases. Reference base cases in **bold.**

Parameter		CH_4	Case#
Dip		1	19
		2	**3**
		5	20
Permeability		100	21
		300	**3**
		600	22
Vertical anisotropy		0.1	23
		0.01	**3**
		0.005	24
Porosity		0.20	39
		0.25	**3**
		0.30	40
CPOR		5×10^{-5}	25
		5×10^{-6}	**3**
PVT	100-0-0	Default	26
		User defined	**16**
	75-25-0	Default	27
		User defined	**13**
	75-0-25	Default	28
		User defined	**14**
Well control	100-0-0	Pressure	29
		Flow rate	**16**
	75-25-0	Pressure	30
		Flow rate	**13**
	75-0-25	Pressure	31
		Flow rate	**14**
Capillary pressure		w/	41
		w/o	**3**

II. Results

Results are summarized according to three metrics (e.g., Kumar, 2008): time to hit the top, maximum lateral extent updip of the injection well, and fraction of gas still mobile after a given time.

Time to hit the top is visually defined in output cross sections as the time at which the first cell of the top layer has nonzero gas saturation. Figure 4 illustrates the process for the base case (Case #3). Maximum lateral extent is the distance from the injected well beyond which there is no gas saturation at 1,000 yr (Figure 4b). In many simulations, this state is reached before the end of the runs. *Time to reach the top* is defined as the time it takes for the model to have nonzero gas saturation in a top-layer cell (Figure 4a).

As noticed by Kumar (2008), a coarse grid overestimates residual saturation by the implicit assumption that CO_2 will uniformly invade the whole available space—an assumption harder to meet as grid-block size increases. Similarly, in theory, mobile fraction of gas or of a gas component in a cell should be computed from the total amount of gas/component from which the dissolved amount has been deducted and from which the amount that will stay immobile behind has been subtracted. The Land formula (e.g., Land, 1971), giving residual saturation as a function of maximum saturation, can be used to compute the future immobile amount. Because

of the coarseness of the grid and of well-known sweep-efficiency problems, however, we thought that the mobile fraction should be defined as total amount minus dissolved amount in cells where gas is still moving (defined by cells with nonzero relative permeability). Figure 5 illustrates the difference in results between the two definitions of mobile gas. Amount of dissolved gas is identical by construction, but there is a big difference in immobilized gas, especially early on, probably because of the high gas saturation (~100%) reached around the well early on. Later, as more and more of the gas is actually trapped, difference between the two approaches decreases.

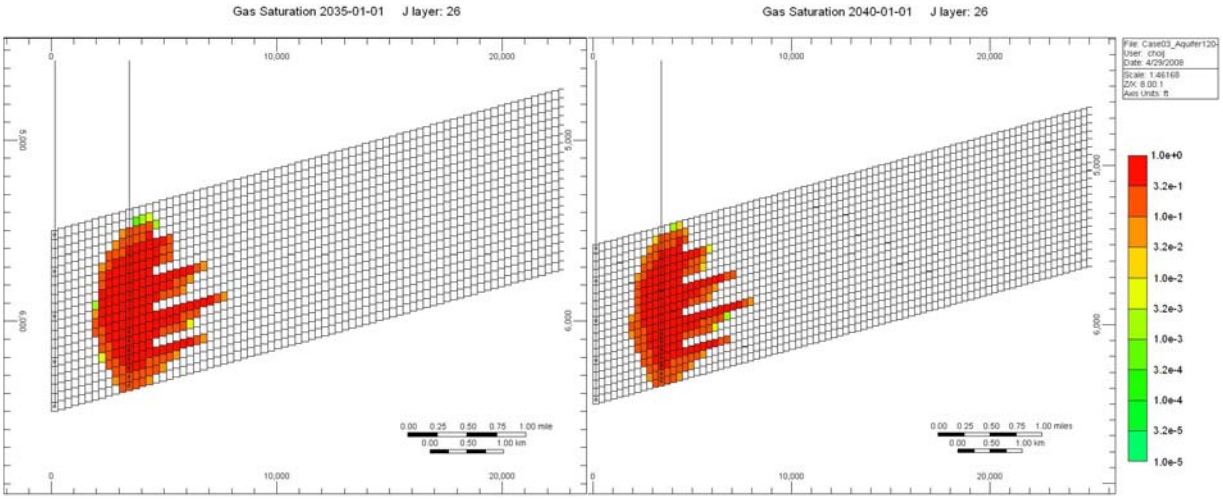

(a)

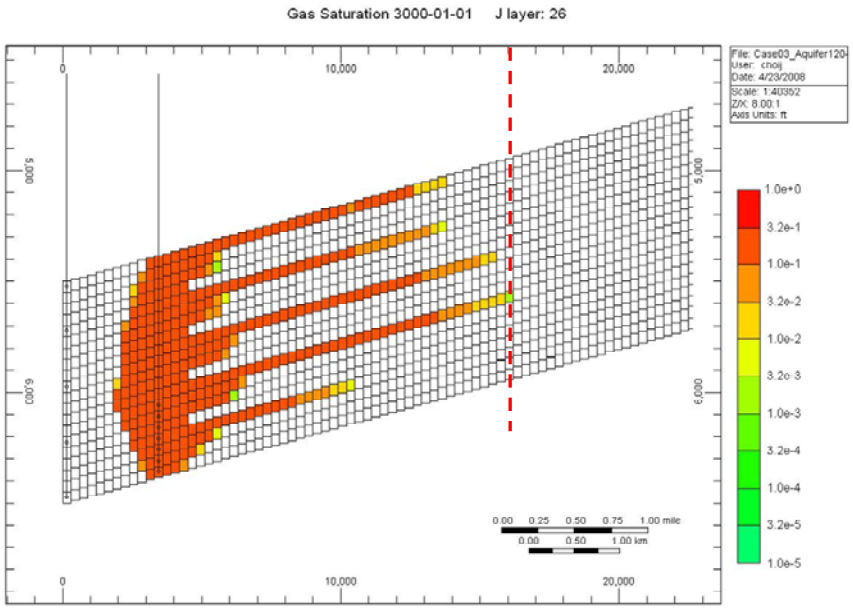

(b)

Figure 4. Illustration of how maximum extent and time to reach the top are extracted from run results. In this case (Case #3), Tongue #4 has the maximum extent.

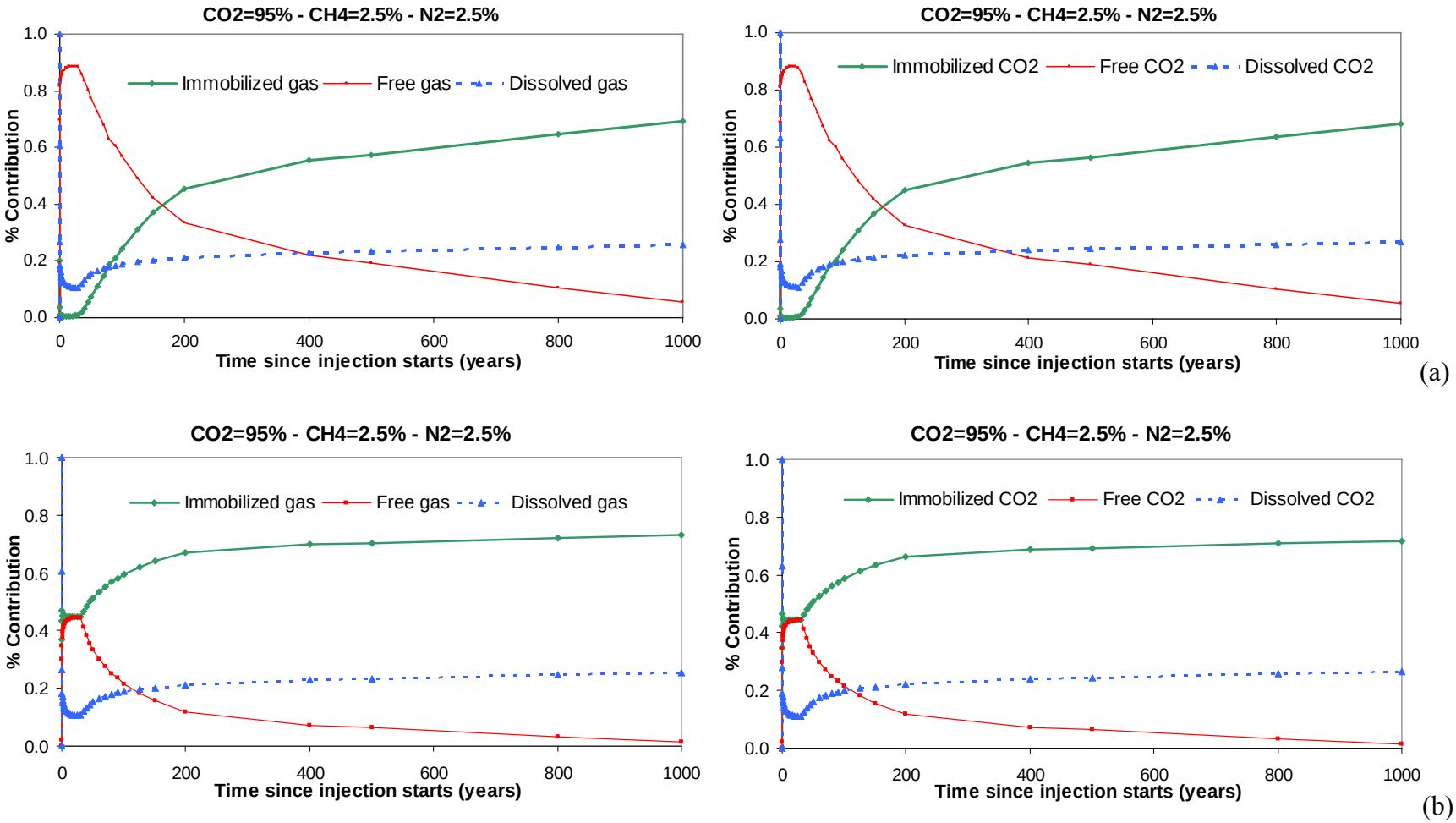

Figure 5. Contrast in phase fraction for the two definitions of mobile gas (using base case = Case #3): (a) assumes that all gas is mobile, including gas that will become trapped later; (b) assumes that some of the mobile gas will never move out of the cell and will be trapped later as residual gas and consequently does not tally it as mobile.

II-1. Generic Model Results

A summary of results in terms of metrics (time to reach the top, maximum extent, and mobile gas as a function of time) for both the parametric study and sensitivity analysis is presented in Table 5. Results display some limited noise because of the added complexity derived from the presence of four baffles.

II-1-1 Parametric Study on Stream Composition

The injection-stream composition fundamentally impacts the three metrics, and plotting results on a ternary diagram is a convenient way to visualize them (Figure 6 through Figure 13). The diagrams are based on the 25% of the injection stream that varies between the three poles of 100% (of the 25%) CO_2, N_2, or CH_4. The remaining 75% is always CO_2, and there is no need to include them in the ternary diagrams. The top pole represents an injection stream of 75% CO_2 and 25% N_2 (Case #14), the left-hand-side bottom pole represents a 100%-CO_2 stream (Case #16), whereas the right-hand-side bottom pole represents 75% CO_2 and 25% CH_4 (Case #13). Only 16 points were used to draw the diagrams and, although the general trends are valid, local deviations in the curves most likely represent a paucity of data points rather than a real fluctuation of isolines. In any case, as expected, metrics vary smoothly with injection-stream composition but not necessarily linearly.

The time to reach the top (Figure 6 and Figure 7) varies from 13.7 to 60 yr for Cases #14 and #16—75% CO_2 and 25% N_2 and 100% CO_2, respectively. Case #15, 75% CO_2 and 25% CH_4, is close to the N_2 case, with a time of 18.1 yr. Injection ended before the gas reached the top only in those cases with a CO_2 fraction of the injection stream more than 91% (75% + 0.65× 25%—Figure 6). Such behavior can be explained if the two following mechanisms were acting in the same direction to maximize time to reach the top: (1) higher dissolution of CO_2 into the aqueous phase attenuating its upward migration but (2) stronger buoyancy forces when the injection stream contains a significant amount of CH_4 and N_2. Kumar (2008) did a detailed analysis of plume dynamics on a simplified system similar to the one used in this study. He determined that time to hit the top was controlled by a Gravity Number N_{gv} defined as

$$N_{gv} = \frac{k_v \Delta\rho g \cos\alpha}{\mu u}$$

where k_v is vertical permeability, $\Delta\rho$ is density difference between brine and gas phase at aquifer temperature and pressure, α is dip angle, μ is gas viscosity, and u is total velocity. The only terms varying with injection-stream composition are $\Delta\rho/\mu$ and u. The term u can be reasonably assumed constant, and changes to $\Delta\rho/\mu$ dominate the behavior of the system. Buoyancy forces are initially stronger in the CO_2-N_2 mixture than in the CO_2-CH_4 mixture (Figure 38—Appendix A), explaining the shorter time to reach the top for the former.

Results for the maximum extent (Figure 8 and Figure 9) can again be explained by relative solubility into saline brine of the three components: CO_2 is much more soluble than CH_4 or N_2, and CH_4 is approximately twice as soluble as N_2 in the reservoir conditions 1.3×10^{-3} and 6×10^{-4} on a mole basis, respectively (Appendix A). The maximum extent varies from 10,350 ft for CO_2 to more than twice the distance for CH_4 (22,250 ft) and N_2 (24,250 ft). As in the time-to-reach-the-top case, buoyant driving force for the CO_2-N_2 mixture is higher, except in later stages of plume evolution, when most of the CO_2 has dissolved. The latter fact, in addition to the larger

solubility of CH_4, explains the close results in terms of maximum lateral extent for the CO_2-CH_4 and CO_2-N_2 mixtures.

Figure 10 and Figure 11 show the fraction of mobile gas 100 yr after start of injection (that is, 70 yr after injection stops). The fraction of mobile gas at 100 yr is sensibly equivalent for CH_4 and N_2, at 0.389 and 0.391, respectively. Both are much smaller than the mobile fraction for the pure CO_2 injection-stream case (0.676). Explanation for the numerical observations is the slower movement of CO_2 in the subsurface. Speed of fluid migration subhorizontally is a function of the ratio of density to viscosity and varies by almost a factor of 2, between CO_2 on one side and CH_4 and N_2 (mixed with CO_2) on the other side (Appendix B). In other words, pure CO_2 is moving slower, leaving behind its trail at residual saturation also at a slower rate. The same pattern still exists at 500 yr after start of injection (Figure 12 and Figure 13)

An important conclusion is that pure CO_2 does not travel as far as a mixed-gas plume does (smaller maximum extent—Figure 8), which, on the positive side, minimizes potential area-of-review for abandoned wells, faults, and other pathways or worries about property rights. And yet, on the other hand, some of the gas stays mobile longer (Figure 10 and Figure 12), which translates into a longer postclosure monitoring period.

II-1-2 Storage Capacity as a Function of Distance

It is interesting to investigate how much CO_2 is stored close to, or at some distance from, the injection well for various injection-stream compositions. Figure 14 displays data for the three bounding injection-stream compositions (75% CO_2 and 25% of either CO_2—Case #16, CH_4—Case #17, and N_2—Case #18), as well as for the base case (95% CO_2, 2.5% CH_4, and 2.5% N_2—Case #3). Two metrics are used, both at a given distance updip of the injection well, as follows: (1) fraction of total injected CO_2 that is nonmobile (that is, at residual saturation or dissolved) within the volume downdip of a selected distance (including that CO_2 downdip of the injection well) and (2) absolute amount of CO_2 stored within that same volume.

Both metrics reflect the observation already made in the discussion on parametric analysis—systems with CH_4 and/or N_2 behave faster than a pure CO_2 system. Right-hand-side plots of Figure 14 show that CH_4/N_2-containing systems trap CO_2 faster. Initially more CO_2 is trapped in these systems, even if less was injected. It is only between 100 and 200 yr after start of injection that the pure CO_2 system is able to secure a larger amount of nonmobile CO_2.

At 1,000 yr after start of injection (Figure 14e), more CO_2 has been immobilized in the pure CO_2 case (~13 Mt) than in the two other bounding cases (~11 Mt); however, approximately 15% of the CO_2 is still mobile in the former case (as confirmed by examination of phase-distribution plots in Appendix C).

Table 5. Summary of results (generic model).

Case number	Case	Plume extension (ft)	Tongue #	Time to reach top (yr)	Contribution of free gas at 100 yr	Contribution of free gas at 500 yr
1	95-5-0 (CO2-CH4-N2)	12,050	3	42.5	0.593	0.203
2	95-0-5 (CO2-CH4-N2)	14,050	1	37.0	0.544	0.186
3	95-2.5-2.5 (CO2-CH4-N2) (base case)	12,550	4	40.0	0.567	0.194
4	90-10-0(CO2-CH4-N2)	15,550	1	31.5	0.494	0.172
5	90-0-10 (CO2-CH4-N2)	17,550	1	26.3	0.413	0.120
6	90-5-5 (CO2-CH4-N2)	16,550	1	28.8	0.455	0.148
7	85-15-0 (CO2-CH4-N2)	17,550	1	25.2	0.422	0.125
8	85-0-15 (CO2-CH4-N2)	19,050	1	20.0	0.359	0.049
9	85-7.5-7.5 (CO2-CH4-N2)	19,050	1	22.2	0.378	0.083
10	80-20-0 (CO2-CH4-N2)	19,550	1	21.9	0.376	0.076
11	80-0-20 (CO2-CH4-N2)	23,050	1	16.4	0.379	0.014
12	80-10-10 (CO2-CH4-N2)	21,050	1	18.1	0.370	0.033
13	75-25-0 (CO2-CH4-N2)	22,250	1	18.1	0.391	0.037
14	75-0-25 (CO2-CH4-N2)	24,250	1	13.7	0.389	0.005
15	75-12.5-12.5 (CO2-CH4-N2)	21,550	1	15.4	0.383	0.010
16	100-0-0 (CO2-CH4-N2)	10,350	4	60.0	0.676	0.226
17	75-25-0 (CO2-CH4-N2) on a mass basis	> 32,550	1	10.1	0.458	0.016
18	75-0-25 (CO2-CH4-N2) on a mass basis	31,550	1	11.3	0.413	0.005
19	Dip = 1°	15,050	1	33.4	0.557	0.203
20	Dip = 5°	19,050	4	70.0	0.676	0.226
21	Permeability = 100 md	10,050	4	125.1	0.779	0.353
22	Permeability = 600 md	17,550	1	21.9	0.429	0.107
23	Permeability anisotropy in K-direction = 0.1	30,550	1	4.8	0.615	0.408
24	Permeability anisotropy in K-direction = 0.005	13,550	4	90.1	0.642	0.213
25	CPOR = 5×10^{-5}	11,550	3	45.0	0.590	0.189
26	Default PVT data 100-0-0 (CO2-CH4-N2)	14,550	4	40.0	0.779	0.358
27	Default PVT data 75-25-0 (CO2-CH4-N2)	28,050	1	15.3	0.581	0.164
28	Default PVT data 75-0-25 (CO2-CH4-N2)	> 32,550	1	12.9	0.580	0.092
29	Fixed pressure 100-0-0 (CO2-CH4-N2)	10,050	4	60.0	0.680	0.222
30	Fixed pressure 75-25-0 (CO2-CH4-N2)	22,550	1	19.5	0.391	0.021

Case number	Case	Plume extension (ft)	Tongue #	Time to reach top (yr)	Contribution of free gas at 100 yr	Contribution of free gas at 500 yr
31	Fixed pressure 75-0-25 (CO2-CH4-N2)	19,550	3	15.1	0.385	0.002
39	Porosity = 0.2	15,550	1	31.5	0.534	0.205
40	Porosity = 0.3	11,350	3	47.9	0.599	0.180
41	Capillary pressure	11,050	1	40.0	0.544	0.017

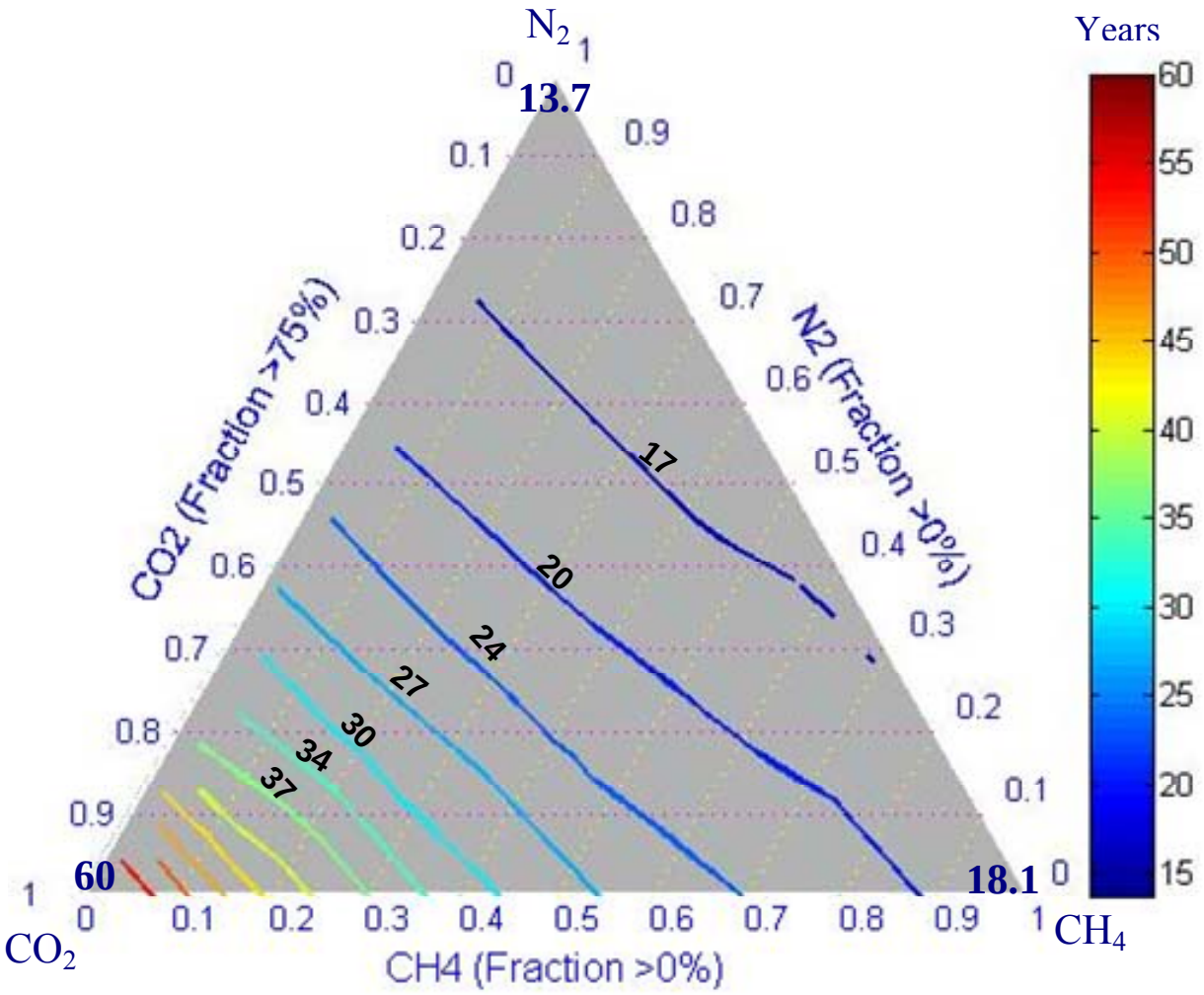

Figure 6. CO_2, CH_4, and N_2 ternary plot of the time (in years) to reach the top after start of injection. Plot based only on the 25% of the injection stream whose composition varies.

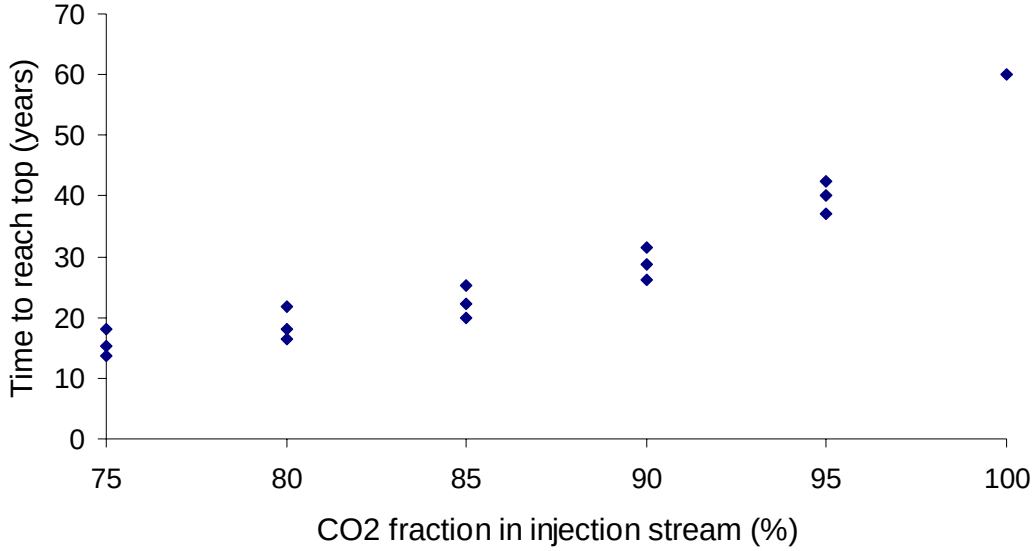

Figure 7. Time to reach the top (after start of injection) as a function of CO_2 fraction in the injection stream.

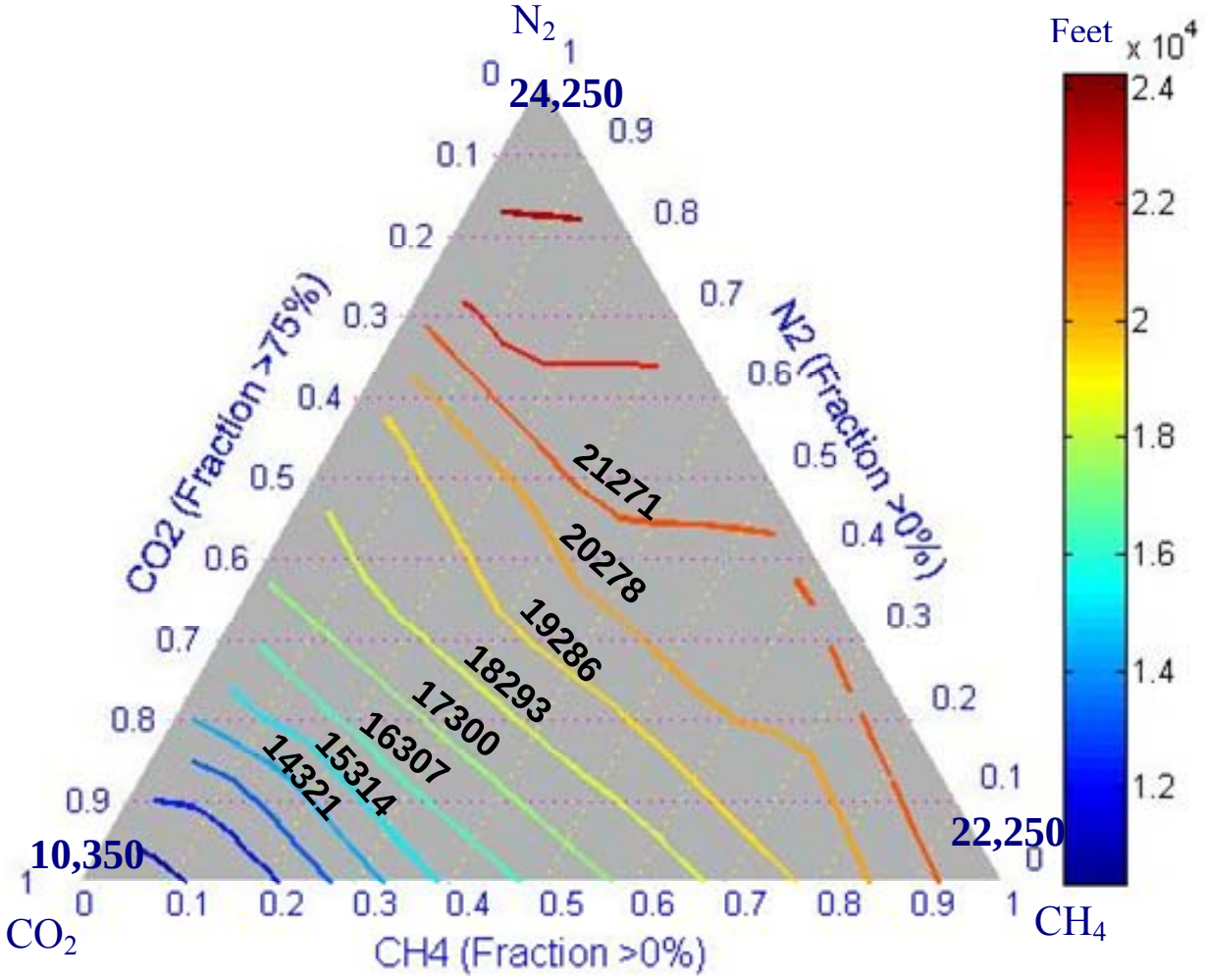

Figure 8. CO_2, CH_4, and N_2 ternary plot of the maximum plume extent (in feet). Plot based only on the 25% of the injection stream whose composition varies.

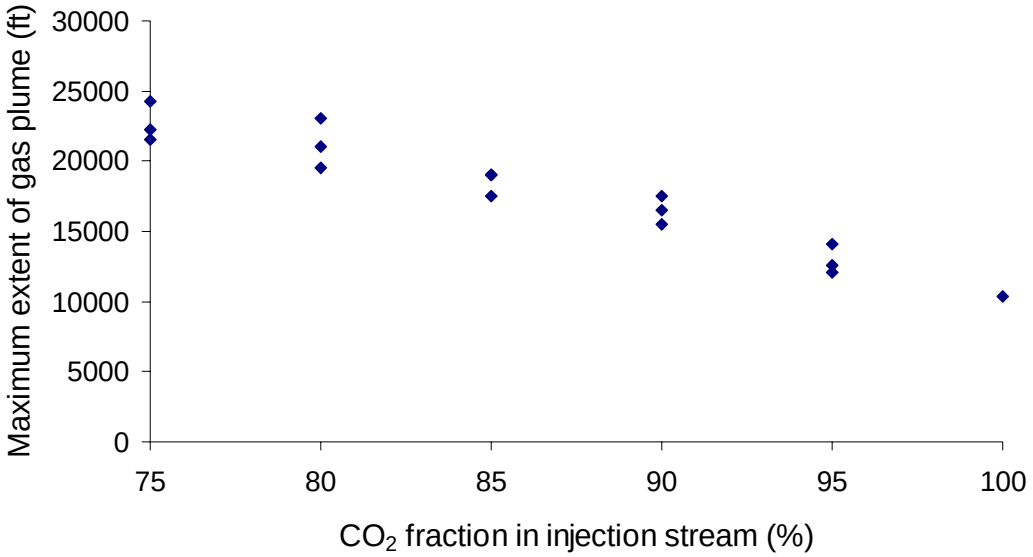

Figure 9. Maximum extent of plume as a function of CO_2 fraction in the injection stream.

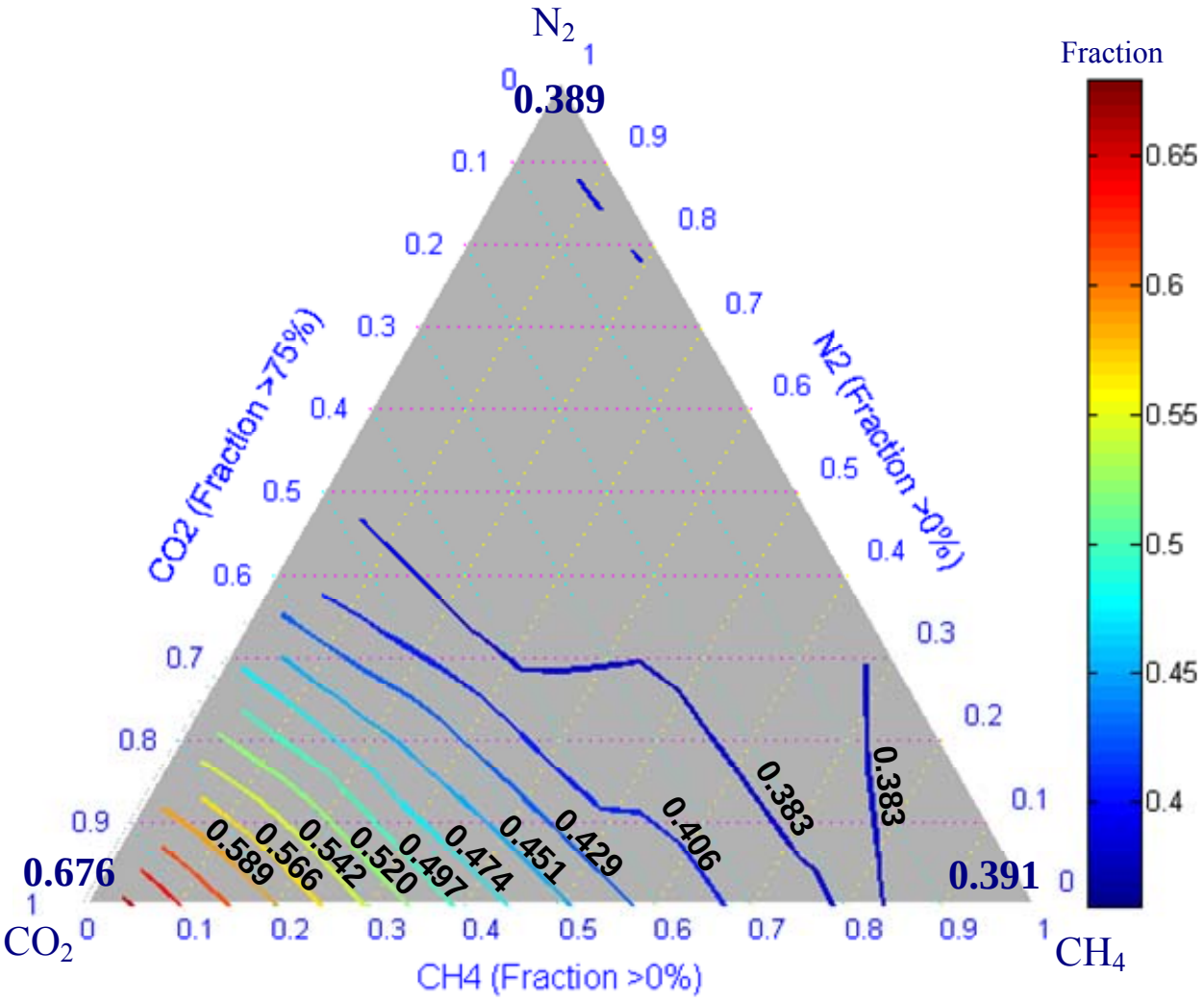

Figure 10. CO_2, CH_4, and N_2 ternary plot of free gas fraction at 100 yr after start of injection. Plot based only on the 25% of the injection stream whose composition varies.

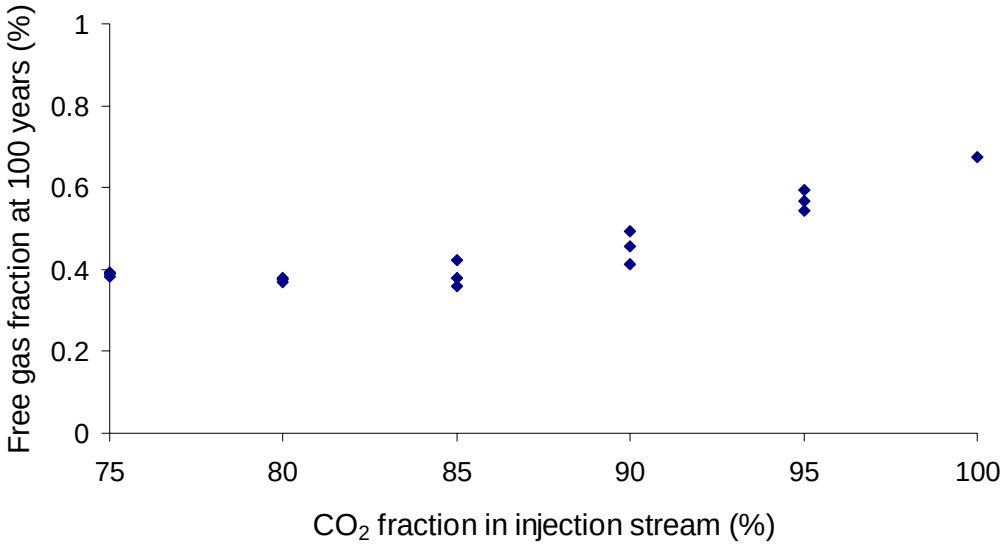

Figure 11. Free gas fraction at 100 yr after start of injection as a function of CO_2 fraction in the injection stream.

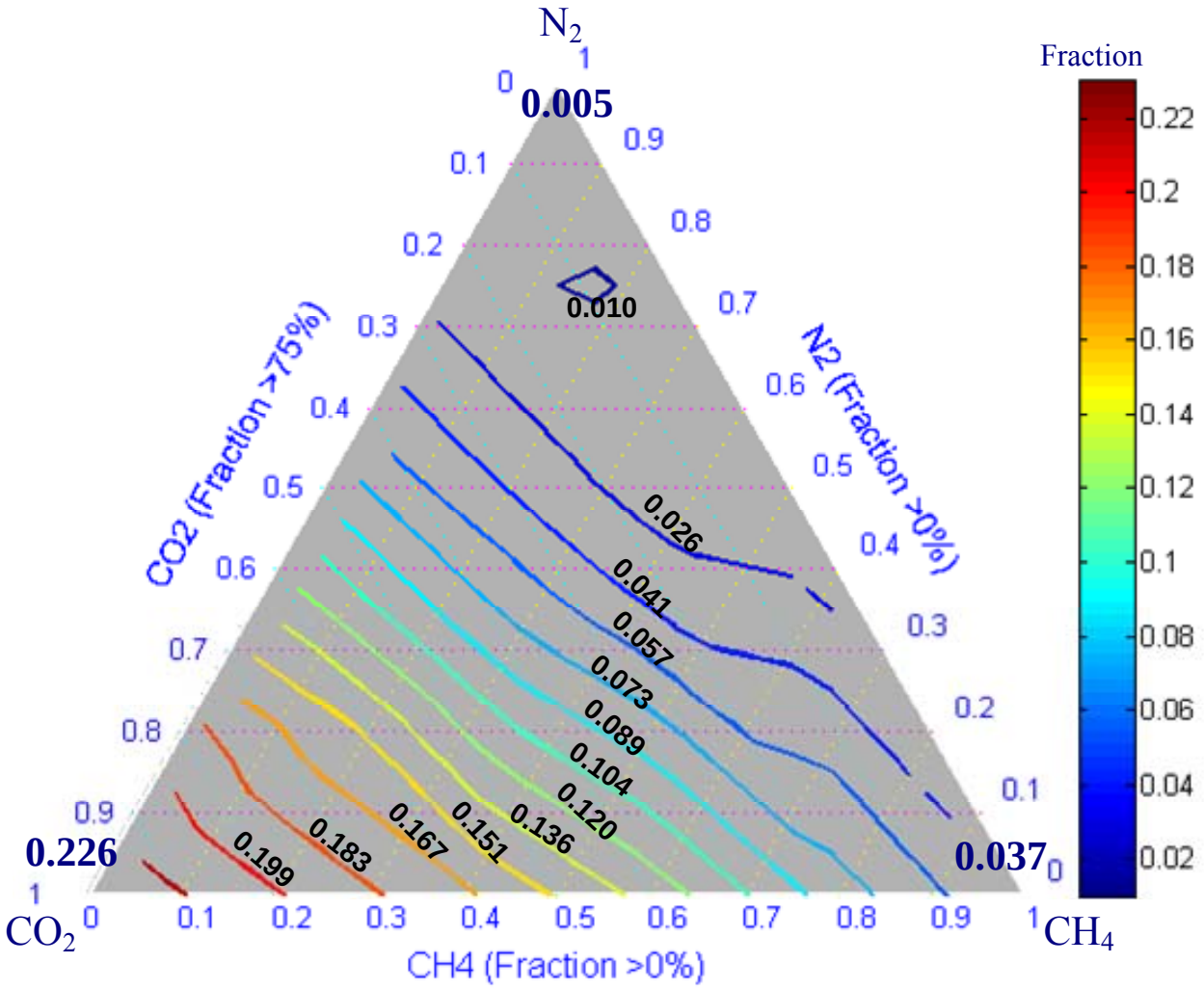

Figure 12. CO_2, CH_4, and N_2 ternary plot of free gas fraction at 500 yr after start of injection. Plot based only on the 25% of the injection stream whose composition varies.

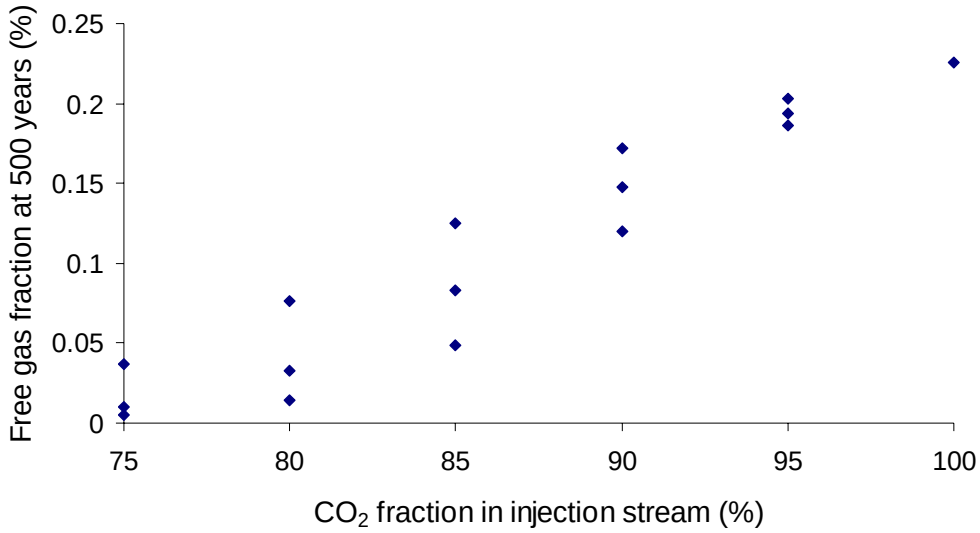

Figure 13. Free gas fraction at 500 yr after start of injection as a function of CO_2 fraction in the injection stream.

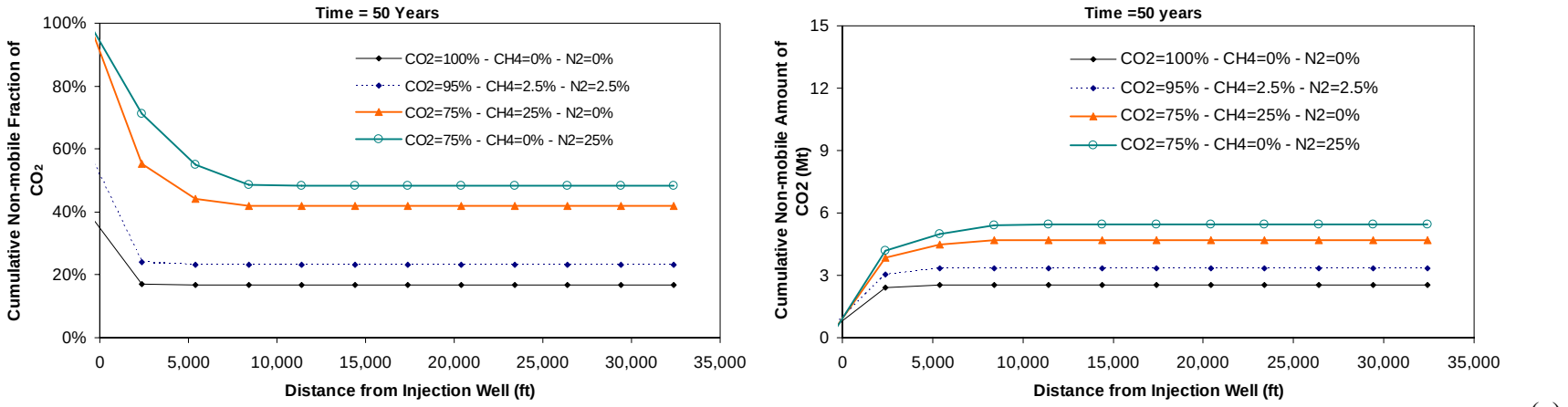

(a)

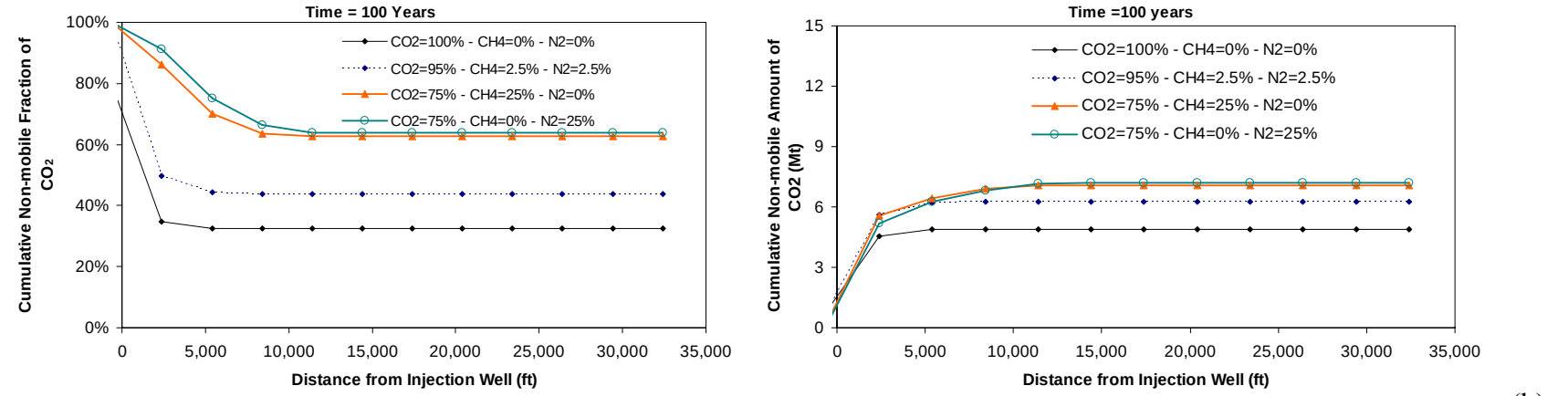

(b)

Figure 14. Nonmobile fraction (at residual saturation and dissolved) and absolute amount of CO_2 present downdip of a given distance from the injection well at selected times: (a) 50, (b) 100, (c) 200, (d) 500, and (e) 1,000 yr after start of 30-yr injection period and for bounding injection-stream composition (75% CO_2 and 25% of CO_2, CH_4, or N_2).

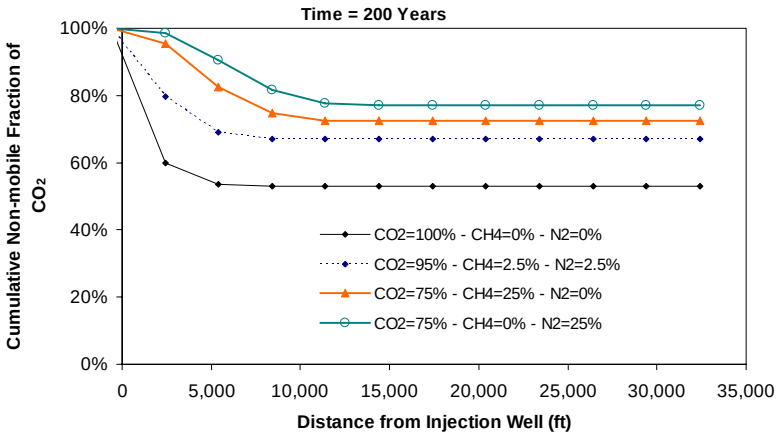

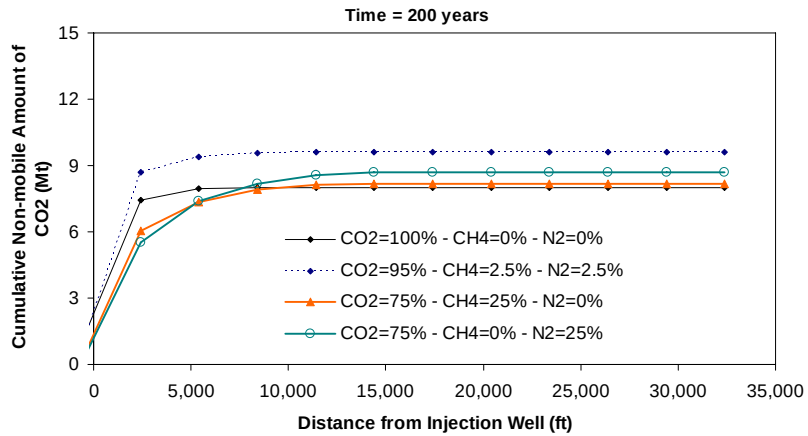

(c)

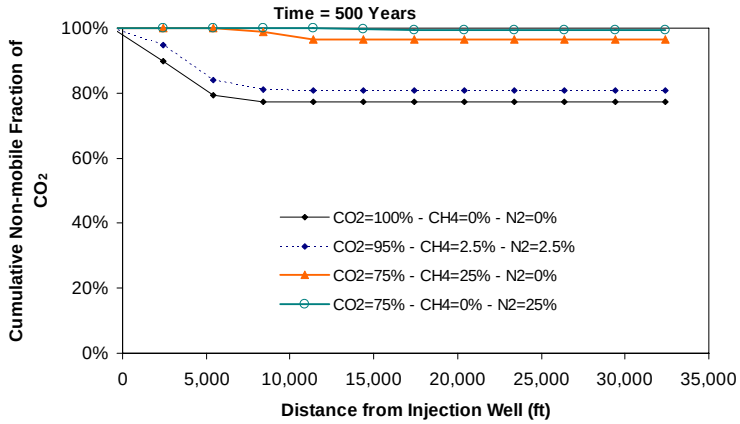

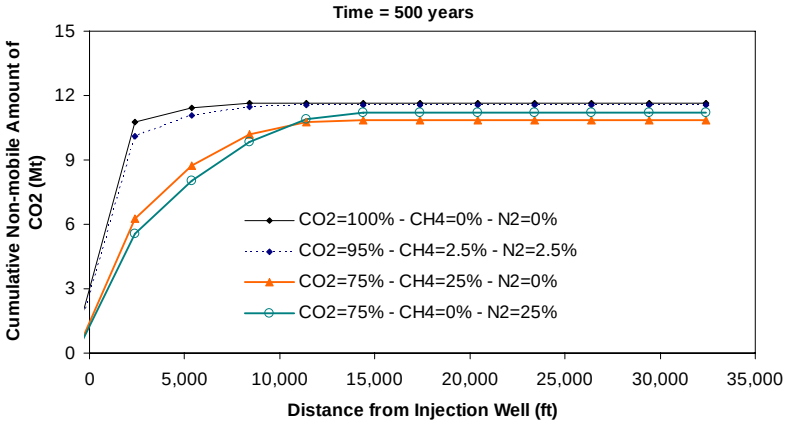

(d)

Figure 14 (continued).

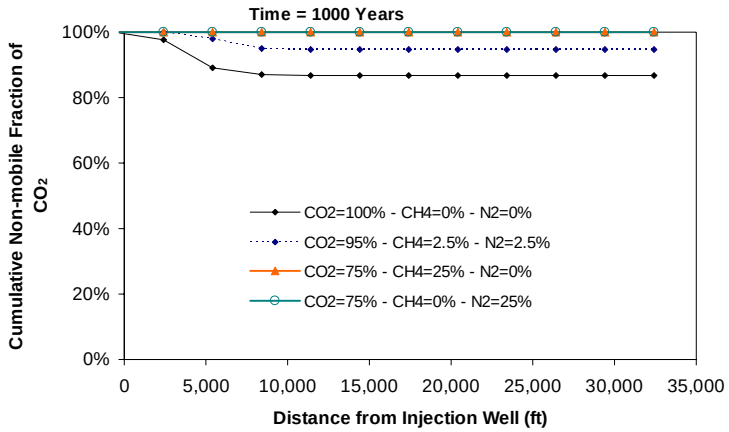

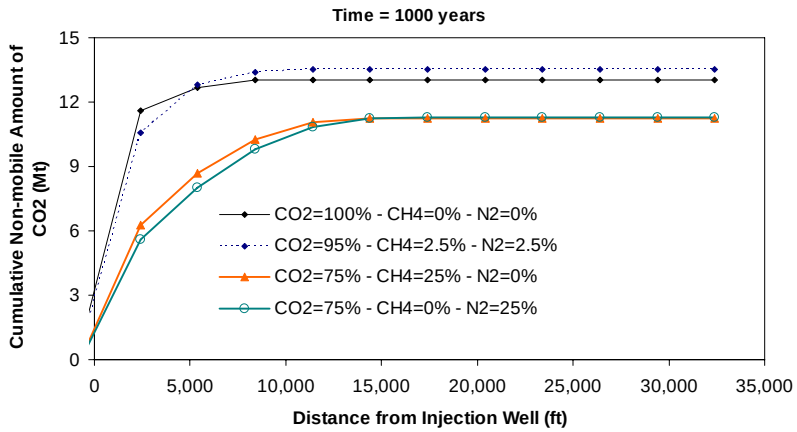

(e)

Figure 14 (continued).

II-1-3 Sensitivity Analysis

For the purpose of comparing results of the sensitivity analysis with results of the parametric study, we present results from the latter in Figure 15 in a manner consistent with the rest of this section. As observable in other plots of this section, variation in injection-stream composition (in the studied range) generates a large change in all metrics. Variations in other parameters generally generate a smaller change in metrics or, if similar in value, a change in only some of the metrics. It follows that injection-stream composition (in the range used in this study) does impact system behavior in important ways.

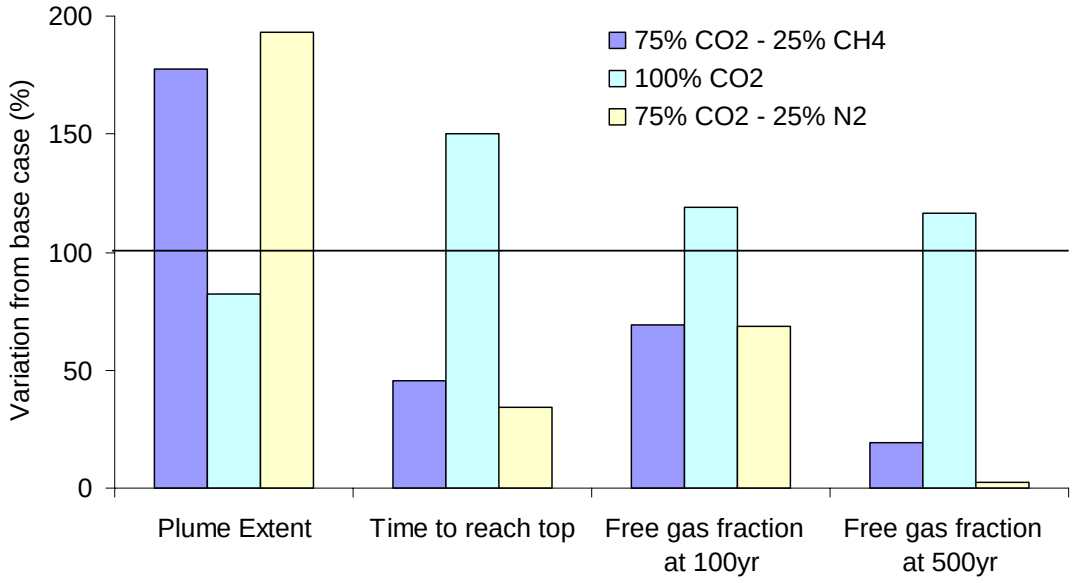

Figure 15. Relative impact of injection-stream composition on parametric-study metrics.

II-1-3.1 Formation Dip

Formation-dip sensitivity analysis included cases #19 (1° dip—p. 73), #3 (2°—base case—p. 57), and #20 (5°—p. 74). Some plots displayed in Appendix C are presented here side by side (Figure 17 and Figure 18) to facilitate discussion of general results (Figure 16). Time to reach the top increases with increasing dip as distance to the top increases as well. Presence of baffles accentuates variation from the base case for the 5° case because a substantial amount of gas is directed toward the baffles and cannot contribute to feeding that part of the plume moving upward to the formation top. Plume extent seems to follow the influence of two opposing effects. When the dip is small, little gas is diverted by the baffles, and most of the gas is directed toward the top of the formation, where the main tongue resides. Similarly, when the dip is large, most of the gas flow is immediately captured by the lowermost tongue. With an intermediate dip, as in the base case, gas distribution is more balanced between the different tongues. It follows that when one tongue dominates, maximum extent is larger than when gas is distributed more uniformly between tongues. The more compact shape of the gas plume next to the well for the larger dip case (Figure 17 and Figure 18) suggests higher gas saturation and subsequently higher free- or mobile-gas fraction.

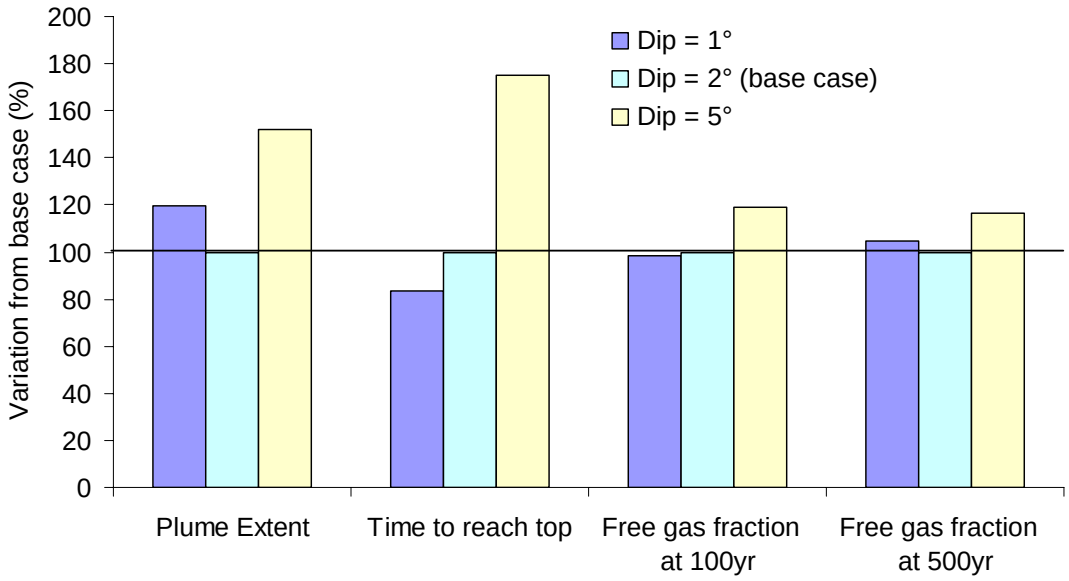

Figure 16. Relative impact of formation dip on parametric-study metrics.

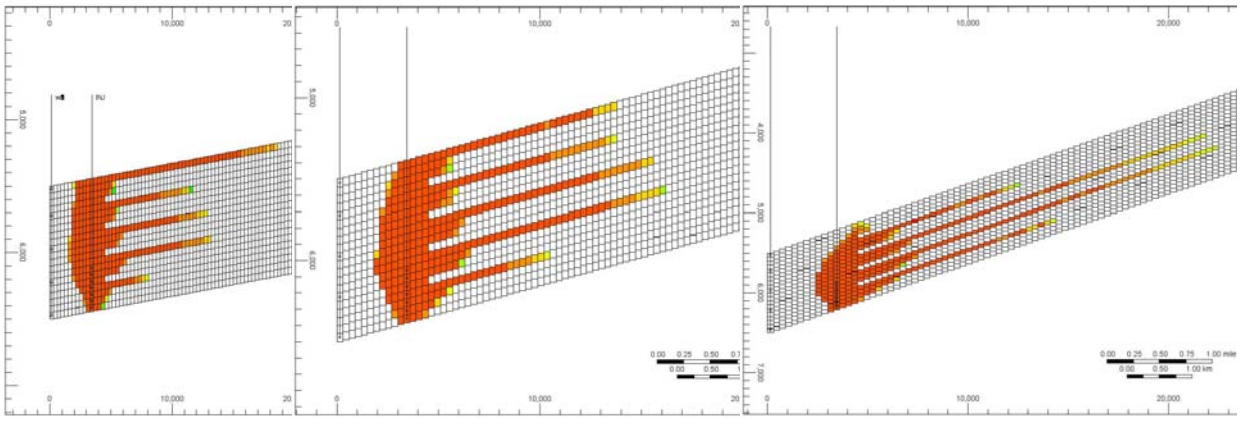

Figure 17. Impact of formation dip on plume extent (at 1,000 yr after start of injection) for dip of 1°, 2°, and 5°.

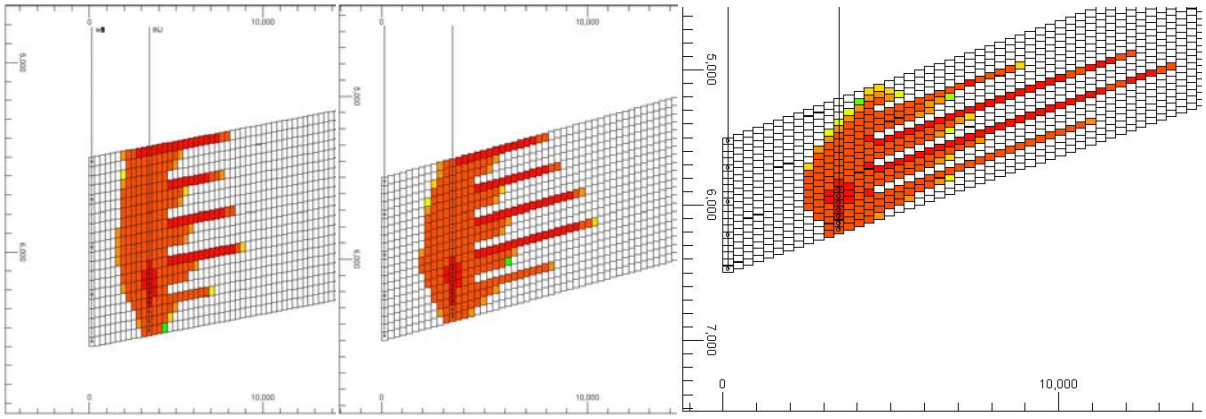

Figure 18. Impact of formation dip on plume extent (at 100 yr after start of injection) for dip of 1°, 2°, and 5°.

II-1-3.2 Formation Permeability

Changes in formation permeability have the expected effect on time to reach the top, which varies almost linearly with the inverse of permeability. For example, reduction of permeability by a factor of 3 generates a threefold increase in time to reach the top (Figure 19). Plume extent, as depicted in cases #21 (100 md—p. 75), #3 (300 md—base case—p. 57), and #22 (600 md—p. 76) increases with increasing permeability (Figure 20). Higher permeability generates a thinner high-saturation area around the injection well, allowing more gas to hit the top of the formation and mechanically produce a longer tongue.

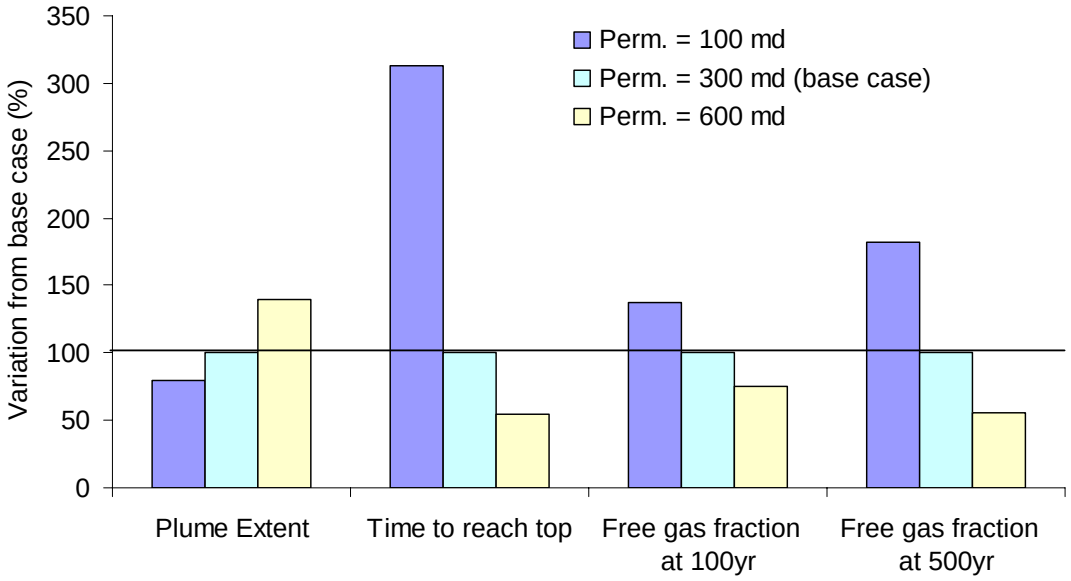

Figure 19. Relative impact of formation permeability on parametric-study metrics.

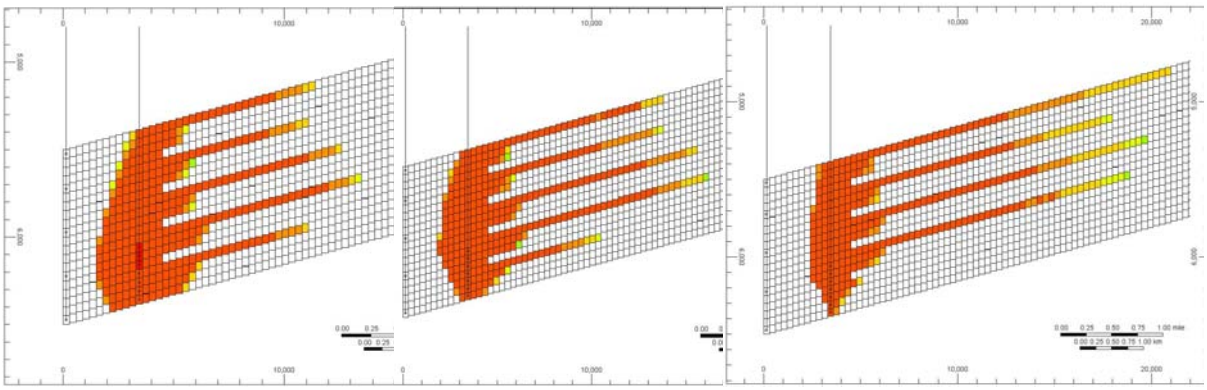

Figure 20. Impact of formation permeability on plume extent (at 1,000 yr after start of injection) for values of 100, 300, and 600 md.

II-1-3.3 Permeability Anisotropy

Permeability anisotropy results (cases #23—0.1 k_v/k_x ratio—p. 77), #3—0.01 ratio—base case—p. 57, and #24—0.005 ratio—p. 78) are displayed in Figure 21. Impact on time to reach the top is similar to that of a change in permeability because of the impact of vertical permeability on vertical movement and is consistent with the relationship between permeability and time to reach

the top, discussed in the previous section. In this case, an increase in vertical permeability by a factor of 10 (anisotropy varying from 0.01 to 0.1) generates a factor-10 decrease in time to reach the top. Plume extent is also much larger with a smaller permeability because much of the gas migrates to the top of the formation to feed only one tongue (in this particular case, #24, some gas escapes the system).

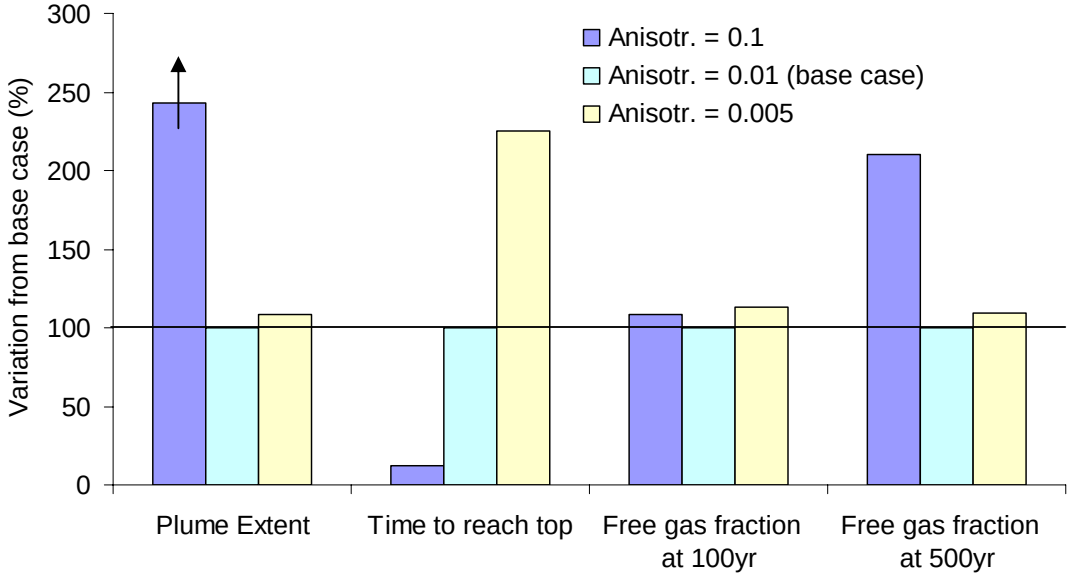

Note: For anisotropy =0.1, the plume reached the boundary, and only minimum plume extent can be displayed.

Figure 21. Relative impact of formation permeability anisotropy on parametric-study metrics.

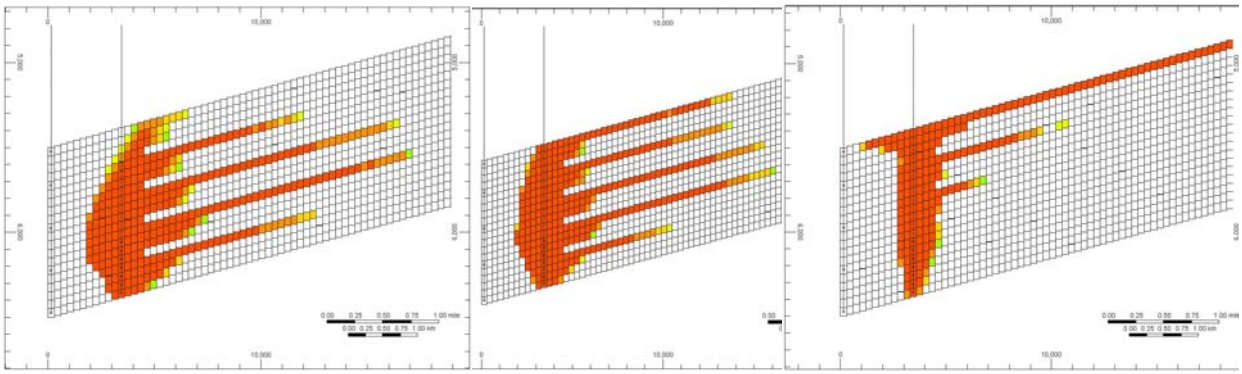

Figure 22. Impact of formation permeability anisotropy on plume extent (at 1,000 yr after start of injection) for values of 0.005, 0.01, and 0.1.

II-1-3.4 Formation Porosity

Porosity variations produce expected variations in time to reach the top (Figure 23). Higher porosity results in a longer time to hit the top. For example, increase in porosity of 20% (from 0.25 to 0.30) translates into a 20% increase in the time to reach the top—in agreement with a somewhat linear variation. Maximum plume extent (Figure 24) also matches porosity variations, with the plume extending farther with a lower porosity because there is less space in which to trap the gas. Trends in amount of mobile gas as a function of porosity are inverted when considering 100 yr and 500 yr after start of injection but do not vary much from the base case.

Porosity sensitivity analysis cases include cases #39 (porosity of 0.20—p. 86), #3 (0.25—base case—p. 57), and #40 (0.30—p. 87). Note that only porosity was varied; no variation in permeability or nonwetting-phase residual saturation was varied as they could have because of the generally recognized and observed correlation between permeability, porosity, and residual saturation.

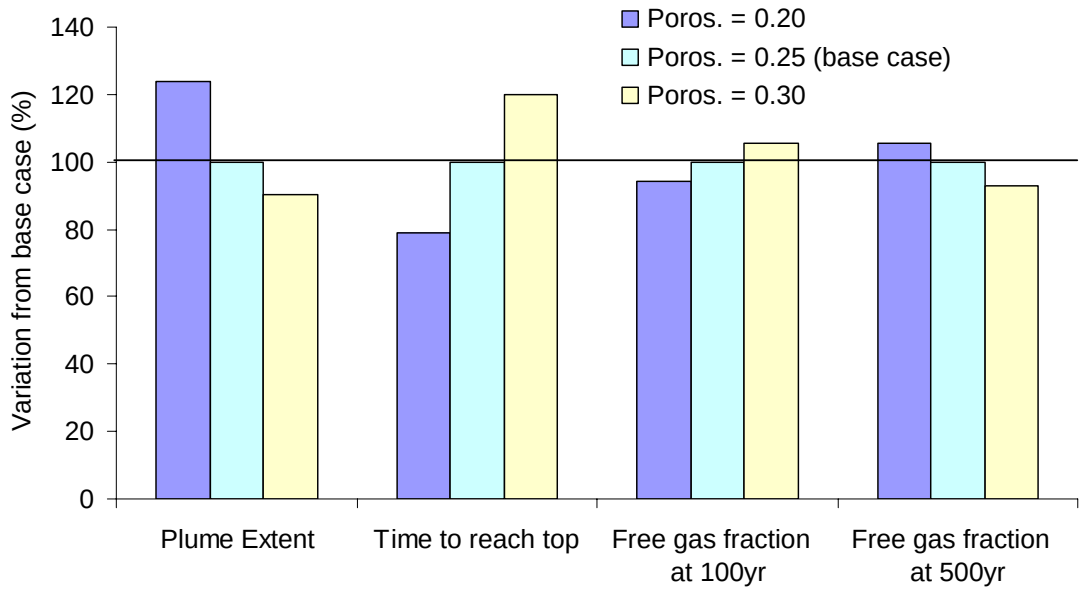

Figure 23. Relative impact of formation porosity on parametric-study metrics.

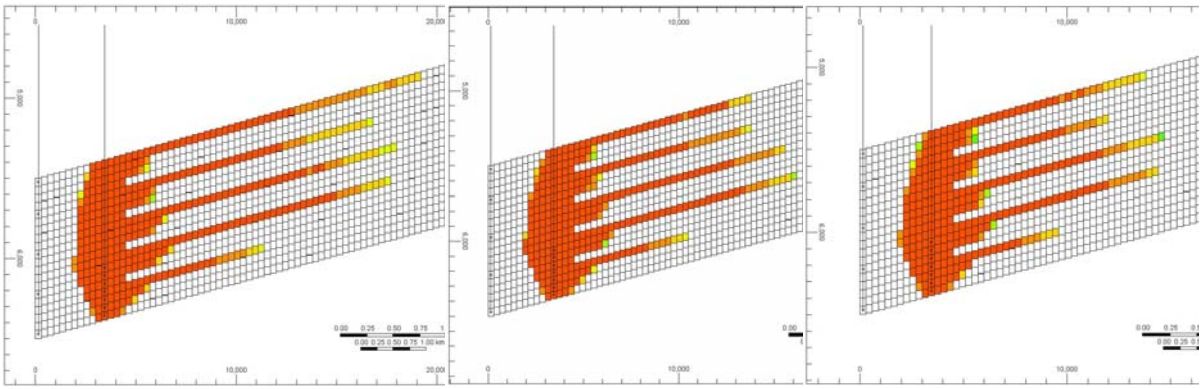

Figure 24. Impact of formation porosity on plume extent (at 1,000 yr after start of injection) for values of 0.20, 0.25, and 0.30.

II-1-3.5 Matrix Compressibility

Matrix compressibility (cases # 3—base case—and #25) is a minor parameter with little impact on results. Increase by 1 order of magnitude of matrix compressibility translates into changes of less than 10% in the four metrics (Figure 25).

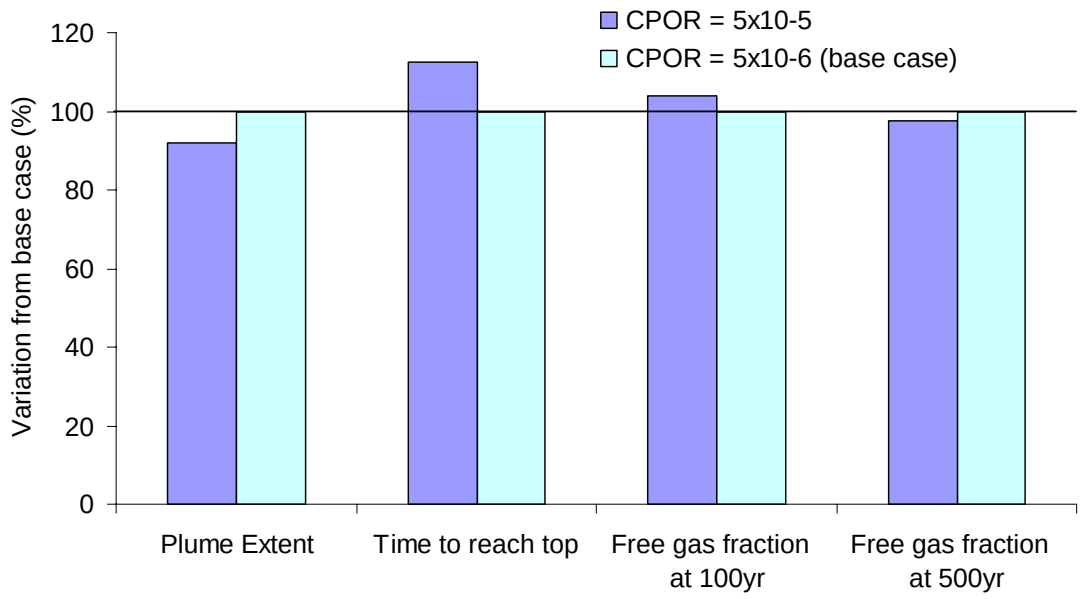

Figure 25. Relative impact of formation matrix compressibility on parametric-study metrics.

II-1-3.6 PVT Data

PVT data could obviously have a large impact on results because they control gas-phase-component solubility, as well as density and viscosity of aqueous and gas phases. Although GEM contains default PVT data for the system of interest, we use user-specified PVT data as described in Appendix A. We investigated the impact of PVT data using three bounding injection-stream compositions run with default and user-specified data: cases #26 and #16 (100% CO_2), cases #27 and #13 (75% CO_2 and 25% CH_4), and cases #28 and #14 (75% CO_2 and 25% N_2). All metrics are impacted by a change in PVT data. Figure 26 displays metric comparisons between default and user-specified data for the three injection-stream compositions. In all cases, choice of PVT data does impact results.

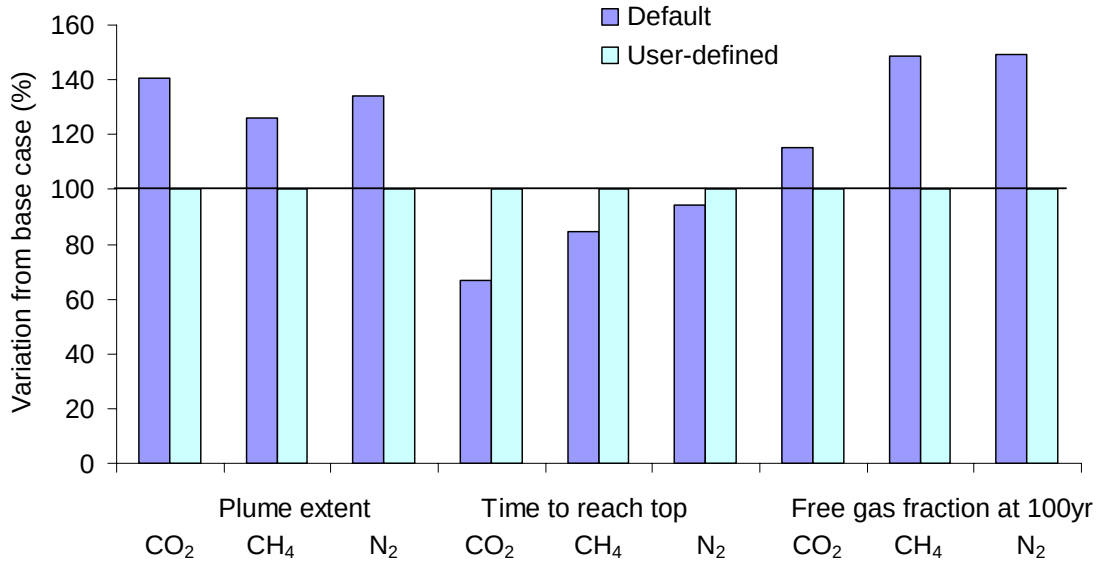

Figure 26. Relative impact of PVT data on parametric-study metrics. "CO_2," "CH_4," and "N_2" stand for 100% CO_2, 75% CO_2 and 25% CH_4, and 75% CO_2 and 25% N_2, respectively.

II-1-3.7 Capillary Pressure

Capillary pressure becomes important only when flow/viscous forces have declined considerably, as shown in Figure 27 (case #3—base case with no capillary pressure—and case #41—with capillary pressure). The mobile gas fraction at later times is impacted the most.

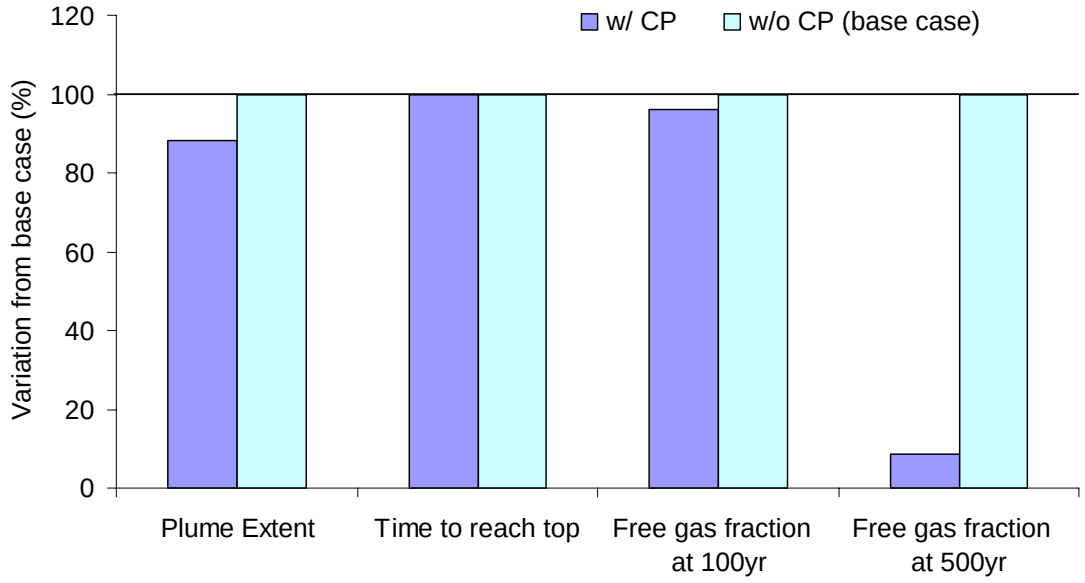

Figure 27. Relative impact of capillary pressure on parametric-study metrics.

II-1-4 Injectivity

Injectivity variations were treated by using either pressure-constrained or flow-rate-constrained (approximately constant injection pressure of ~2,900 psi was chosen as base-case steady-state pressure) gas-stream injection. Note that overall injectivity probably depends more on relative permeability properties (e.g., Burton, 2008) than on stream composition. Injecting at constant pressure, the total amount injected for a mixture of 75% CO_2 and 25% of either CH_4 or N_2 is approximately 80% of the amount of the 100%-CO_2 gas stream (Figure 28), suggesting that the injectivity index (MSCFD/psi) would also decrease by 20%.

The model as it stands is too crude for detailed injectivity analysis. However, impact of lower injectivity of CH_4/N_2-rich cases on the metrics is limited in most cases (Figure 29). Three bounding injection-stream compositions were again used: cases #29 and #16 (100% CO_2), cases #30 and #13 (75% CO_2 and 25% CH_4), and cases #31 and #14 (75% CO_2 and 25% N_2). The reason for the jump in plume extent for the 75% CO_2-25% N_2 case is unclear.

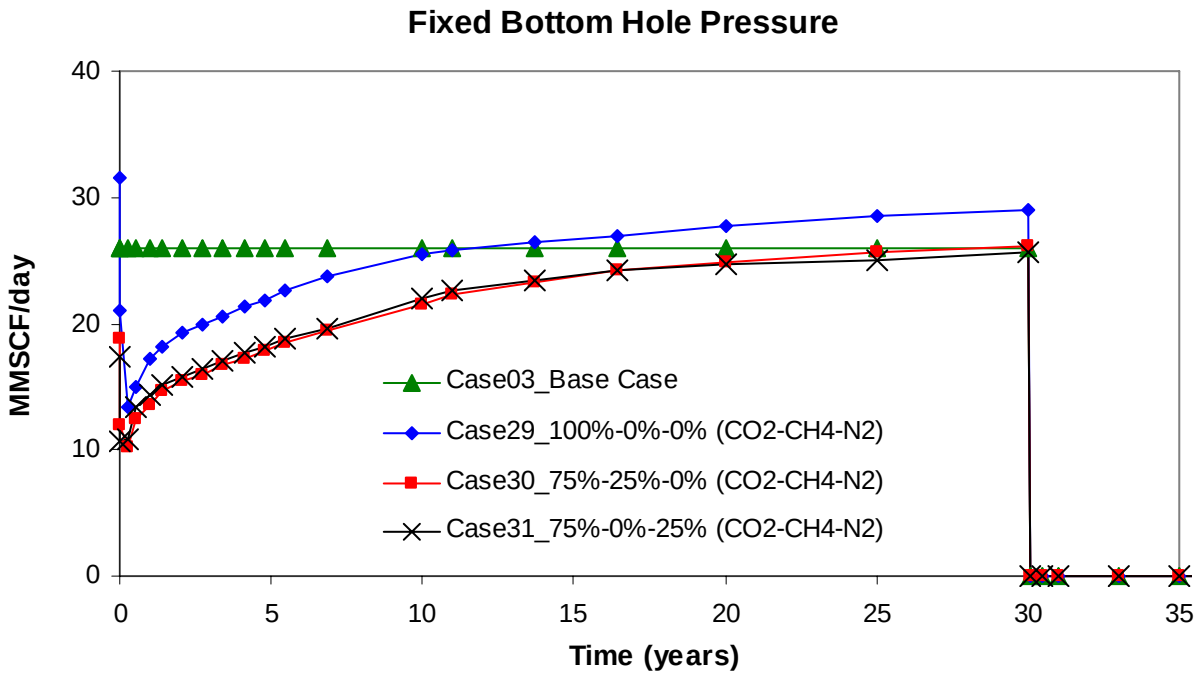

(a)

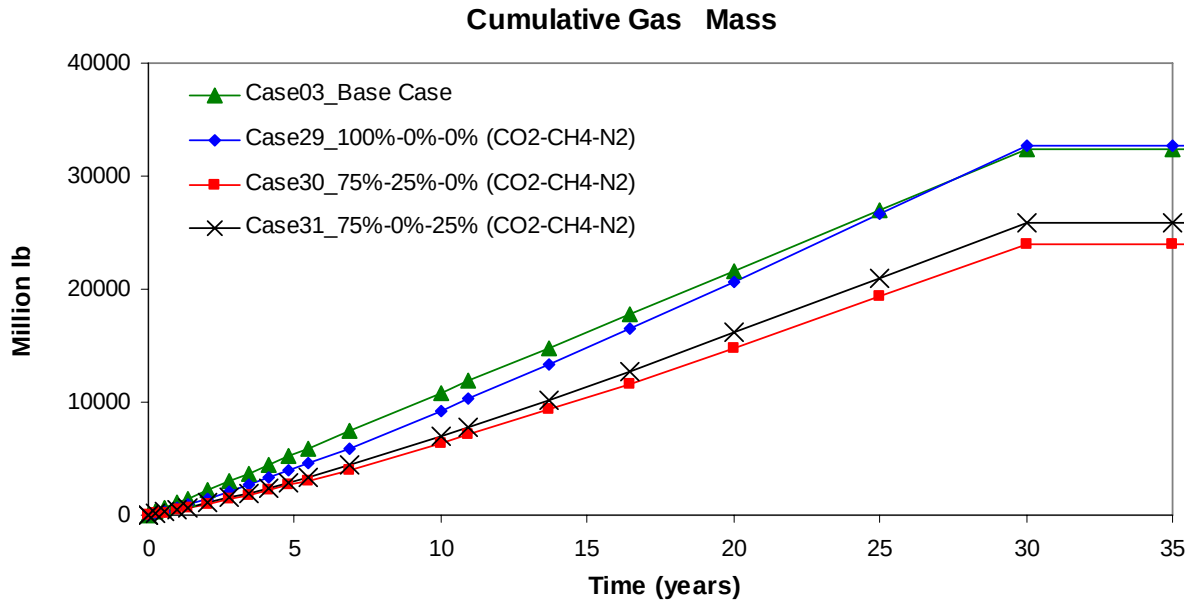

(b)

Figure 28. (a) Instantaneous and (b) cumulative injection flow rate at fixed pressure (target injection pressure is 2,900 psi).

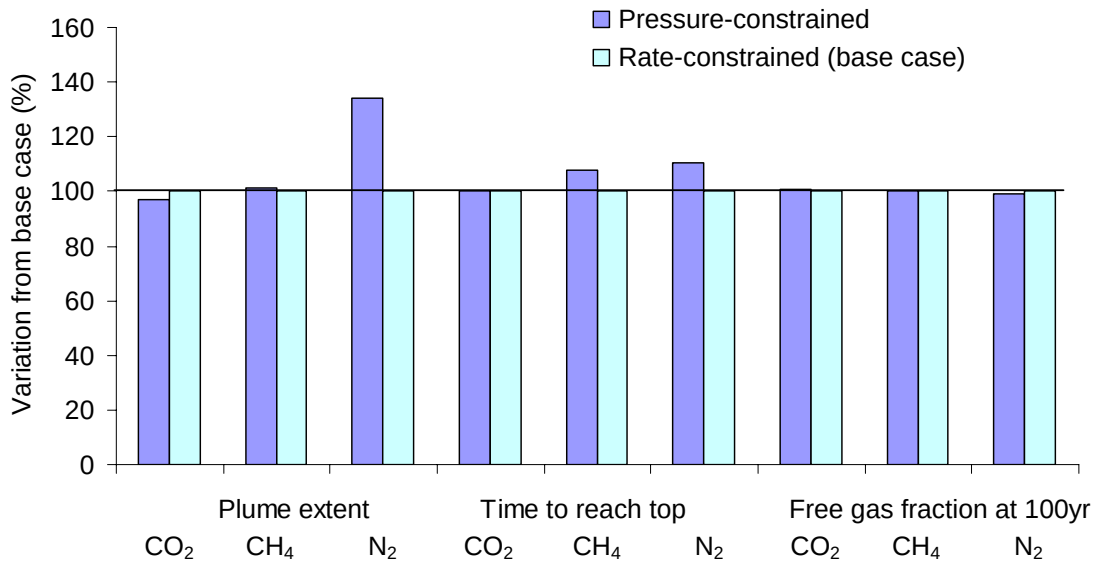

Figure 29. Relative impact of injectivity on parametric-study metrics.

II-2. Gulf Coast Model Results

Modeling results from the Gulf Coast case are displayed in Appendix D. Overall the system behaves much like the generic case. Main differences between the models themselves are variable permeability distribution, variable and generally larger dip, presence of a few faults parallel to general flow, shorter injection time (5 years as opposed to 30 years) and the much smaller total volume in the Gulf Coast case (2×10^8 ft^3 as opposed to 2×10^{11} ft^3). Time to reach the top is much shorter than in the generic case owing to a small injection formation thickness of 60ft. However, relative order and ratios stay similar (Table 6). In addition, the Gulf coast model stabilizes much faster than the generic case owing to its much smaller size. Only dissolution is occurring in the Gulf Coast model at both 100 and 500 yr in contrast to the generic model in which fluids are actively responding to buoyancy forces. Values for contribution of free gas remain higher in the CO_2-CH_4 and CO_2-N_2 Gulf Coast cases because of the updip closed boundary allowing for structural storage.

Table 6. Summary of results (Gulf Coast model) and comparison with generic case

Case	Time to reach top	Contribution of free gas at:					
Gulf Coast	**(day)**	**10**	**50**	**60 yr**	**80 yr**	**100 yr**	**500 yr**
100-0-0 (CO2-CH4-N2)	300	0.659	0.296	0.282	0.268	0.262	0.234
75-25-0 (CO2-CH4-N2)	130	0.635	0.491	0.489	0.487	0.484	0.476
75-0-25 (CO2-CH4-N2)	100	0.633	0.509	0.506	0.504	0.503	0.499
Generic	**(year)**					**100 yr**	**500 yr**
100-0-0 (CO2-CH4-N2)	60.0					0.676	0.226
75-25-0 (CO2-CH4-N2)	18.1					0.391	0.037
75-0-25 (CO2-CH4-N2)	13.7					0.389	0.005

III. Conclusions and Future Work

This simple study underlines the conflicting effects of having a significant amount of CH_4 and/or N_2 in a CO_2-dominated injection stream: the plume stabilizes faster with these impurities but also flows farther from the injection well. In contrast, a pure CO_2 plume travels less because of higher solubility but stays mobile longer. This general conclusion should hold under different sets of reservoir parameters, as suggested by the sensitivity analysis of these parameters and the Gulf Coast case. However, mobility of CH_4 and N_2 can be an issue since, at sufficiently high concentrations, they can become a health and safety risk (asphyxiation/explosion) if leakage occurs.

However, sensitivity analysis needs to be expanded to simulations with, for example, at least a couple more sets of relative-permeability data, horizontal wells, stochastic permeability field, baffles of different sizes and discontinuous, more sophisticated treatment of heterogeneities, impact of closed boundary conditions, and addition of other impurities such as H_2S or SO_2, etc. From a numerical modeling standpoint, effect of grid size needs to be investigated. In particular, maximum plume extent depends somewhat on size of top-layer cells and volume injected. A proper treatment of injectivity also requires better grid resolution around the well.

Other interesting exercises such as monitoring leakage through a (leaking) well located at some distance from the injection well as a function of injection-stream composition could also be performed. More far-reaching and more demanding tasks would be to improve PVT properties and residual saturation understanding, mostly through experiments, for input in the numerical model.

IV. References

Bennion, B. and Bachu, S., 2005, Relative permeability characteristics for supercritical CO_2 displacing water in a variety of potential sequestration zones in the western Canada sedimentary basin, SPE95547.

Burton, M., 2008, *Surface Dissolution: Addressing Technical Challenges of CO_2 Injection and Storage in Brine Aquifers*, MS thesis, The University of Texas at Austin.

Doughty, C., 2007, Modeling geologic storage of carbon dioxide: Comparison of non-hysteretic and hysteretic characteristic curves, *Energy Conversion and Management*, 48, 1768-1781.

Duan, Z., Moller, N., Greenberg, J., and Weare, H., 1992, The prediction of methane solubility in natural waters to high ionic strength from 0 to 250°C and from 0 to 1600 bar, *Geochimica et Cosmochimica Acta*, 56, 1451-1460.

Ghomian, Y., Pope, G. A., and Sepehrnoori, K., 2008, Reservoir simulation of CO2 sequestration pilot in Frio brine formation, USA Gulf Coast, *Energy*, doi:10.1016/j.energy.2008.02.011.

Holtz, M. H., 2002, Residual gas saturation to aquifer influx: A calculation method for 3-D computer reservoir model construction, SPE75502.

Hovorka, S. D., Doughty, Christine, Benson, S. M., Freifeld, B. M., Sakurai, Shinichi, Daley, T. M., Kharaka, Y. K., Holtz, M. H., Trautz, R. C., Nance, H. S., Myer, L. R., and Knauss, K. G.,

2006, Measuring permanence of CO_2 storage in saline formations: the Frio experiment, *Environmental Geosciences*, 13, 105-121.

Hovorka, S. D., Doughty, C. Benson, S. M., Pruess, K., and Knox, P. R., 2004, The impact of geological heterogeneity on CO_2 storage in brine formations: a case study from the Texas Gulf Coast, in Baines, S. J., and Worden, R. H., eds., Geological storage of carbon dioxide: Geological Society, London, Special Publications, 233, p. 147-163.

Knauss, K.G., Johnson, J. W., Steefel, C. I., 2005, Evaluation of the impact of CO_2, co-contaminant gas, aqueous fluid and reservoir rock interactions on the geologic sequestration of CO_2, *Chemical Geology*, 217(3-4), 339-350.

Kumar, A., 2004, *A Simulation Study of Carbon Sequestration in Deep Saline Aquifers*, MS thesis, The University of Texas at Austin.

Kumar, N., 2008, *CO_2 Sequestration: Understanding Plume Dynamics and Estimating Risks*, MS thesis, The University of Texas at Austin.

Kumar, A., Noh, M., Pope, G. A., Sepehrnoori, K., Bryant, S., and Lake, L. W., 2004, Reservoir simulation of CO_2 storage in deep Saline aquifers, SPE 89343.

Land, C.S., 1971, Comparison of calculated with experimental imbibition relative permeability, SPE 3360.

Ozah, R., 2005, *Numerical Simulation of the Storage of CO_2 and CO_2-H_2S Gas Mixture in Deep Saline Aquifers*, MS thesis, The University of Texas at Austin.

Pedersen, K. S., Fredenslund, A., Christensen, P. L., and Thomassen, P., 1984, Viscosity of crude oils, *Chemical Engineering Science*, 36(6).

Perry, R. H., and Green, D. W., 1997, Perry's Chemical Engineers' Handbook, 7th Edition, McGraw-Hill.

Pruess, K., Xu, T., Apps, J., and Garcia, J., 2001, Numerical modeling of aquifer disposal of CO_2, SPE 66537.

Sun, R., Hu, W., Duan, Z., 2001, Prediction of nitrogen solubility in pure water and aqueous NaCl solutions up to high temperature, pressure, and ionic strength, *Journal of Solution Chemistry*, 30(6).

Vicencio, O. A., 2007, *Nitrogen Injection into Naturally Fractured Reservoirs*, Ph.D. Dissertation, The University of Texas at Austin, 238 p.

Weast, R. C., 1972, *Handbook of Chemistry and Physics*, 53rd edition, CRC Press, USA.

Zaytsev, I. D., and Aseyev, G. G., 1992, *Properties of Aqueous Solutions of Electrolytes,* CRC Press, Boca Raton, FL, 1729 p.

V. Appendix A: Phase Behavior Modeling of CH_4-CO_2-N_2 Gas Mixture and Brine

The Peng-Robinson Equation-of-State (EOS) is used to predict phase equilibrium compositions of N_2-CH_4-CO_2-H_2O mixtures. EOS parameters for all of the components were tuned to match the experimental data for density, viscosity, and solubility in the brine. Some general properties of individual gas-phase components are given in Table 7. PVT properties were adjusted to a brine salinity of 100,000 mg/L.

Table 7. Characteristics of gas-phase components.

	CO_2	CH_4	N_2	H_2O
Critical pressure (atm)	73	45.4	33.5	218
Critical temperature (°C)	31	-82.7	-147	374
Molecular weight (g/mol)	44	16	28	18

V-1. Solubility of Gas-Mixture Components in the Brine

V-1-1 CO_2 Solubility

Kumar et al. (2004) tuned the Binary Interaction Coefficient (BIC) between CO_2 and H_2O to match experimental data for CO_2 solubility in the brine. They presented a correlation between $BIC_{H2O\text{-}CO2}$ values, temperature, and brine salinity, which was used to determine the $BIC_{H2O\text{-}CO2}$.used in PTS environmental conditions of the models.

V-1-2 CH_4 Solubility

Binary interaction coefficients between brine and CH_4 at reservoir temperature (~135°F), limited range of reservoir pressure (2,000–2,400 psi) and at brine salinity of 100,000 ppm was tuned to match experimental data for CH_4 solubility in the brine (Duan et al., 1992). At reservoir temperature, pressure of 2,000 psi, and mentioned brine salinity, CH_4 solubility is 1.224×10^{-3} mole fraction. If reservoir pressure is increased to 2,300 psi, CH_4 solubility will increase slightly to 1.314×10^{-3} mole fraction. BIC value between CH_4 and brine was then determined to be -0.1804. Figure 30 shows the plot of BIC versus CH_4 solubility under the aforementioned conditions. These points are in fact all trial and error points to determine the correct BIC value, considering available experimental data.

V-1-3 N_2 Solubility

Binary interaction coefficients between brine and N_2 at reservoir temperature (130 °F), limited range of reservoir pressure (2,000–2,400 psi), and at a brine salinity of 110,000 ppm were tuned to match experimental data for N_2 solubility in the brine (Sun et al., 2001). At reservoir temperature, a pressure of 2,000 psi, and the earlier mentioned brine salinity, N_2 solubility is 5.94×10^{-4} mole fraction. If reservoir pressure is increased to 2,300 psi, N_2 solubility will increase to 6.8×10^{-4} mole fraction. BIC value between N_2 and brine was determined to be -0.465, which can

model experimental solubility data accurately. Figure 31 shows the plot of BIC versus N_2 solubility at aforementioned conditions. These points are in fact all trial and error points to determine the correct BIC value, considering available experimental data.

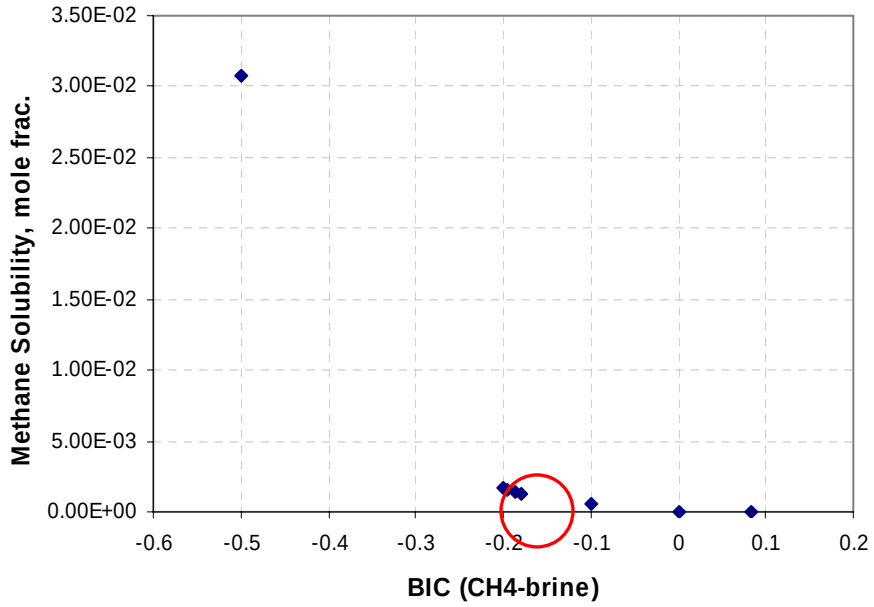

Figure 30. CH_4 solubility data versus binary interaction coefficients between CH_4 and brine and final trial and error values inside the circle.

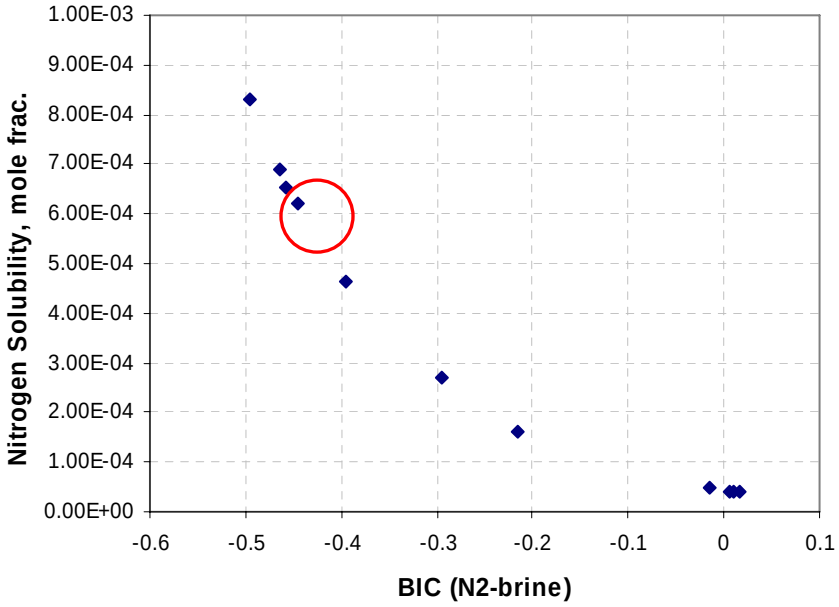

Figure 31. N_2 solubility data versus binary interaction coefficients between N_2 and brine and final trial and error values inside the circle.

V-2. Brine and Gas-Mixture Density

V-2-1 CO_2 Saturated-Brine Density

Kumar et al. (2004) tuned Volume Shift Parameter (VSP) for H_2O as a component (brine) to match CO_2-saturated brine density with the experimental data. He presented a correlation between VSP of brine, temperature, and brine salinity, which was used to determine the VSP of H_2O in our study.

Because of the presence of other gases in the model and because experimental data for brine density saturated with a mixture of CO_2, CH_4, and N_2 are not available, VSP for CO_2, CH_4 and N_2 was tuned to match experimental single gas-phase densities, and it was assumed that these correct VSP values would provide accurate density values for brine saturated with this mixture. Following are steps taken to model the density data using PR-EOS.

V-2-2 CH_4 Density

Table 8 shows CH_4 density at reservoir temperature and different reservoir pressure obtained from Setzmann and Wagner (1991), reported in the National Institute of Standards and Technology (NIST) web book. CH_4 VSP was tuned to match these data. Final VSP value for CH_4 was determined at -0.194004 to provide an accurate range of gas density.

Table 8. Experimental data for CH_4 density at T=130°F and different pressure values.

Temperature (°F)	Pressure (psi)	Density (lbm/ft^3)
130	1,900	5.426
130	2,100	6.0238
130	2,300	6.6123
130	2,500	7.1882

(1 lbm/ft^3 = 16 kg/m^3)

V-2-3 N2 Density

Table 9 shows N_2 density at reservoir temperature and different reservoir pressure obtained from Span et al. (2000), reported in the National Institute of Standards and Technology (NIST) web book. N_2 VSP was tuned to match these data. Final VSP value for N_2 was determined at -0.17587.

Table 9. Experimental data for N_2 density at T=130°F and different pressure values.

Temperature (°F)	Pressure (psi)	Density (lbm/ft^3)
130	1,900	8.1478
130	2,100	8.9456
130	2,300	9.7273
130	2,500	10.492

(1 lbm/ft^3 = 16 kg/m^3)

V-2-4 CO_2 Density

Table 10 shows CO_2 density at reservoir temperature and different reservoir pressure obtained from Span and Wagner (1996), reported in the National Institute of Standards and Technology (NIST) web book. CO_2 VSP was tuned to match these data. Final VSP value for CO_2 was determined at 0.024668 to provide accurate range of gas density.

Table 10. Experimental data for CO_2 density at T=130°F and different pressure values.

Temperature (°F)	Pressure (psi)	Density (lbm/ft^3)
130	1,900	36.462
130	2,100	40.087
130	2,300	42.595
130	2,500	44.498

(1 lbm/ft^3 = 16 kg/m^3)

V-3. Brine and Gas-Mixture Viscosity

By running several simulations, we performed brine viscosity calibration against experimental data. According to experimental data (Zaytsev and Aseyev, 1992) for temperature, pressure, and salinity similar to those in our aquifer, brine viscosity is 0.51 cp. Using the Pedersen et al. (1984) correlation for different fluids' viscosity, we found Pedersen's coefficients, as well as critical volumes for different components for which viscosity values in the simulation and experimental data matched. These coefficients and EOS parameters were then used as simulation input data. Table 11 shows viscosity values for three gases (N_2, CH_4, and CO_2) at reservoir temperature and different reservoir pressure obtained from different sources reported in the National Institute of Standards and Technology (NIST) web book. Final viscosity coefficients for viscosity calculations are: 0.291, 1.4, 0.0005747, 4.265, and 1.0579.

Table 11. Experimental viscosity data for all three gases at T=130 °F and different pressure values.

Temperature (°F)	Pressure (psi)	CO_2 viscosity (cp)	N_2 viscosity (cp)	CH_4 viscosity (cp)
130	1,900	0.0439	0.02163	0.01539
130	2,100	0.0498	0.02197	0.01593
130	2,300	0.0545	0.02232	0.01650
130	2,500	0.0584	0.02268	0.017100

V-4. Ternary Diagrams

To better grasp the range of variations in fluid density and viscosity, we extracted data from the PVT model at pressures of 2,250 and 2,500 psi and temperature of 135°F (Table 12 and Table 13). Data extracted using CMG-Winprop software are consistent with data used in simulation runs. In addition, for better visualization, we prepared ternary diagrams of solubility (Figure 32), brine density (Figure 33), gas-phase density (Figure 34), gas-phase viscosity (Figure 35), gas-phase density and viscosity ratio (Figure 36), and ratio of gas- and aqueous-phase density difference to gas-phase viscosity (Figure 37). Note that, unlike the ternary diagrams included in the main text, the six ternary diagrams presented in this appendix plot data for 100% of each of the three components. CO_2 is approximately 10 times more soluble than CH_4 and N_2 on a mole fraction basis (Figure 32), but brine density varies little (Figure 33). Single-component CO_2 gas-phase density is about two-thirds that of the brine, whereas single-component CH_4 and N_2 gas-phase density is smaller by factors of about 6 and 4, respectively. Figure 37 suggests that the driving force for CO_2 is approximately one order of magnitude less than that of CH_4 and N_2 for single-component gas phase. At the injection composition (at least 75% CO_2), the contrast is less but still of approximately a factor of 3. Figure 38 illustrates that a CO_2-N_2 mixture (CO_2 >75%) has initially a stronger buoyancy driving force than that of a CO_2-CH_4 mixture, but that as the

gas is progressively depleted from CO_2 by differential dissolution, the CO_2-CH_4 mixture (CO_2 <25%) becomes more buoyant.

Table 12. PVT data table extracted from CMG-WinProp (user-specified input), 2,500 psi, and 135°F.

Mole Fraction (%)			Gas phase		Aqueous phase		Solubility in aqueous phase (mole %)		
			Density	Viscosity	Density	Viscosity			
CO_2	CH_4	N_2	lb/ft^3	cp	lb/ft^3	cp	CO_2	CH_4	N_2
100	**0**	**0**	**41.19**	**0.0714**	**62.45**	**0.500**	**1.7102**	**0**	**0**
95	0	5	36.61	0.0582	62.42	0.499	1.6295	0	0.0077
95	2.5	2.5	36.79	0.0608	62.42	0.499	1.6283	0.0050	0.0039
95	5	0	36.98	0.0634	62.42	0.499	1.6274	0.0100	0
80	0	20	26.15	0.0360	62.36	0.496	1.4304	0	0.0224
80	10	10	26.52	0.0397	62.35	0.495	1.4178	0.0159	0.0117
80	20	0	26.99	0.0450	62.34	0.495	1.4085	0.0324	0
75	0	25	23.82	0.0331	62.34	0.495	1.3666	0	0.0261
75	12.5	12.5	24.10	0.0362	62.33	0.494	1.3505	0.0189	0.0137
75	25	0	24.51	0.0410	62.31	0.494	1.3385	0.0385	0
60	0	40	18.94	0.0289	62.28	0.491	1.1608	0	0.03657
60	20	20	18.80	0.0307	62.26	0.490	1.1378	0.02749	0.01905
60	40	0	18.85	0.0338	62.24	0.490	1.1211	0.05551	0
50	0	50	16.73	0.0276	62.23	0.488	1.0074	0	0.0433
50	25	25	16.29	0.0288	62.21	0.488	0.9827	0.0331	0.0225
50	50	0	16.05	0.0309	62.18	0.487	0.9654	0.0664	0
40	0	60	14.99	0.0266	62.18	0.485	0.8396	0	0.0501
40	20	40	14.50	0.0270	62.16	0.485	0.8224	0.0260	0.0341
40	40	20	14.08	0.0276	62.14	0.484	0.8087	0.0515	0.0176
40	60	0	13.74	0.0286	62.12	0.484	0.7989	0.0773	0
25	0	75	12.93	0.0255	62.10	0.481	0.5582	0	0.0606
25	25	50	12.19	0.0254	62.07	0.480	0.5440	0.0319	0.0410
25	50	25	11.51	0.0253	62.05	0.480	0.5332	0.0628	0.0211
25	75	0	10.88	0.0253	62.03	0.479	0.5263	0.0938	0
20	0	80	12.35	0.0252	62.06	0.479	0.4559	0	0.0641
20	20	60	11.73	0.0249	62.05	0.478	0.4464	0.0256	0.0485
20	40	40	11.14	0.0246	62.03	0.478	0.4385	0.0504	0.0329
20	60	20	10.58	0.0243	62.01	0.478	0.4326	0.0748	0.0169
20	80	0	10.04	0.0241	62.00	0.477	0.4287	0.0994	0
12.5	12.5	75	11.14	0.0243	62.00	0.476	0.2900	0.0161	0.0598
12.5	75	12.5	9.23	0.0225	61.96	0.475	0.2766	0.0927	0.0106
10	10	80	10.97	0.0241	61.99	0.475	0.2351	0.0130	0.0636
10	80	10	8.79	0.0217	61.94	0.474	0.2231	0.0986	0.0085
2.5	2.5	95	10.51	0.0237	61.94	0.472	0.0612	0.0033	0.0751
2.5	95	2.5	7.49	0.0185	61.87	0.471	0.0572	0.1166	0.0021
0	**0**	**100**	**10.37**	**0.0236**	**61.92**	**0.471**	**0**	**0**	**0.0790**
0	5	95	10.20	0.0234	61.92	0.471	0	0.0066	0.0751

Mole Fraction (%)			Gas phase		Aqueous phase		Solubility in aqueous phase (mole %)		
			Density	Viscosity	Density	Viscosity			
CO_2	CH_4	N_2	lb/ft^3	cp	lb/ft^3	cp	CO_2	CH_4	N_2
0	20	80	9.70	0.0227	61.91	0.470	0	0.0258	0.0634
0	25	75	9.53	0.0225	61.91	0.470	0	0.0321	0.0595
0	40	60	9.04	0.0218	61.89	0.470	0	0.0505	0.0480
0	50	50	8.71	0.0212	61.89	0.470	0	0.0626	0.0402
0	60	40	8.38	0.0206	61.88	0.470	0	0.0746	0.0325
0	75	25	7.89	0.0196	61.87	0.470	0	0.0925	0.0207
0	80	20	7.72	0.0192	61.87	0.470	0	0.0985	0.0166
0	95	5	7.23	0.0177	61.86	0.470	0	0.1166	0.0043
0	**100**	**0**	**7.06**	**0.0172**	**61.85**	**0.470**	**0**	**0.1227**	**0**

Table 13. PVT data table extracted from CMG-WinProp (user-specified input), 2,250 psi, and 135°F.

Mole Fraction (%)			Gas Phase		Aqueous phase		Solubility in aqueous phase (mole %)		
			Density	Viscosity	Density	Viscosity			
CO_2	CH_4	N_2	lb/ft^3	cp	lb/ft^3	cp	CO_2	CH_4	N_2
100	**0**	**0**	**38.16**	**0.0648**	**62.39**	**0.498**	**1.6755**	**0**	**0**
95	0	5	33.23	0.0512	62.37	0.497	1.5969	0	0.0068
95	2.5	2.5	33.50	0.0538	62.36	0.497	1.5956	0.0045	0.0035
95	5	0	33.77	0.0565	62.36	0.497	1.5946	0.0091	0
80	0	20	23.18	0.0322	62.31	0.493	1.4001	0	0.0198
80	10	10	23.55	0.0349	62.30	0.493	1.3884	0.0145	0.0103
80	20	0	24.05	0.0391	62.28	0.493	1.3794	0.0295	0
75	0	25	21.14	0.0302	62.29	0.492	1.3352	0	0.0232
75	12.5	12.5	21.39	0.0324	62.27	0.492	1.3207	0.0173	0.0121
75	25	0	21.80	0.0360	62.26	0.491	1.3095	0.0352	0
60	0	40	16.93	0.0273	62.22	0.489	1.1266	0	0.033
60	20	20	16.76	0.0285	62.20	0.488	1.1066	0.02538	0.01712
60	40	0	16.79	0.0306	62.18	0.488	1.0919	0.05119	0
50	0	50	15.02	0.0263	62.18	0.486	0.9733	0	0.0393
50	25	25	14.59	0.0271	62.15	0.485	0.9518	0.0307	0.0203
50	50	0	14.34	0.0285	62.13	0.485	0.9369	0.0615	0
40	0	60	13.50	0.0256	62.13	0.483	0.8075	0	0.0457
40	20	40	13.04	0.0258	62.11	0.483	0.7926	0.0241	0.0310
40	40	20	12.64	0.0261	62.09	0.482	0.7808	0.0479	0.0159
40	60	0	12.31	0.0267	62.08	0.482	0.7725	0.0718	0
25	0	75	11.69	0.0247	62.04	0.479	0.5335	0	0.0553
25	25	50	11.01	0.0245	62.02	0.478	0.5212	0.0297	0.0374
25	50	25	10.37	0.0242	62.00	0.478	0.5120	0.0585	0.0192
25	75	0	9.78	0.0239	61.98	0.477	0.5061	0.0874	0
20	0	80	11.18	0.0245	62.01	0.477	0.4349	0	0.0586
20	20	60	10.61	0.0241	62.00	0.476	0.4266	0.0238	0.0443
20	40	40	10.06	0.0237	61.98	0.476	0.4199	0.0469	0.0300

Mole Fraction (%)			Gas Phase		Aqueous phase		Solubility in aqueous phase (mole %)		
			Density	Viscosity	Density	Viscosity			
CO_2	CH_4	N_2	lb/ft^3	cp	lb/ft^3	cp	CO_2	CH_4	N_2
20	60	20	9.54	0.0233	61.97	0.476	0.4148	0.0697	0.0154
20	80	0	9.03	0.0228	61.95	0.475	0.4115	0.0927	0
12.5	12.5	75	10.10	0.0237	61.96	0.474	0.2762	0.0150	0.0547
12.5	75	12.5	8.32	0.0215	61.91	0.473	0.2646	0.0864	0.0096
10	10	80	9.95	0.0235	61.94	0.473	0.2236	0.0120	0.0582
10	80	10	7.93	0.0208	61.89	0.472	0.2133	0.0920	0.0077
2.5	2.5	95	9.55	0.0232	61.90	0.470	0.0580	0.0031	0.0688
2.5	95	2.5	6.76	0.0178	61.83	0.469	0.0546	0.1088	0.0020
0	**0**	**100**	**9.43**	**0.0231**	**61.88**	**0.469**	**0**	**0**	**0.0723**
0	5	95	9.27	0.0228	61.88	0.469	0	0.0061	0.0687
0	20	80	8.81	0.0222	61.87	0.469	0	0.0240	0.0580
0	25	75	8.65	0.0220	61.86	0.469	0	0.0298	0.0545
0	40	60	8.20	0.0212	61.85	0.469	0	0.0470	0.0439
0	50	50	7.89	0.0206	61.85	0.469	0	0.0583	0.0368
0	60	40	7.59	0.0200	61.84	0.468	0	0.0696	0.0297
0	75	25	7.14	0.0189	61.83	0.468	0	0.0863	0.0188
0	80	20	6.98	0.0185	61.83	0.468	0	0.0919	0.0152
0	95	5	6.53	0.0170	61.82	0.468	0	0.1088	0.0039
0	**100**	**0**	**6.37**	**0.0165**	**61.81**	**0.468**	**0**	**0.1145**	**0**

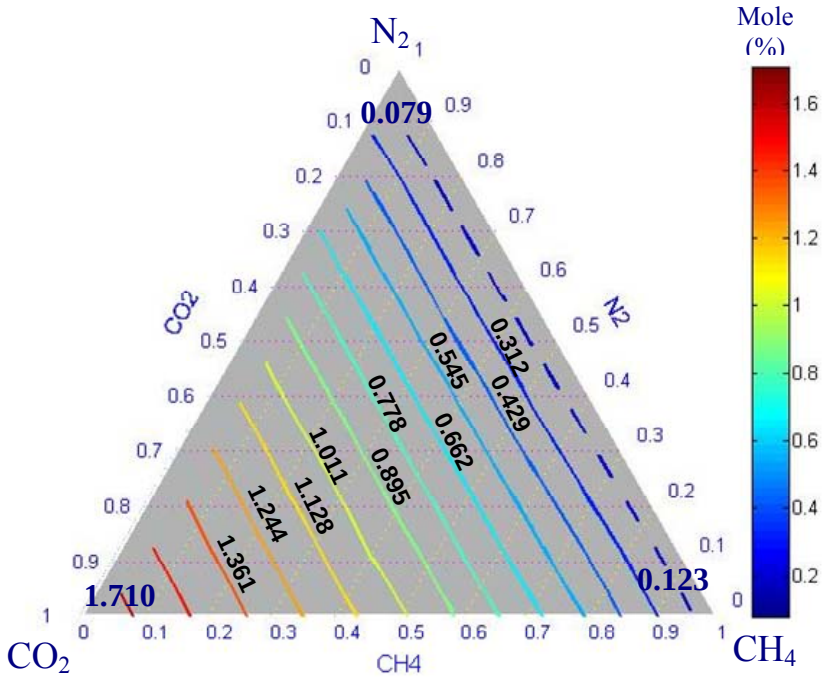

Figure 32. Solubility of all gas components (mole percent), 2,500 psi, and 135°F.

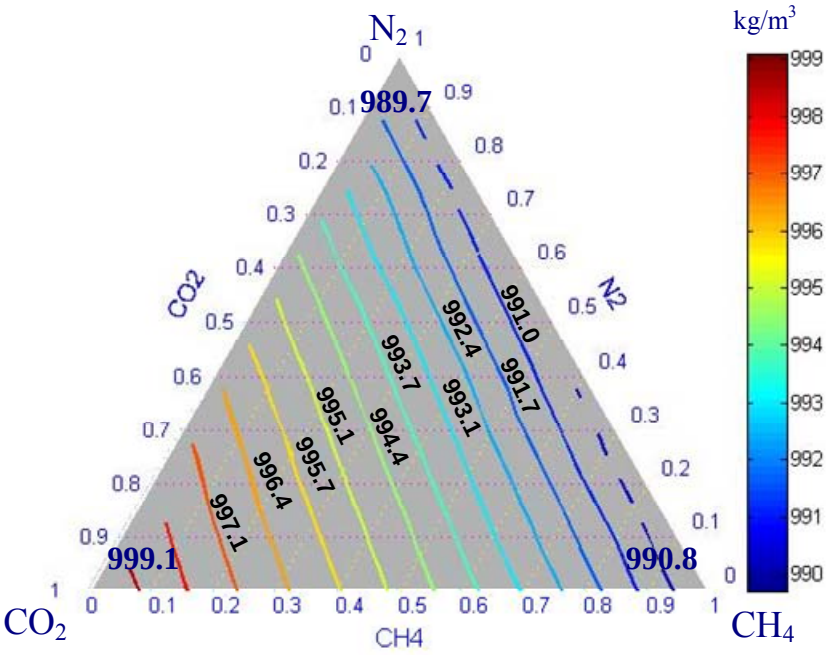

Figure 33. Brine density, ρ_b (kg/m^3), 2,500 psi, and 135°F.

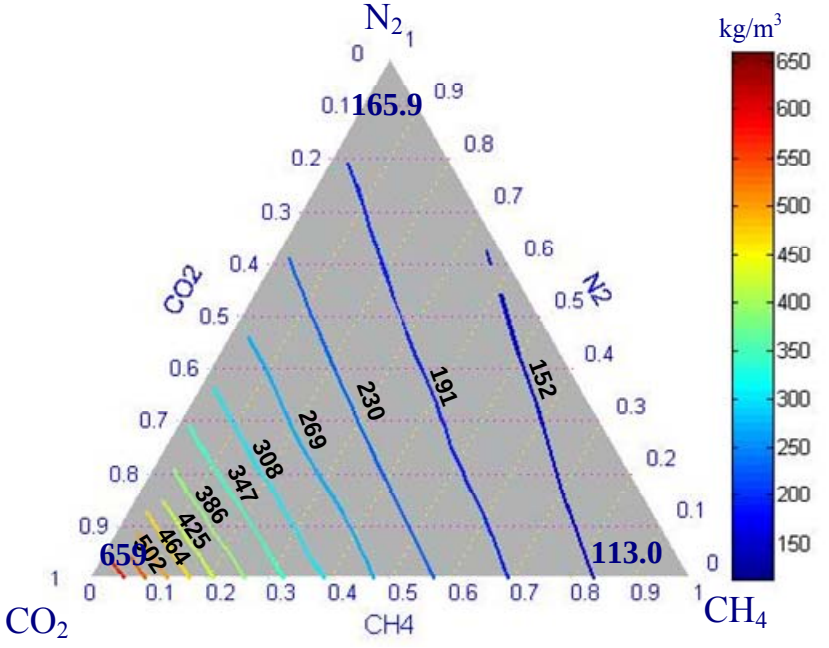

Figure 34. Gas-phase density, ρ_g (kg/m^3), 2,500 psi, and 135°F.

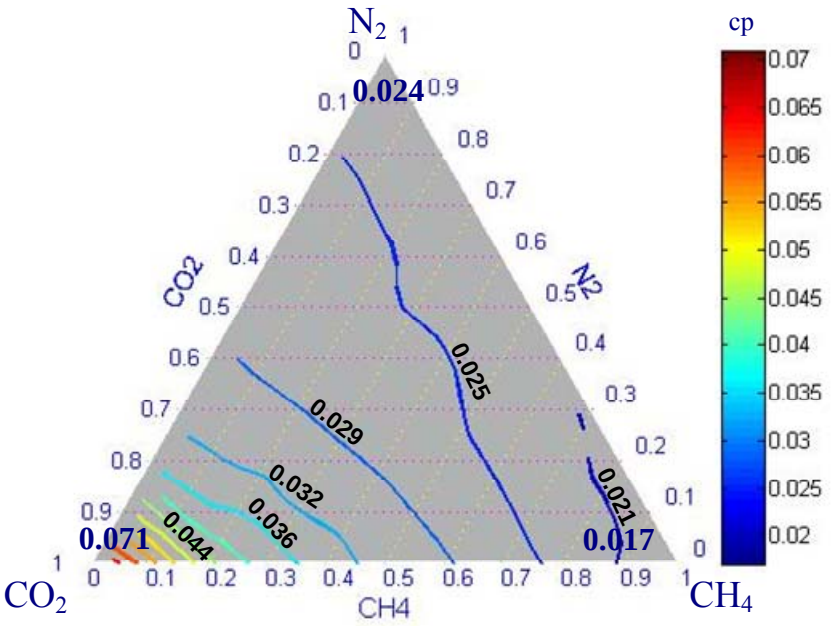

Figure 35. Gas-phase viscosity, μ_g (cp), 2,500 psi, and 135°F.

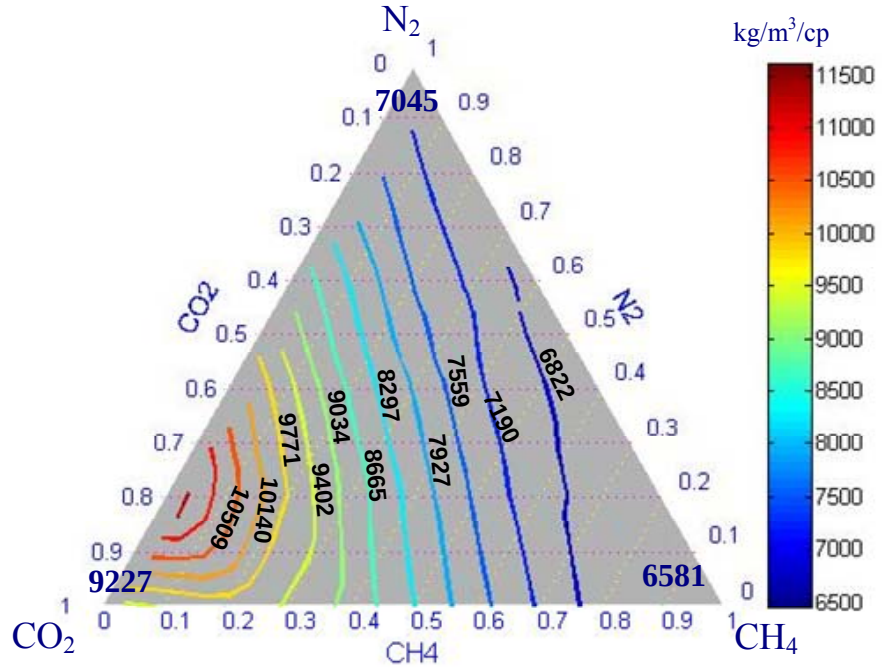

Figure 36. Gas-phase density–viscosity ratio, ρ_g / μ_g (kg/m^3/cp), 2,500 psi, and 135°F.

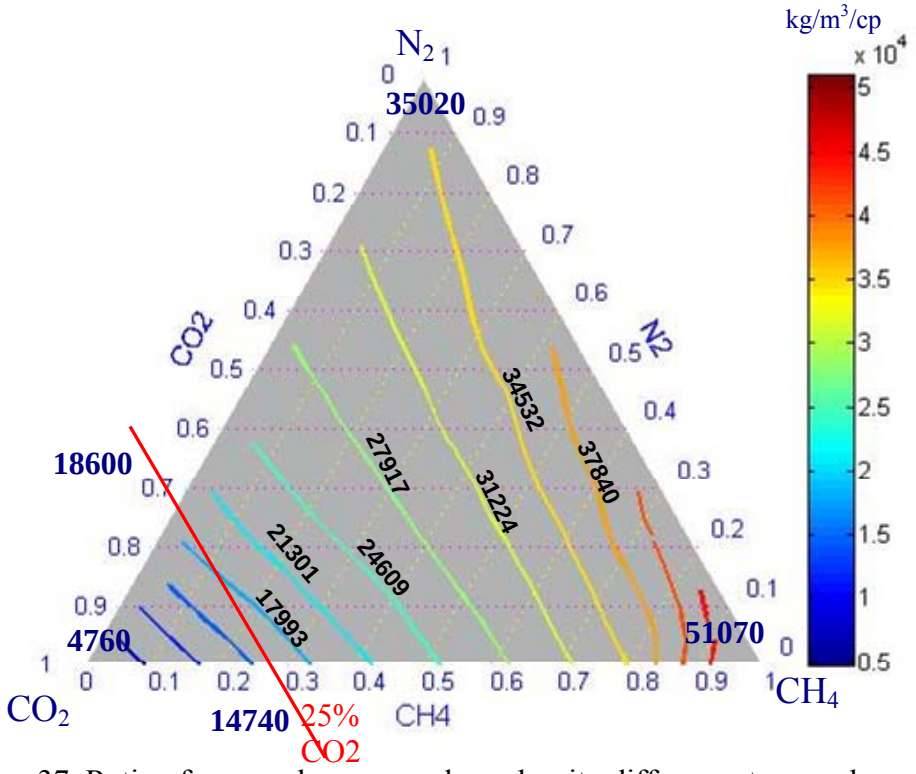

Figure 37. Ratio of gas- and aqueous-phase density difference to gas-phase viscosity (buoyant driving force), $(\rho_b - \rho_g)/\mu_g$ (kg/m^3/cp), 2,500 psi, and 135°F.

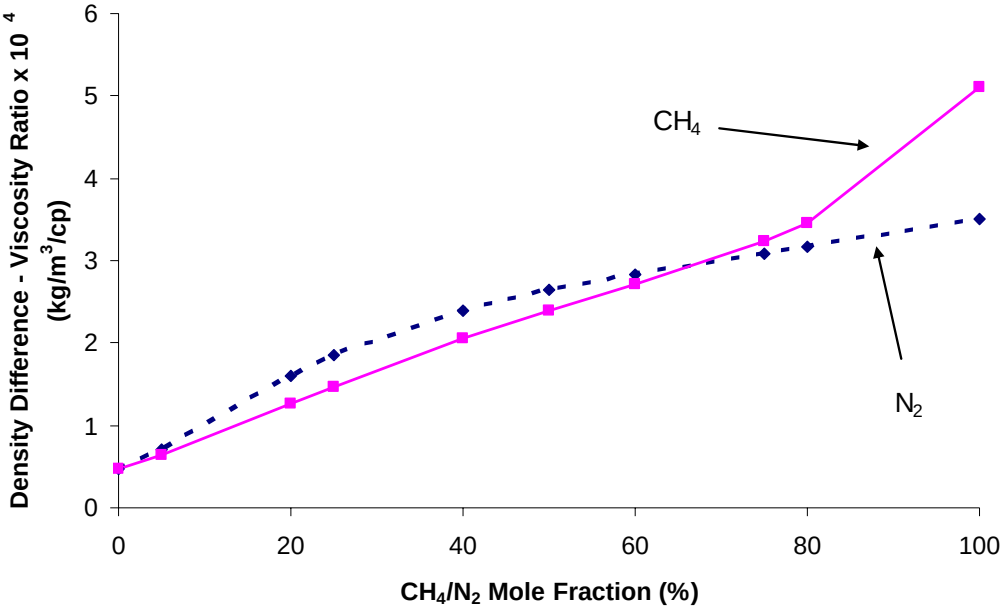

Figure 38. Comparison of buoyancy pull for a CO_2 stream with variable amounts of either CH_4 and N_2 or 2500 psi and 135°F.

VI. Appendix B: GEM Input Files

VI-1. Generic Case

This is Case 16 of Table 3

```
** FILE: Aquifer120-51-20-BaseCase6.dat **
** **
** MODEL: 120-51-20 CARTESIAN GRID CO2 Storage Gas Mixture **
** FIELD UNITS **
** **
**---------------------------------------------------------------------**

** ---------------------------------------------------------------------**
** I/O CONTROL DATA
** ---------------------------------------------------------------------**
RESULTS SIMULATOR GEM 200710
*INUNIT *FIELD
*DIM MDJCS 200
*INTERRUPT *INTERACTIVE
*XDR *ON
*MAXERROR 20
*WPRN *WELL *TIME
*WPRN *GRID *TIME
*WPRN *ITER *NONE
*WSRF *WELL *TIME
*WSRF *GRID *TIME
*DIARY *CHANGES
*RANGECHECK ON

*OUTPRN *RES *ALL
*OUTPRN *GRID
*POROS
*KRG
*SG
*RHOG
*Y 'CO2'
*Y 'CH4'
*Y 'N2'
*SO
*RHOO
*X 'CO2'
*X 'CH4'
*X 'N2'

*OUTSRF *WELL *PSPLIT
*OUTSRF *GRID DENG RHOG MWG FRG SG
                DENO RHOO PCG PCW SO DENW SW KRG VISG
 MWO KRO VISO PRES KRW
                K 'CO2' Z 'CO2' Y 'CO2' X 'CO2'
 K 'H2O' Z 'H2O' Y 'H2O' X 'H2O'
 K 'CH4' Z 'CH4' Y 'CH4' X 'CH4'
 K 'N2' Z 'N2' Y 'N2' X 'N2'
*OUTSRF *RES *ALL

**---------------------------------------------------------------------**
** RESERVOIR DATA
**---------------------------------------------------------------------**

*GRID *CART 120 51 20
*KDIR *DOWN

*DEPTH *TOP 1 1 1 5500.0
*DIP 2 0

*DI *CON 300.0
*DJ *CON 300.0
```

```
*DK *CON 50.0
**$ Property: NULL Blocks Max: 1 Min: 1
**$ 0 = null block, 1 = active block
*NULL CON 1
*IJK
16:116 1:51 16 0
16:116 1:51 12 0
16:116 1:51 8 0
16:116 1:51 4 0

*POR *CON 0.25
*PERMI *CON 300
*PERMJ EQUALSI
*PERMK EQUALSI * 0.01
PINCHOUTARRAY CON 1

*CPOR 5.0E-06
*PRPOR 14.7

**----------------------------------------------------------------------**
** FLUID COMPONENT DATA
**----------------------------------------------------------------------**
*MODEL *PR
*NC 4 4
*COMPNAME 'CO2' 'H2O' 'CH4'    'N2'
*HCFLAG 0 0 0 0
*VISCOR *PEDERSEN
*VISCOEFF 0.291
 1.4
 0.0005747
 4.265
 1.0579
*MIXVC 1
*TRES 135
*PCRIT 72.809000 217.75460 45.400000  33.5000
*TCRIT 304.12780 647.09440 190.60000  126.200
*AC 0.223940 0.344000 0.008000        0.04000
*VCRIT 0.094000 0.056000 0.099000     0.08950
*MW 44.01000 18.01500 16.04300        28.013
*PCHOR 78.00000 52.00000 77.00000     41.0000
*SG 0.818000 1.000000 0.300000        0.80900
*VISVC 0.094000 0.056000 0.099000     0.08950
*VSHIFT 0.024668 0.233645 -0.194004   -0.17587
*OMEGA 0.457235530 0.457235530 0.457235530 0.457235530
*OMEGB 0.077796074 0.077796074 0.077796074 0.077796074
*BIN
 -0.0603
 0.1     -0.1804
 -0.017  -0.465         0.0311

*PHASEID *DEN

**----------------------------------------------------------------------**
** ROCK FLUID
**----------------------------------------------------------------------**

*ROCKFLUID
RPT 1 DRAINAGE SCALING-OLD
*SWT
** Not used
0       0               1               **290
0.05    1E-10           0.95            **105.044278
0.1     0.00000001      0.86            **50.89774296
0.15    0.000001        0.76            **32.84889794
0.2     0.0001          0.65            **23.82447543
0.25    0.002923977     0.5265          **18.40982192
0.3     0.016391711     0.416           **14.80005292
0.35    0.044319935     0.3185          **12.22164649
0.4     0.088235294     0.234           **10.28784166
0.45    0.147653281     0.1625          **8.783771243
0.5     0.220387362     0.104           **7.580514909
```

```
0.55    0.303070525    0.0585         **6.596032453
0.6     0.391805812    0.026          **5.775630407
0.65    0.482781457    0.0065         **5.08144406
0.7     0.572718844    0.001          **4.486427191
0.75    0.659104078    0.0001         **3.970745905
0.8     0.740228803    0.00001        **3.519524779
0.85    0.815104022    0.000001       **3.121388492
0.9     0.88331325     0.0000001      **2.76748957
0.95    0.94485456     0.00000001     **2.450843166
1       1              0              **2.165861402

*SLT
** water/gas
**Sw    krg krw        Pc
0               1              0              **221.2336384
0.05            0.894160584    0.0000002      **107.9838121
0.1             0.788321168    0.000005       **52.70673921
0.137           0.71           0.00005        **31
0.190938        0.604208       0.000561       **14.3
0.244875        0.508485       0.003645       **7.76
0.298813        0.42249        0.010892       **5.02
0.35275         0.345869       0.023683       **3.8
0.406688        0.278253       0.043261       **3
0.460625        0.21926        0.070776       **2.8
0.514563        0.168486       0.10731        **2.35
0.5685          0.125512       0.153893       **2.28
0.622438        0.089888       0.21151        **2.16
0.676375        0.061142       0.28111        **2.01
0.730313        0.03876        0.36361        **1.91
0.78425         0.022188       0.459902       **1.86
0.838188        0.010808       0.570851       **1.75
0.892125        0.003922       0.697303       **1.69
0.946063        0.000693       0.840084       **1.54
1               0              1              **1.4

*HYSKRG 0.300


**------------------------------------------------------------------------**
** INITIAL CONDITIONS
**------------------------------------------------------------------------**
INITIAL
** Set up brine aquifer
[Under *VERTICAL *DEPTH_AVE *WATER_OIL, the water-oil contact depth (*DWOC), together with a
reference pressure (*REFPRES) at a reference depth (*REFDEPTH) must be specified. One composition
vector (entered under *ZOIL), representing the averaged reservoir fluid composition, is required.
This composition is assigned to all grid blocks. This option is used for undersaturated oil
reservoirs in which the added accuracy in initial amounts in place made possible by the depth
averaging is wanted.]

*VERTICAL *DEPTH_AVE *WATER_OIL
*NREGIONS 1
*ZOIL 0. 1. 0. 0.
*REFDEPTH 5500 **FT
*REFPRES 2557.5 **PSI
*DWOC 4264 **FT

**------------------------------------------------------------------------**
** NUMERICAL METHODS CONTROL
**------------------------------------------------------------------------**

*NUMERICAL
*DTMAX 1
*DTMIN 1.E-06
*NORM *PRESS 2000
*MAXCHANGE *GMOLAR 0.2
*MAXCHANGE *SATUR 0.2
*AIM *STAB 1
*CONVERGE *PRESS 0.15
*MAXSTEPS 1000000
```

```
**------------------------------------------------------------------------**
** WELL DATA
**------------------------------------------------------------------------**

*RUN
*DATE 2000 1 1
 *DTWELL 1.0

 *WELL 1 'INJ'
 *INJECTOR 1
** 'CO2' 'H2O' 'CH4' 'N2'
 INCOMP SOLVENT 1.00 0.0 0.0 0.0
 *OPERATE *MAX *STG 2.603E+7  CONT
 *GEOMETRY *K 0.5 0.37 1. 0.
 *PERF *GEO 1
 12 26 14:20 1 OPEN

 *WELL  2      'w1'
 *INJECTOR 2
 INCOMP SOLVENT 0. 1 0. 0.
 *OPERATE *MAX *STG 0.0E+3    CONT
 GEOMETRY      K       40      0.35    1       0
 PERF   GEO     'w1'
 **1     1:25   1       1       OPEN
 1       1:51   1       1       OPEN

 *WELL  3      'w2'
 *INJECTOR 3
 INCOMP SOLVENT 0. 1 0. 0.
 *OPERATE *MAX *STG 0.0E+3    CONT
 GEOMETRY      K       40      0.35    1       0
 PERF   GEO     'w2'
 **1     1:25   5       1       OPEN
 1       1:51   5       1       OPEN

 *WELL  4      'w3'
 *INJECTOR 4
 INCOMP SOLVENT 0. 1 0. 0.
 *OPERATE *MAX *STG 0.0E+3    CONT
 GEOMETRY      K       40      0.35    1       0
 PERF   GEO     'w3'
 **1     1:25   10      1       OPEN
 1       1:51   10      1       OPEN

 *WELL  5      'w4'
 *INJECTOR 5
 INCOMP SOLVENT 0. 1 0. 0.
 *OPERATE *MAX *STG 0.0E+3    CONT
 GEOMETRY      K       40      0.35    1       0
 PERF   GEO     'w4'
 **1     1:25   15      1       OPEN
 1       1:51   15      1       OPEN

 *WELL  6      'w5'
 *INJECTOR 6
 INCOMP SOLVENT 0. 1 0. 0.
 *OPERATE *MAX *STG 0.0E+3    CONT
 GEOMETRY      K       40      0.35    1       0
 PERF   GEO     'w5'
 **1     1:25   20      1       OPEN
 1       1:51   20      1       OPEN

 *WELL  7      'Prod1'
 *PRODUCER     'Prod1'
 OPERATE       MIN     BHP     2003.0  CONT
 GEOMETRY      K       40      0.35    1       0
 PERF   GEO     'Prod1'
 **60    1:25   1       1       OPEN
 120     1:51   1       1       OPEN

 *WELL  8      'Prod2'
```

```
 *PRODUCER     'Prod2'
 OPERATE       MIN     BHP     2093.6  CONT
 GEOMETRY      K       40      0.35    1       0
 PERF   GEO    'Prod2'
 **60    1:25  5       1       OPEN
 120     1:51  5       1       OPEN

 *WELL  9      'Prod3'
 *PRODUCER     'Prod3'
 OPERATE       MIN     BHP     2206.9  CONT
 GEOMETRY      K       40      0.35    1       0
 PERF   GEO    'Prod3'
 **60    1:25  10      1       OPEN
 120     1:51  10      1       OPEN

 *WELL  10     'Prod4'
 *PRODUCER     'Prod4'
 OPERATE       MIN     BHP     2320.2  CONT
 GEOMETRY      K       40      0.35    1       0
 PERF   GEO    'Prod4'
 **60    1:25  15      1       OPEN
 120     1:51  15      1       OPEN

 *WELL  11     'Prod5'
 *PRODUCER     'Prod5'
 OPERATE       MIN     BHP     2433.5  CONT
 GEOMETRY      K       40      0.35    1       0
 PERF   GEO    'Prod5'
 **60    1:25  20      1       OPEN
 120     1:51  20      1       OPEN



*OPEN 1
*OPEN 2
*OPEN 3
*OPEN 4
*OPEN 5
*OPEN 6
*OPEN 7
*OPEN 8
*OPEN 9
*OPEN 10
*OPEN 11

TIME    1
TIME    10

*DTMAX 100

TIME    100
TIME    200
TIME    365
TIME    500
TIME    750
TIME    1000
TIME    1250
TIME    1500
TIME    1750
TIME    2000
TIME    2500
TIME    3653
TIME    4000
TIME    5000
TIME    6000
TIME    7305
TIME    9131
TIME    10958

*SHUTIN 1
```

```
*DTMAX 200

TIME    12784
TIME    14610
TIME    16436
TIME    18263
TIME    21915

*DTMAX 1000

TIME    25568
TIME    29220
TIME    32873
TIME    36525
TIME    45656
TIME    54788
TIME    73050

*DTMAX 3000

TIME    146100
TIME    182625
TIME    292200
TIME    365243


*STOP
```

VI-2. Gulf Coast Brine Case

Input consists of 1 main input files and 6 “include” files

Main input file

```
** Revised data received from BEG in Sept.
** Added the real location of monitoring well
** Included first shale layer above the reservoir
** Horizontal K revised according new correlation between Phi and K=6E6*Phi^7.5054
** T and P updated so all tuning have been done
** New Pc and Rel. Perm models inserted (7 Rock Type)
** Kv/Kh=1
** 2008-02-14, 1:46:19 PM, yousef
** 2008-05-05              Jong-Won Choi
**********************************************************************************************
RESULTS SIMULATOR GEM 200600

** ----------------------------------------------------------------**
** I/O CONTROL DATA
** ----------------------------------------------------------------**
*INUNIT *FIELD
DIM   MDJCS   200
*INTERRUPT *INTERACTIVE
*XDR *ON
*MAXERROR  20
*WPRN *WELL  *TIME
*WPRN *GRID  *TIME
*WPRN *ITER  *NONE
*WSRF *WELL *TIME
*WSRF *GRID *TIME
*DIARY *CHANGES
RANGECHECK ON

*OUTPRN *RES *ALL
*OUTPRN *GRID
*POROS
*KRG
*SG
*RHOG
```

```
*Y 'CO2'
*Y 'CH4'
*Y 'N2'
*SO
*RHOO
*X 'CO2'
*X 'CH4'
*X 'N2'

*OUTSRF *WELL  *PSPLIT
*OUTSRF *GRID DENG RHOG MWG FRG SG
                 DENO RHOO PCG PCW SO DENW SW KRG VISG
              MWO KRO VISO PRES KRW
                 K 'CO2' Z 'CO2' Y 'CO2' X 'CO2'
              K 'H2O' Z 'H2O' Y 'H2O' X 'H2O'
              K 'CH4' Z 'CH4' Y 'CH4' X 'CH4'
              K 'N2'  Z 'N2'  Y 'N2'  X 'N2'
*OUTSRF *RES *ALL

**----------------------------------------------------------------------**
** RESERVOIR DATA
**----------------------------------------------------------------------**
*INCLUDE 'New_Frio_Model_GRID.inc'
*INCLUDE 'New_Frio_Model_POR.inc'
*INCLUDE 'New_Frio_Model_PERMS.inc'
CPOR  MATRIX   10e-6
PRPOR MATRIX   14.7

**----------------------------------------------------------------------**
** FLUID COMPONENT DATA
**----------------------------------------------------------------------**

** FLUID COMPONENT DATA FROM GENERIC CASE
**
*MODEL        *PR
*NC           4   4
*COMPNAME     'CO2'          'H2O'         'CH4'           'N2'
*HCFLAG       0               0             0                   0
*VISCOR       *PEDERSEN
*VISCOEFF     0.291
              1.4
              0.0005747
              4.265
              1.0579
*MIXVC        1
*TRES          135
*PCRIT         72.809000    217.75460    45.400000       33.5000
*TCRIT         304.12780    647.09440    190.60000       126.200
*AC             0.223940    0.344000     0.008000        0.04000
*VCRIT          0.094000    0.056000     0.099000        0.08950
*MW             44.01000    18.01500     16.04300        28.013
*PCHOR          78.00000    52.00000     77.00000        41.0000
*SG             0.818000    1.000000     0.300000        0.80900
*VISVC          0.094000    0.056000     0.099000        0.08950
*VSHIFT         0.024668    0.233645     -0.194004       -0.17587
*OMEGA          0.457235530  0.457235530  0.457235530     0.457235530
*OMEGB          0.077796074  0.077796074  0.077796074     0.077796074
*BIN
**PVTSIM defaults
     -0.0603
      0.1           -0.1804
     -0.017         -0.465    0.0311

*PHASEID      *DEN

**----------------------------------------------------------------------**
** ROCK FLUID
**----------------------------------------------------------------------**
*ROCKFLUID
RPT 1 DRAINAGE SCALING-OLD
*SWT
```

```
0       0               1               790
0.05    1E-11           0.99            671.0894325
0.1     1E-10           0.98            325.1670446
0.15    0.000000001     0.965           209.859582
0.2     0.00000001      0.955           152.2058507
0.25    0.0000001       0.93            117.6136119
0.3     0.000001        0.9             94.55211935
0.35    0.00001         0.75            78.07962469
0.4     0.0001          0.55            65.7252537
0.45    0.001           0.4             56.11629848
0.5     0.007438417     0.2048          48.4291343
0.55    0.041128264     0.0864          42.13963634
0.6     0.108130899     0.0256          36.89838804
0.65    0.206313361     0.0032          32.46348563
0.7     0.326837256     0.0001          28.66214071
0.75    0.457947732     0.000001        25.36764178
0.8     0.588750003     0.00000001      22.48495521
0.85    0.711413919     1E-10           19.94140824
0.9     0.821582858     1E-12           17.6804776
0.95    0.917695358     1E-14           15.65753966
1       1               0               13.83689552

*SLT
0.91        0.01        0                1190
0.915625     0.00851    0.0005609       1060
0.92125     0.0071618   0.0036447       900
0.926875     0.0059506  0.0108919       751
0.9325      0.0048714   0.0236831       610
0.938125     0.0039191  0.0432609       490
0.94375     0.0030882   0.0707757       430
0.949375     0.002373   0.1073101       360
0.955       0.0017678   0.1538931       290
0.960625     0.001266   0.21151          250
0.96625     0.0008611   0.2811098       180
0.971875     0.0005459  0.3636104       145
0.9775      0.0003125   0.4599021       120
0.983125     0.0001522  0.5708514       98
0.98875     0.0000552   0.6973033       89
0.994375     0.0000098  0.8400835       83
1           0           1               80

*HYSKRG 0.04503
RPT 2 SCALING-OLD
*SWT
0       0               1               290
0.05    1E-10           0.95            105.044278
0.1     0.00000001      0.86            50.89774296
0.15    0.000001        0.76            32.84889794
0.2     0.0001          0.65            23.82447543
0.25    0.002923977     0.5265          18.40982192
0.3     0.016391711     0.416           14.80005292
0.35    0.044319935     0.3185          12.22164649
0.4     0.088235294     0.234           10.28784166
0.45    0.147653281     0.1625          8.783771243
0.5     0.220387362     0.104           7.580514909
0.55    0.303070525     0.0585          6.596032453
0.6     0.391805812     0.026           5.775630407
0.65    0.482781457     0.0065          5.08144406
0.7     0.572718844     0.001           4.486427191
0.75    0.659104078     0.0001          3.970745905
0.8     0.740228803     0.00001         3.519524779
0.85    0.815104022     0.000001        3.121388492
0.9     0.88331325      0.0000001       2.76748957
0.95    0.94485456      0.00000001      2.450843166
1       1               0               2.165861402

*SLT

0.137000  0.710000  0.000000  31.0
0.190938  0.604208  0.000561  14.3
0.244875  0.508485  0.003645  7.76
```

```
0.298813  0.422490  0.010892  5.02
0.352750  0.345869  0.023683  3.8
0.406688  0.278253  0.043261  3.0
0.460625  0.219260  0.070776  2.8
0.514563  0.168486  0.107310  2.35
0.568500  0.125512  0.153893  2.28
0.622438  0.089888  0.211510  2.16
0.676375  0.061142  0.281110  2.01
0.730313  0.038760  0.363610  1.91
0.784250  0.022188  0.459902  1.86
0.838188  0.010808  0.570851  1.75
0.892125  0.003922  0.697303  1.69
0.946063  0.000693  0.840084  1.54
1.000000  0.000000  1.000000  1.4

*HYSKRG 0.276

*KROIL *STONE2 *SWSG

*INCLUDE 'New_Frio_Model_ROCKARRAY.inc'

**---------------------------------------------------------------------**
** INITIAL CONDITIONS
**---------------------------------------------------------------------**
*INITIAL
*USER_INPUT
*INCLUDE 'New_Frio_Model_INITARRAYS_95_2_2.inc'

**---------------------------------------------------------------------**
** NUMERICAL METHODS CONTROL
**---------------------------------------------------------------------**
*NUMERICAL
*DTMAX 1.0
*DTMIN 1.E-06
*NORM *PRESS 2000
*MAXCHANGE *GMOLAR 0.2
*MAXCHANGE *SATUR 0.2
*AIM *STAB 1
*CONVERGE *PRESS 0.15

**---------------------------------------------------------------------**
** WELL DATA
**---------------------------------------------------------------------**
*INCLUDE 'New_Frio_Model_WELL_95_2_2.inc'
```

File 'New_Frio_Model_GRID.inc'

```
GRID CORNER 83 62 26
COORD
3429.819 8952.988 4610.684 3429.819 8952.988 4610.684
3500.602 8882.205 4610.684 3500.602 8882.205 4610.684
3571.386 8811.422 4610.684 3571.386 8811.422 4610.684
3642.169 8740.639 4610.684 3642.169 8740.639 4610.684
…….(data deleted – see DVD)
      4610.68    4610.68   4610.68    4610.68   4610.68    4610.68
      4610.68    4610.68   4610.68    4610.68   4610.68    4610.68
      4610.68    4610.68   4610.68    4610.68   4610.68    4610.68
      4610.68    4610.68   4610.68    4610.68
NULL
0
0
0
…….(data deleted – see DVD)
1
…….(data deleted – see DVD)
0
0
PINCHOUTARRAY ALL
 9*0 42*1 32*0 61*1 22*0 64*1 19*0 68*1 15*0 74*1 9*0 79*1 4*0 81*1 2*0 497*1 0 82*1 0
…….(data deleted – see DVD)
```

File 'New_Frio_Model_POR.inc'

```
POR
0
…….(data deleted – see DVD)
0
0.247903
0.178193
…….(data deleted – see DVD)
*MOD

   48:52       15:23       22:22    = 0.3315
   48:52       15:23       21:21    = 0.322
…….(data deleted – see DVD)
```

File 'New_Frio_Model_PERMS.inc'

```
PERMI
0
…….(data deleted – see DVD)
0
153.545
12.8833
…….(data deleted – see DVD)
PERMJ EQUALSI
PERMK EQUALSI * 0.1
*MOD
   48:52       15:23       15:15    = 614
   48:52       15:23       16:16    = 1403
…….(data deleted – see DVD)
```

File 'New_Frio_Model_ROCKARRAY.inc'

```
RTYPE ALL
1
…….(data deleted – see DVD)
2
…….(data deleted – see DVD)
1
1
*MOD
   48:52       15:23       15:15    = 2
   48:52       15:23       16:16    = 2
   48:52       15:23       17:17    = 2
…….(data deleted – see DVD)
```

File 'New_Frio_Model_INITARRAYS_95_2_2.inc'

```
**$ RESULTS PROP SW  Units: Dimensionless
**$ RESULTS PROP Minimum Value: 0  Maximum Value: 0
SW CON 0

**$ RESULTS PROP PRES  Units: psi
**$ RESULTS PROP Minimum Value: 2265  Maximum Value: 2265
PRES CON 2196.5

**$ RESULTS PROP ZGLOBALC 'CO2'  Units: Dimensionless
**$ RESULTS PROP Minimum Value: 0  Maximum Value: 0
ZGLOBALC 'CO2' CON 0

**$ RESULTS PROP ZGLOBALC 'H2O'  Units: Dimensionless
**$ RESULTS PROP Minimum Value: 1  Maximum Value: 1
ZGLOBALC 'H2O' CON 1.
ZGLOBALC 'CH4' CON 0.
ZGLOBALC 'N2'  CON 0.
```

File 'New_Frio_Model_WELL_95_2_2.inc'

```
RUN
DATE 2000 01 01
**$
WELL  'NewWell113'
PRODUCER       'NewWell113'
OPERATE MIN    BHP    2196.5  CONT
**$          rad  geofac  wfrac  skin
```

```
GEOMETRY  K  0.5  0.35  1.  0.
PERF  GEO  'NewWell113'
**$ UBA       ff  Status  Connection
    23 40 15  1.  OPEN    FLOW-TO  'SURFACE'  REFLAYER
    23 40 16  1.  OPEN    FLOW-TO  1
    23 40 17  1.  OPEN    FLOW-TO  2
    23 40 18  1.  OPEN    FLOW-TO  3
    23 40 19  1.  OPEN    FLOW-TO  4
    23 40 20  1.  OPEN    FLOW-TO  5
    23 40 21  1.  OPEN    FLOW-TO  6
    23 40 22  1.  OPEN    FLOW-TO  7
    23 40 23  1.  OPEN    FLOW-TO  8
    23 40 24  1.  OPEN    FLOW-TO  9
    23 40 25  1.  OPEN    FLOW-TO  10
    23 40 26  1.  OPEN    FLOW-TO  11
```

…….(data deleted – see DVD)

```
WELL  'InjectionWell'
INJECTOR       'InjectionWell'
**                    'CO2' 'H2O' 'CH4' 'N2'
      INCOMP  SOLVENT  0.95  0.0   0.025   0.025
OPERATE MAX     STG     3.0E+6  CONT
OPERATE MAX     BHP     3600    CONT
**$          rad  geofac  wfrac  skin
GEOMETRY  K  0.5  0.35  1.  0.
PERF  GEO  'InjectionWell'
**$ UBA               ff  Status  Connection
    35 29 26           1.  OPEN    FLOW-FROM  'SURFACE'  REFLAYER

OPEN 'InjectionWell'
TIME    1
TIME    10

*DTMAX 100

TIME    100
TIME    200
TIME    365
TIME    500
TIME    750
TIME    1000
TIME    1250

TIME    1826

*SHUTIN 'InjectionWell'

TIME    2500
TIME    3653
TIME    5000
TIME    6000
TIME    7305
TIME    9131
TIME    10958

*DTMAX 200

TIME    12784
```

…….(data deleted – see DVD)

```
TIME    292200
TIME    365243

STOP
```

VII. Appendix C: Figures for Generic Cases

1. Case 1: 95-5-0 (CO_2-CH_4-N_2) in volume

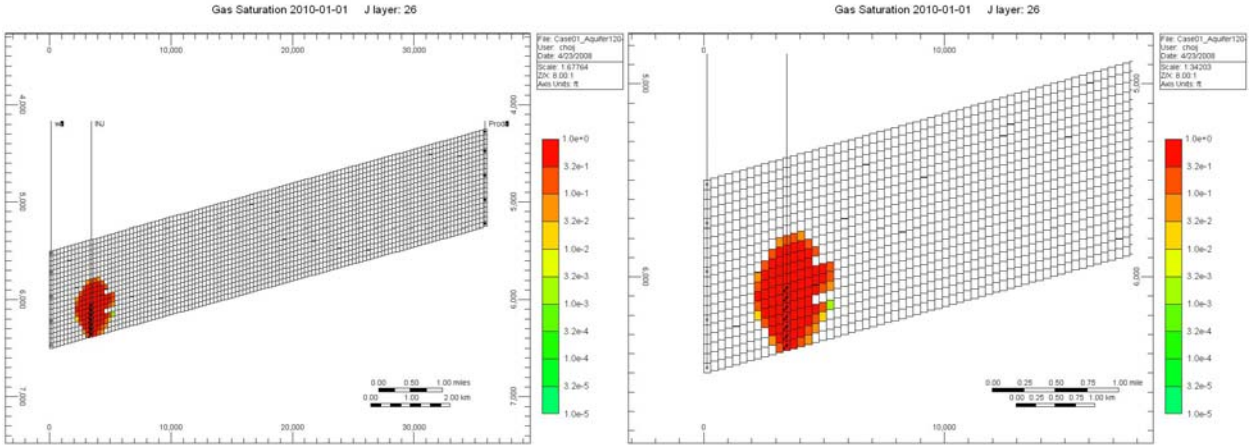

Time = 10 yr

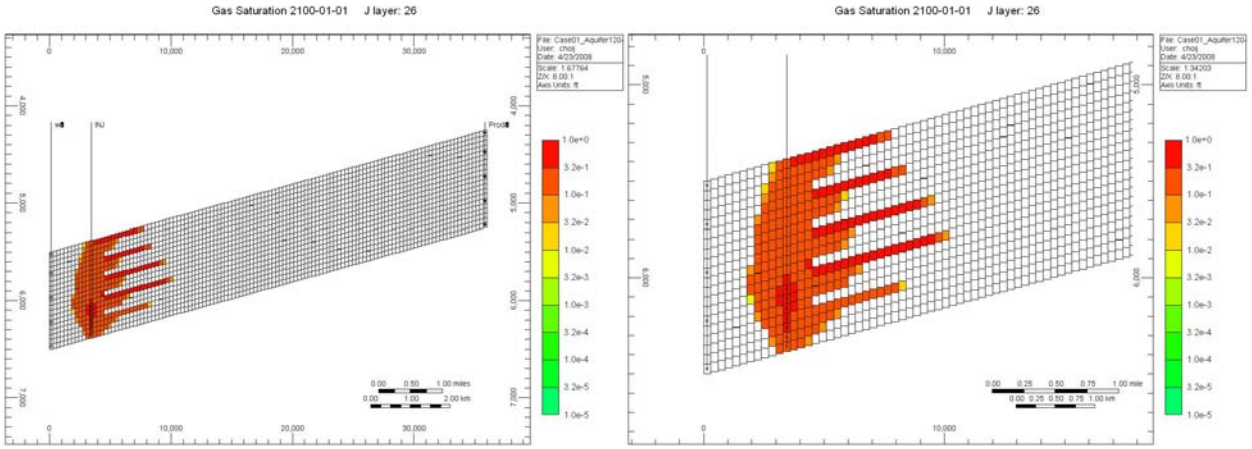

Time = 100 yr

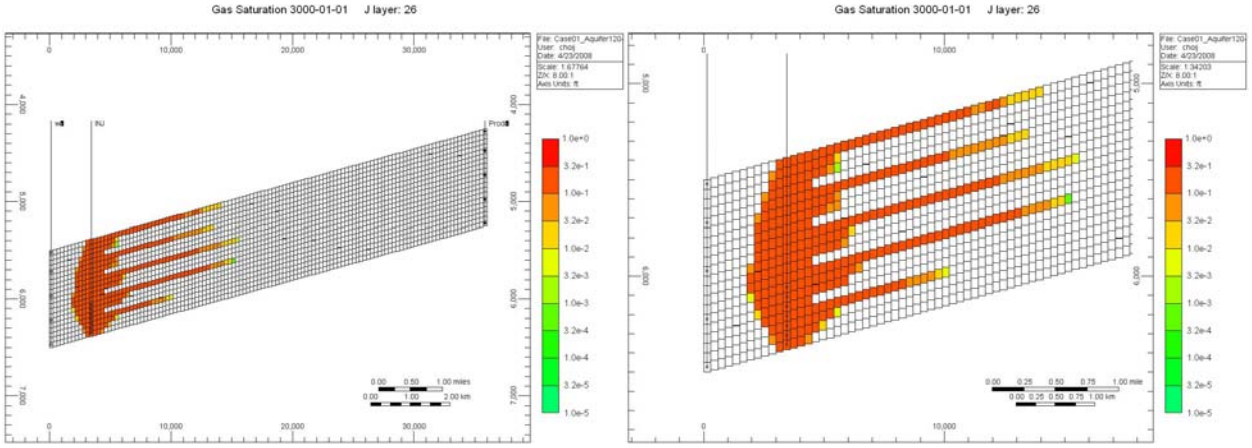

Time = 1,000 yr

2. Case 2: 95-0-5 (CO_2-CH_4-N_2) in volume

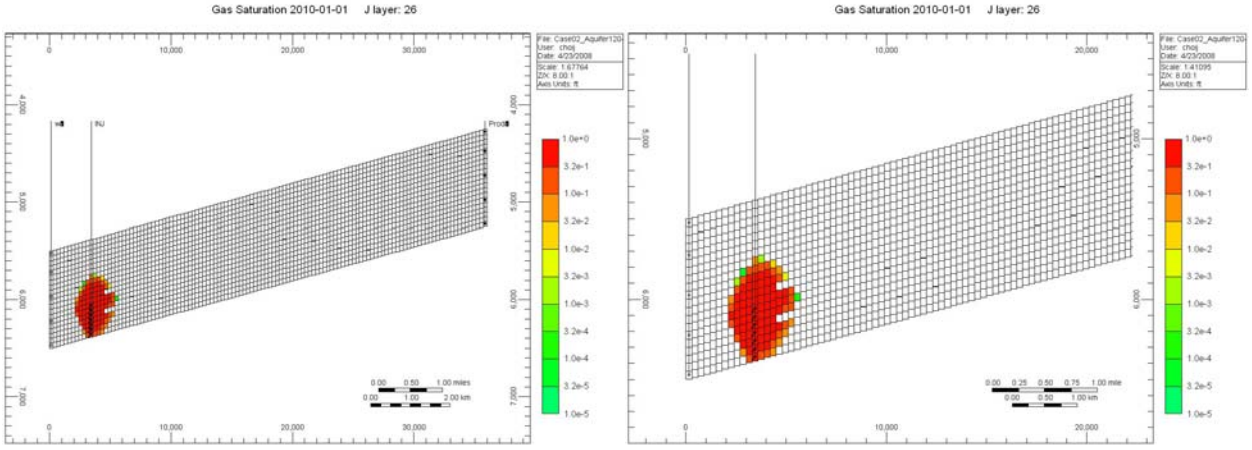

Time = 10 yr

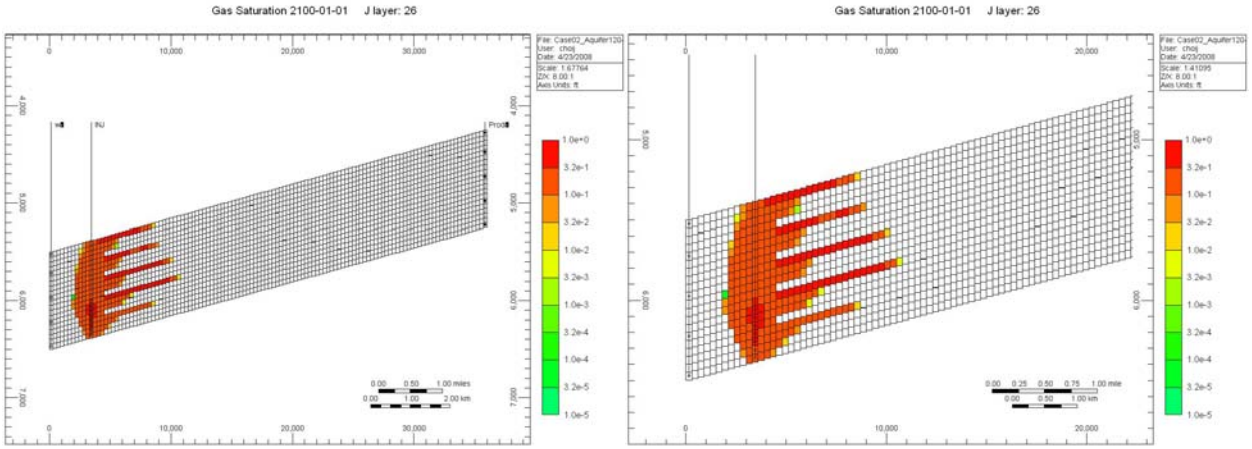

Time = 100 yr

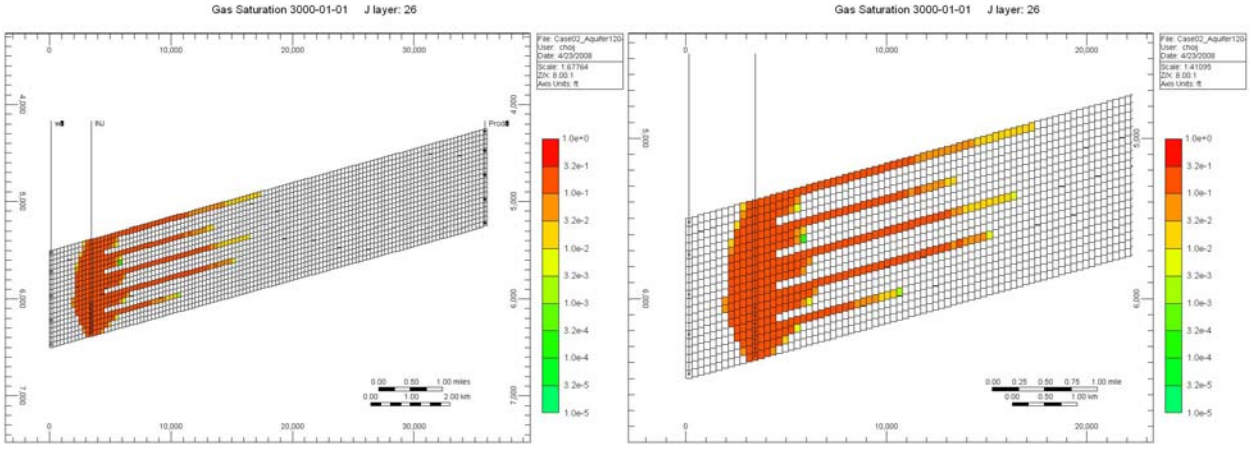

Time = 1,000 yr

3. Case 3: 95-2.5-2.5 (CO_2-CH_4-N_2) in volume

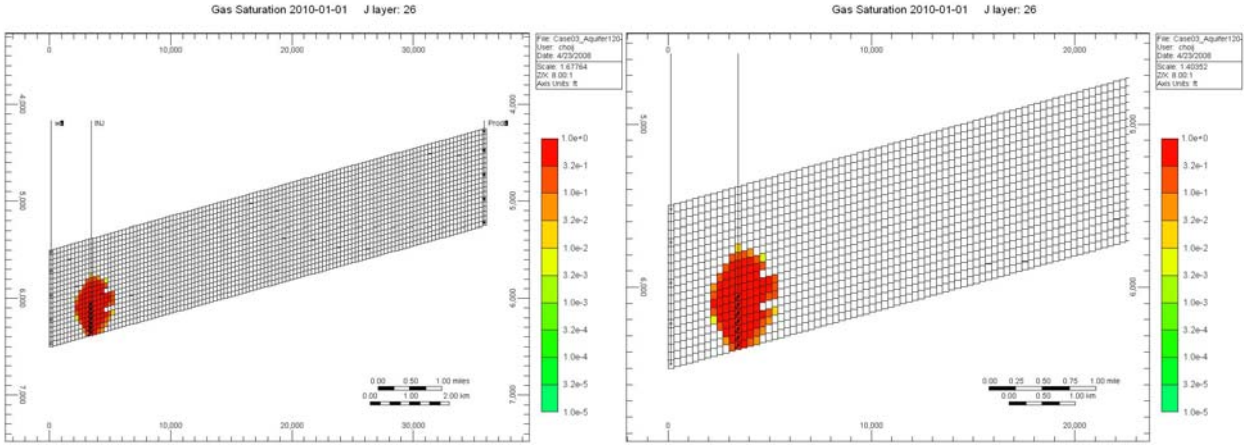

Time = 10 yr

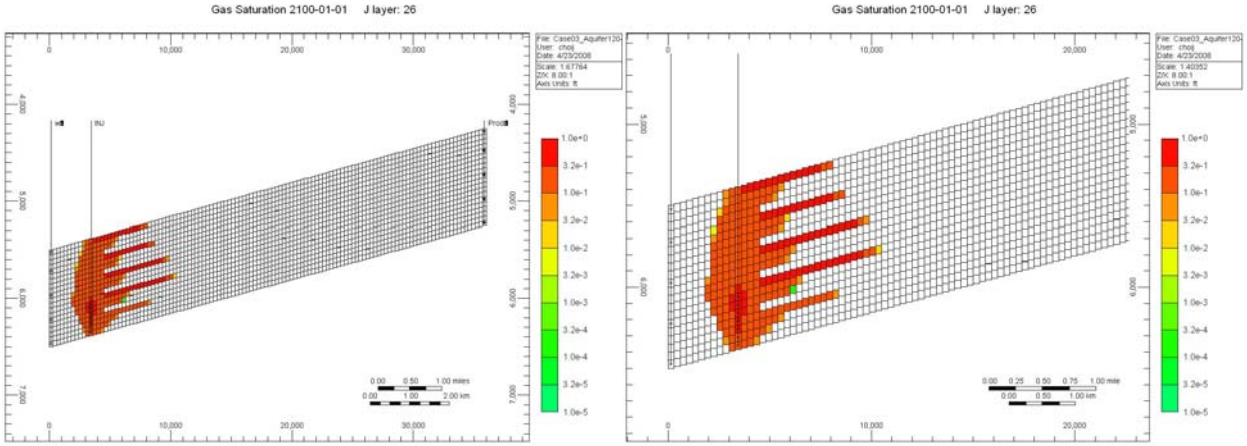

Time = 100 yr

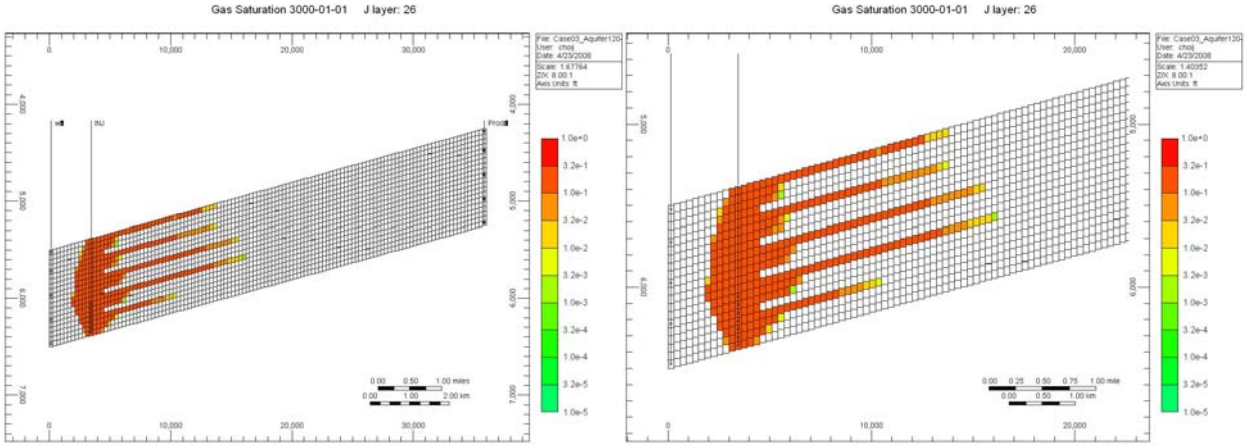

Time = 1,000 yr

4. Case 4: 90-10-0 (CO_2-CH_4-N_2) in volume

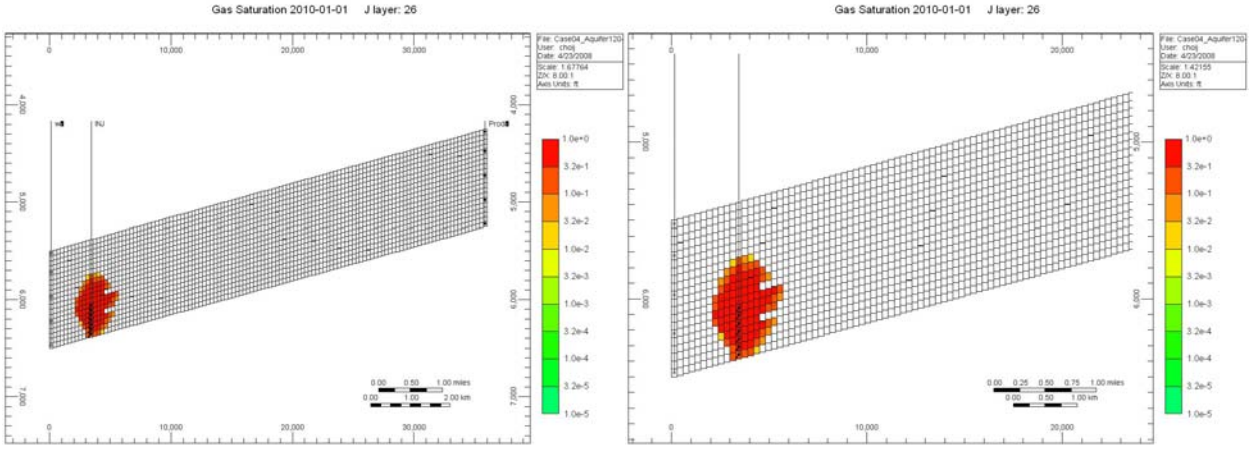

Time = 10 yr

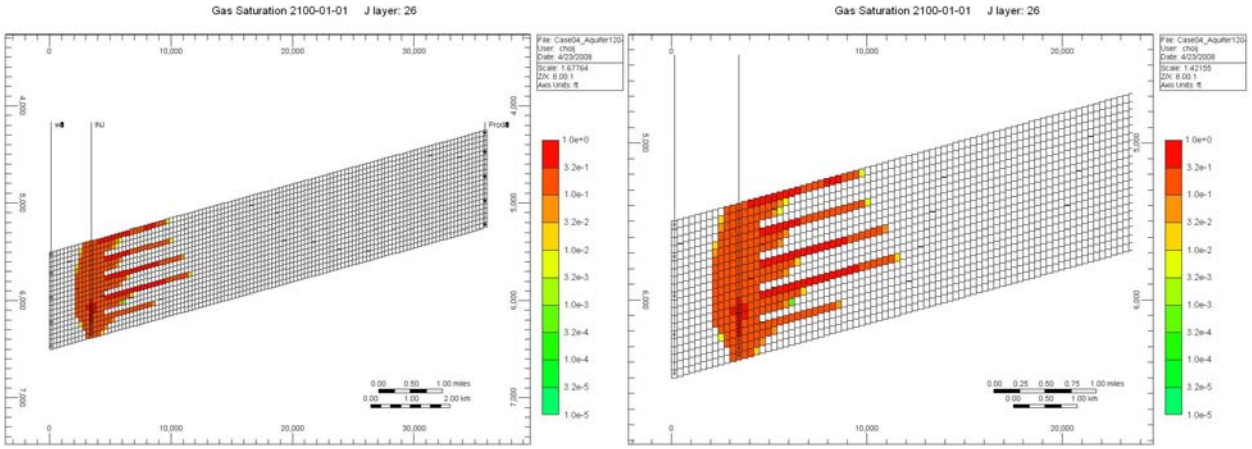

Time = 100 yr

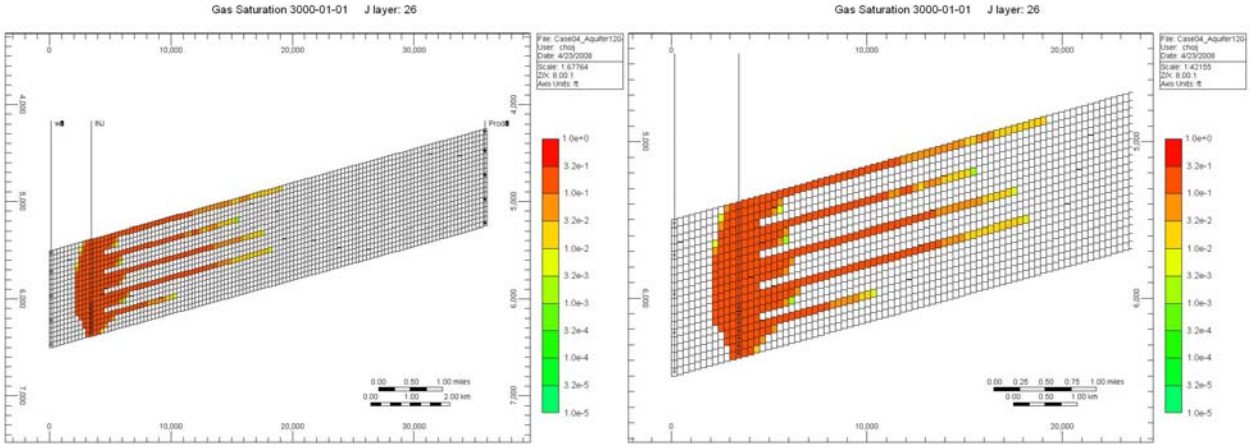

Time = 1,000 yr

5. Case 5: 90-0-10 (CO_2-CH_4-N_2) in volume

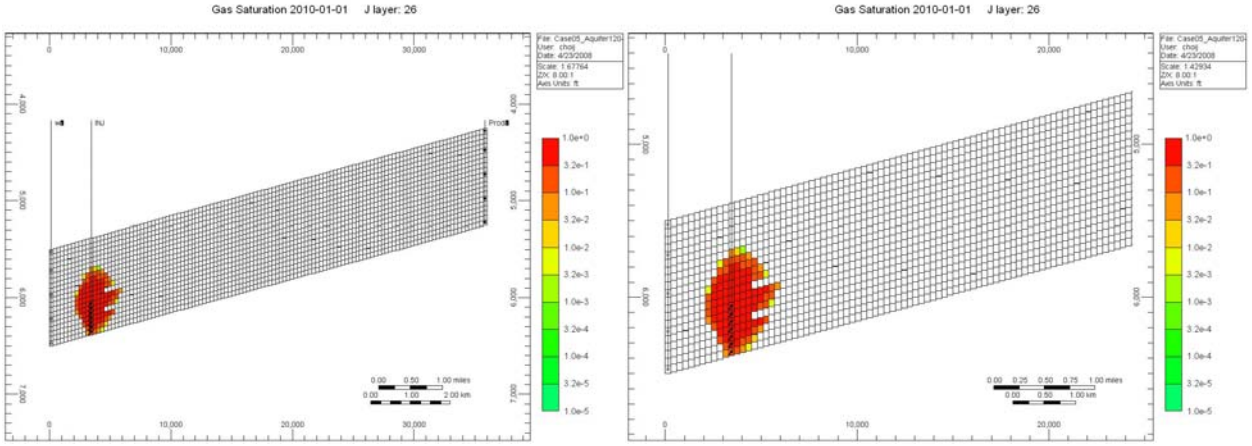

Time = 10 yr

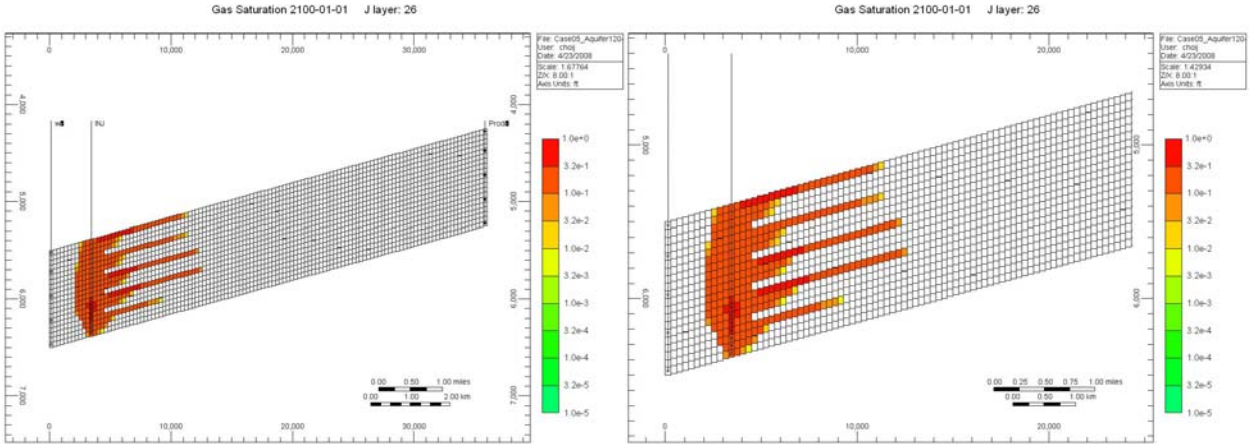

Time = 100 yr

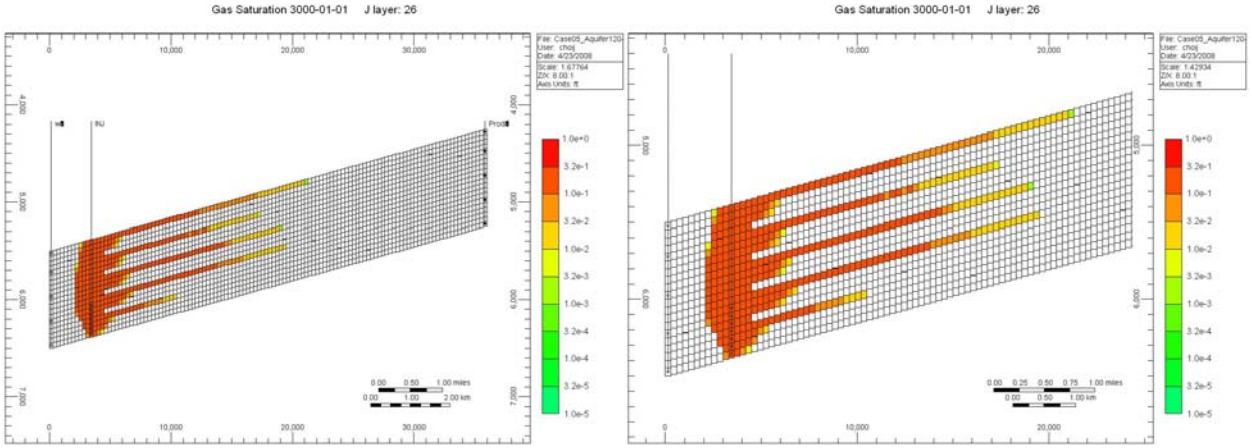

Time = 1,000 yr

6. Case 6: 90-5-5 (CO_2-CH_4-N_2) in volume

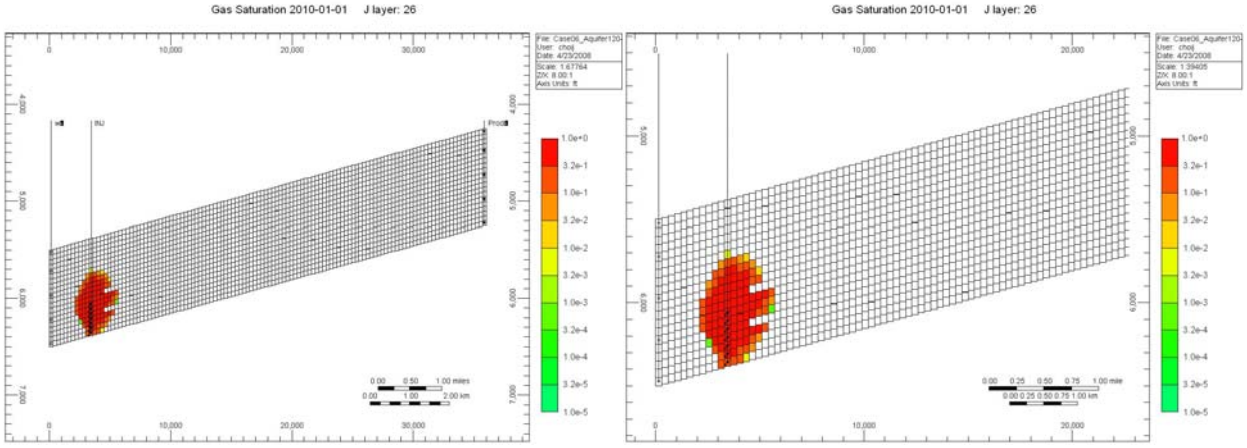

Time = 10 yr

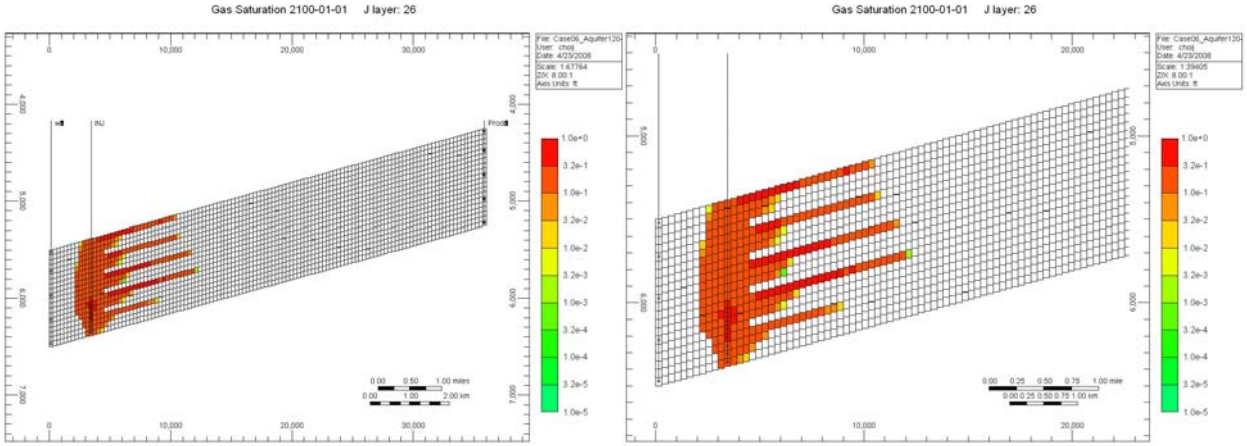

Time = 100 yr

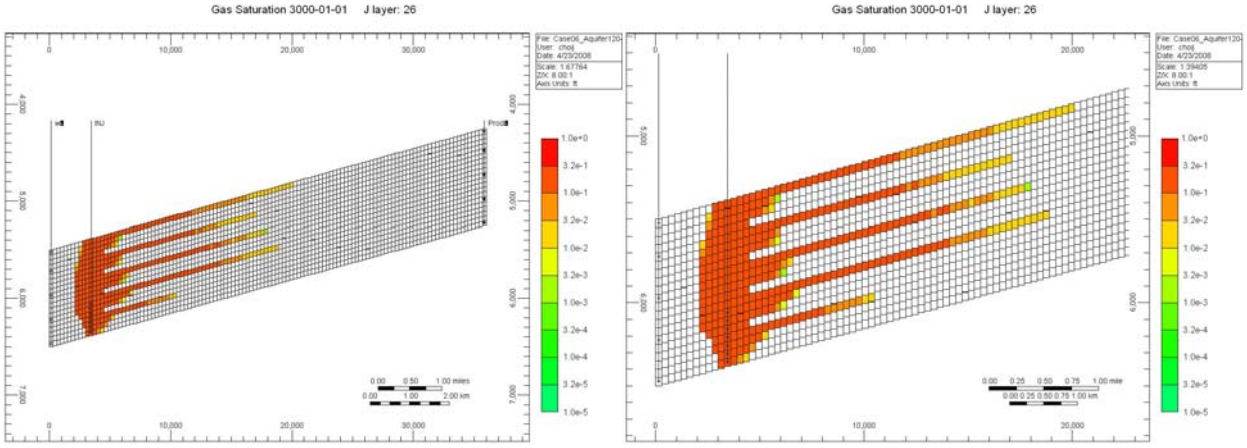

Time = 1,000 yr

7. Case 7: 85-15-0 (CO_2-CH_4-N_2) in volume

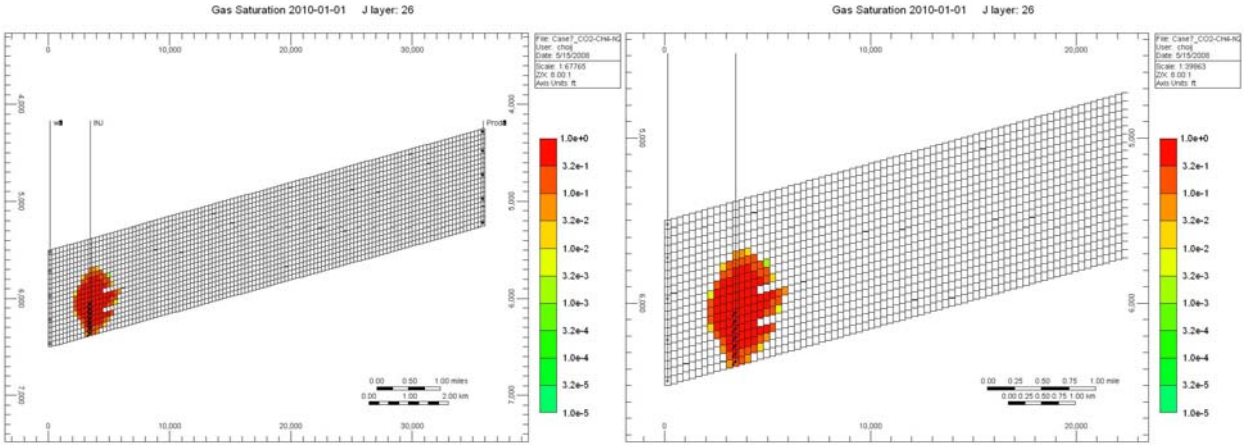

Time = 10 yr

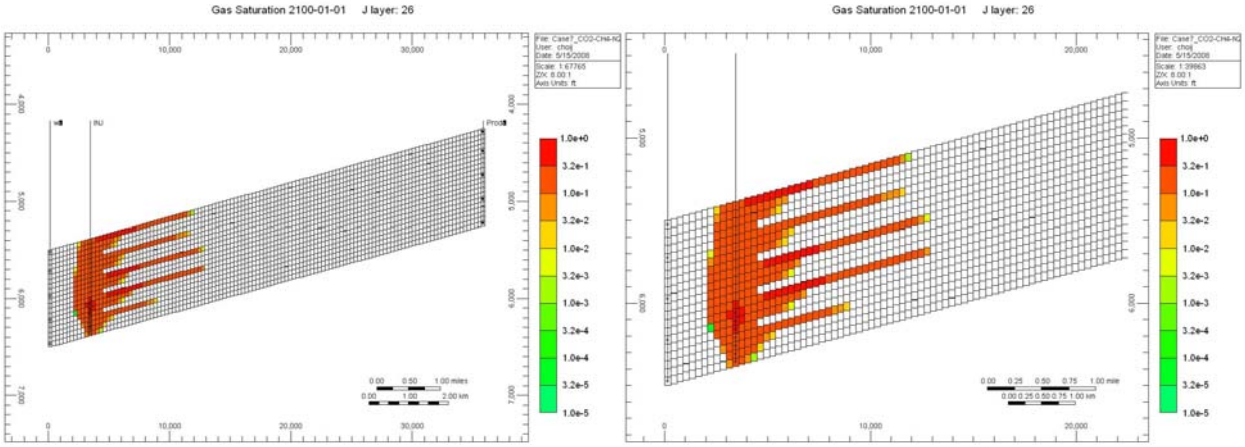

Time = 100 yr

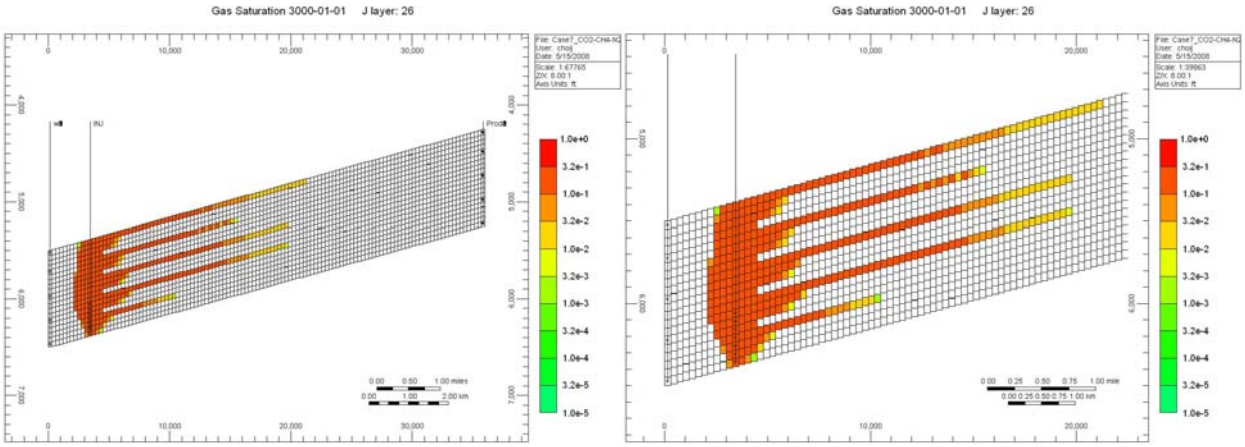

Time = 1,000 yr

8. Case 8: 85-0-15 (CO_2-CH_4-N_2) in volume

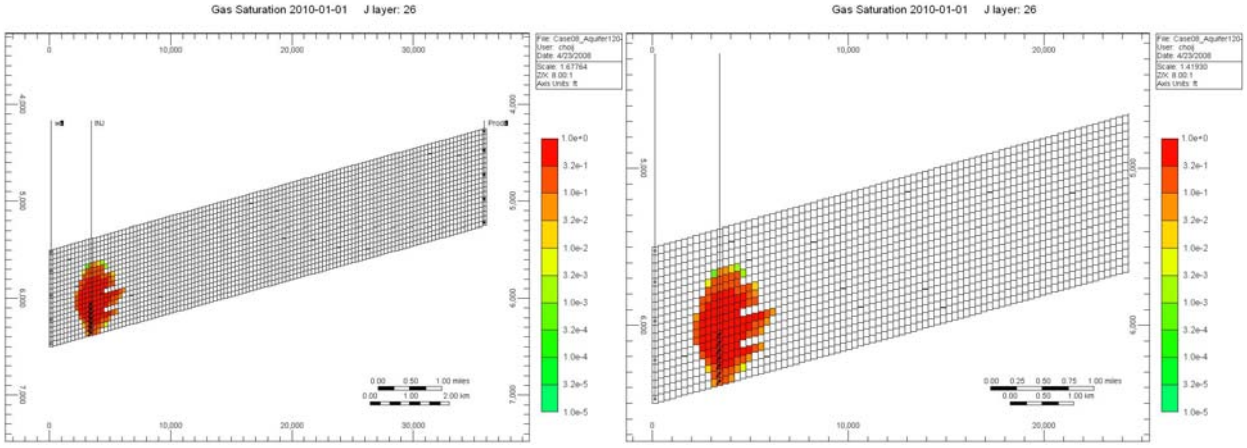

Time = 10 yr

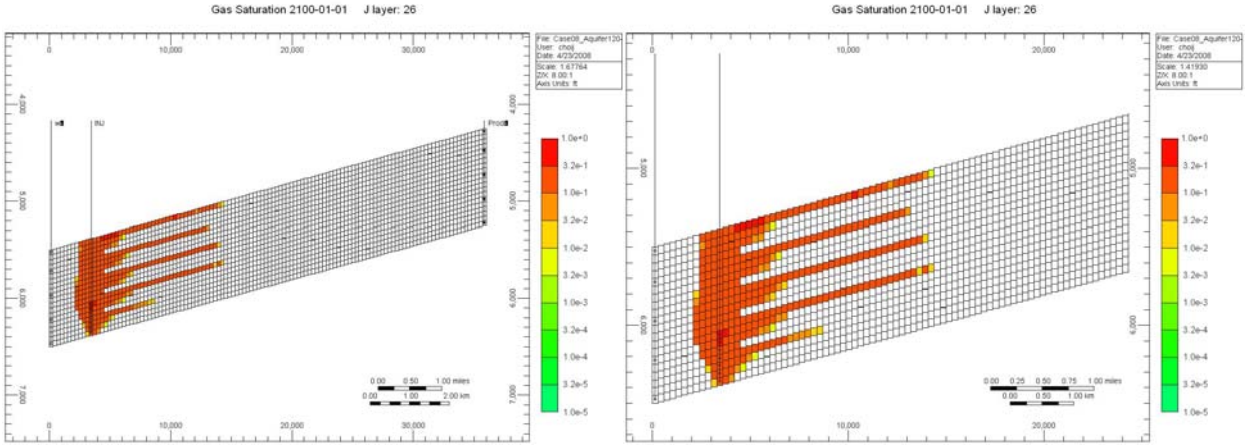

Time = 100 yr

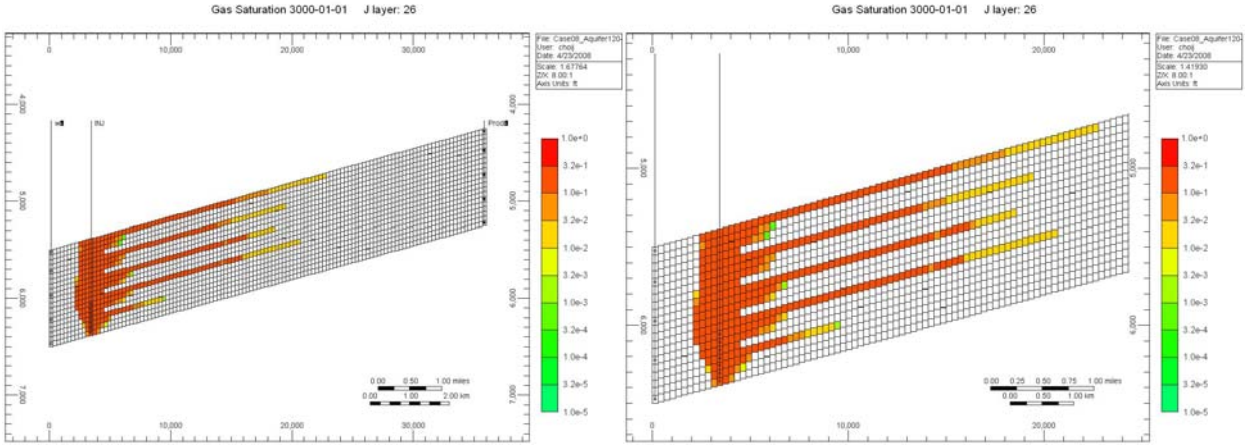

Time = 1,000 yr

9. Case 9: 85-7.5-7.5 (CO_2-CH_4-N_2) in volume

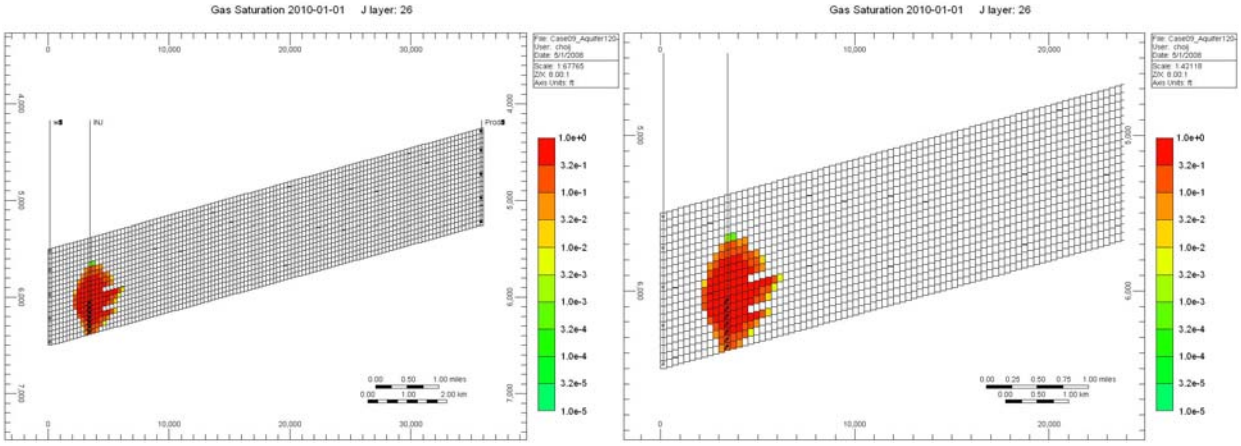

Time = 10 yr

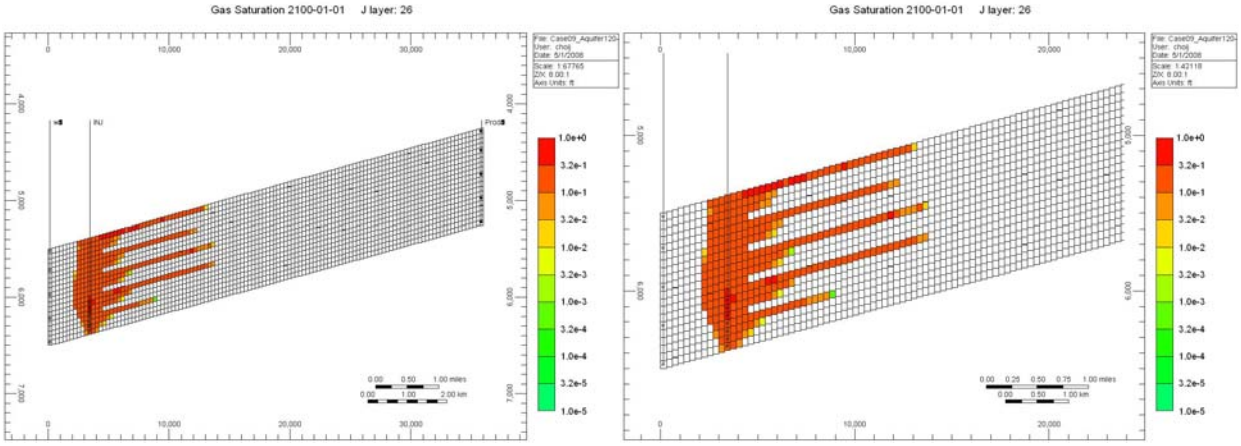

Time = 100 yr

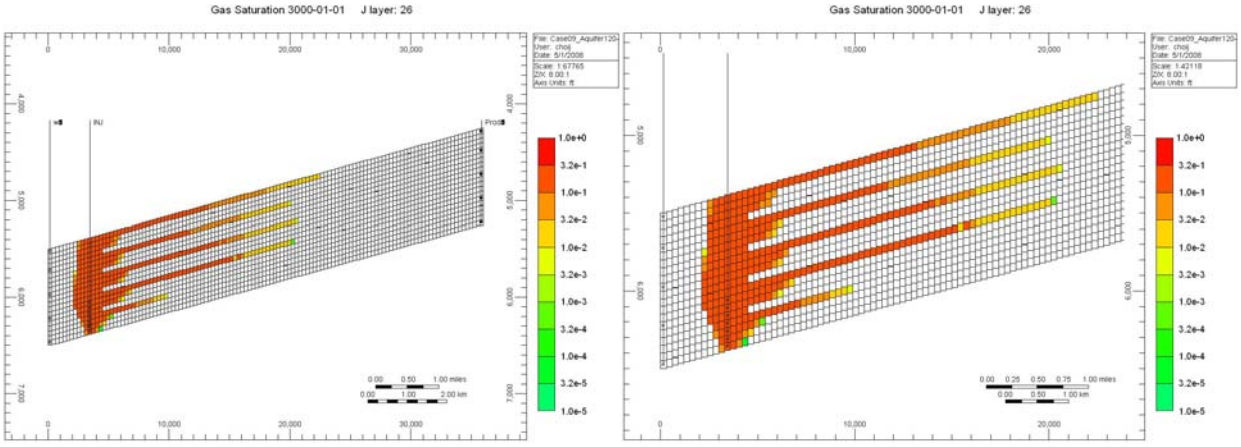

Time = 1,000 yr

10. Case 10: 80-20-0 (CO_2-CH_4-N_2) in volume

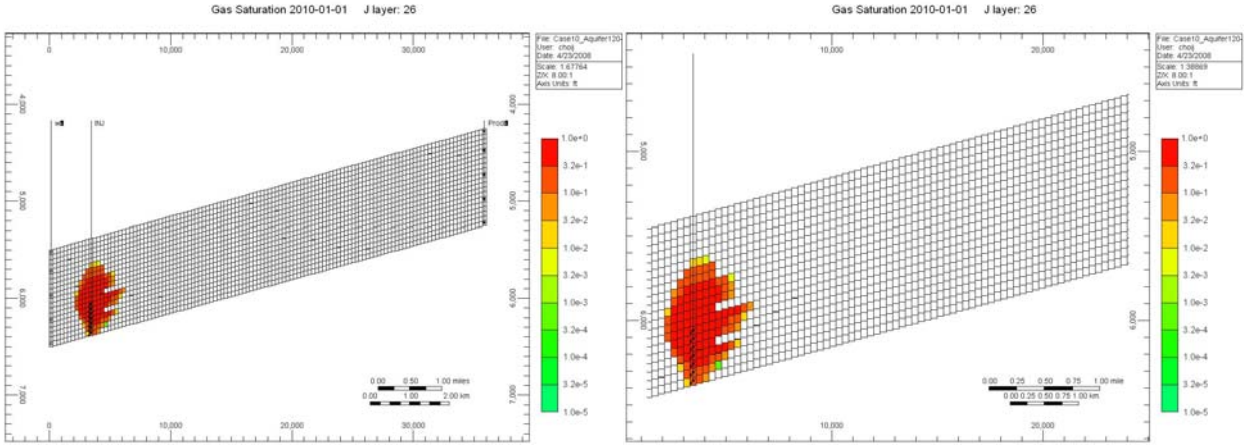

Time = 10 yr

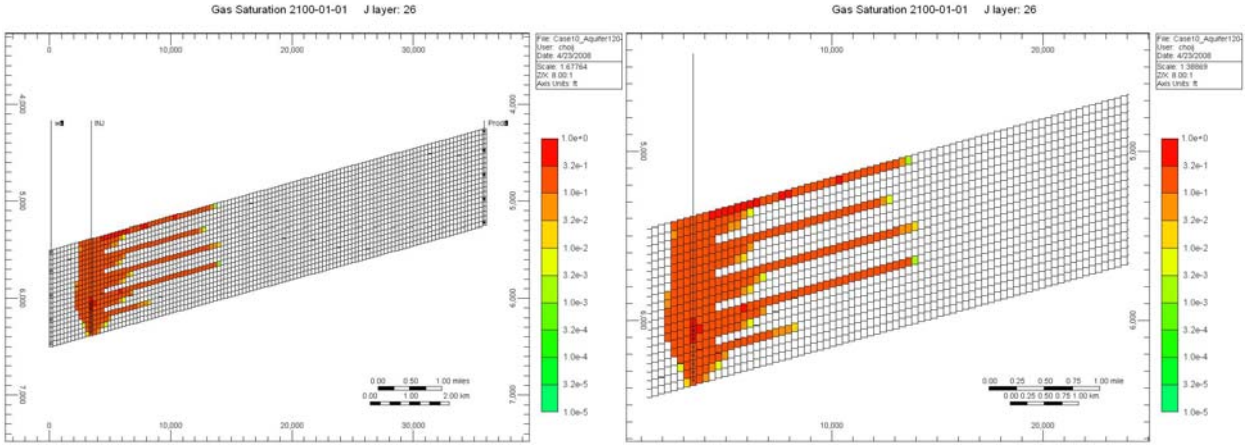

Time = 100 yr

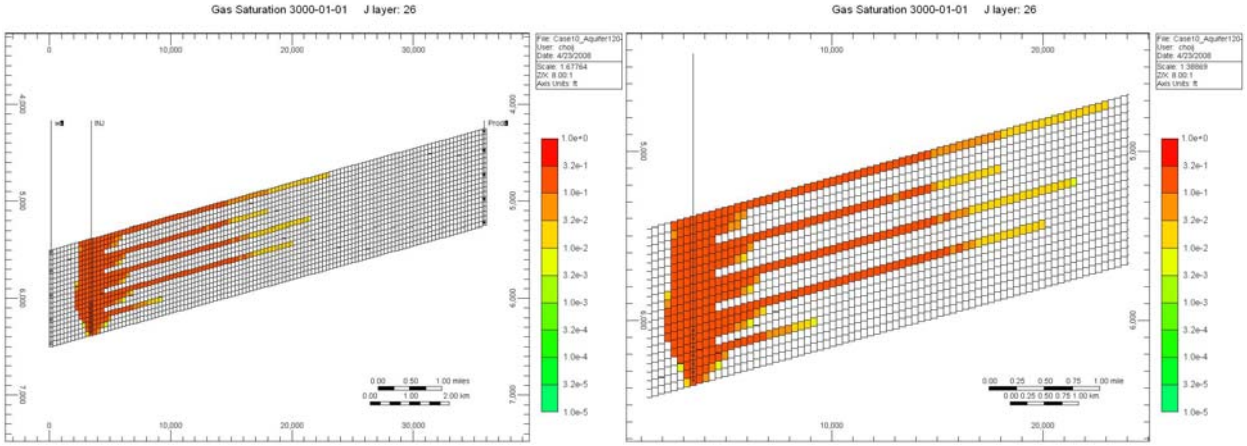

Time = 1,000 yr

11. Case 11: 80-0-20 (CO_2-CH_4-N_2) in volume

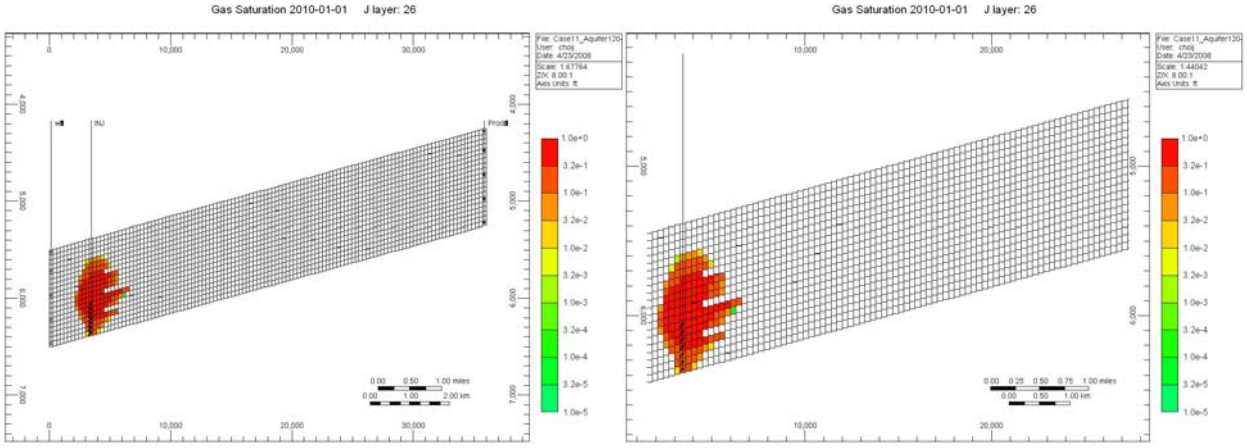

Time = 10 yr

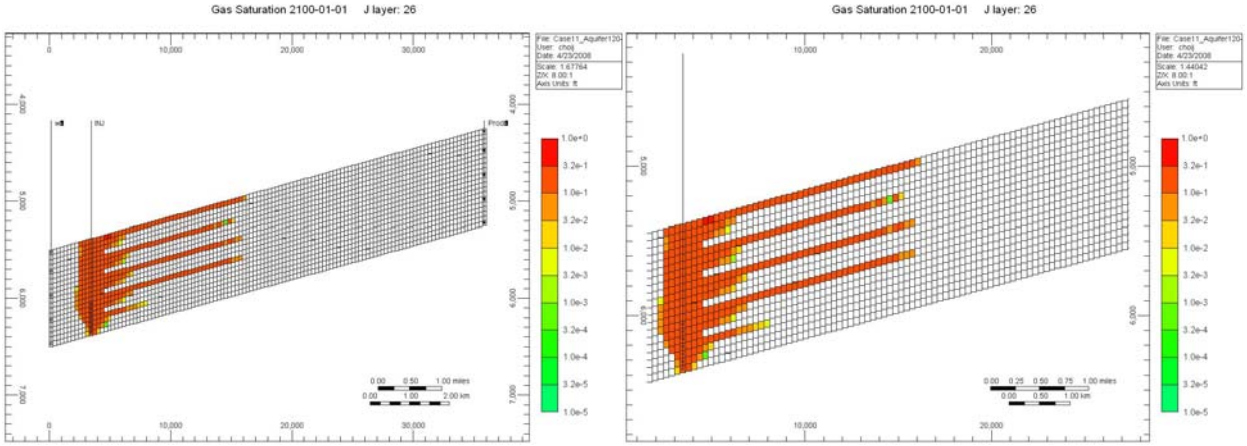

Time = 100 yr

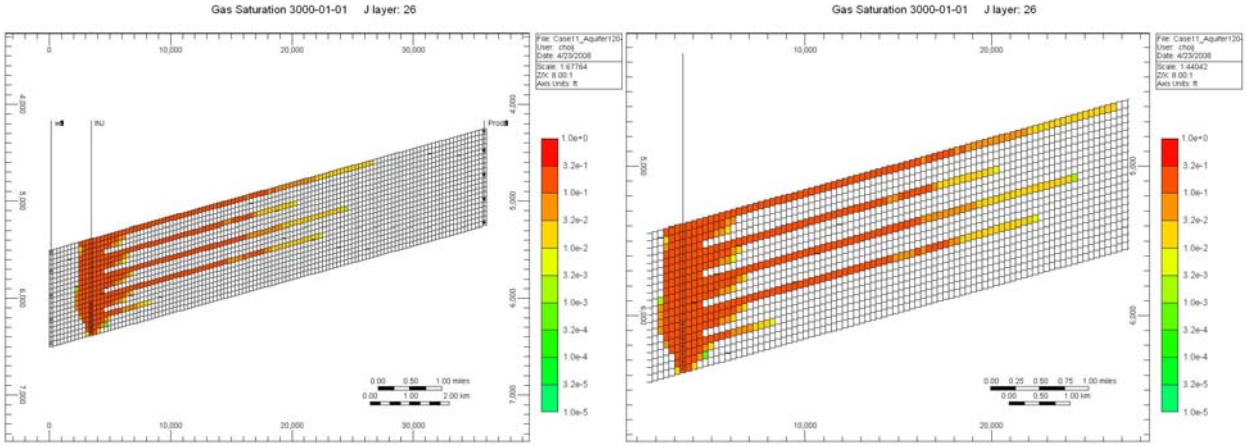

Time = 1,000 yr

12. Case 12: 80-10-10 (CO_2-CH_4-N_2) in volume

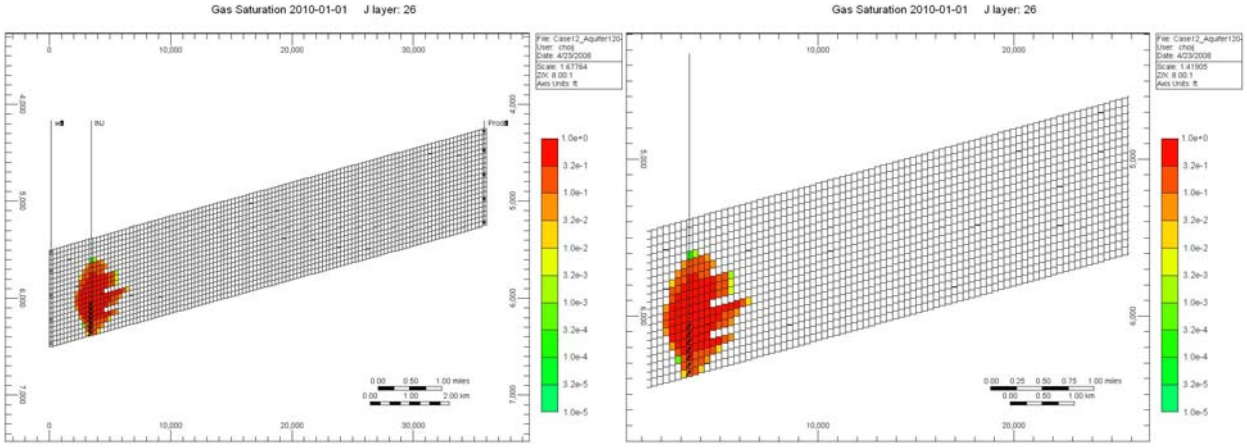

Time = 10 yr

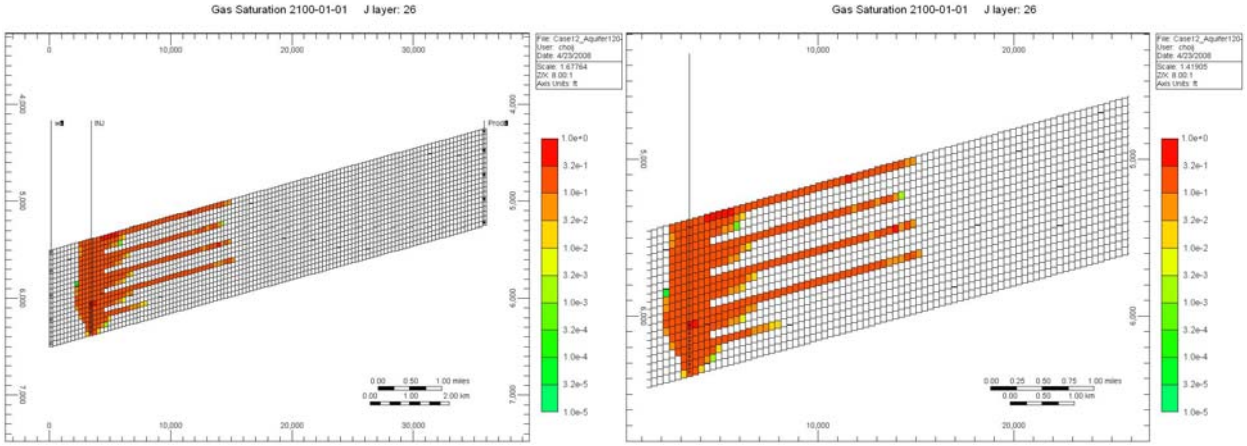

Time = 100 yr

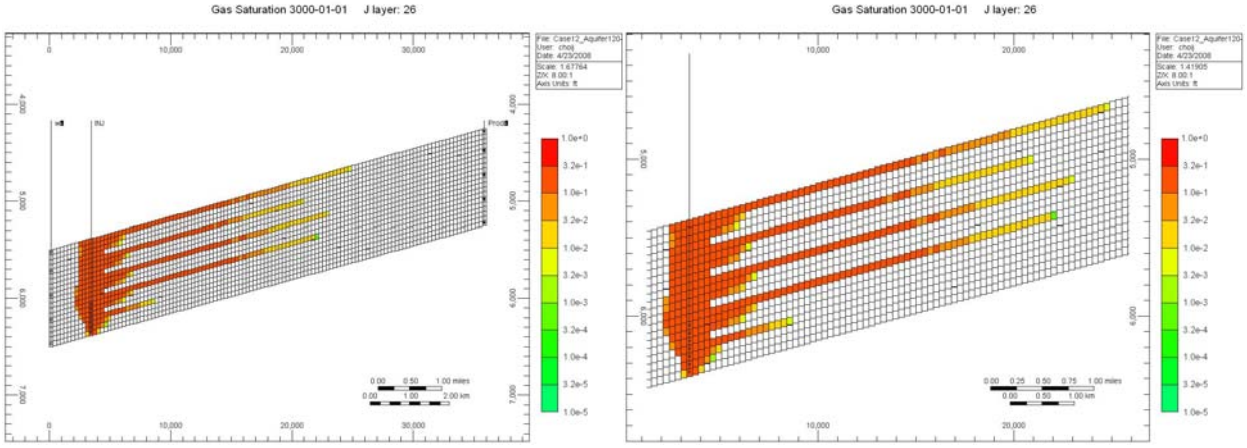

Time = 1000 yr

13. Case 13: 75-25-0 (CO_2-CH_4-N_2) in volume

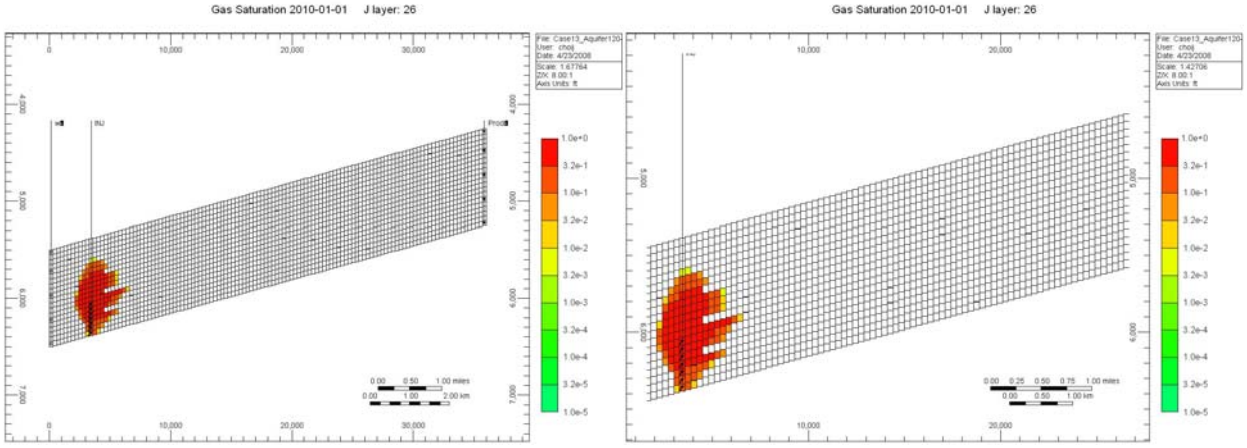

Time = 10 yr

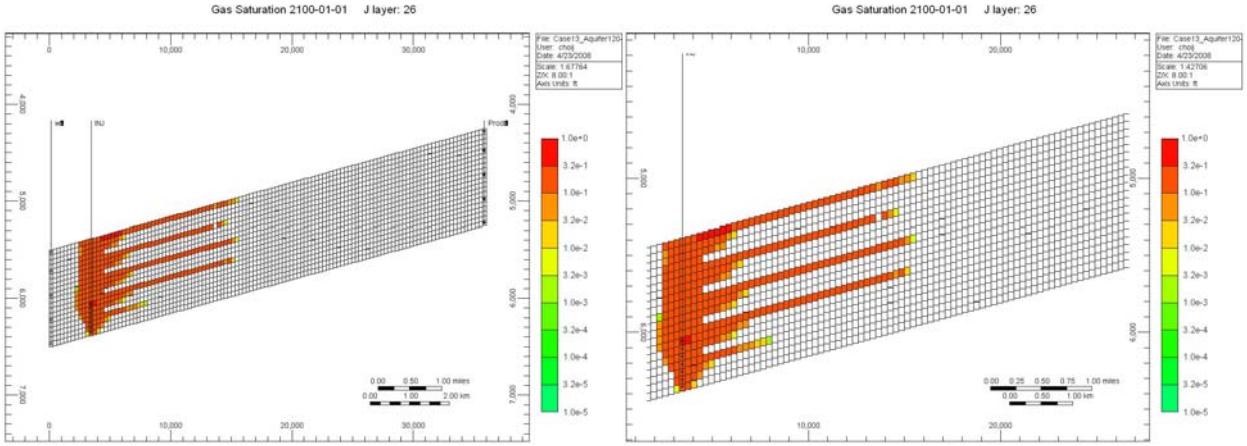

Time = 100 yr

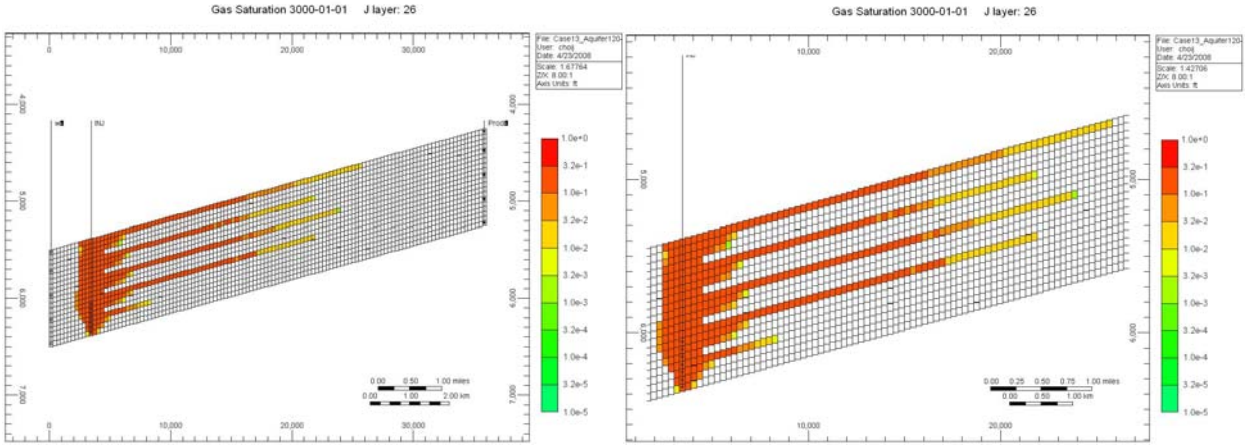

Time = 1,000 yr

14. Case 14: 75-0-25 (CO_2-CH_4-N_2) in volume

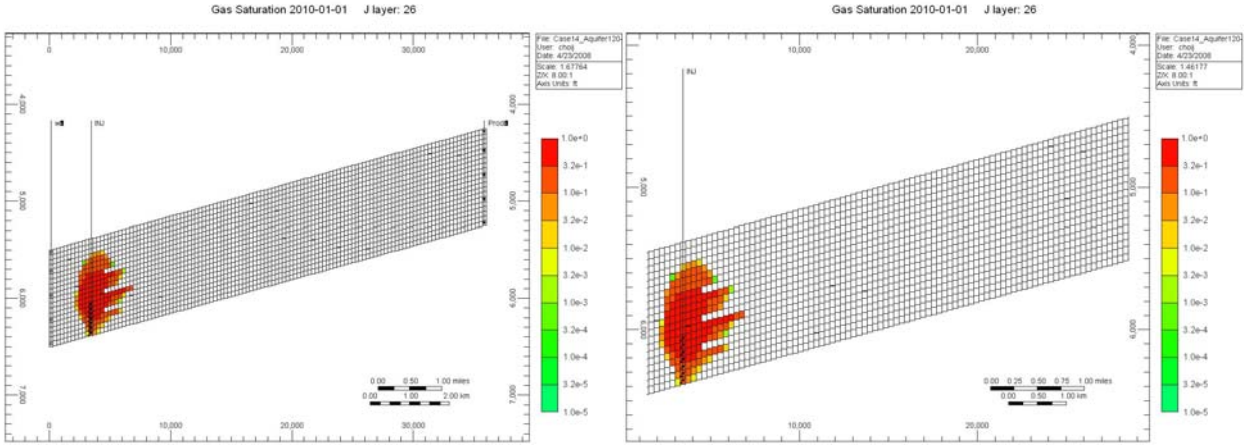

Time = 10 yr

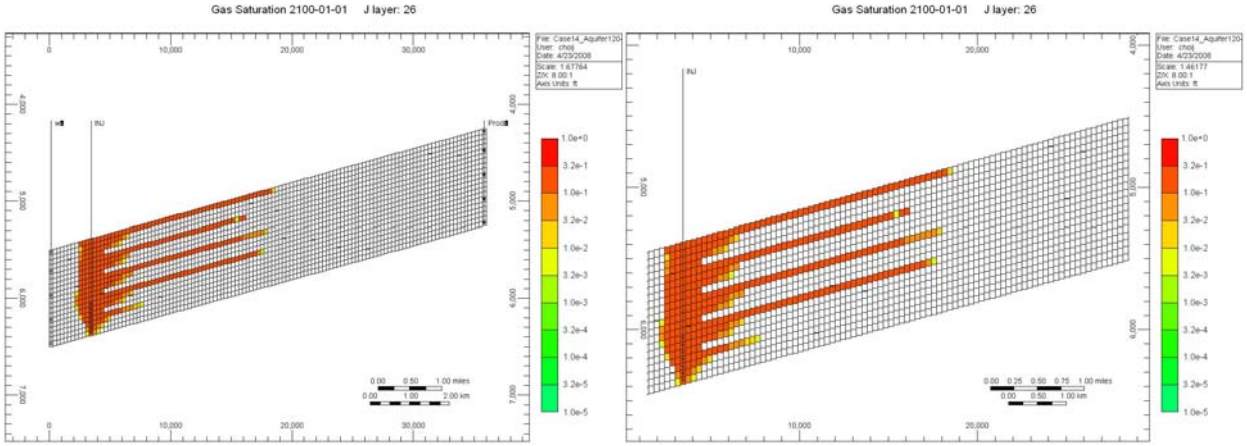

Time = 100 yr

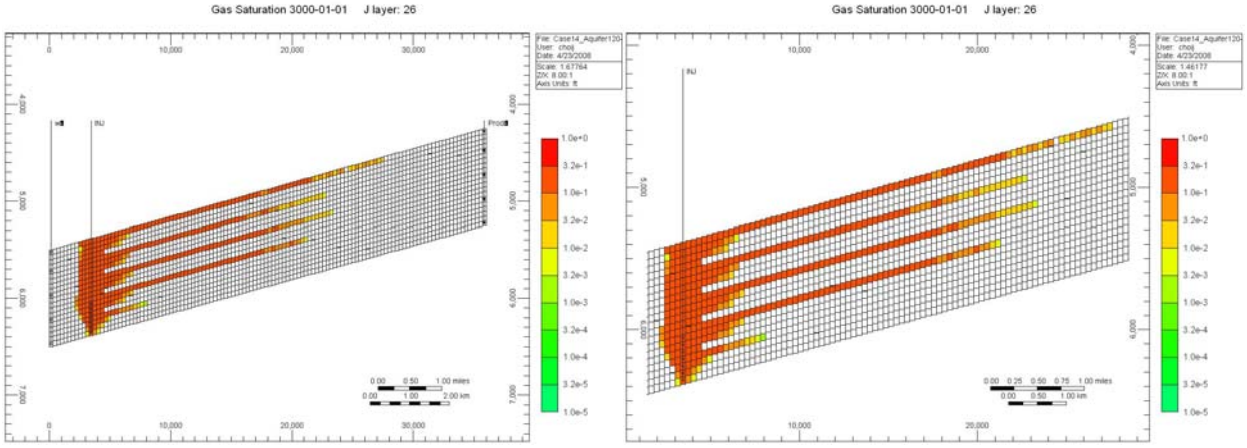

Time = 1,000 yr

15. Case 15: 75-12.5-12.5 (CO_2-CH_4-N_2) in volume

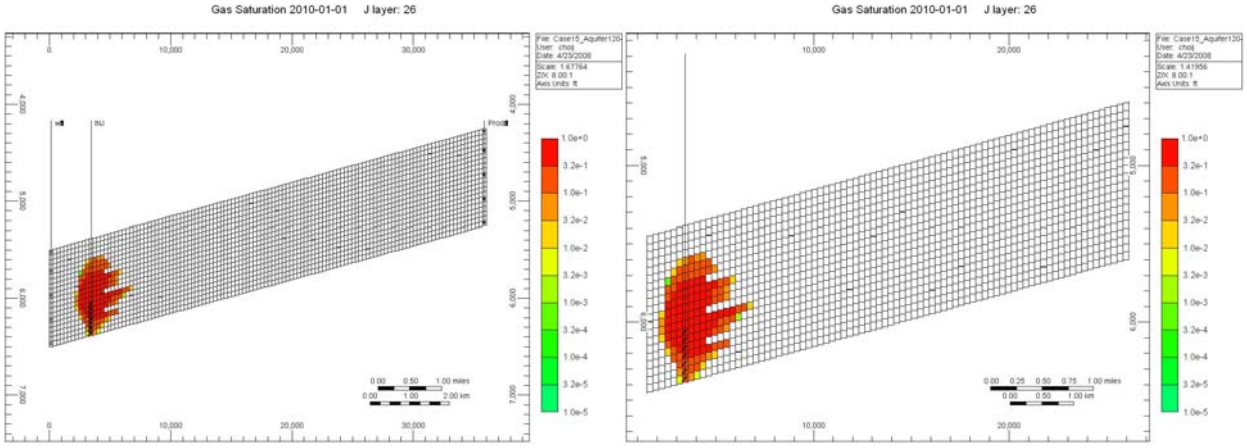

Time = 10 yr

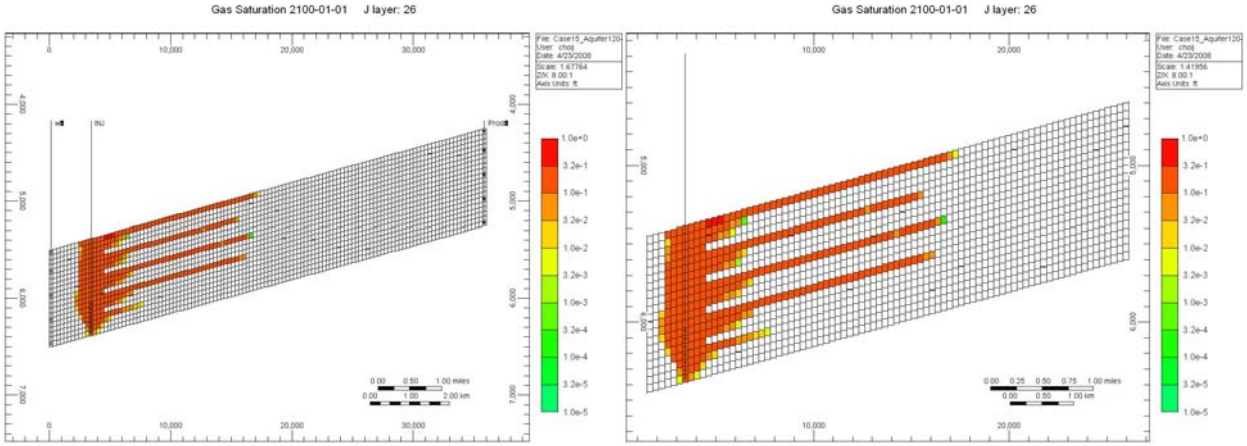

Time = 100 yr

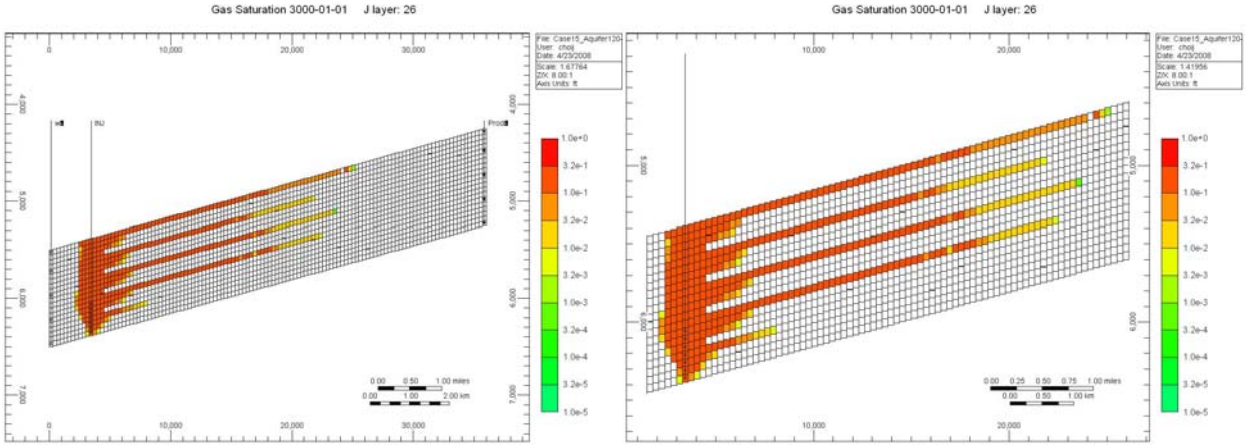

Time = 1,000 yr

16. Case 16: 100-0-0 (CO_2-CH_4-2)

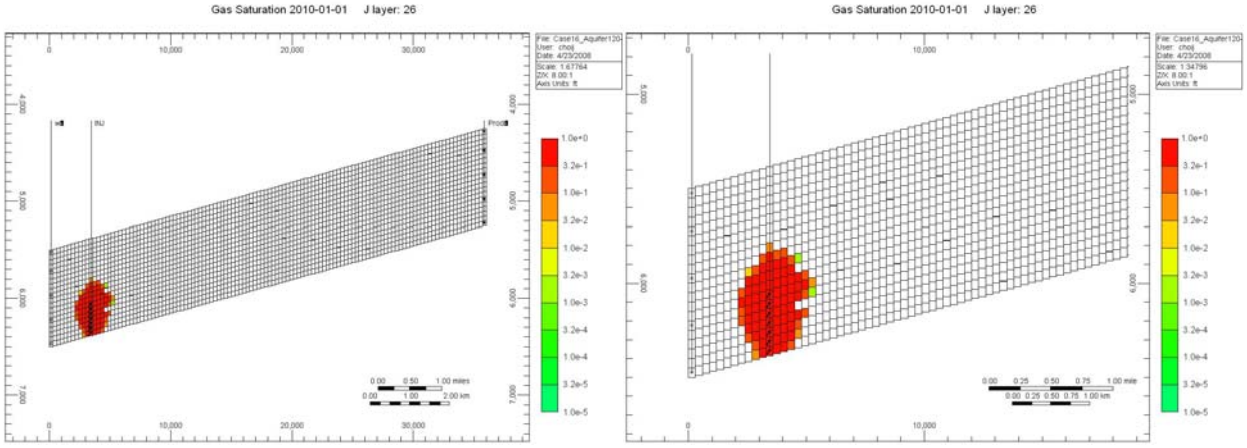

Time = 10 yr

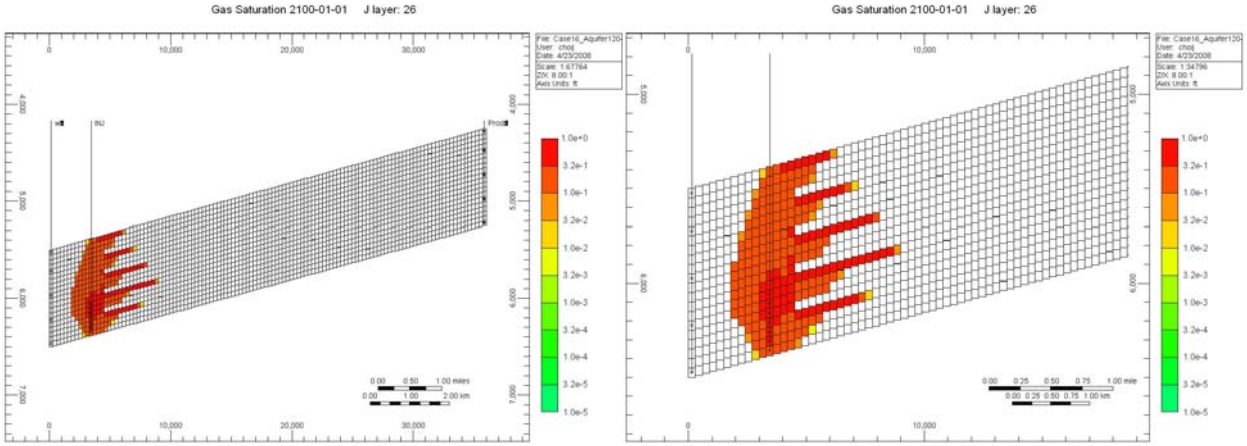

Time = 100 yr

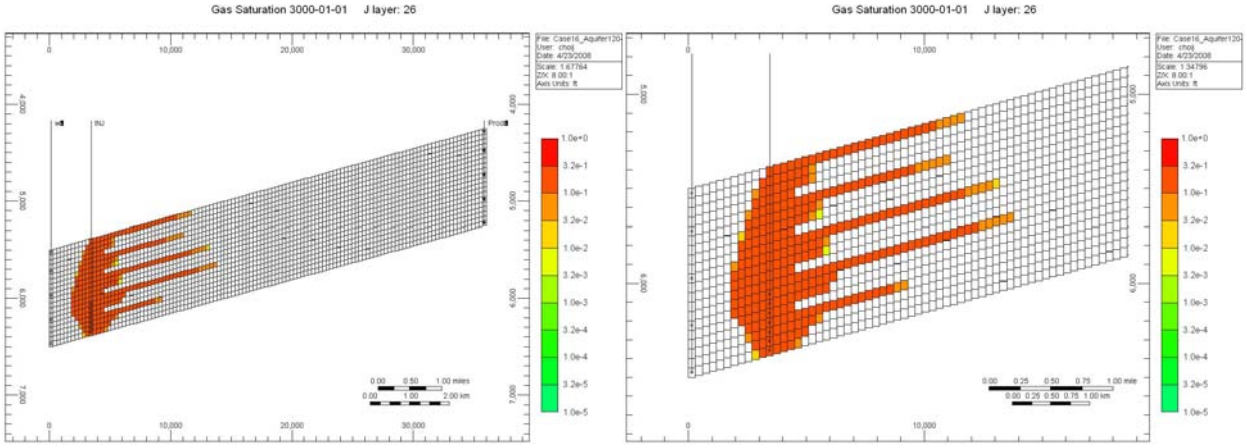

Time = 1,000 yr

17. Case 17: 75-25-0 (CO_2-CH_4-N_2) in mass

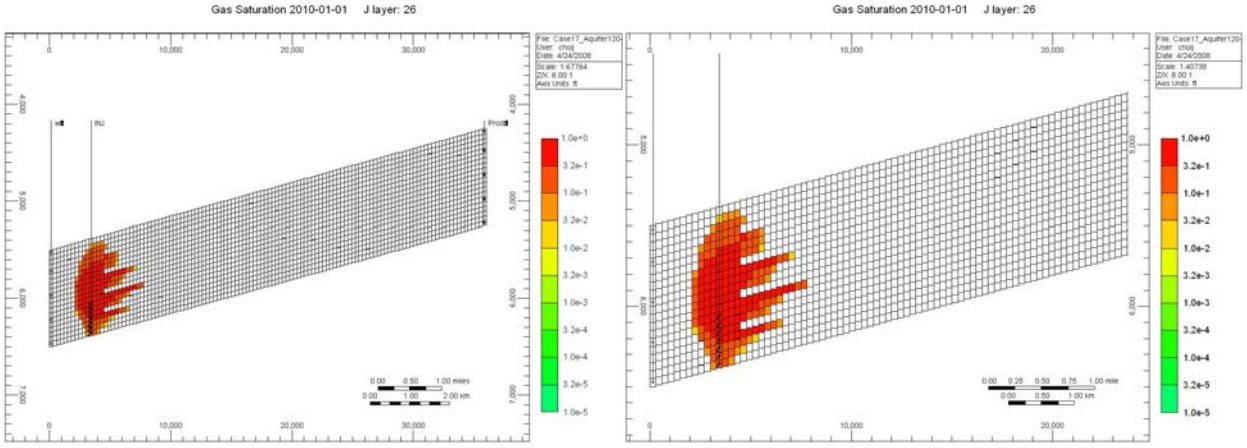

Time = 10 yr

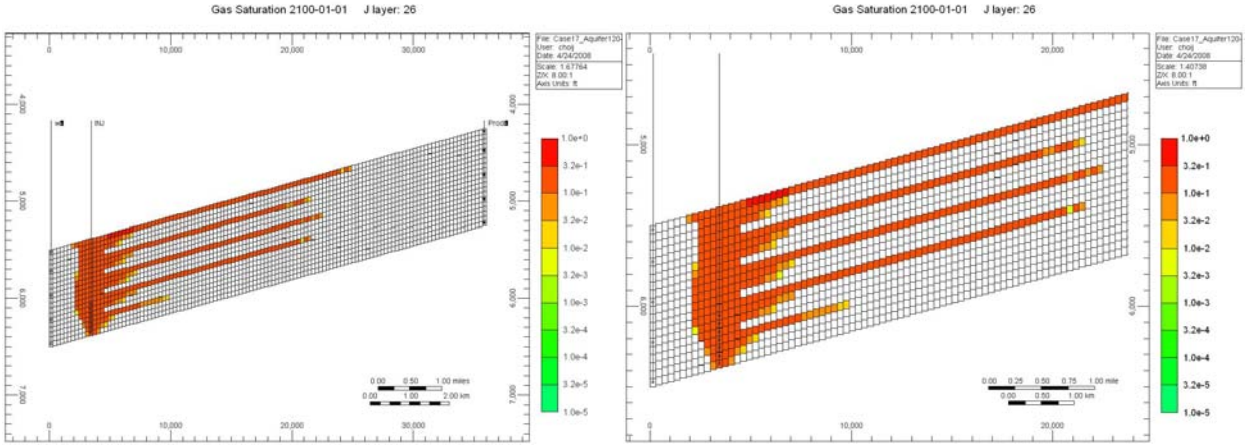

Time = 100 yr

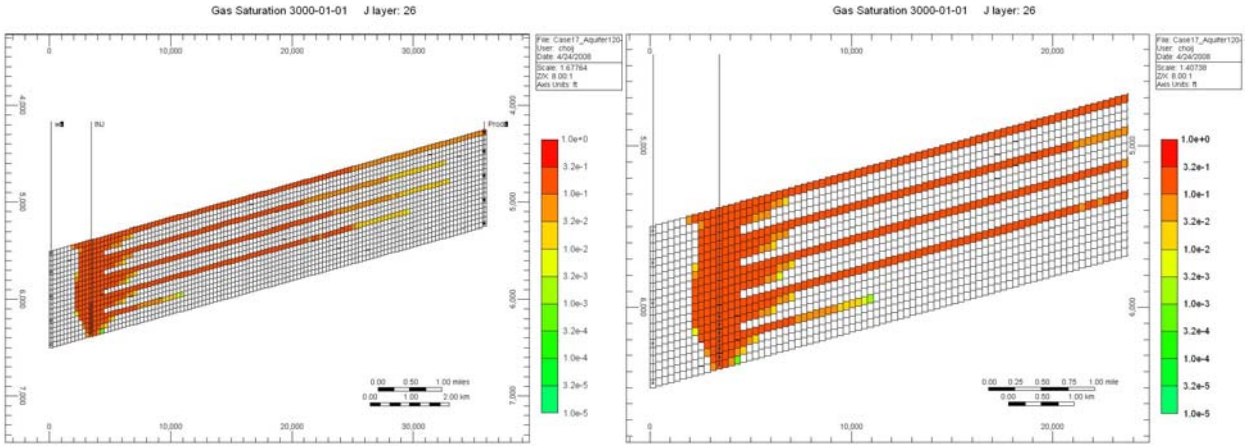

Time = 1,000 yr

18. Case 18: 75-0-25 (CO_2-CH_4-N_2) in mass

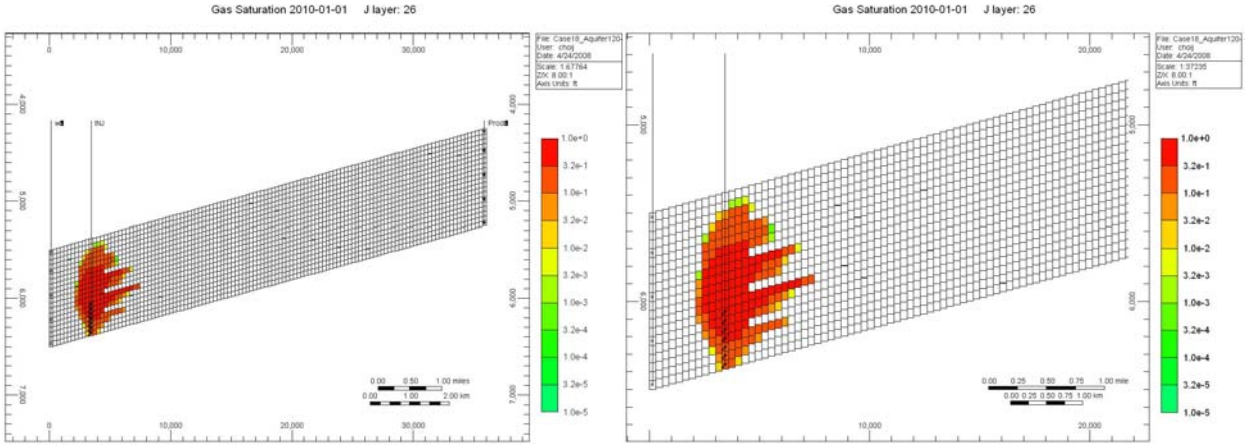

Time = 10 yr

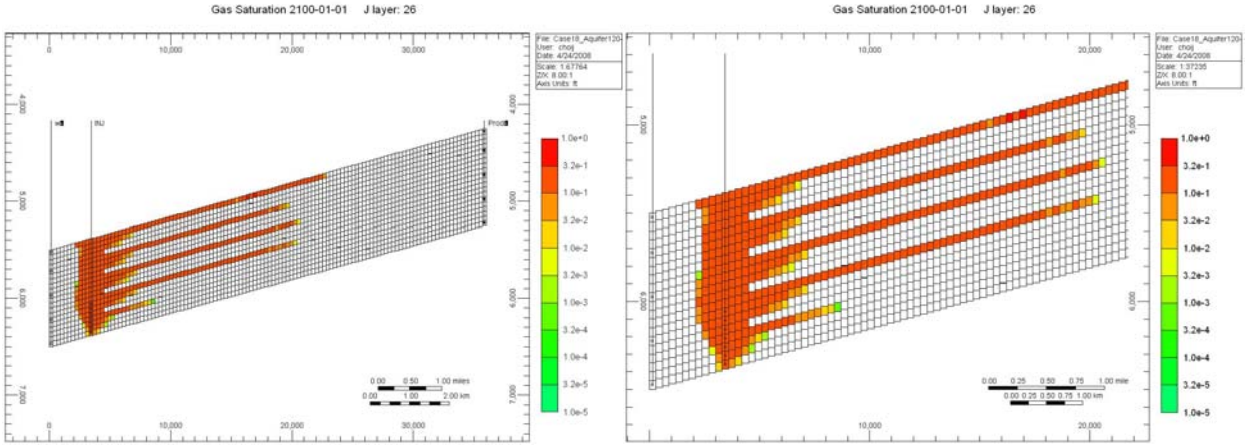

Time = 100 yr

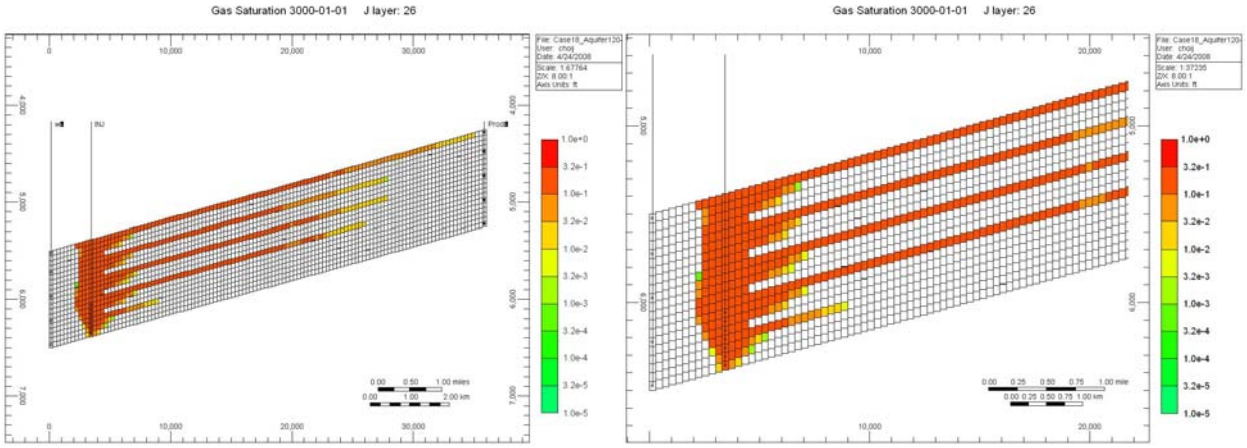

Time = 1,000 yr

19. Case 19: Dip = 1°

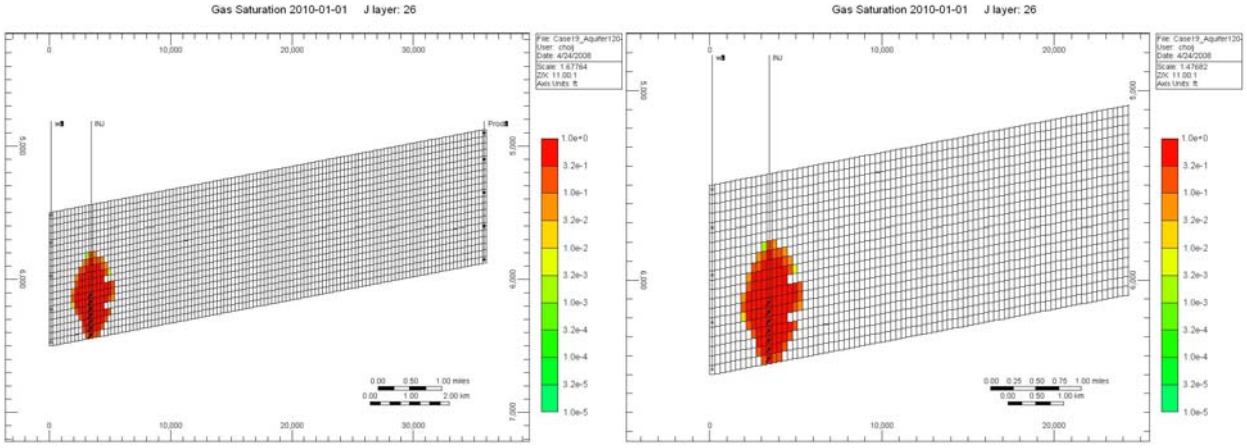

Time = 10 yr

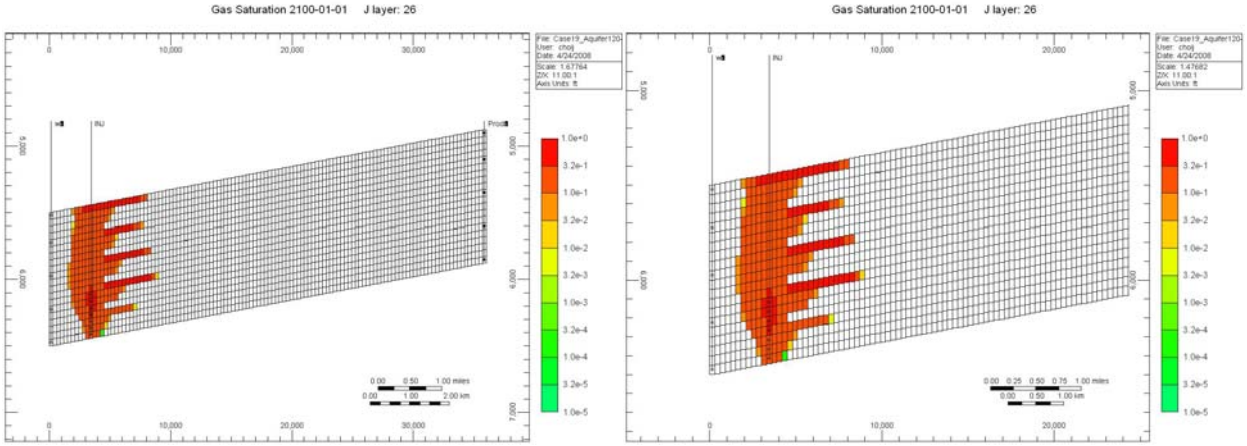

Time = 100 yr

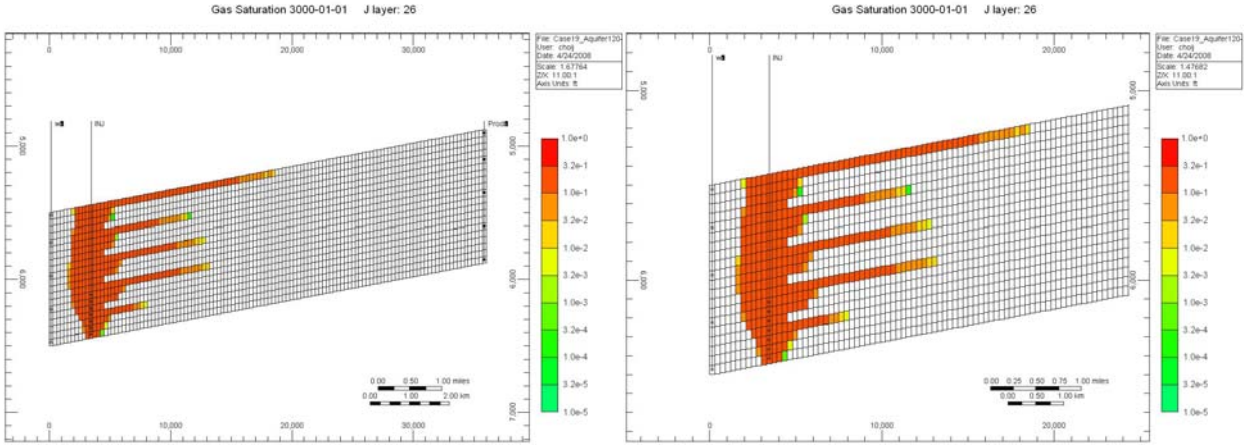

Time = 1,000 yr

20. Case 20: Dip = 5°

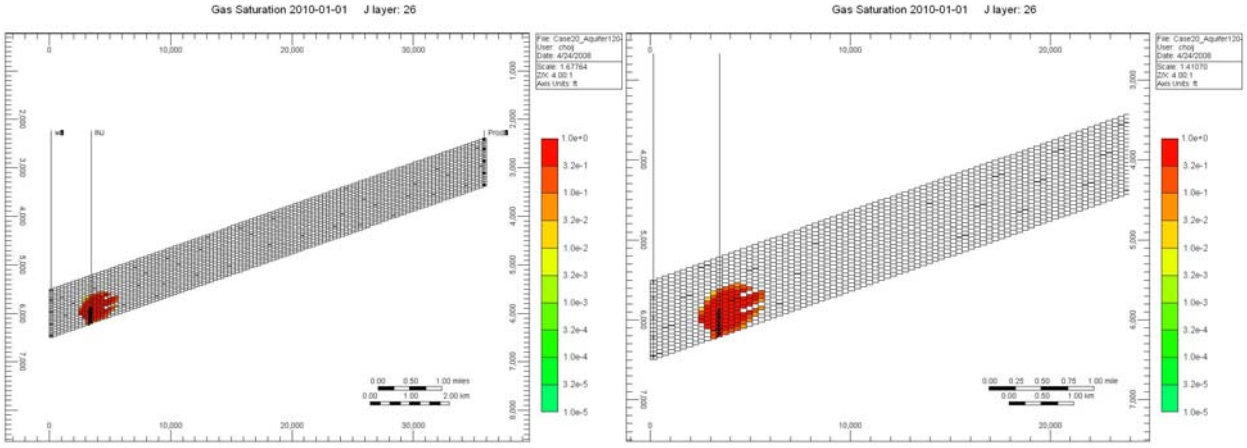

Time = 10 yr

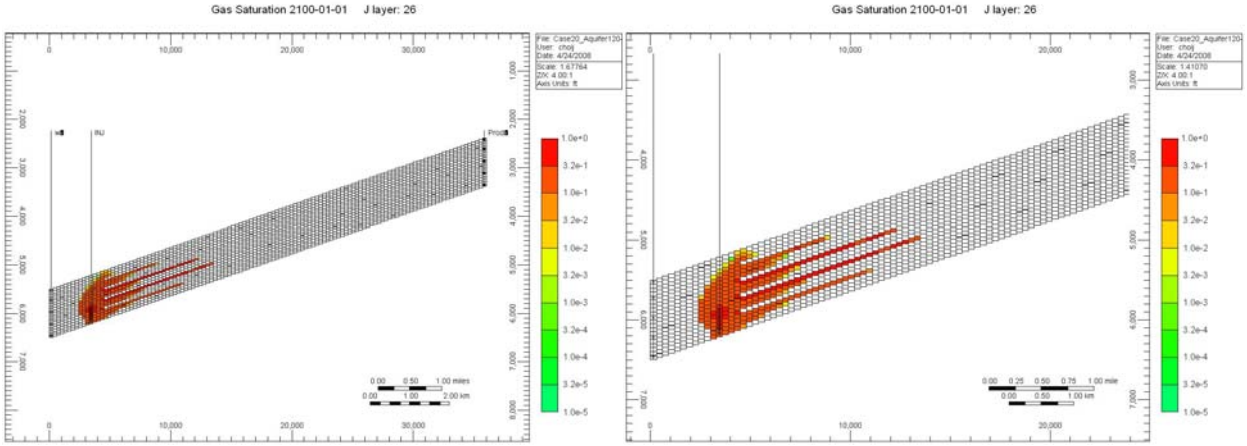

Time = 100 yr

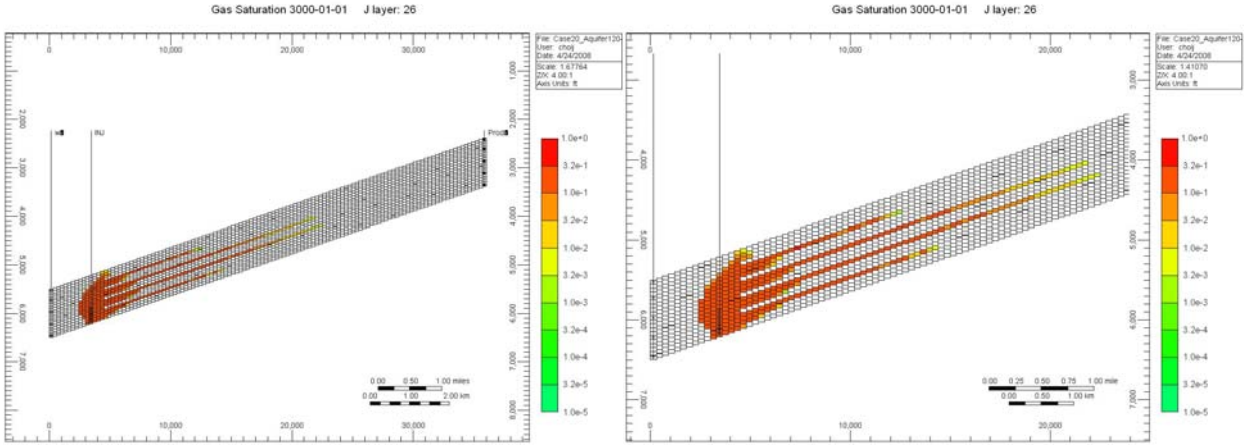

Time = 1,000 yr

21. Case 21: Permeability in I direction = 100 md

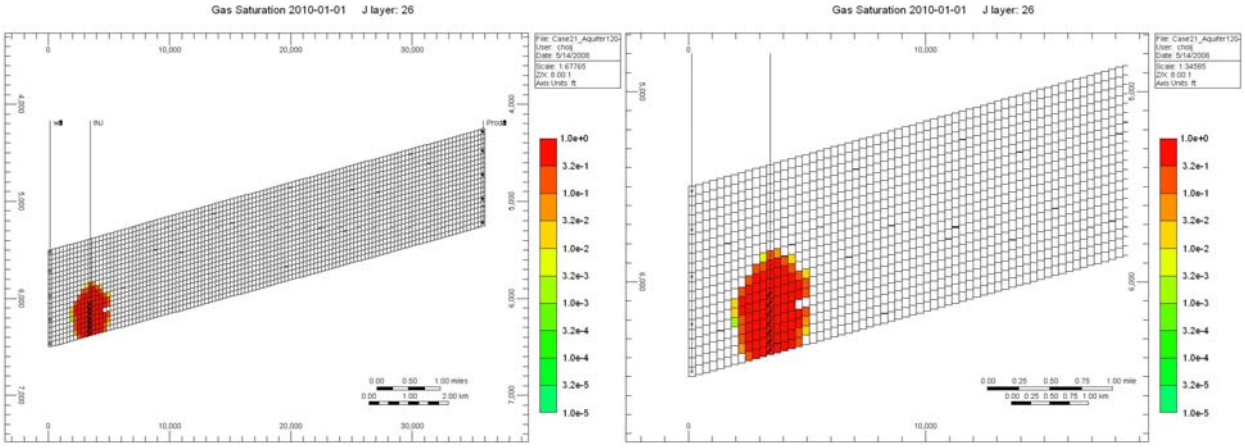

Time = 10 yr

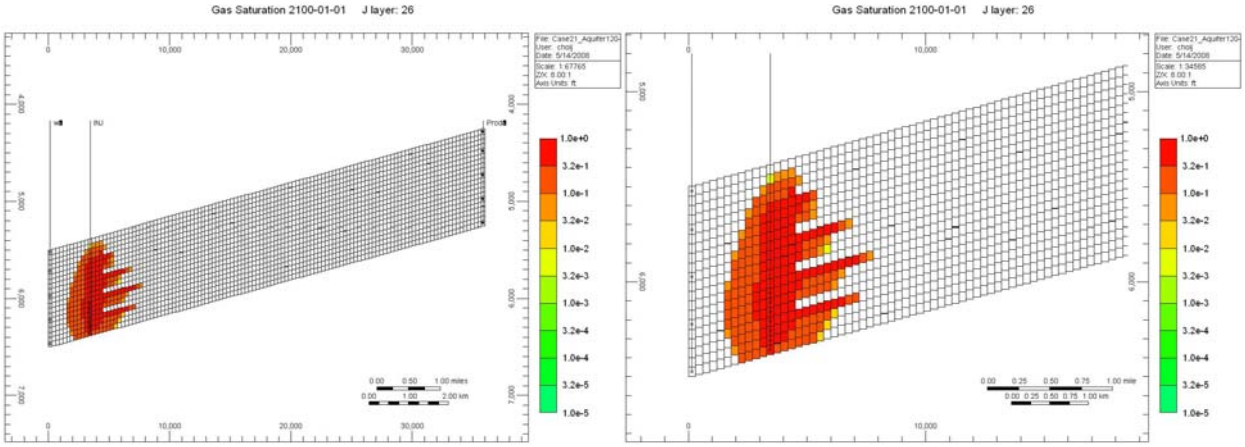

Time = 100 yr

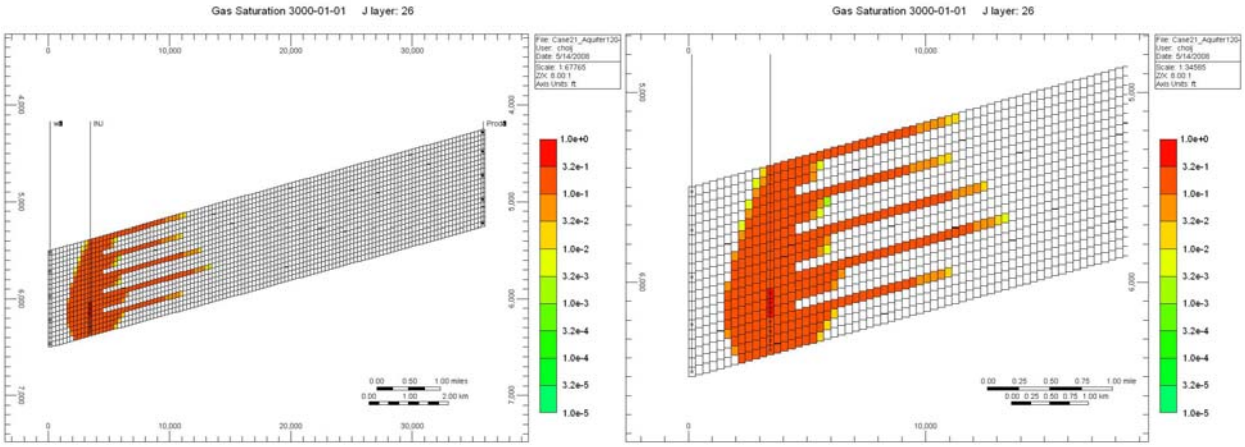

Time = 1,000 yr

22. Case 22: Permeability in I direction = 600 md

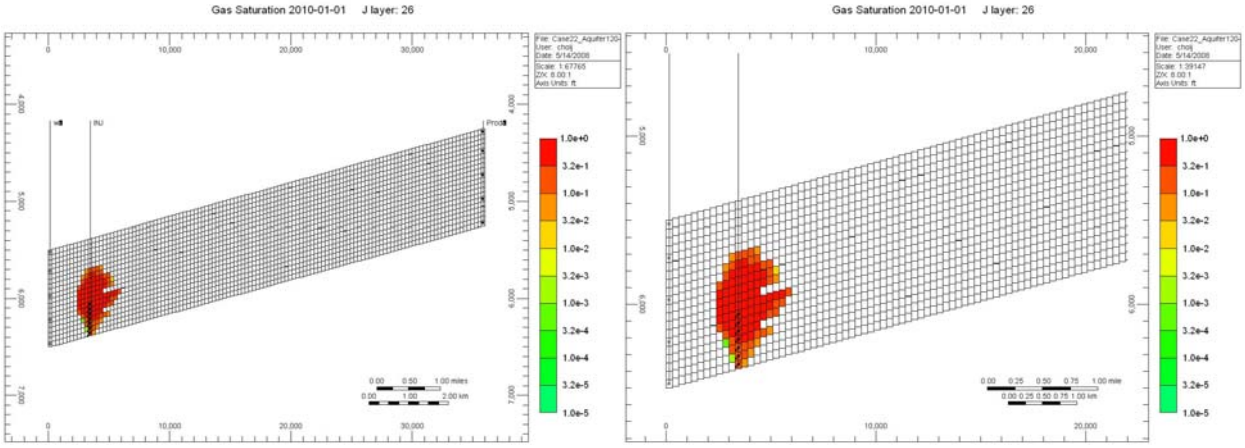

Time = 10 yr

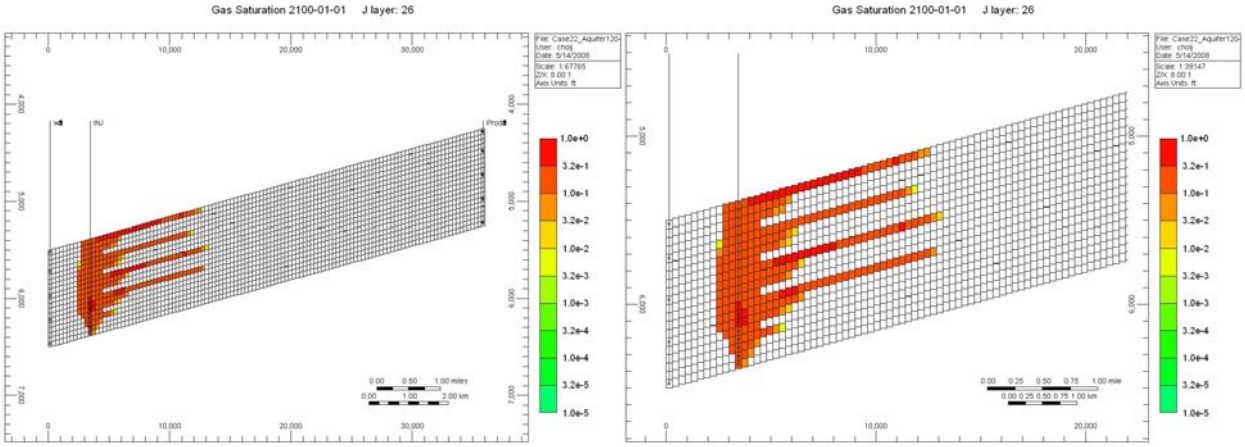

Time = 100 yr

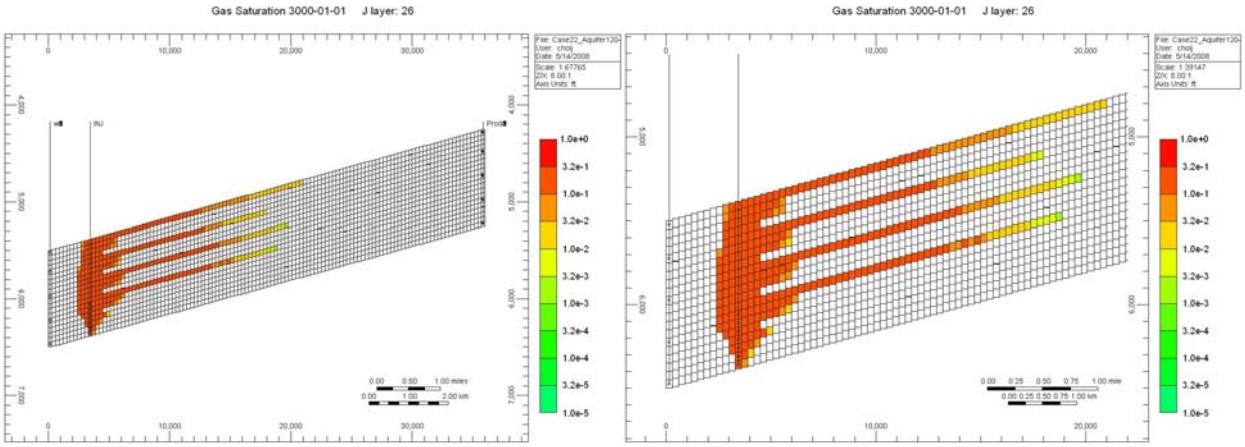

Time = 1,000 yr

23. Case 23: Permeability anisotropy in K direction = 0.1

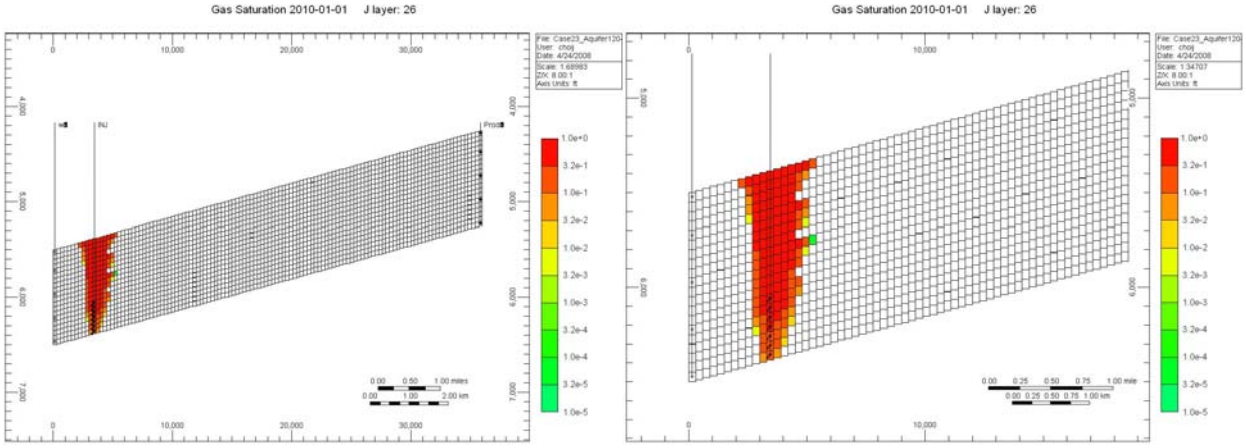

Time = 10 yr

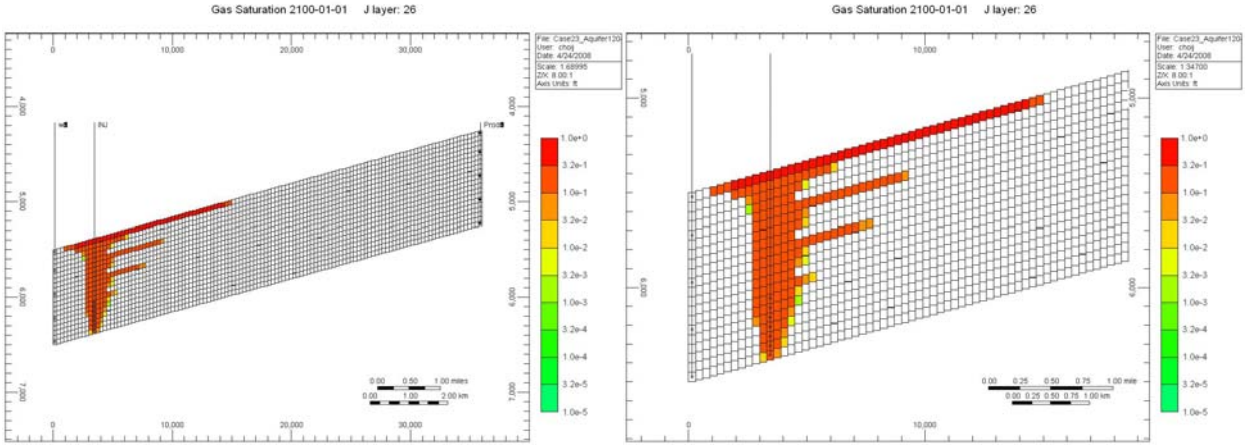

Time = 100 yr

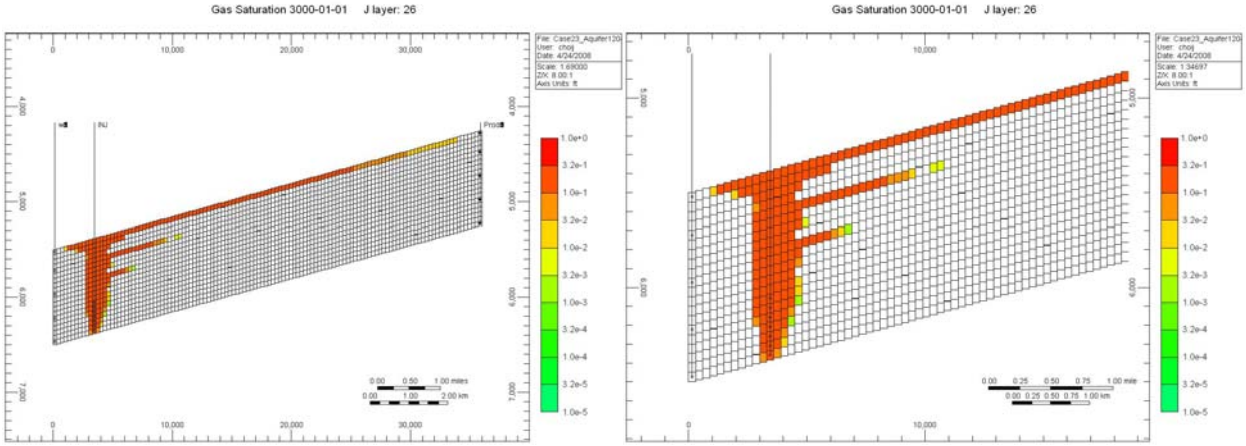

Time = 1,000 yr

24. Case 24: Permeability anisotropy in K direction = 0.005

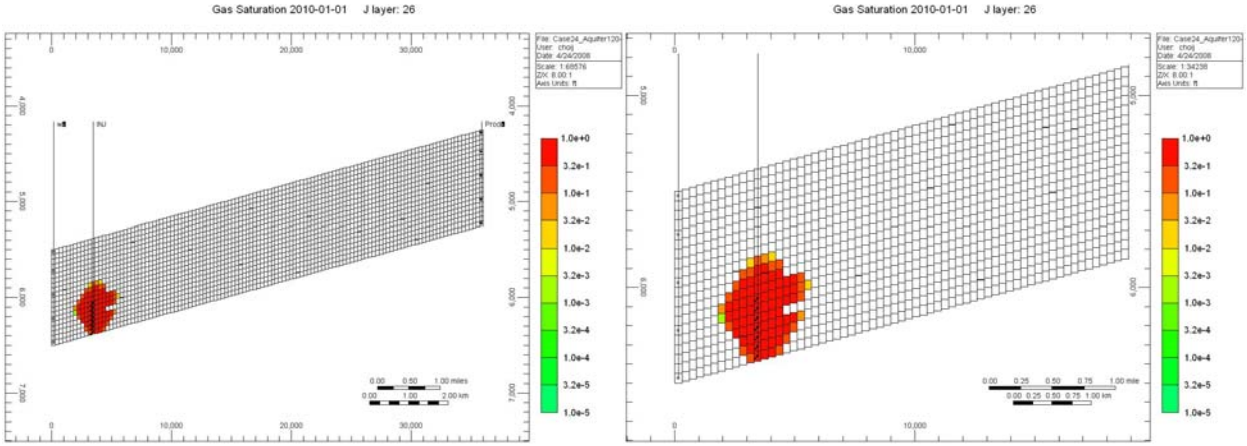

Time = 10 yr

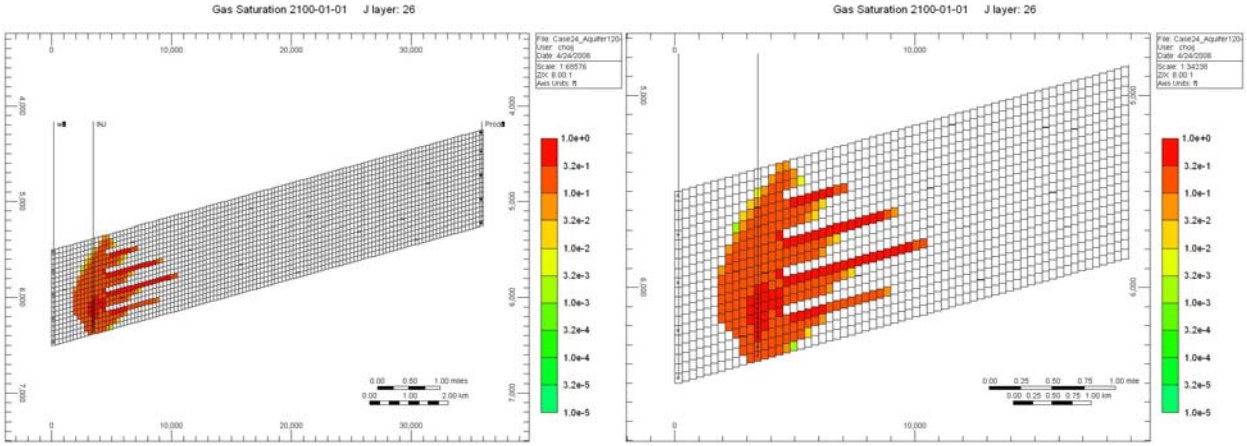

Time = 100 yr

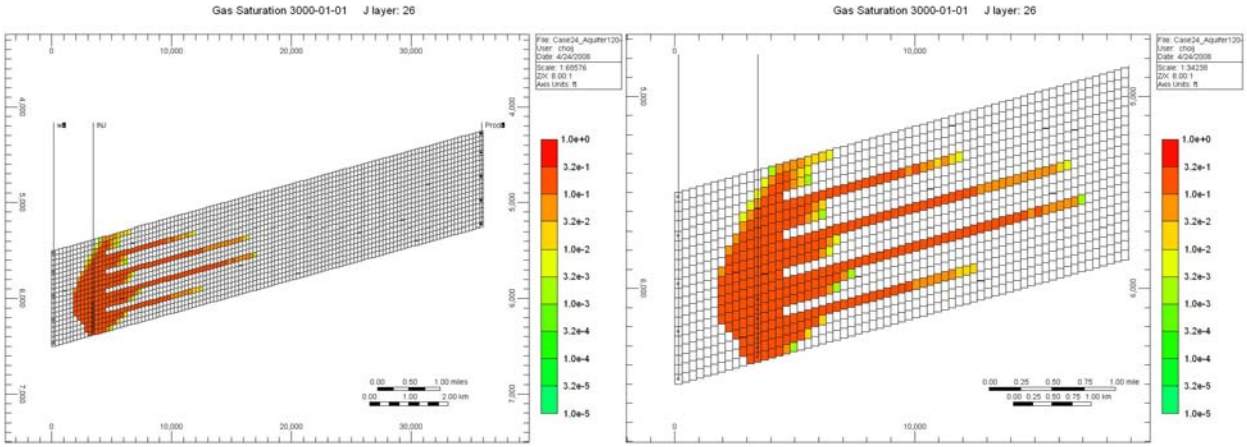

Time = 1,000 yr

25. Case 25: CPOR = 5×10^{-5}

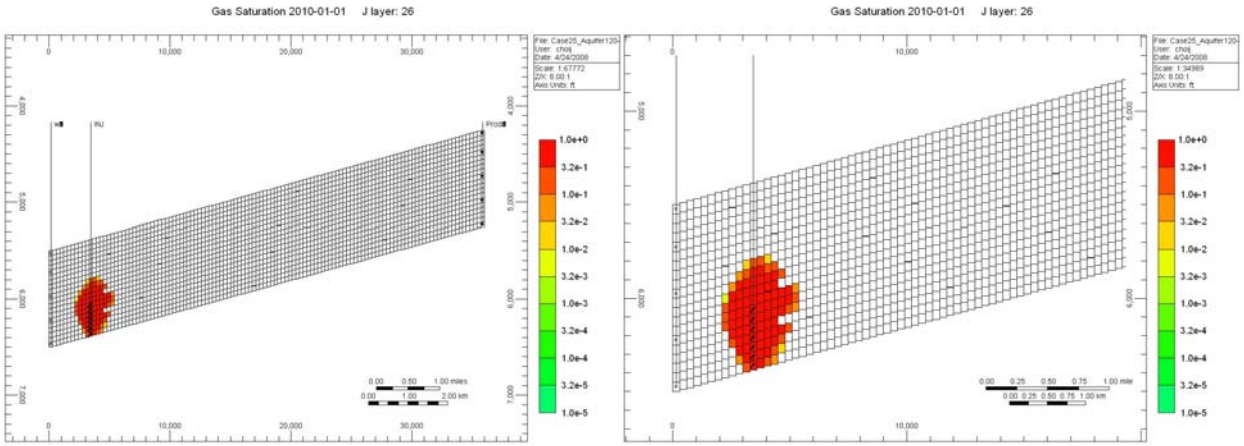

Time = 10 yr

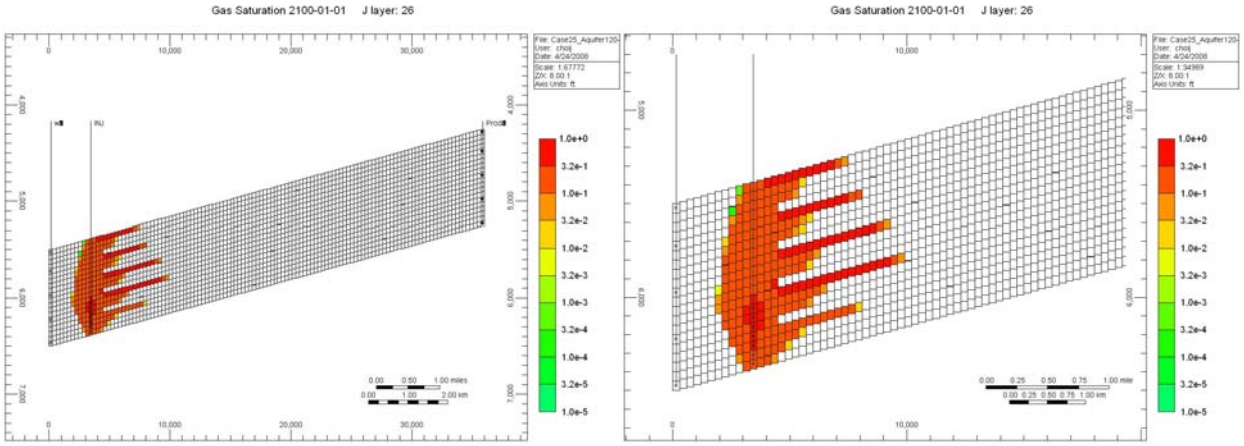

Time = 100 yr

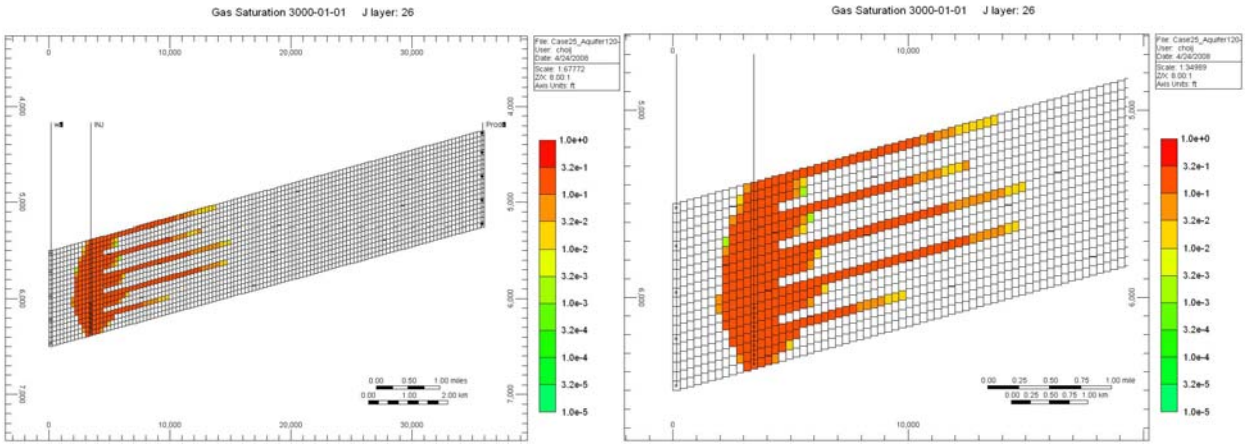

Time = 1,000 yr

26. Case 26: Default PVT properties 100-0-0 (CO2-CH4-N2) in volume

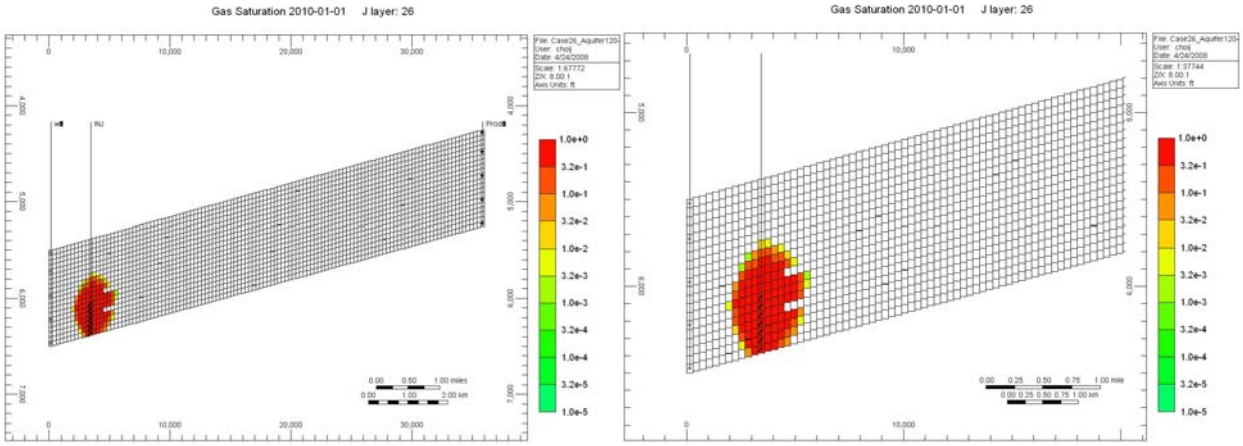

Time = 10 yr

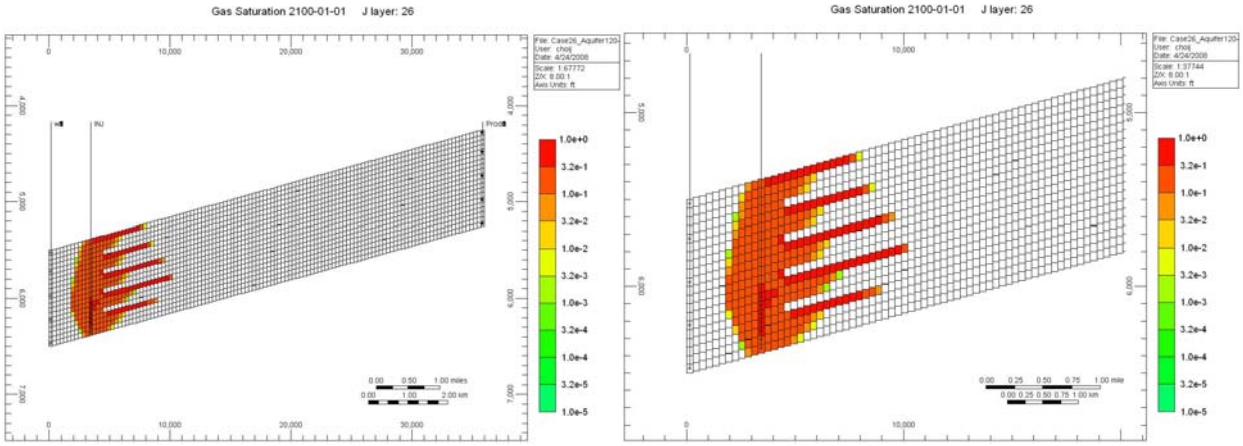

Time = 100 yr

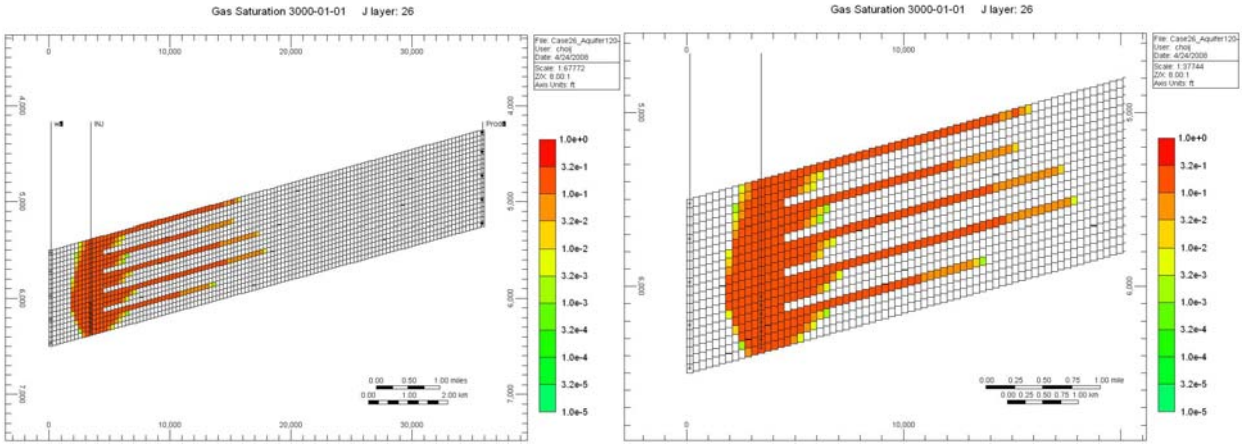

Time = 1,000 yr

27. Case 27: Default PVT properties 75-25-0 (CO_2-CH_4-N_2) in volume

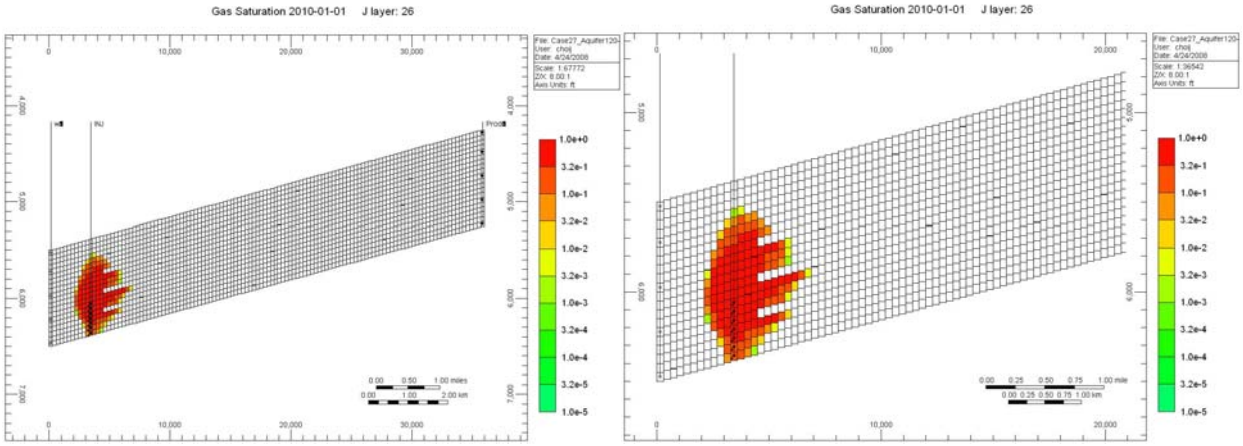

Time = 10 yr

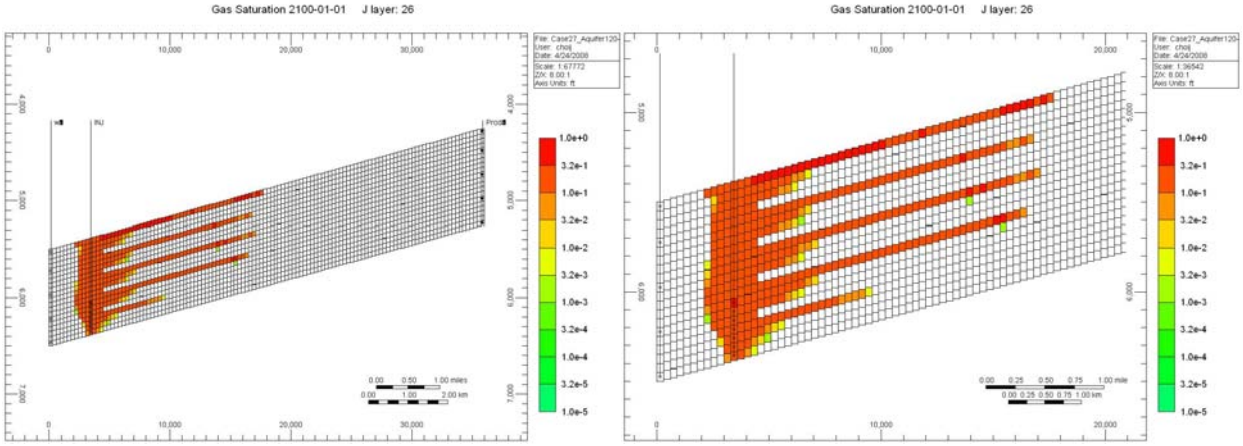

Time = 100 yr

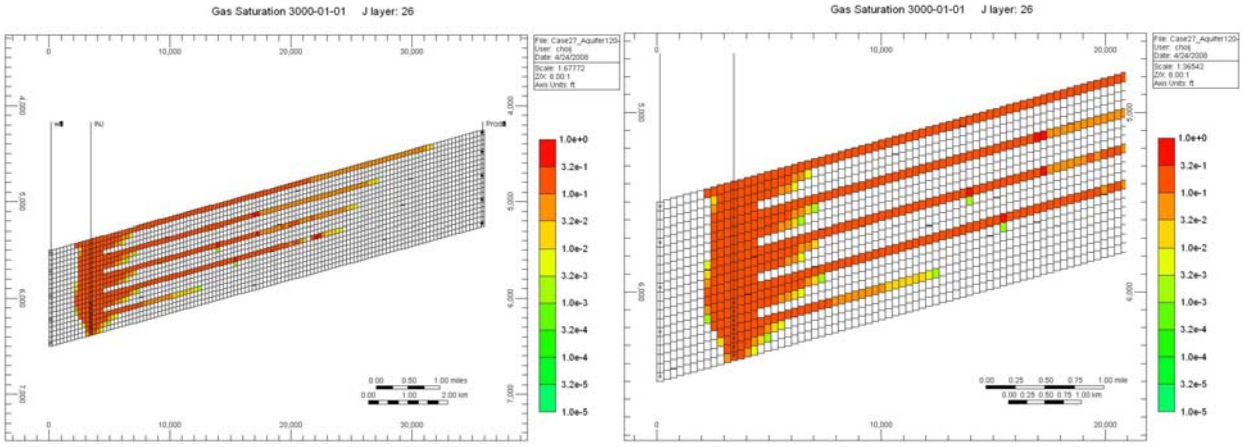

Time = 1,000 yr

28. Case 28: Default PVT properties a 75-0-25 (CO_2-CH_4-N_2) in volume

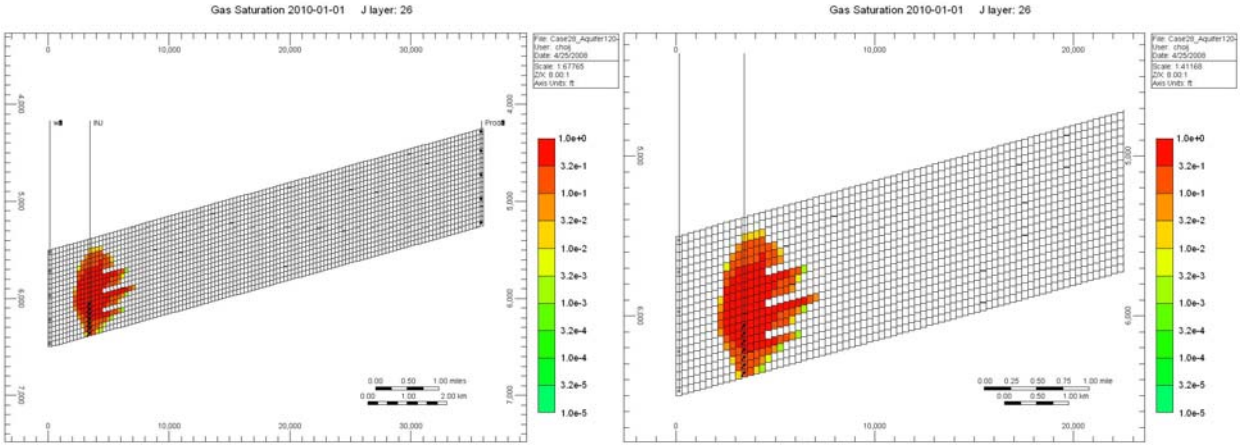

Time = 10 yr

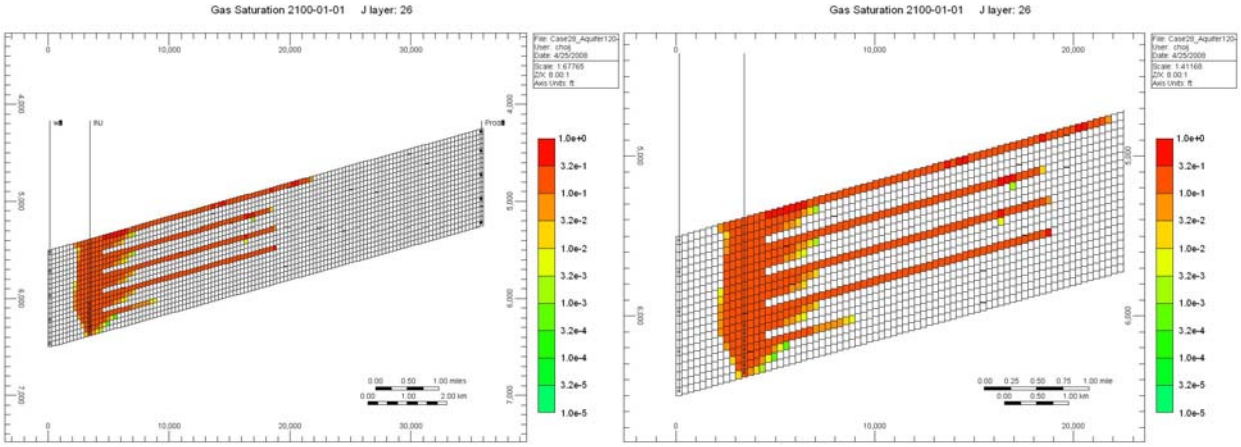

Time = 100 yr

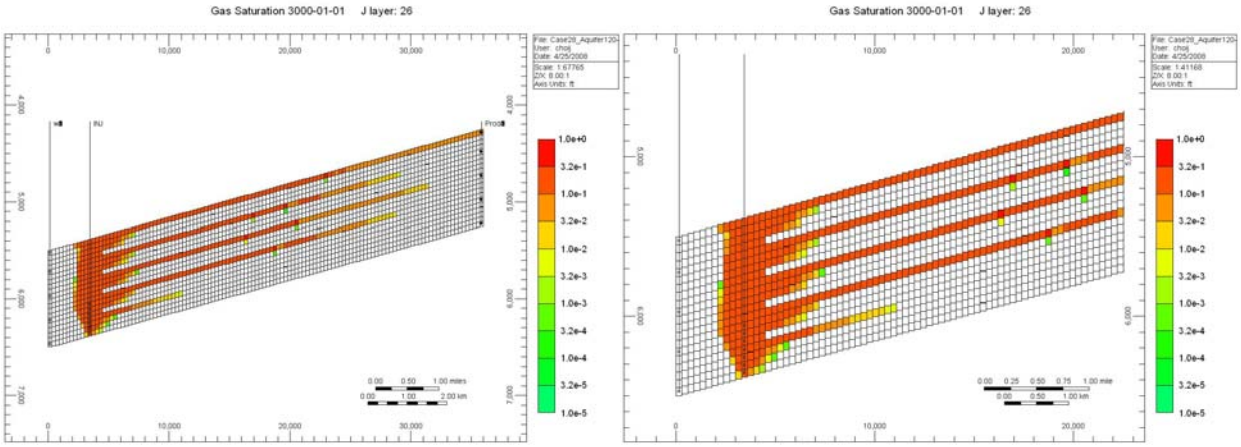

Time = 1,000 yr

29. Case 29: Fixed pressure 100-0-0 (CO_2-CH_4-N_2) in volume

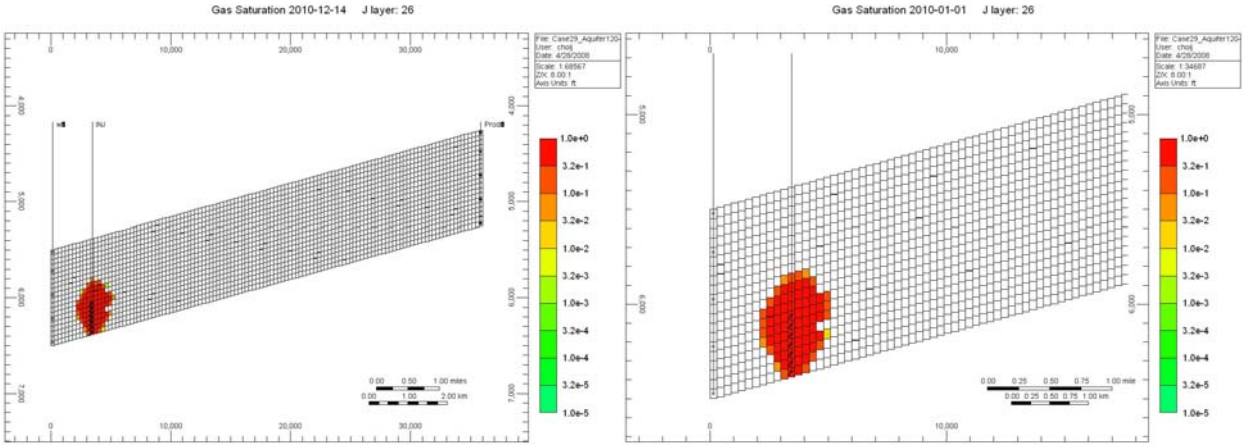

Time = 10 yr

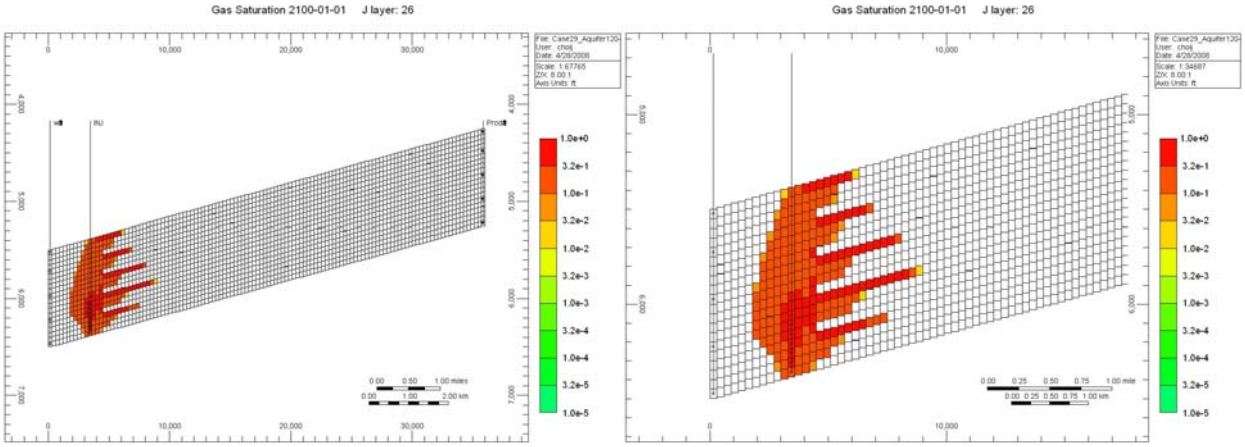

Time = 100 yr

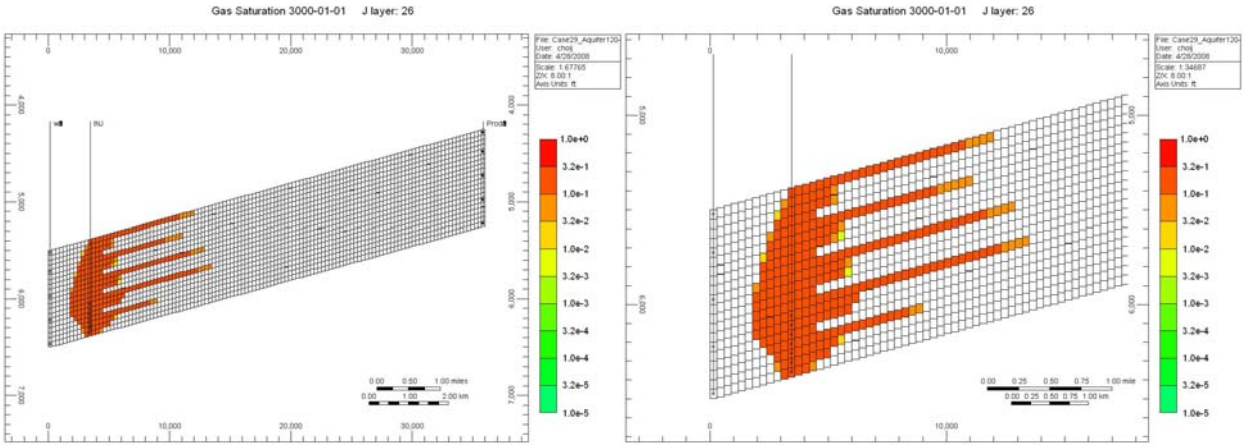

Time = 1,000 yr

30. Case 30: Fixed pressure 75-25-0 (CO_2-CH_4-N_2) in volume

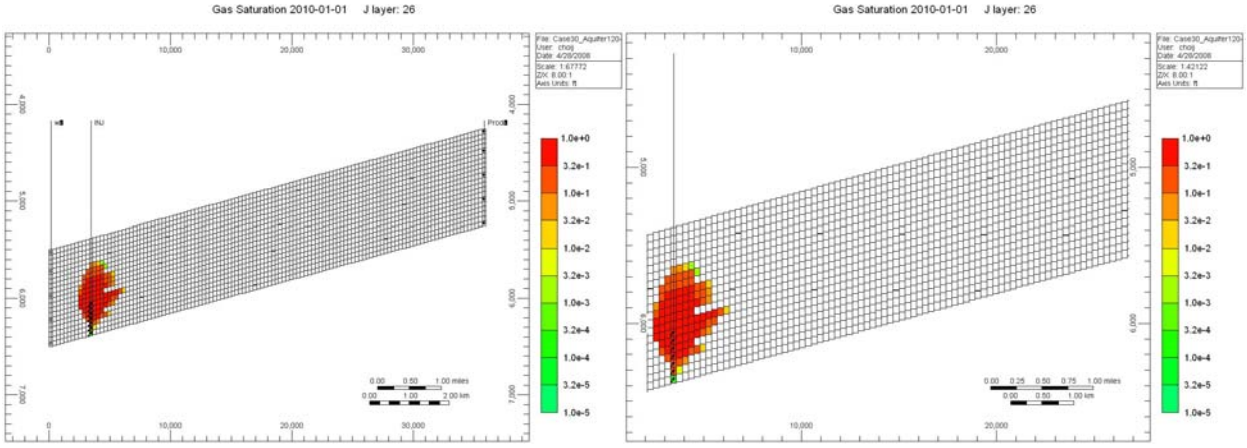

Time = 10 yr

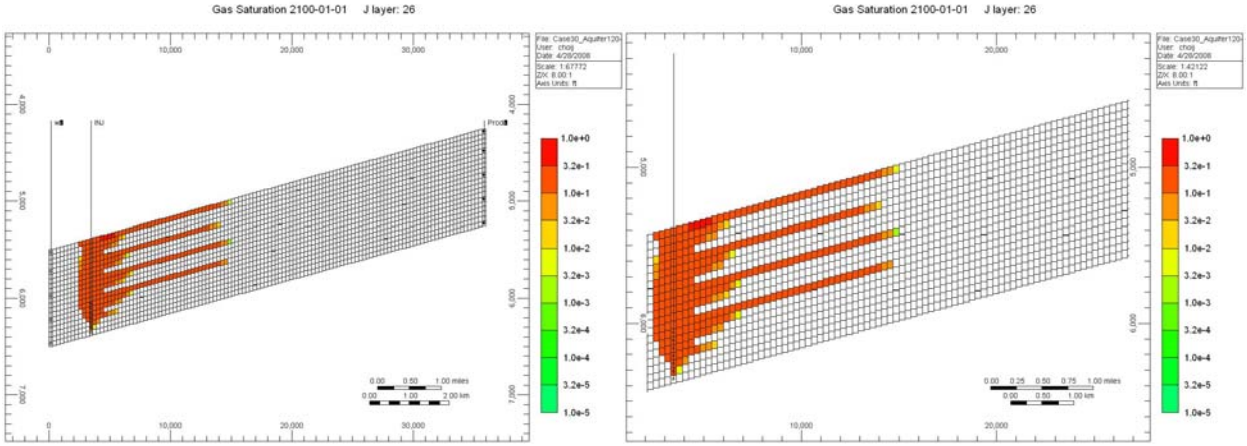

Time = 100 yr

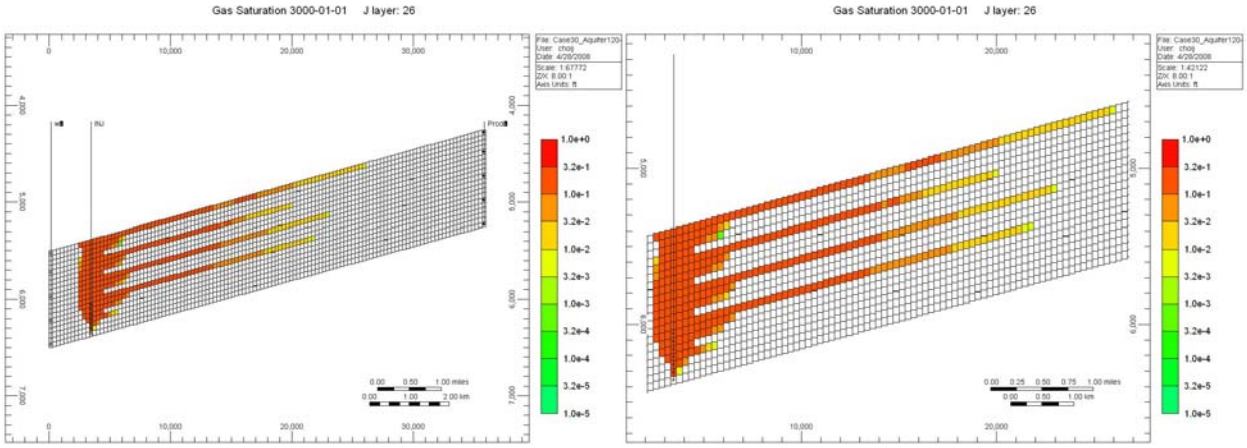

Time = 1,000 yr

31. Case 31: Fixed pressure 75-0-25 (CO_2-CH_4-N_2) in volume

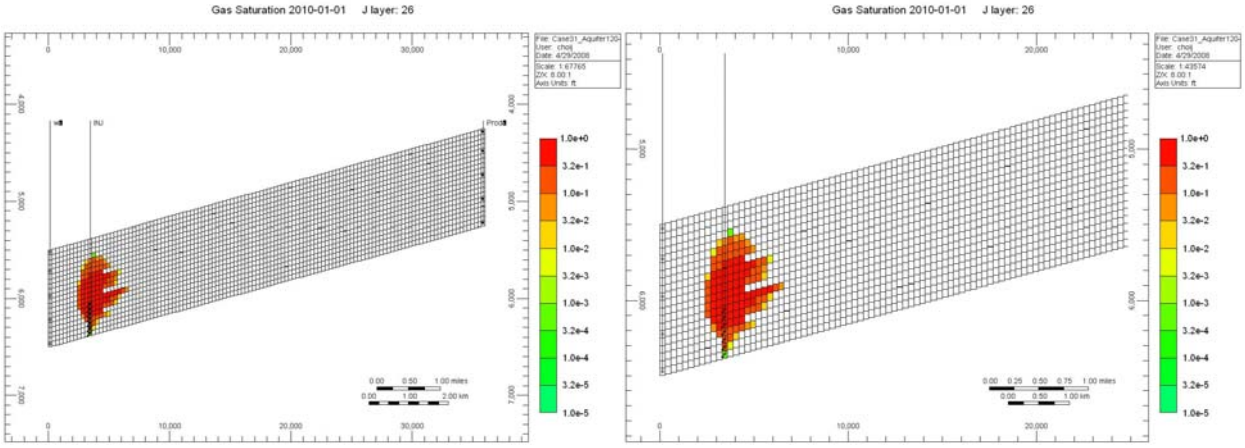

Time = 10 yr

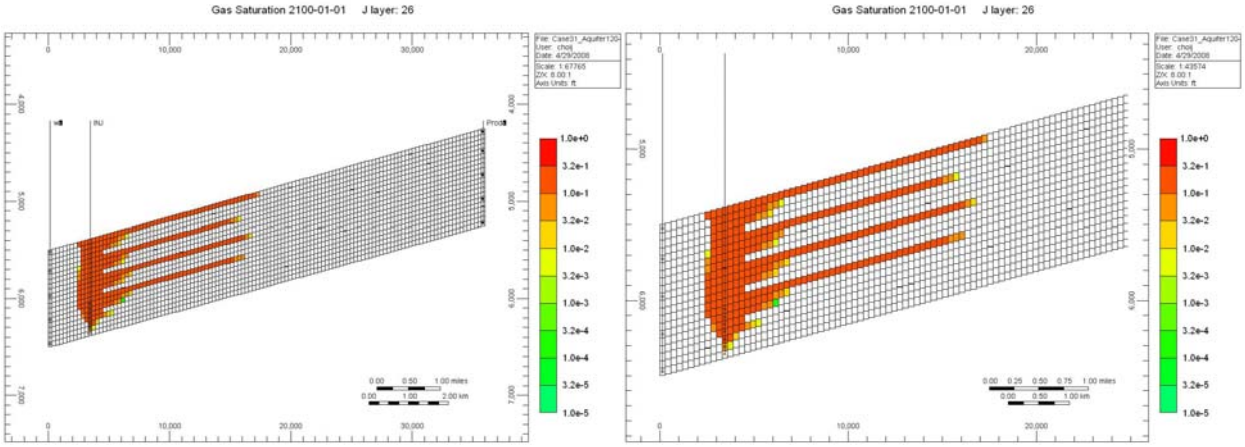

Time = 100 yr

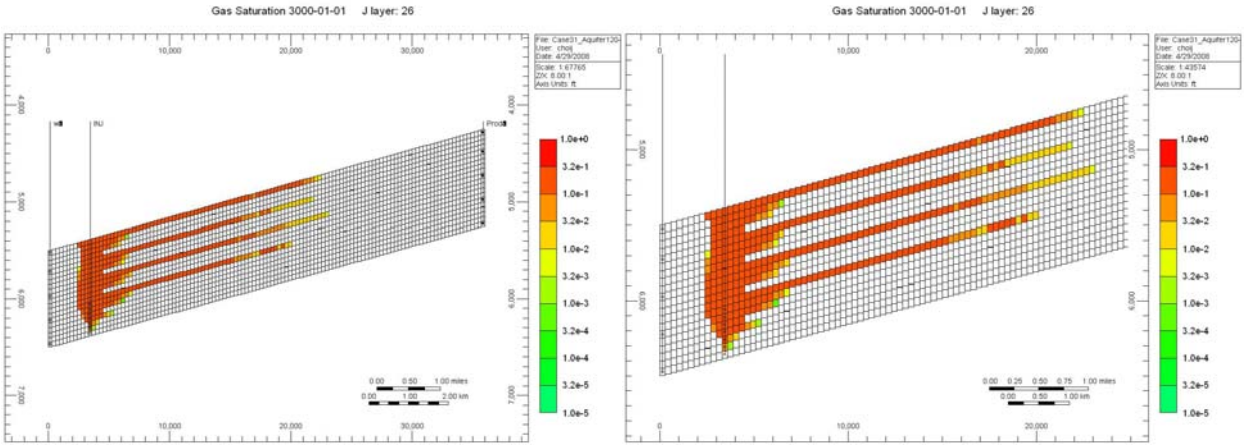

Time = 1,000 yr

32. Case 39: Porosity = 0.2 with 95-2.5-2.5 (CO_2-CH_4-N_2) in volume

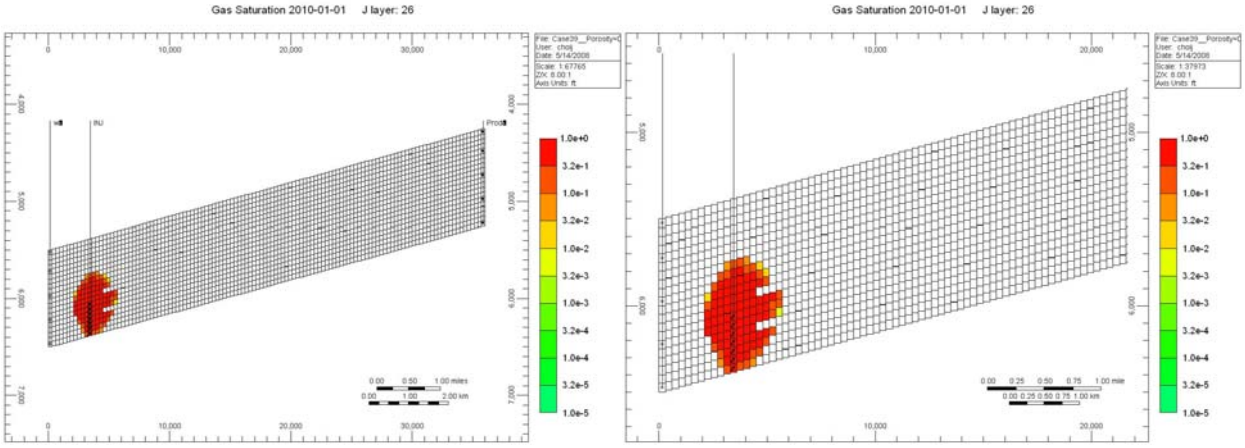

Time = 10 yr

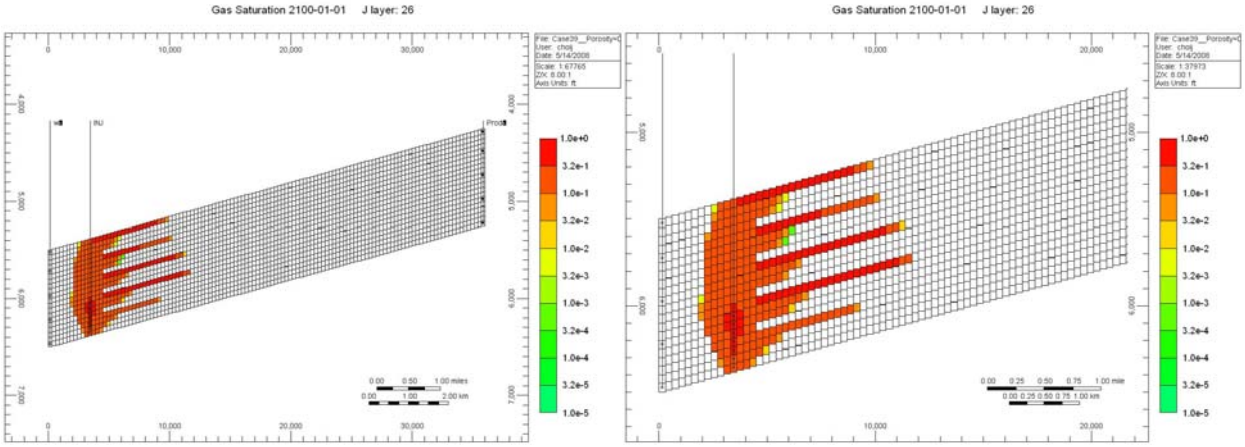

Time = 100 yr

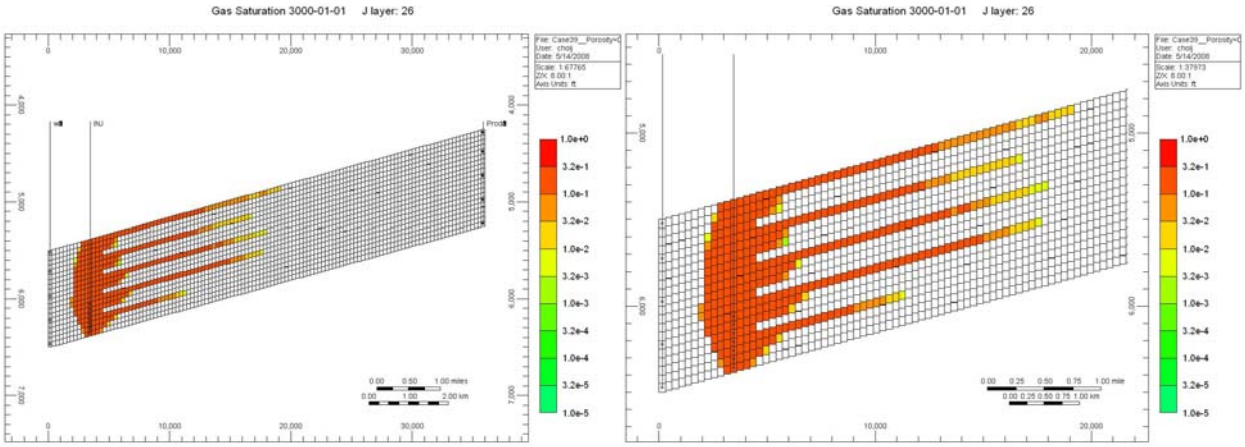

Time = 1,000 yr

33. Case 40: Porosity = 0.3 with 95-2.5-2.5 (CO_2-CH_4-N_2) in volume

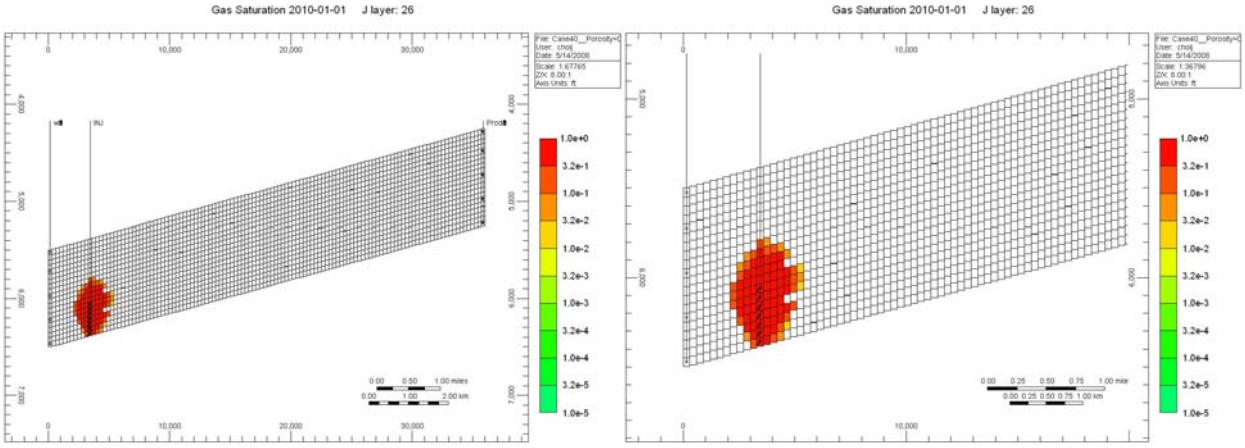

Time = 10 yr

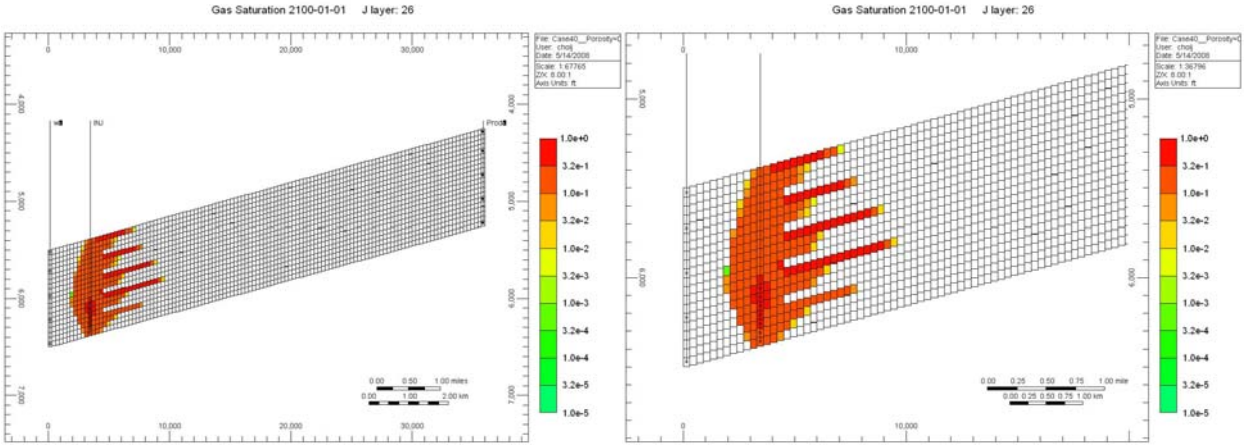

Time = 100 yr

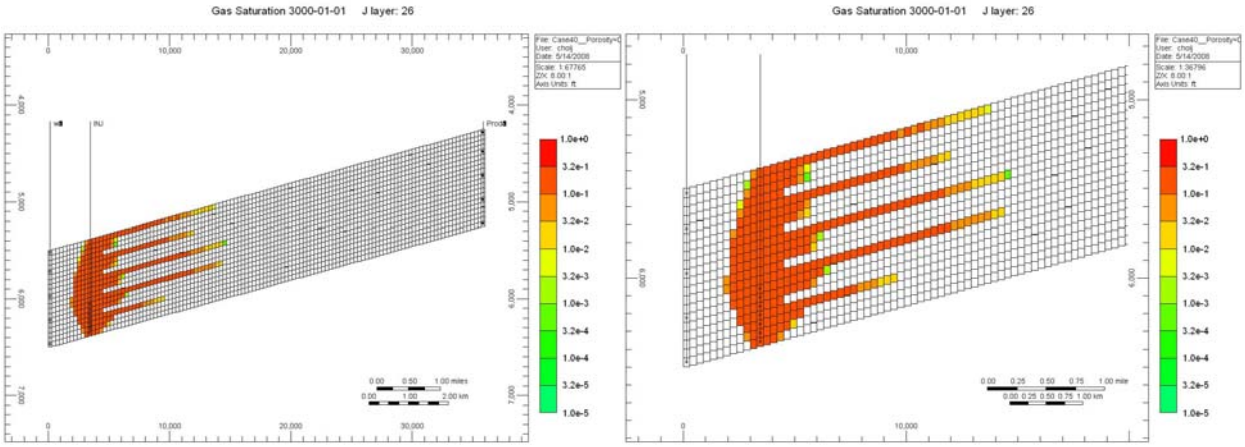

Time = 1,000 yr

34. Case 41: capillary pressure included with 95-2.5-2.5 (CO_2-CH_4-N_2) in volume

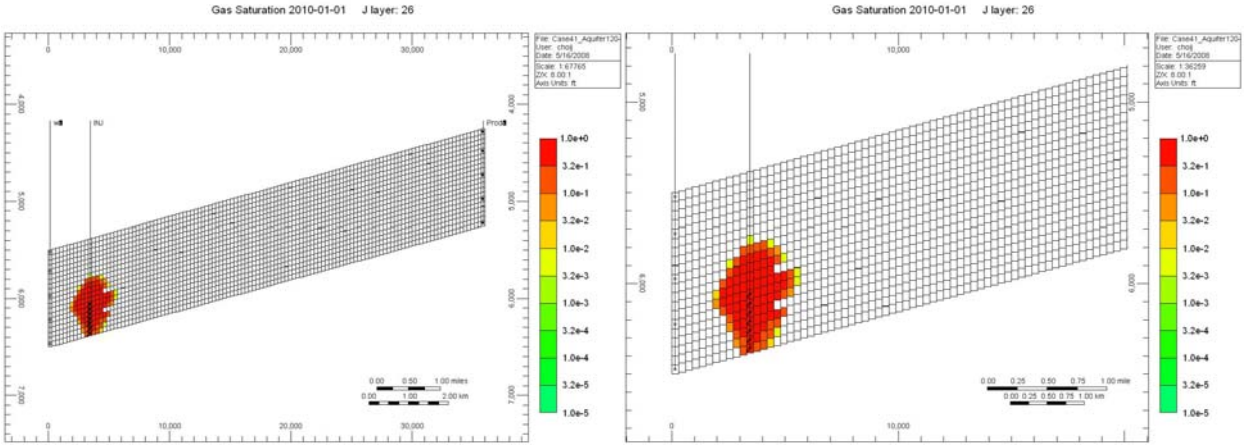

Time = 10 yr

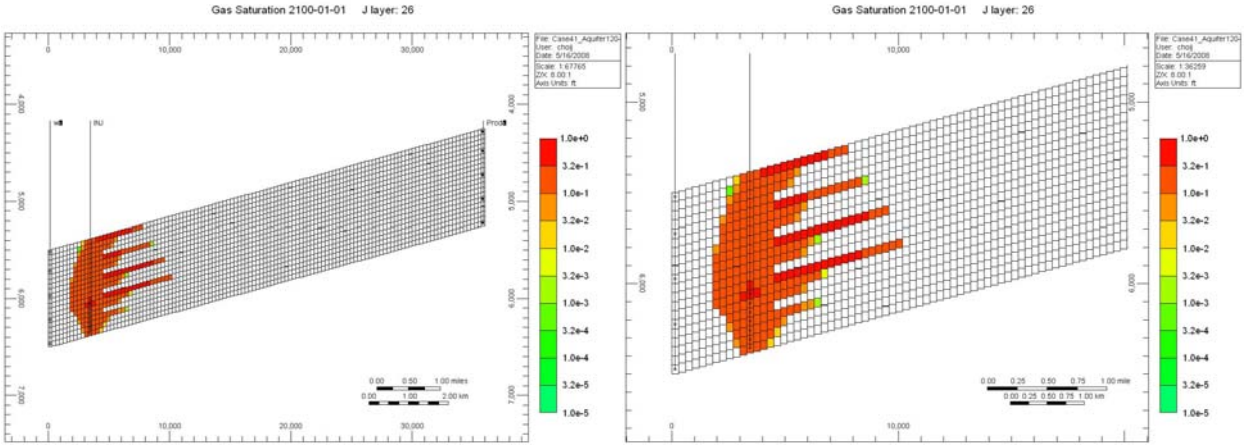

Time = 100 yr

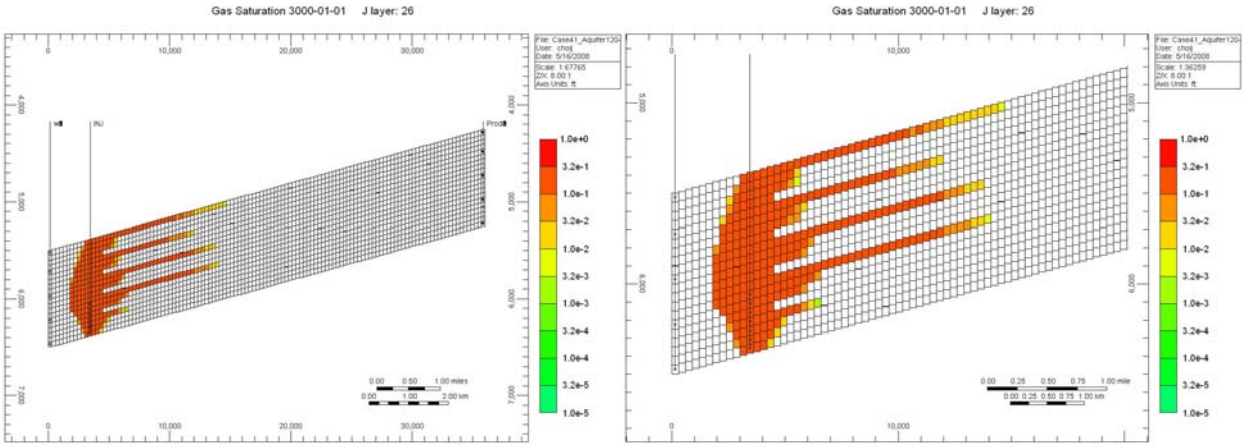

Time = 1,000 yr

35. Case 1: 95-5-0 (CO_2-CH_4-N_2) in volume

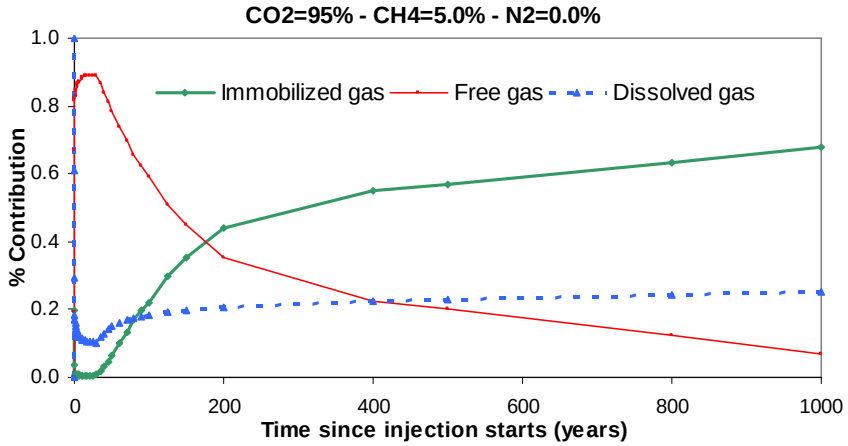

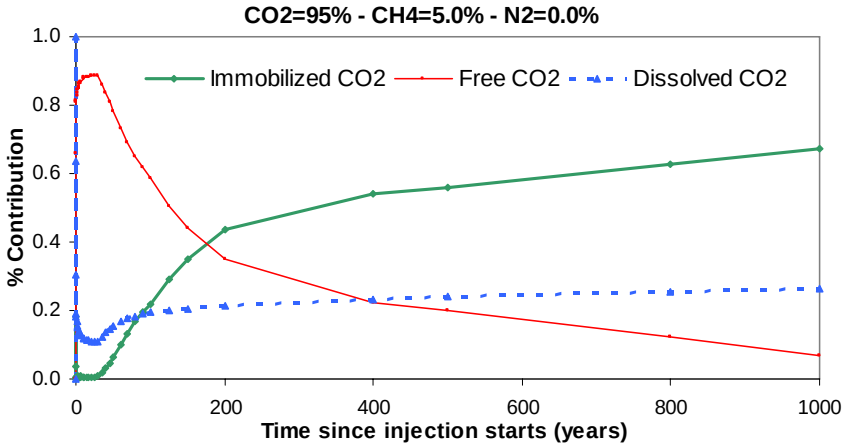

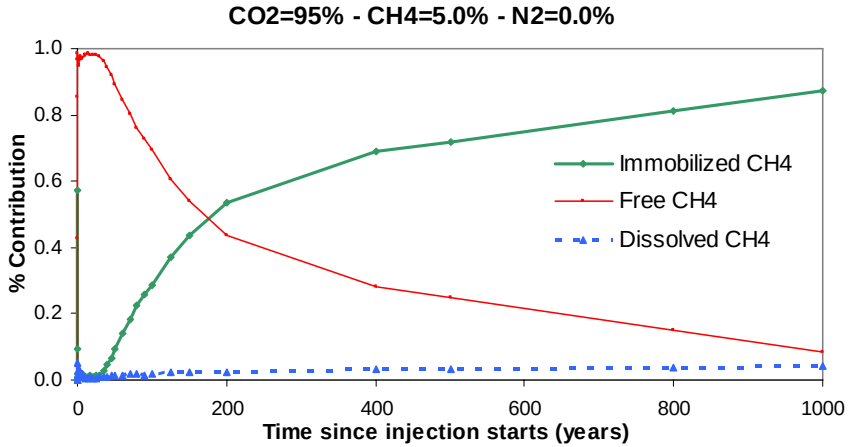

36. Case 2: 95-0-5 (CO_2-CH_4-N_2) in volume

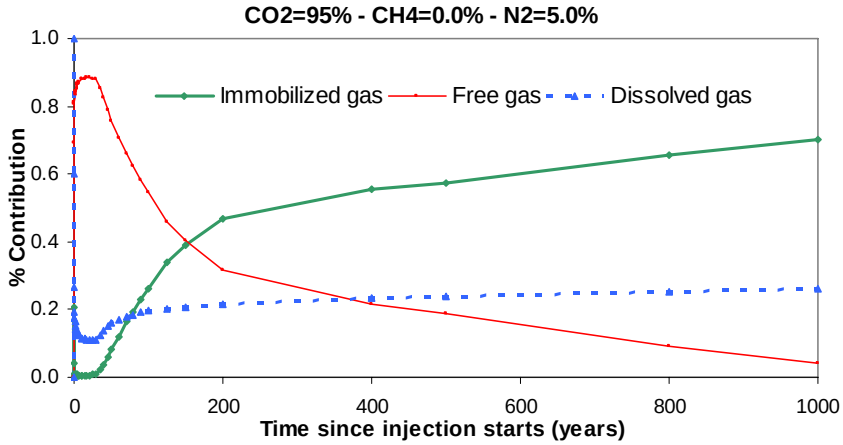

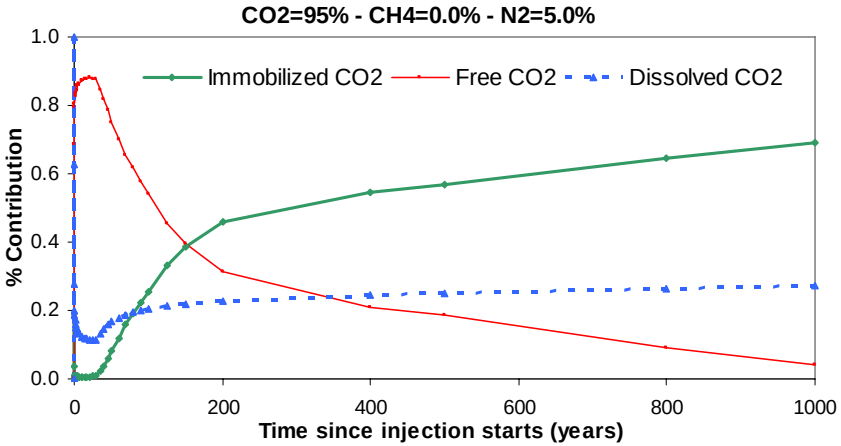

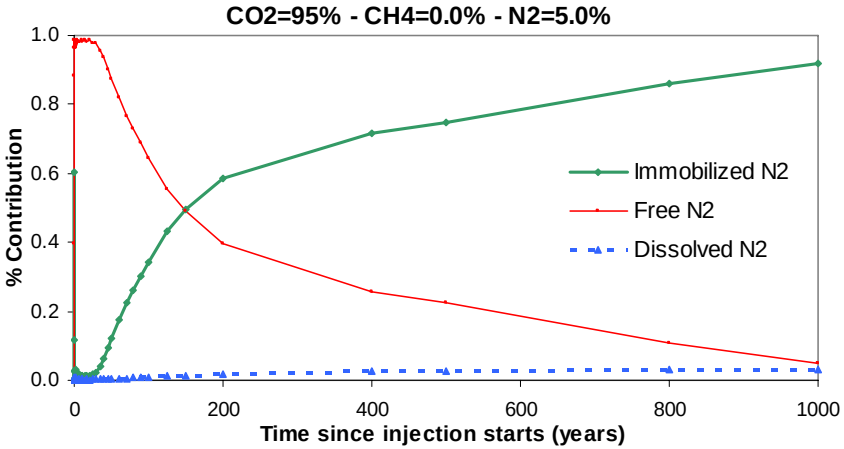

37. Case 3: 95-2.5-2.5 (CO_2-CH_4-N_2) in volume

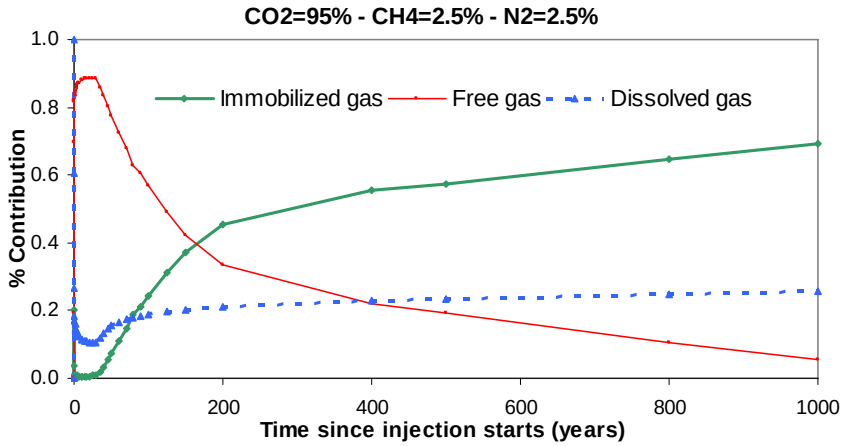

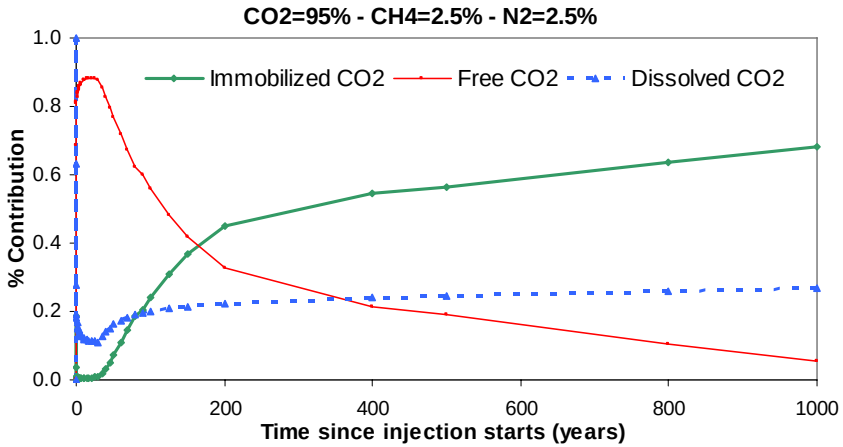

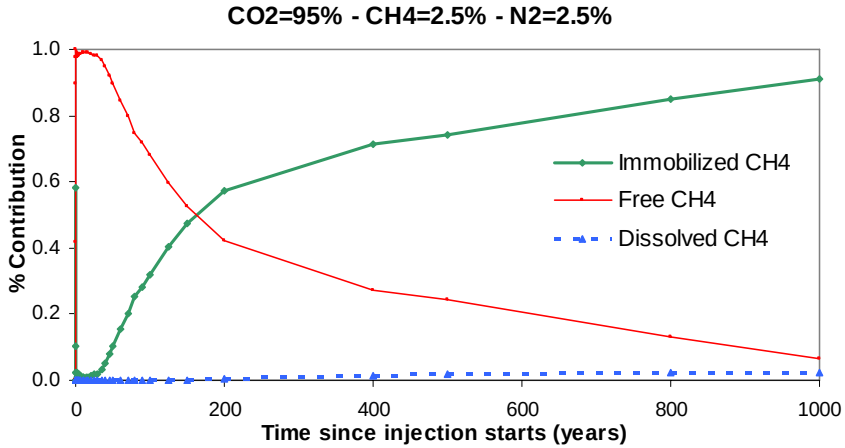

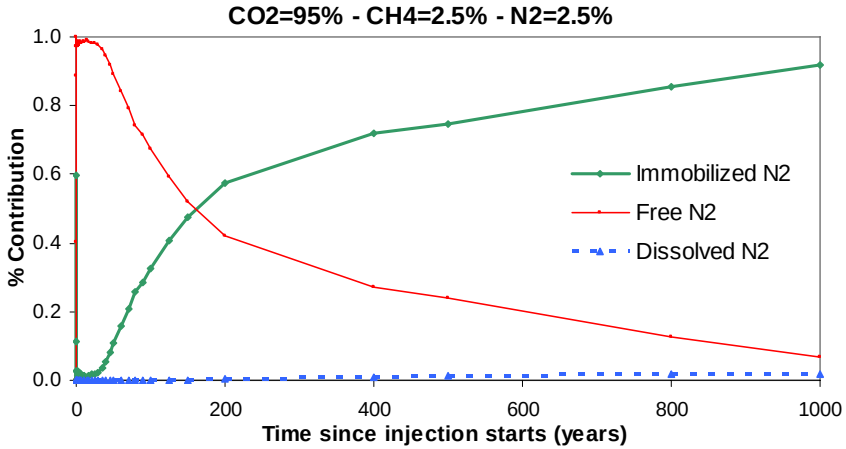

38. Case 4: 90-10-0 (CO_2-CH_4-N_2) in volume

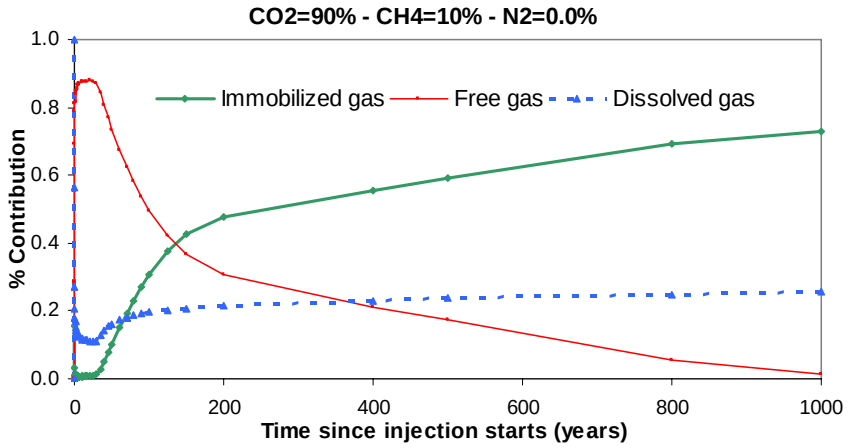

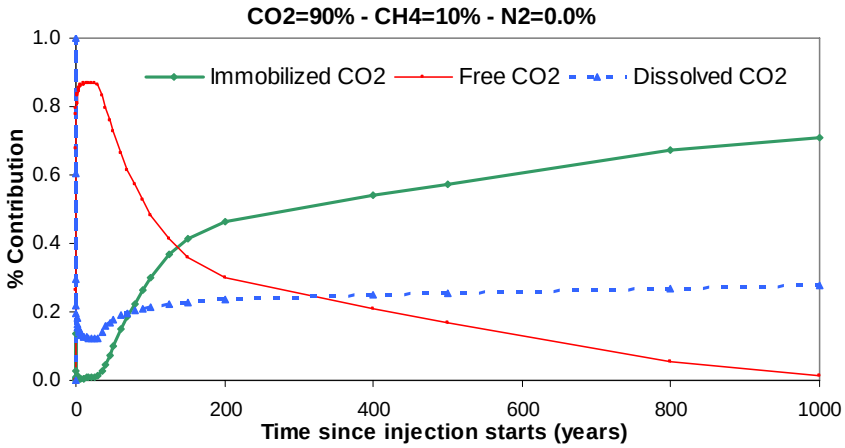

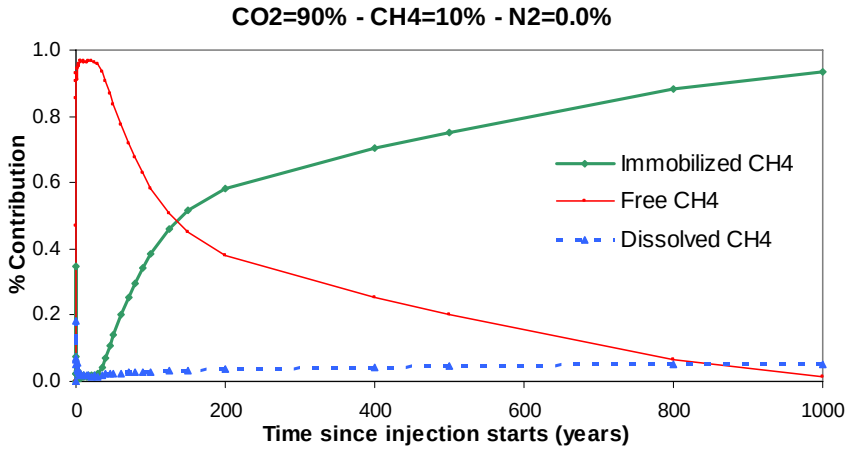

39. Case 5: 90-0-10 (CO_2-CH_4-N_2) in volume

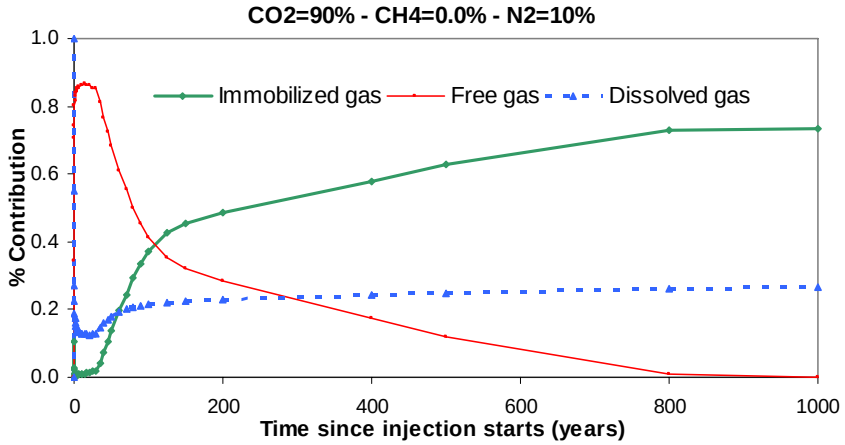

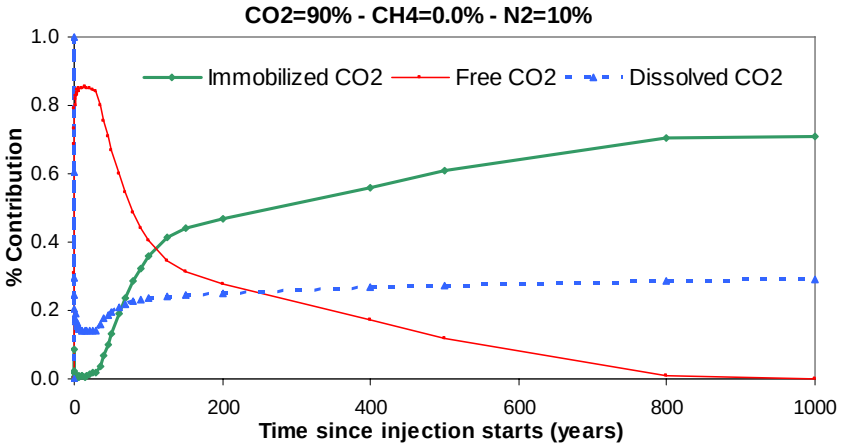

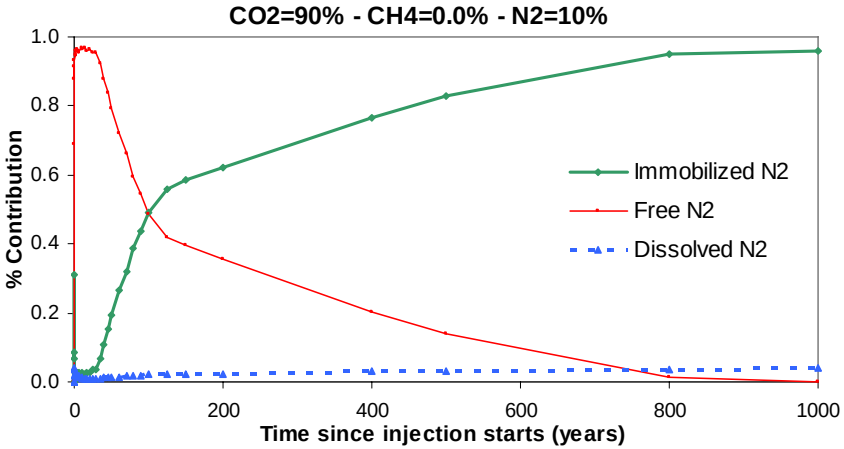

40. Case 6: 90-5-5 (CO_2-CH_4-N_2) in volume

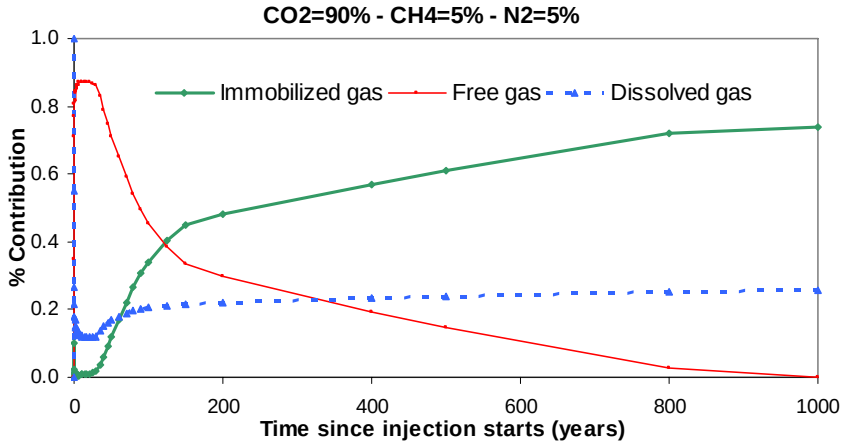

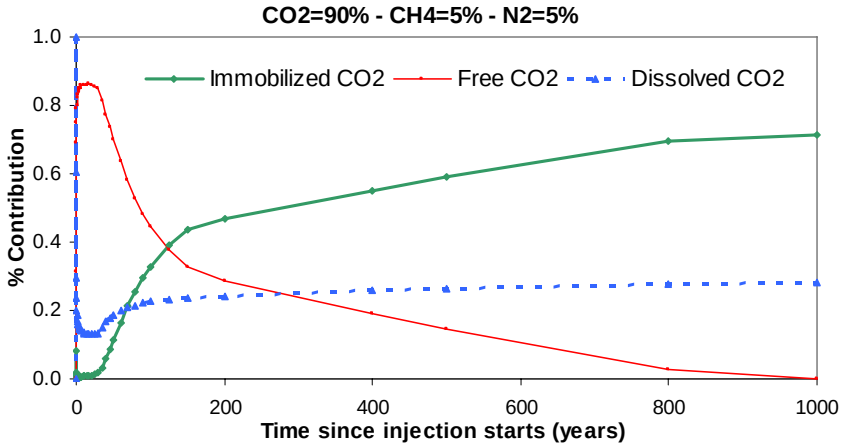

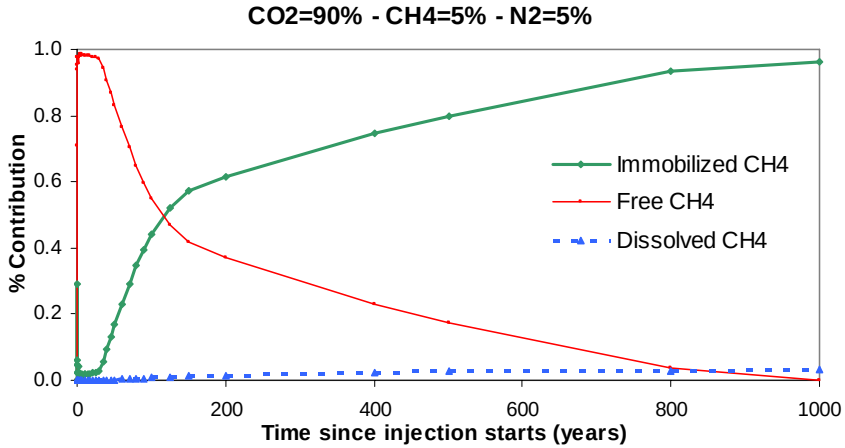

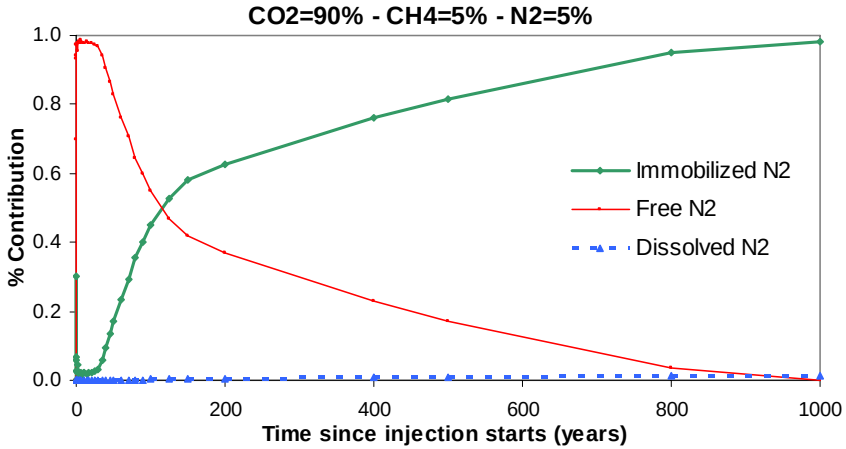

41. Case 7: 85-15-0 (CO_2-CH_4-N_2) in volume

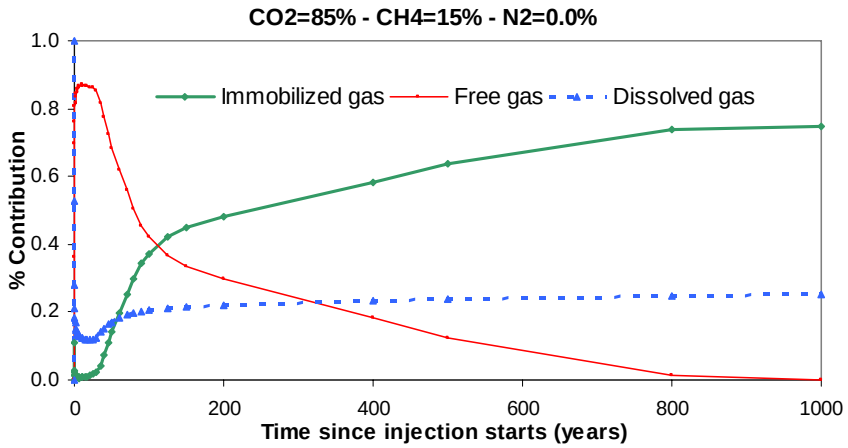

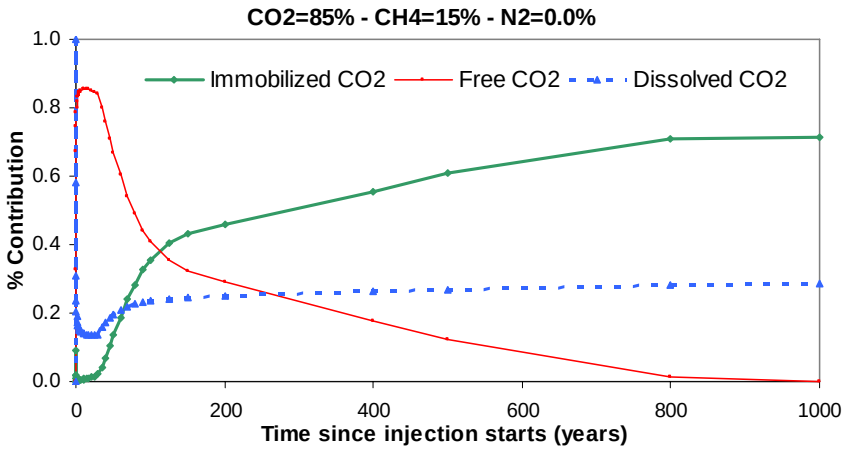

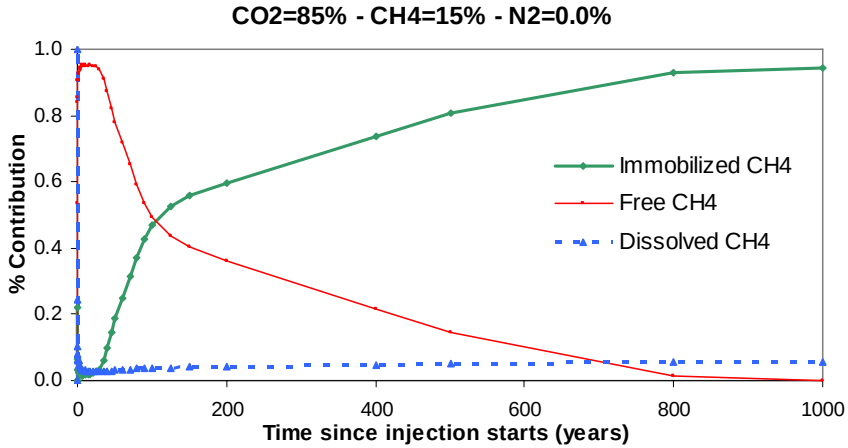

42. Case 8: 85-0-15 (CO_2-CH_4-N_2) in volume

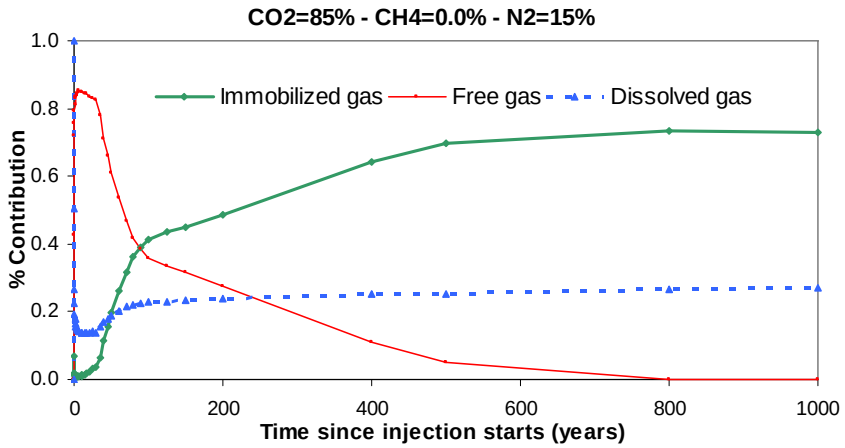

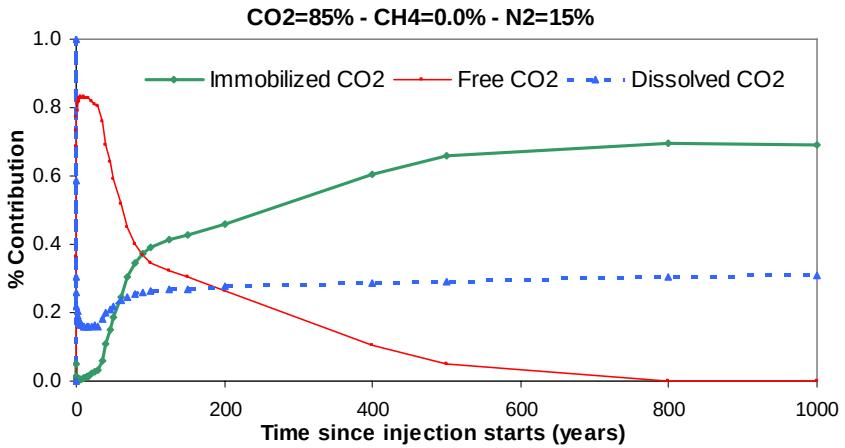

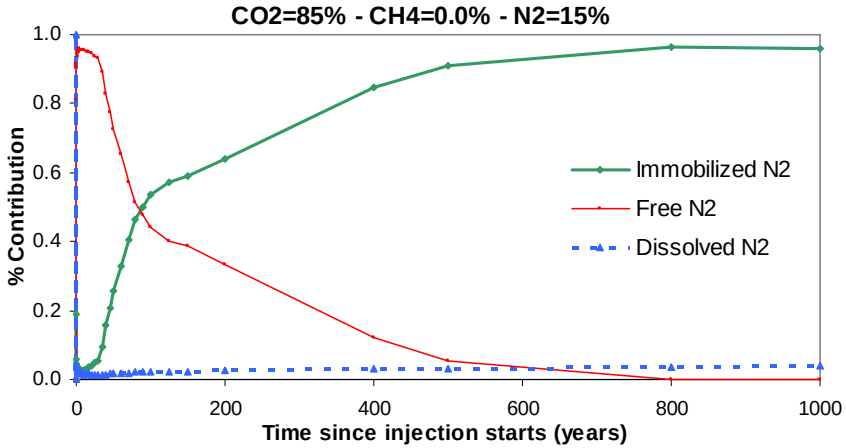

43. Case 9: 85-7.5-7.5 (CO_2-CH_4-N_2) in volume

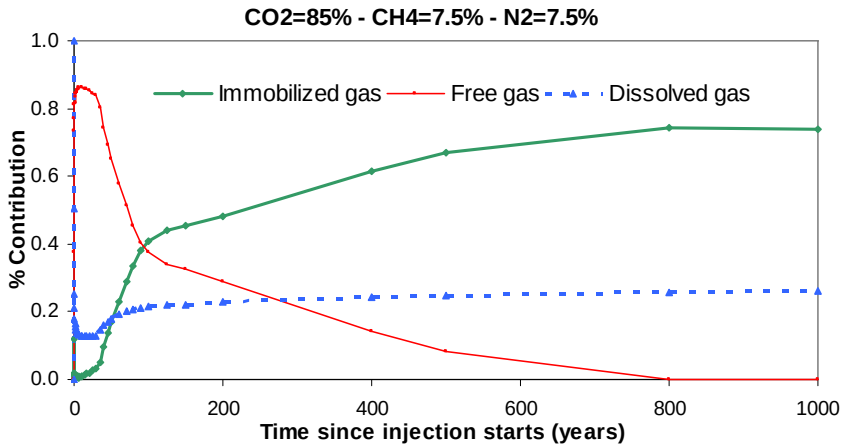

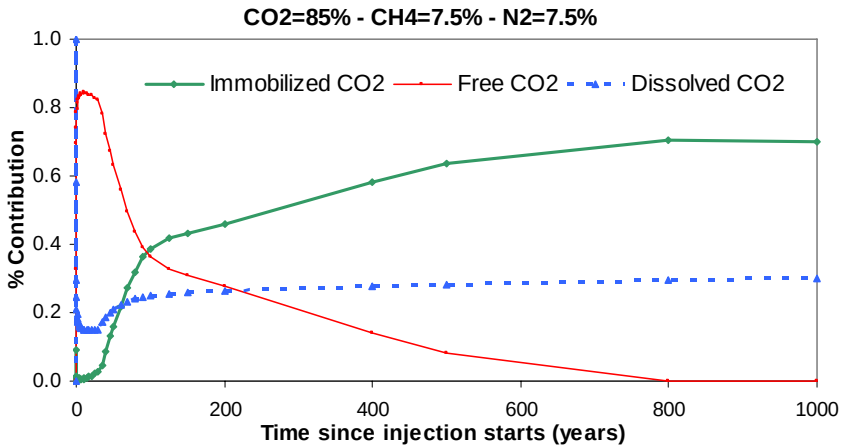

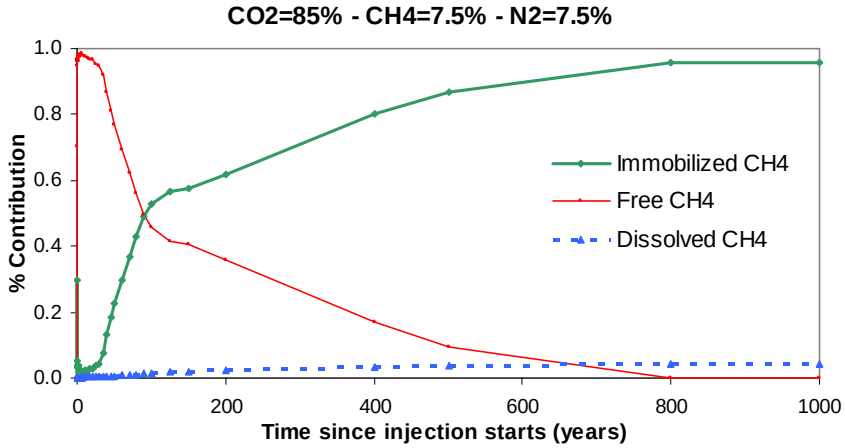

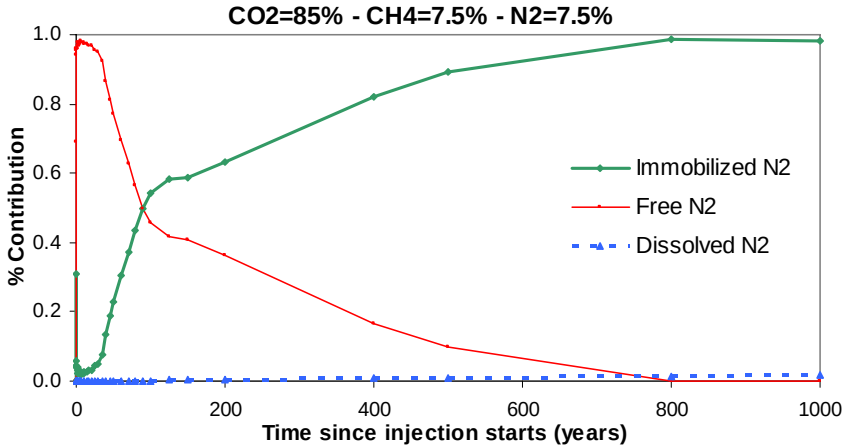

44. Case 10: 80-20-0 (CO_2-CH_4-N_2) in volume

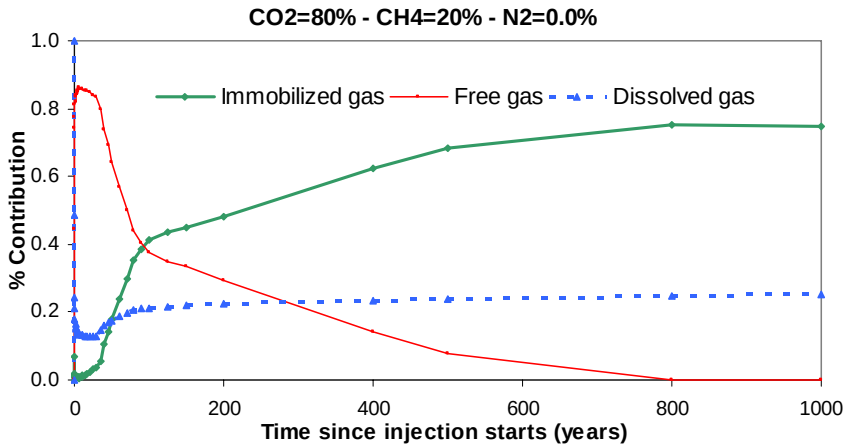

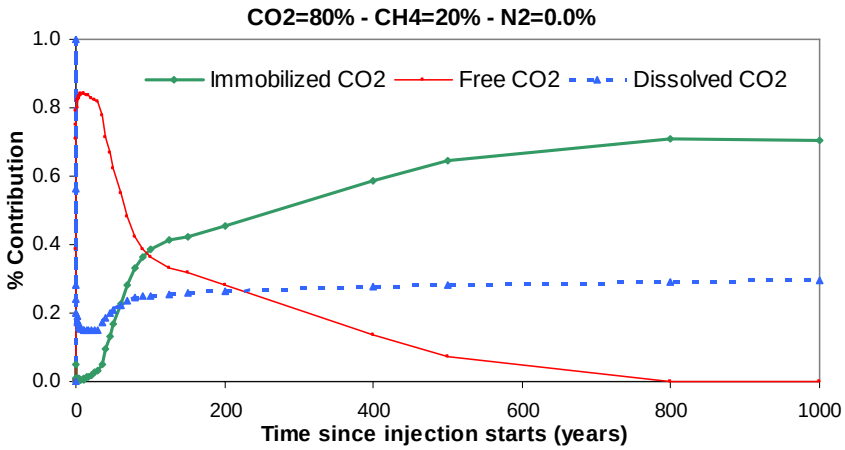

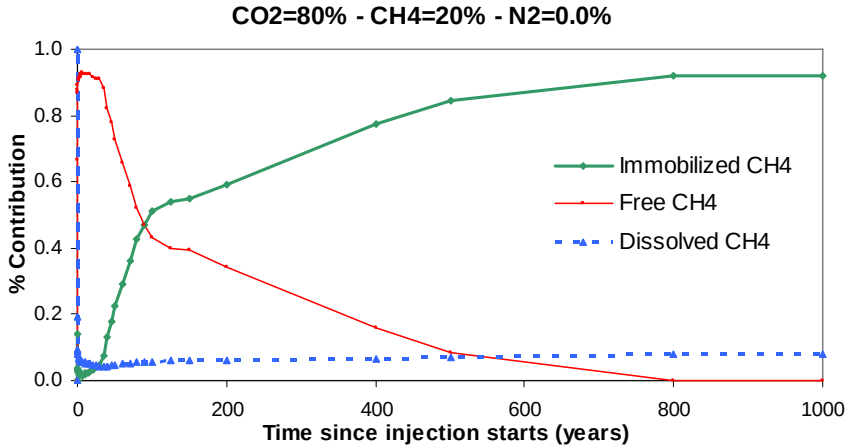

45. Case 11: 80-0-20 (CO_2-CH_4-N_2) in volume

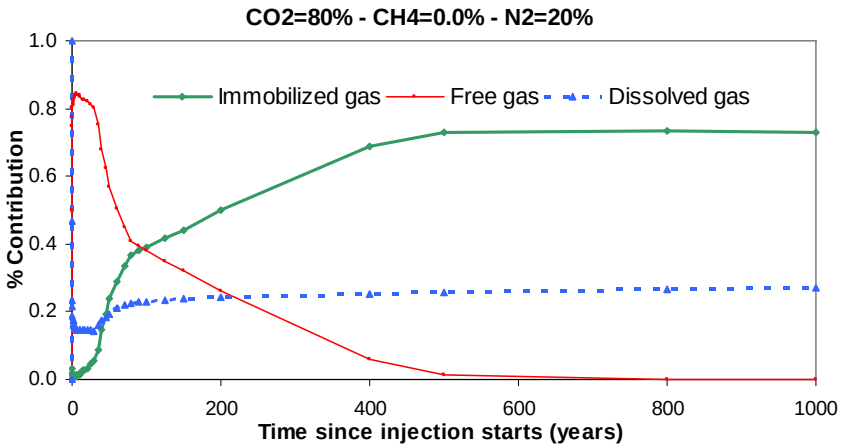

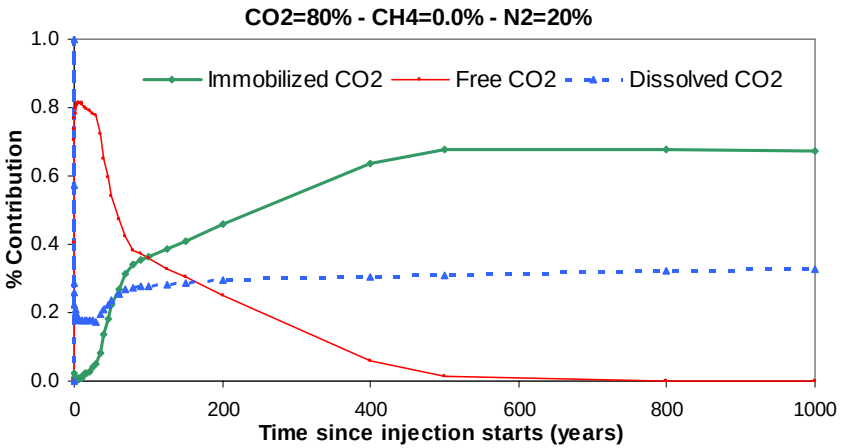

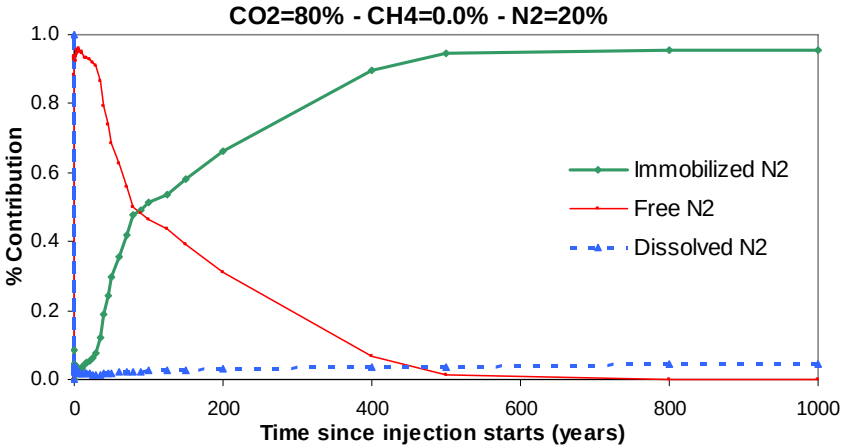

46. Case 12: 80-10-10 (CO_2-CH_4-N_2) in volume

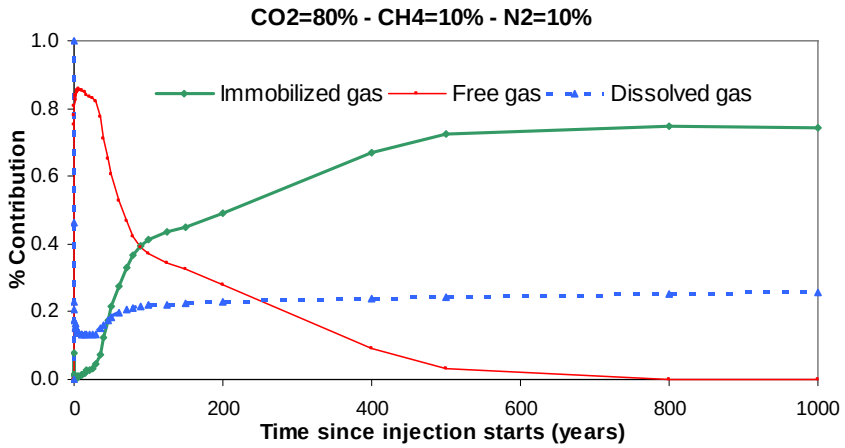

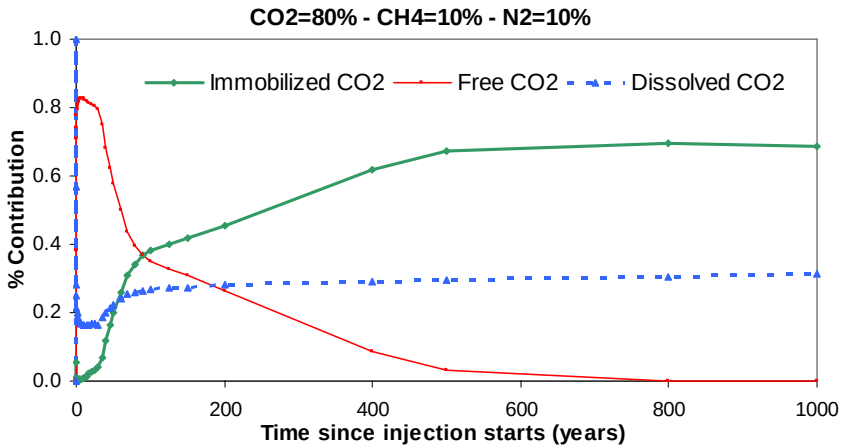

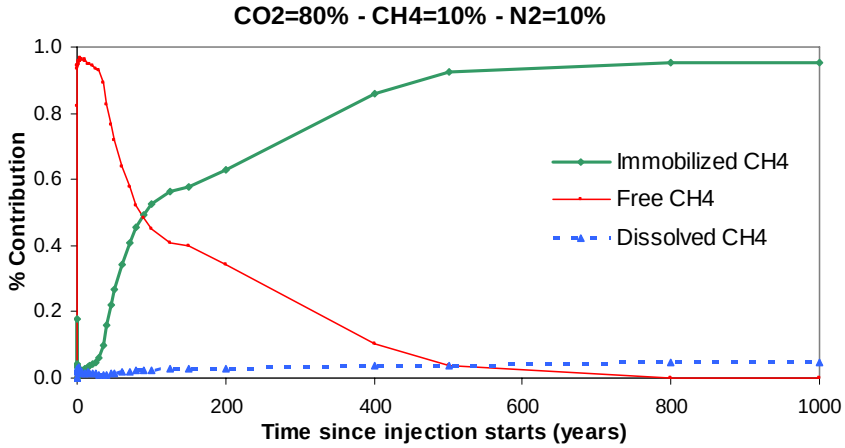

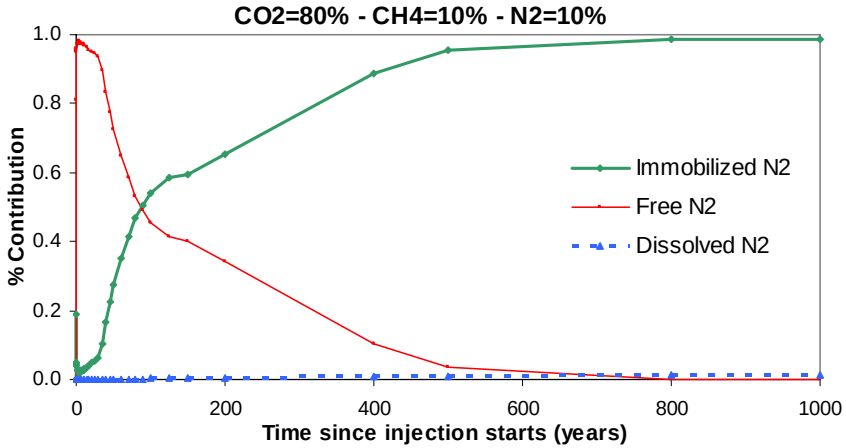

47. Case 13: 75-25-0 (CO_2-CH_4-N_2) in volume

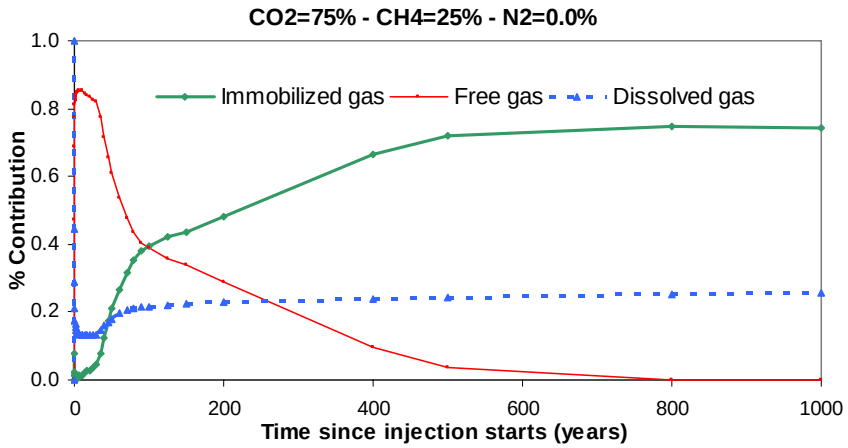

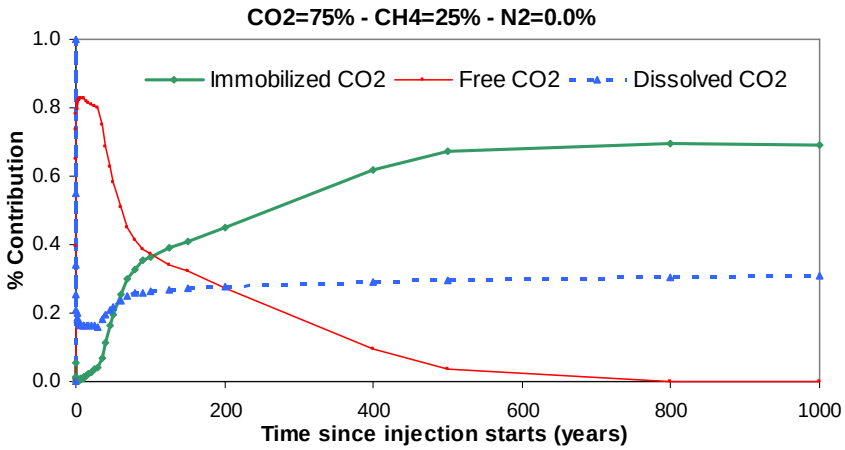

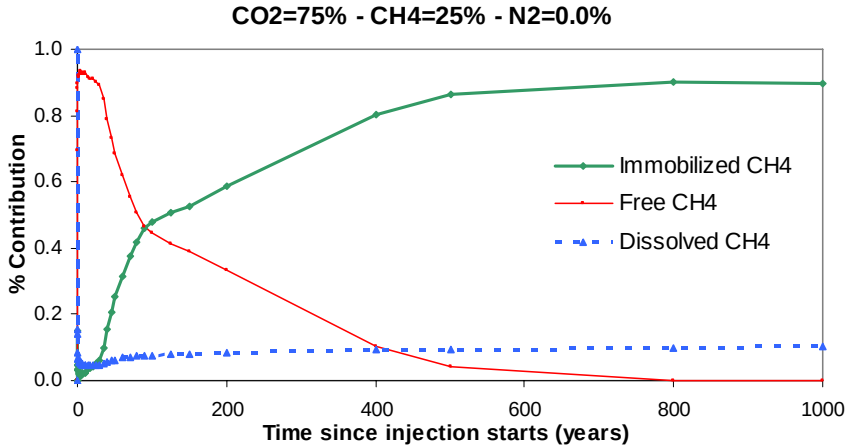

48. Case 14: 75-0-25 (CO_2-CH_4-N_2) in volume

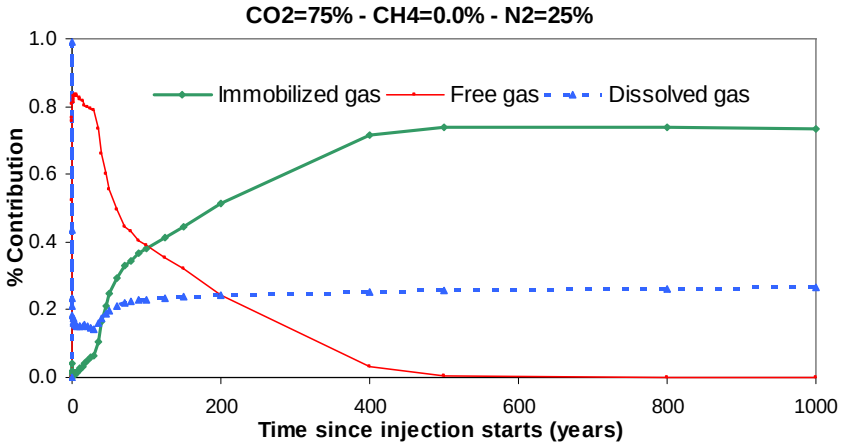

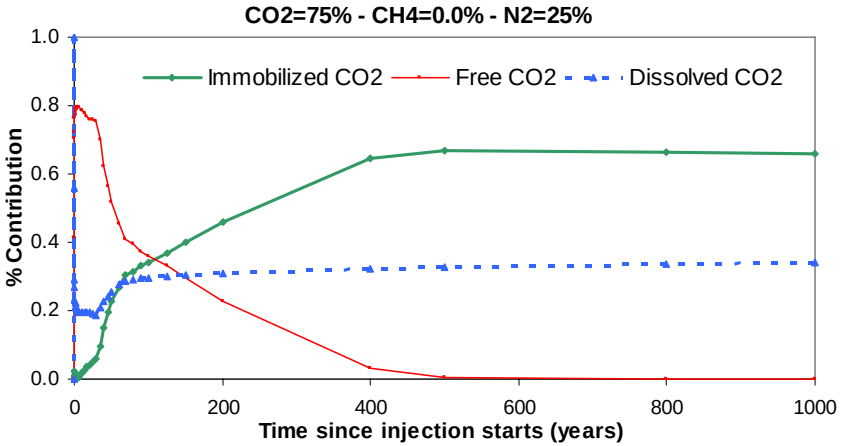

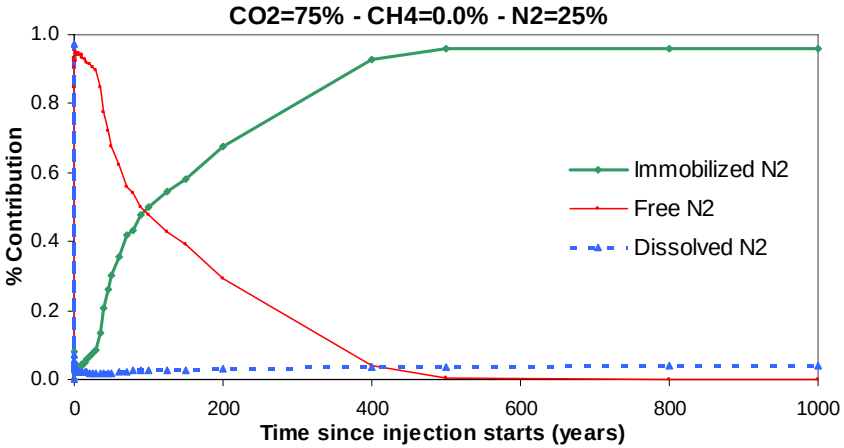

49. Case 15: 75-12.5-12.5 (CO_2-CH_4-N_2) in volume

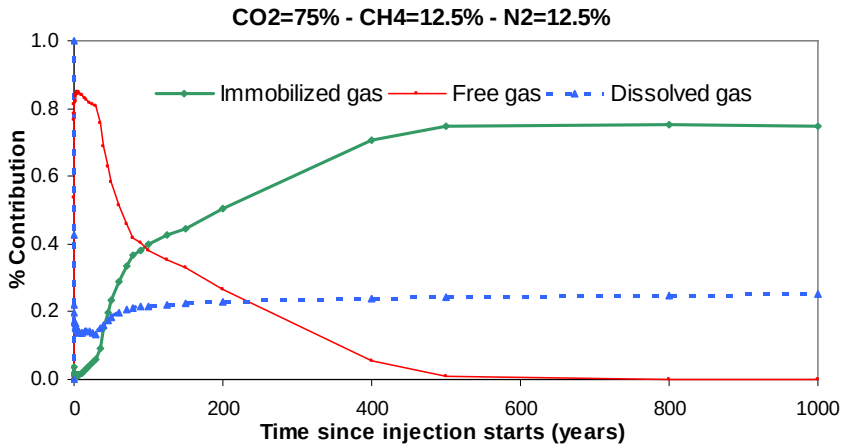

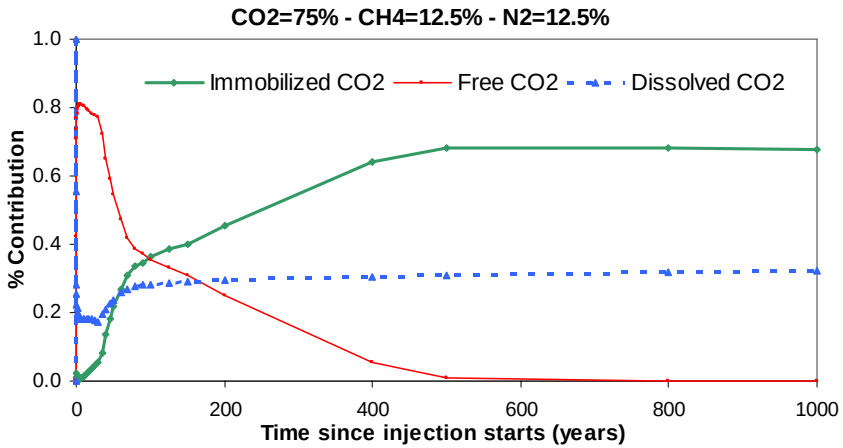

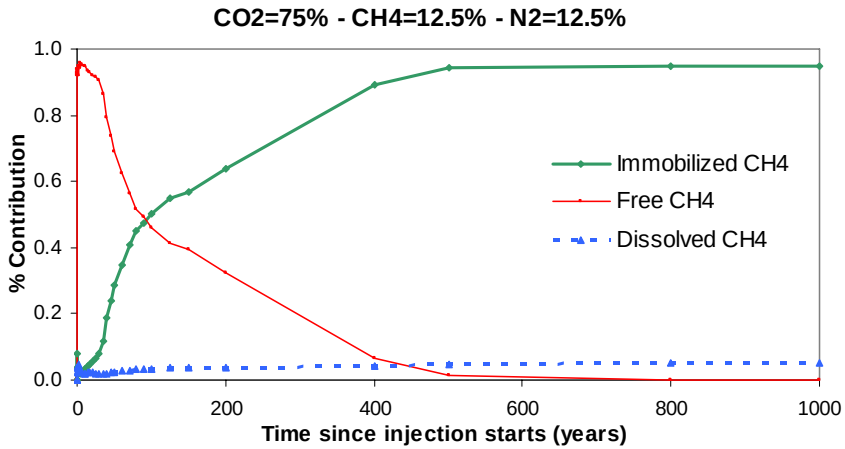

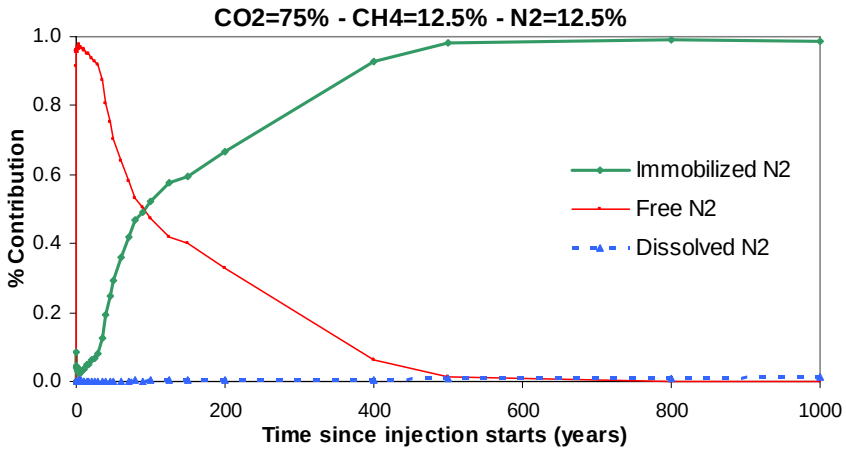

50. Case 16: 100-0-0 (CO_2-CH_4-N_2)

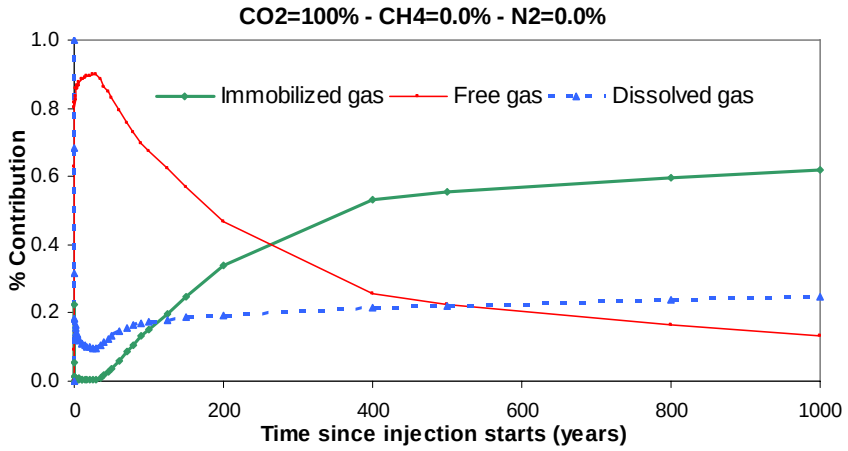

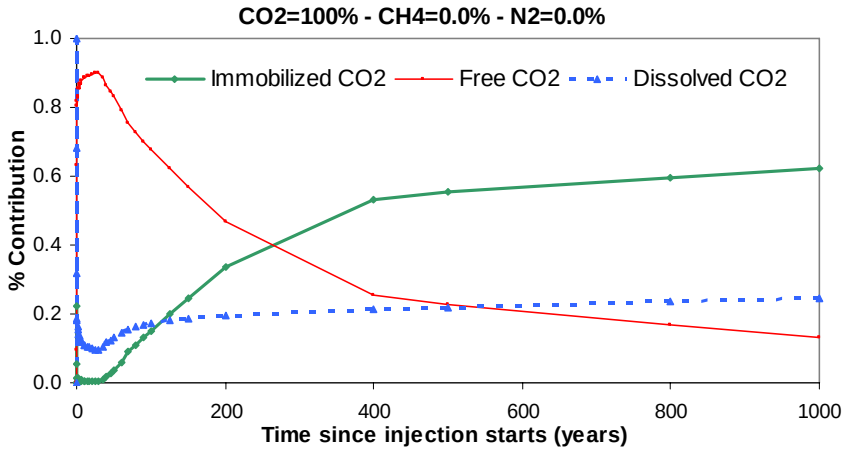

51. Case 17: 75-25-0 (CO_2-CH_4-N_2) in mass

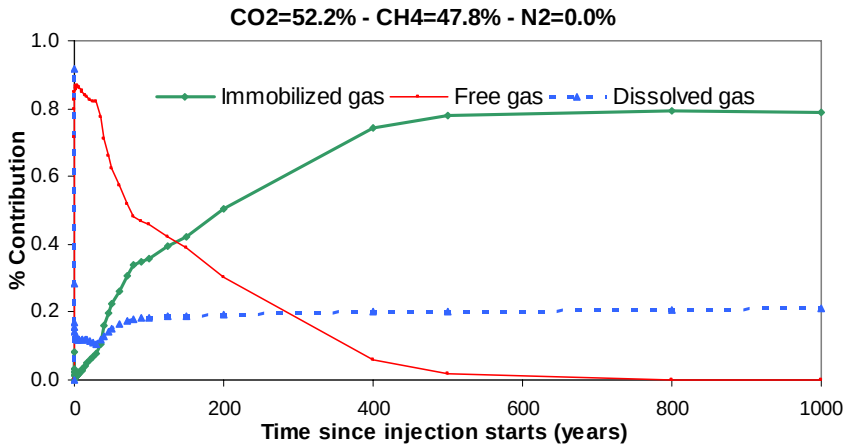

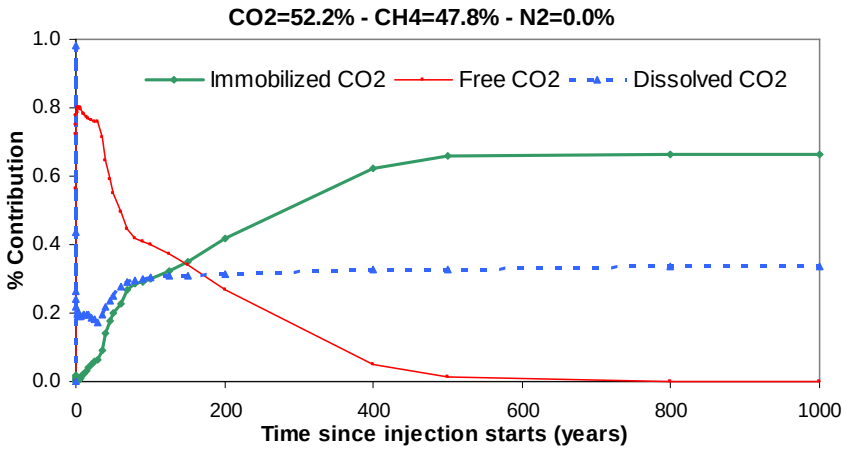

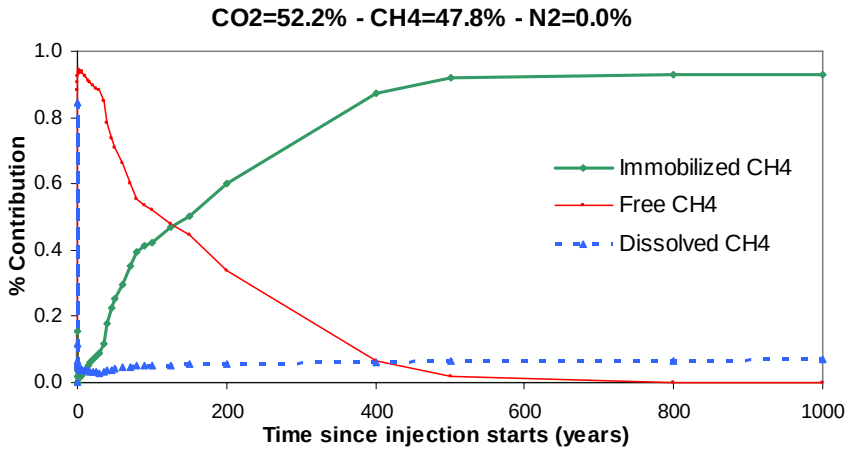

52. Case 18: 75-0-25 (CO_2-CH_4-N_2) in mass

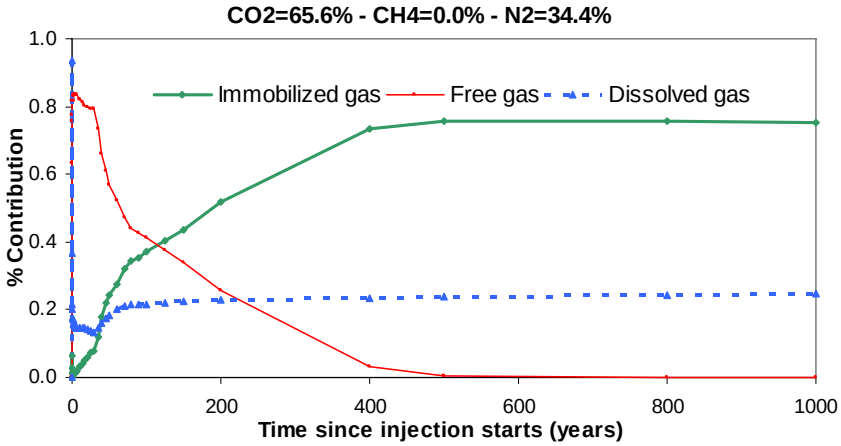

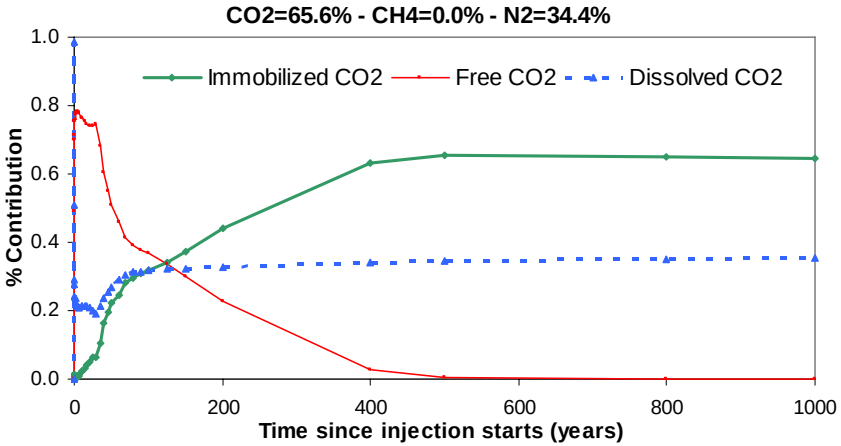

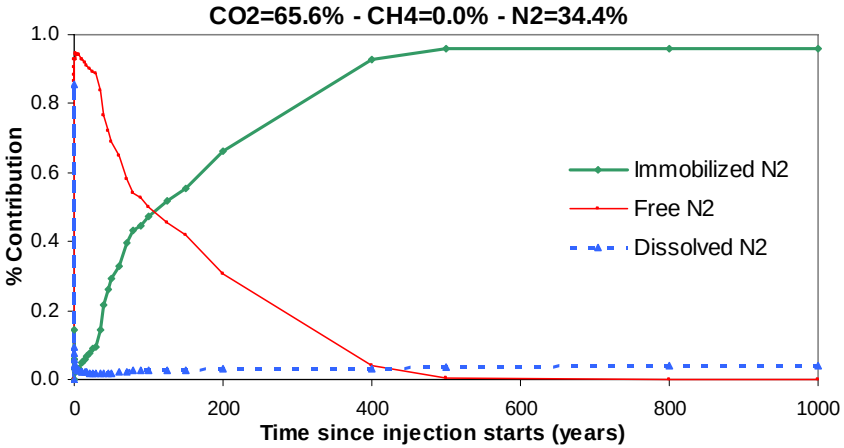

53. Case 19: Dip = 1°

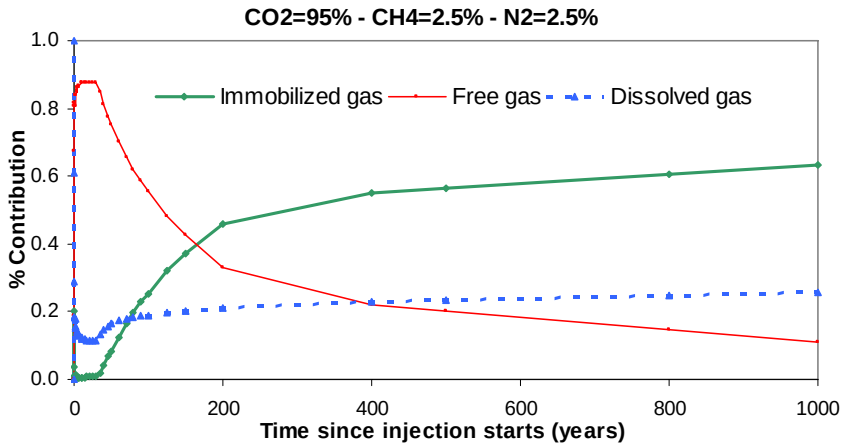

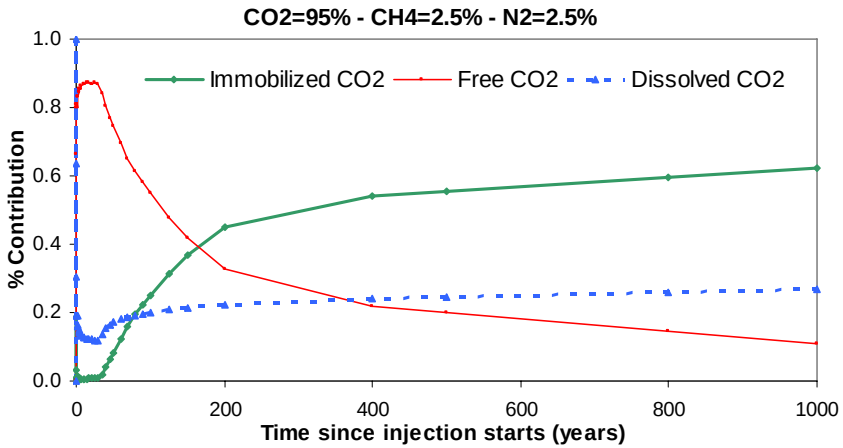

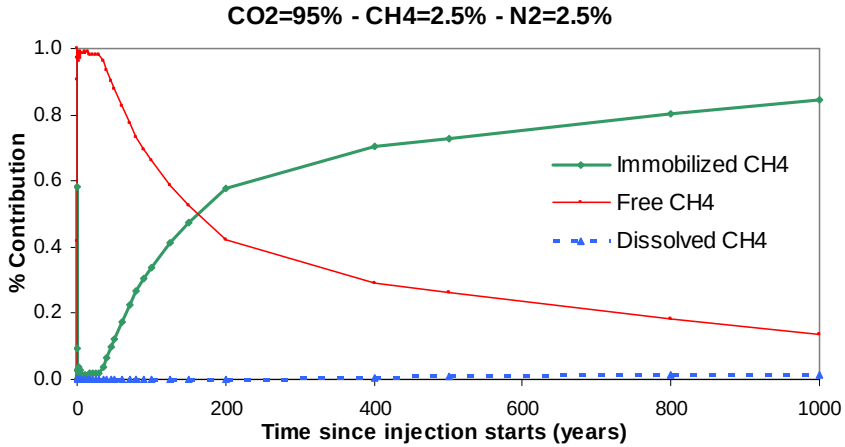

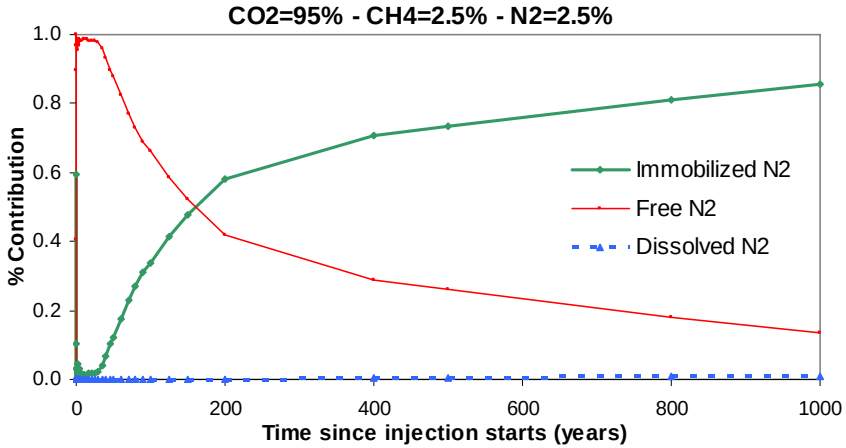

54. Case 20: Dip = 5°

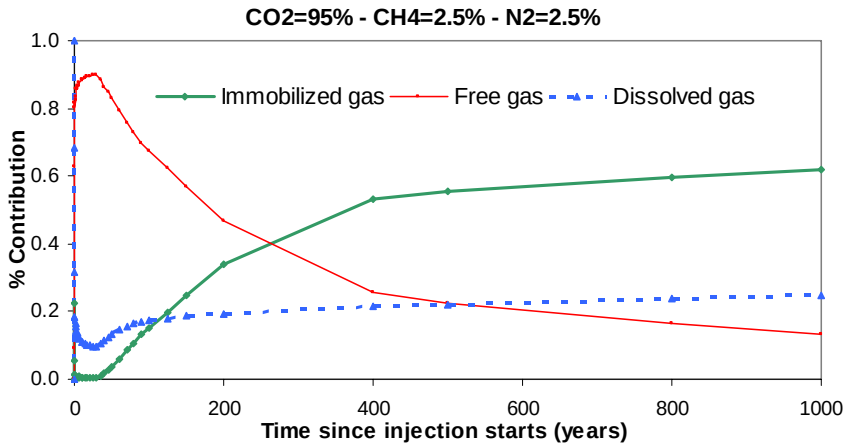

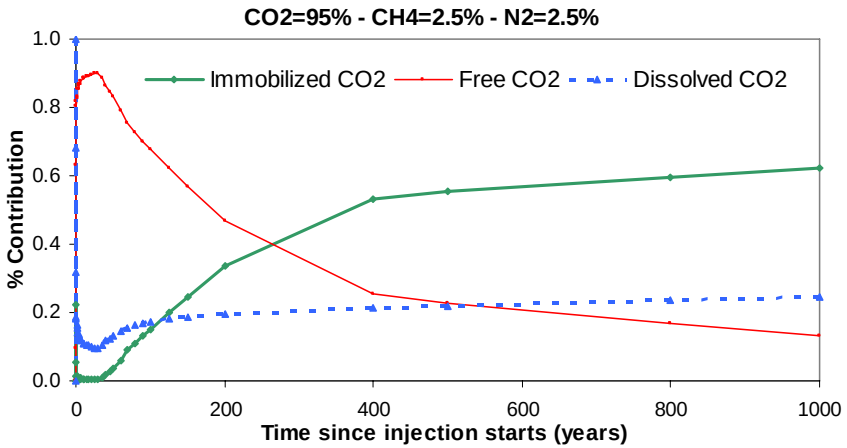

55. Case 21: Permeability in I direction = 100 md

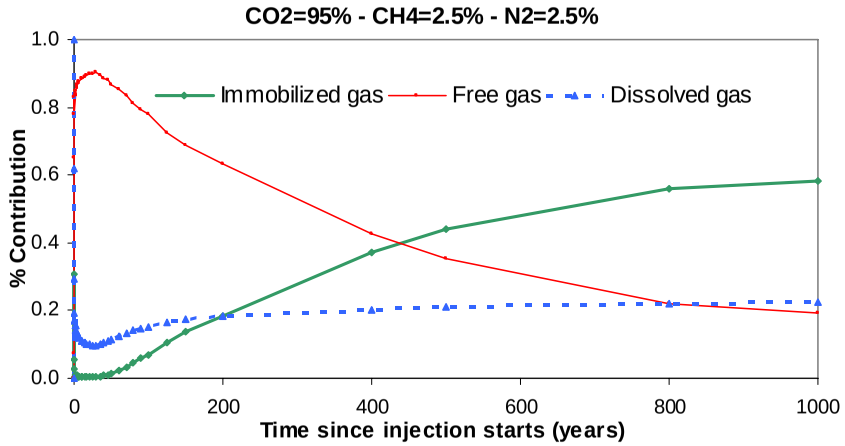

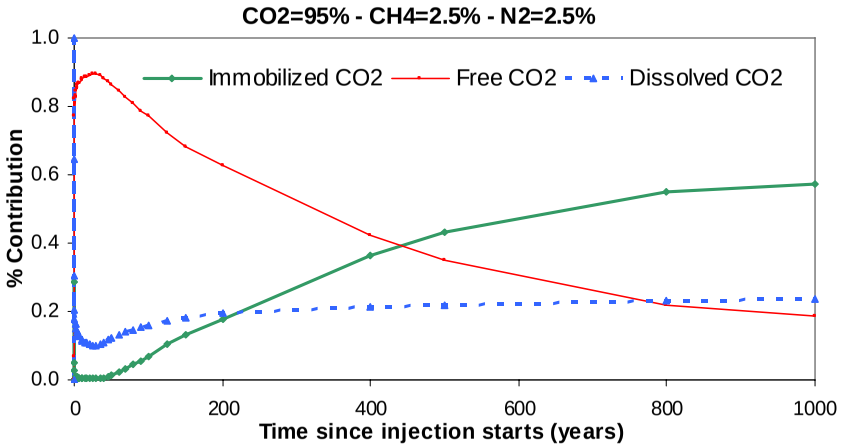

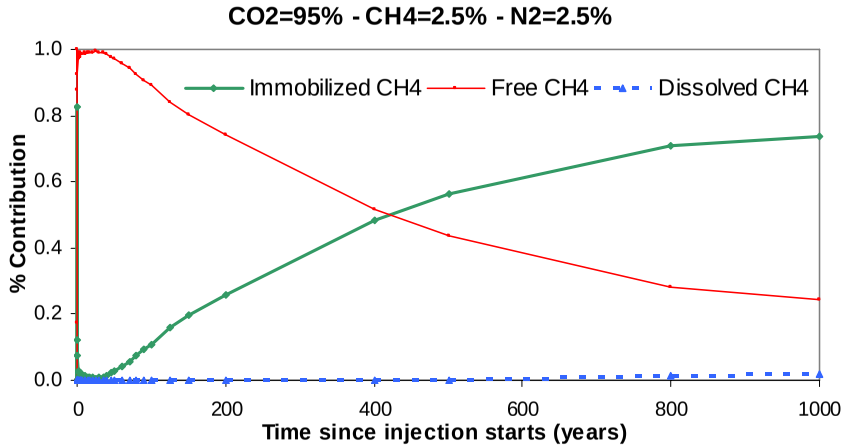

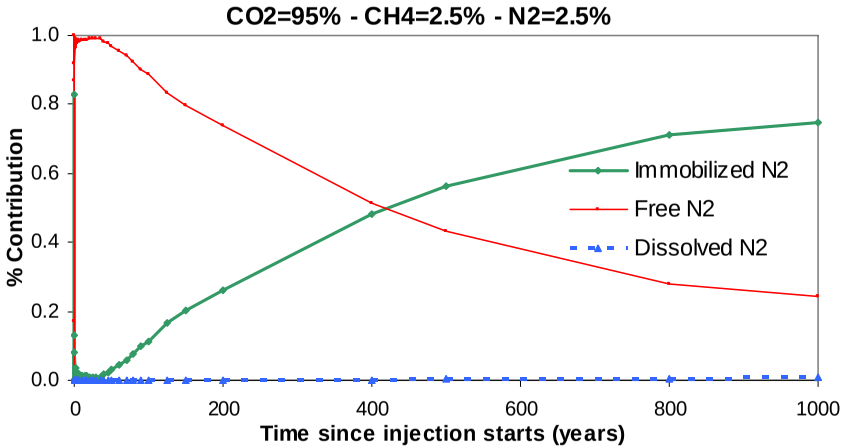

56. Case 22: Permeability in I direction = 600 md

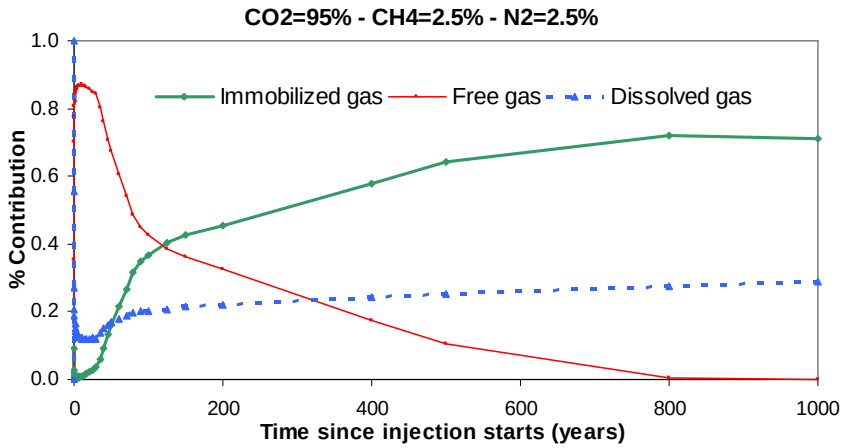

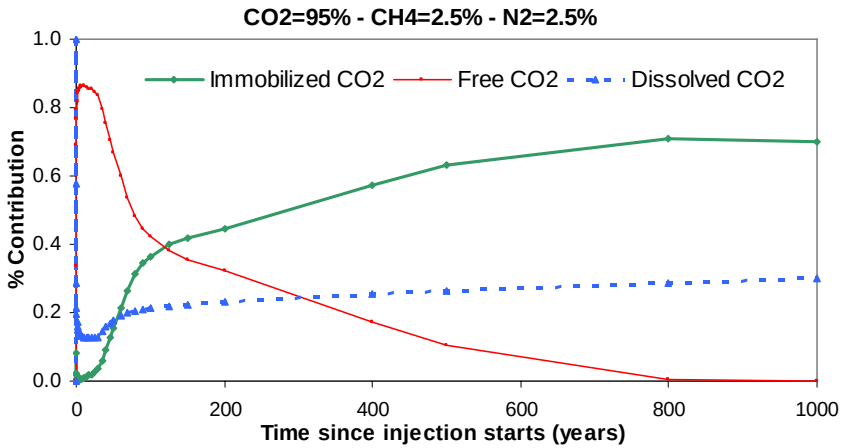

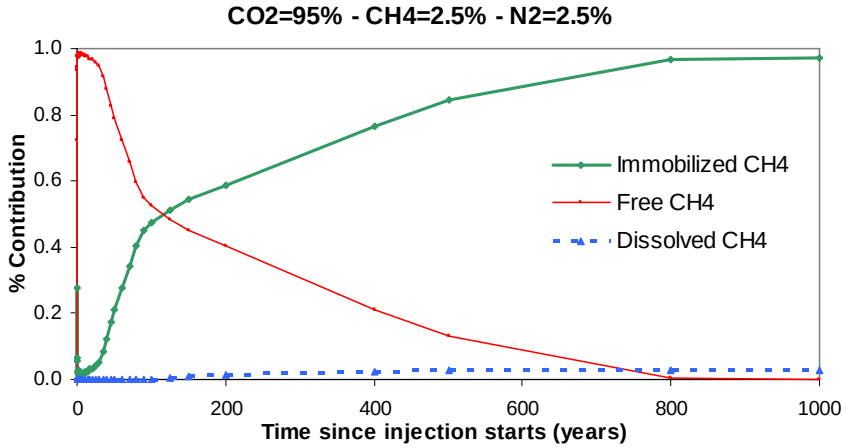

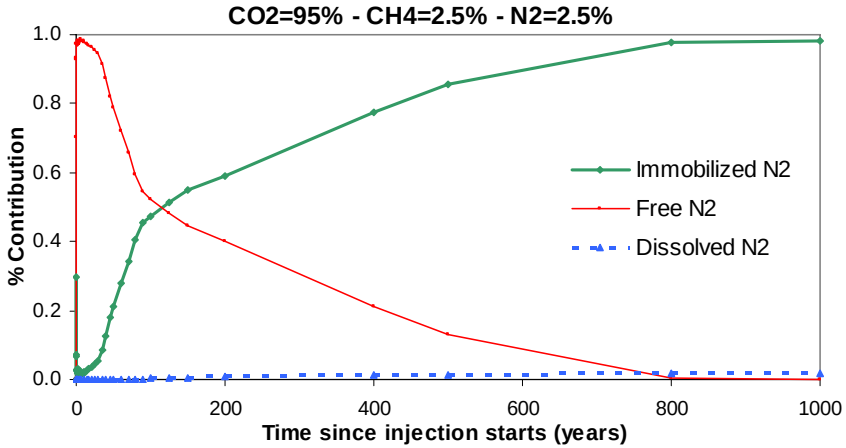

57. Case 23: Permeability anisotropy in K direction = 0.1

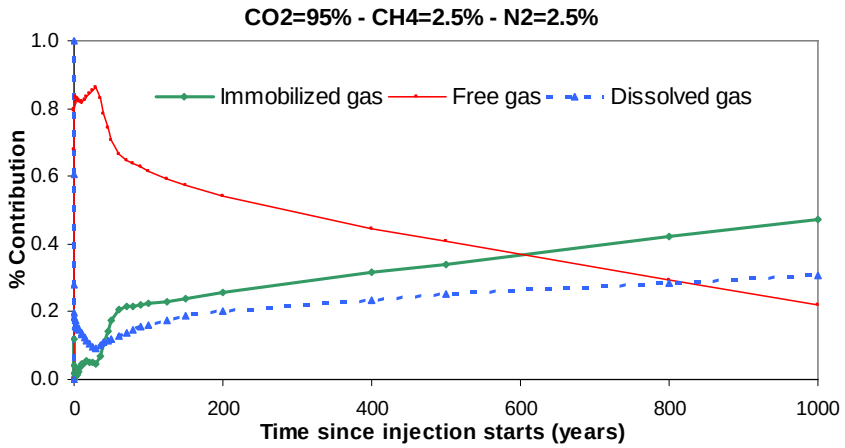

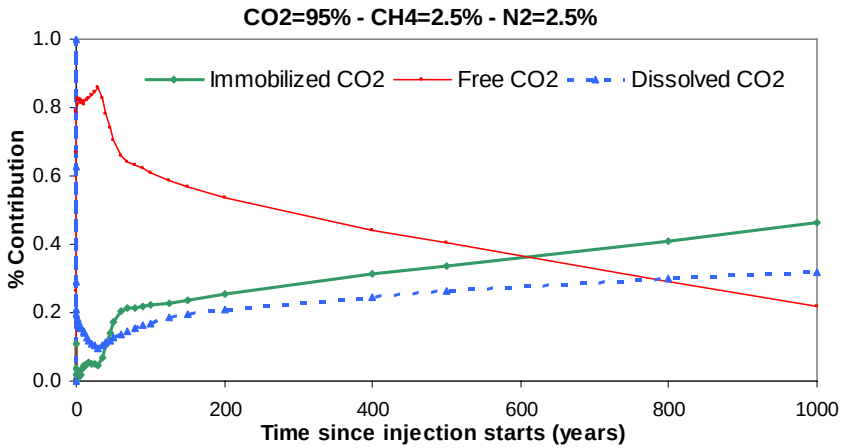

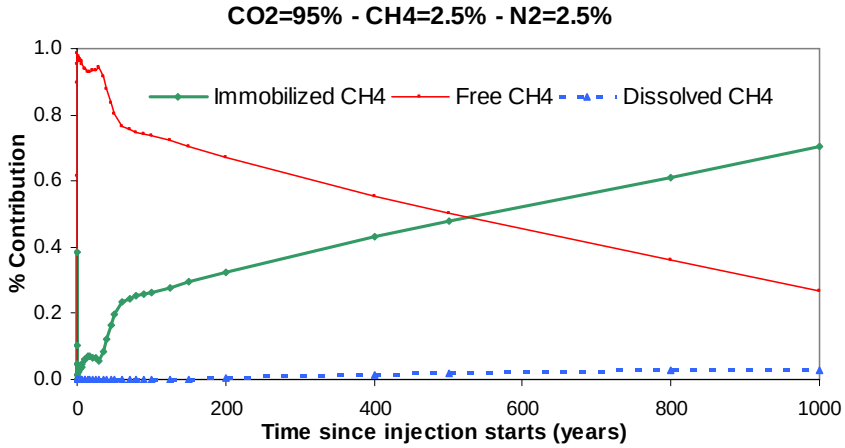

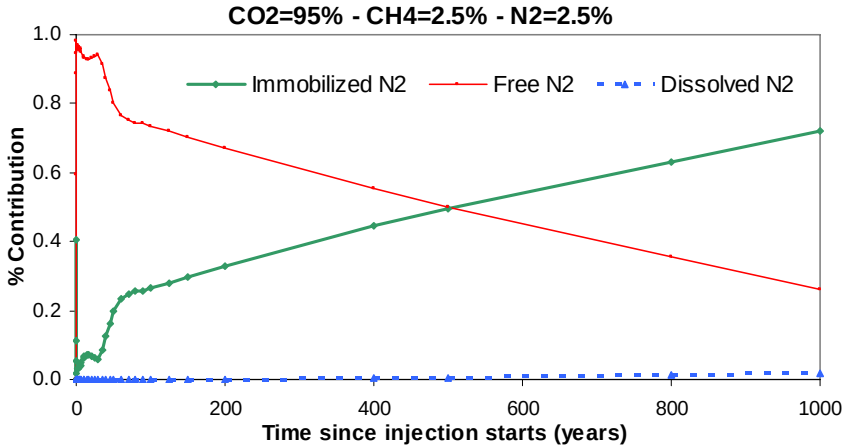

58. Case 24: Permeability anisotropy in K direction = 0.005

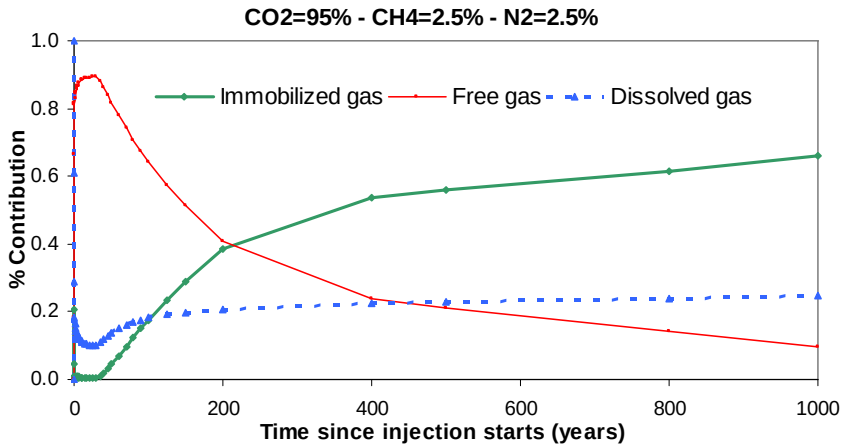

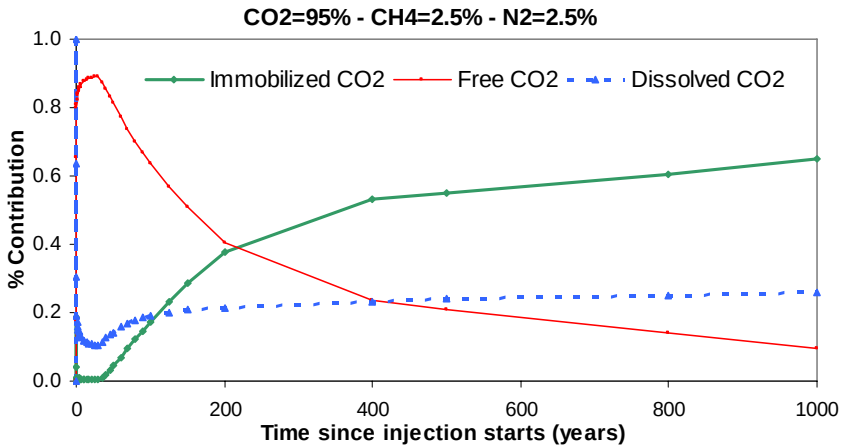

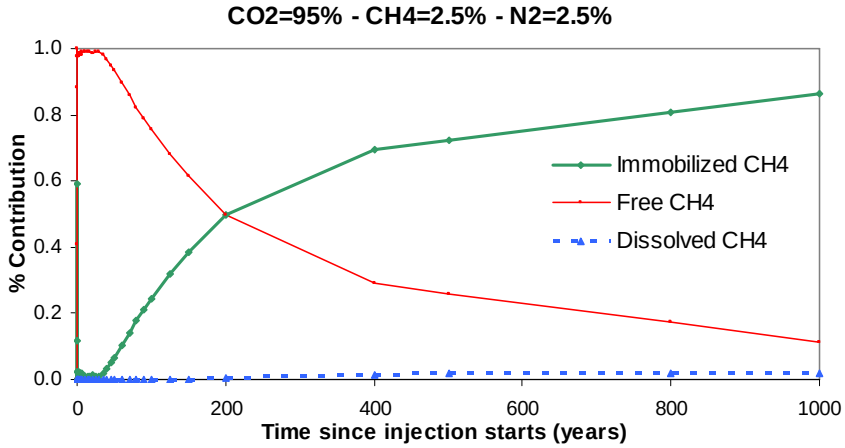

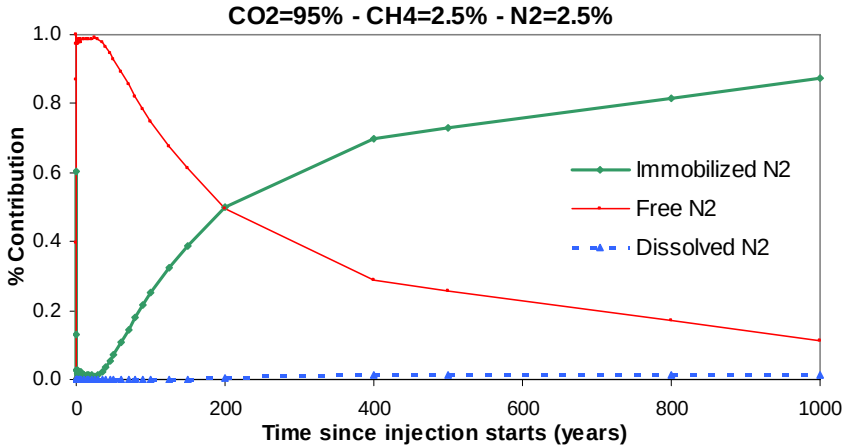

59. Case 25: CPOR = 5×10^{-5}

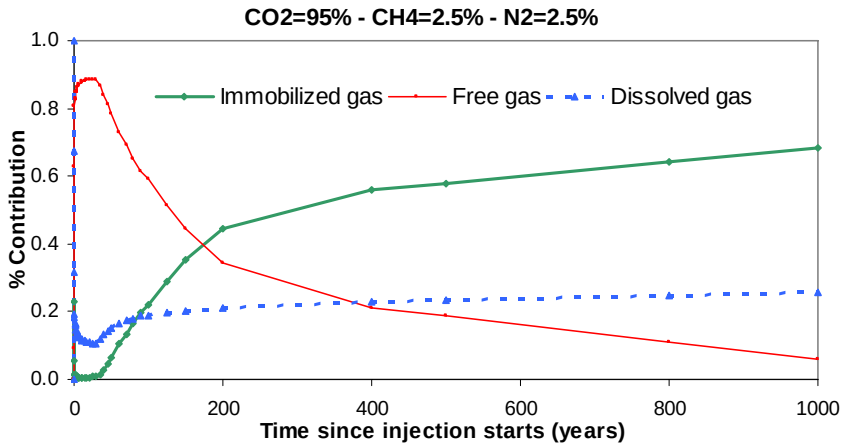

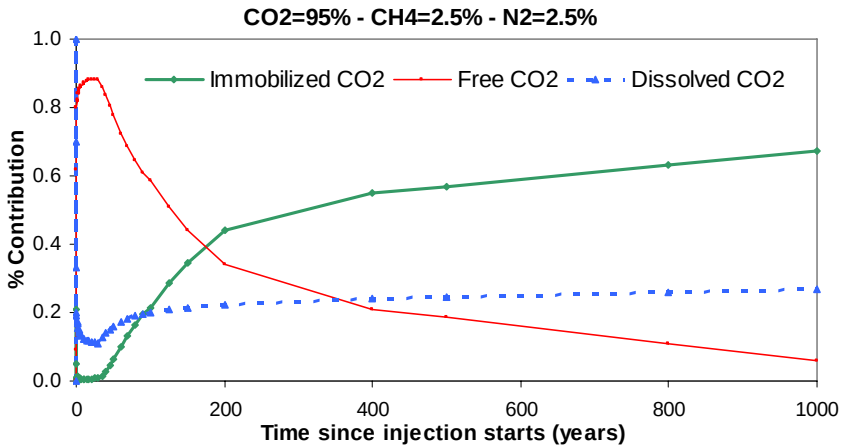

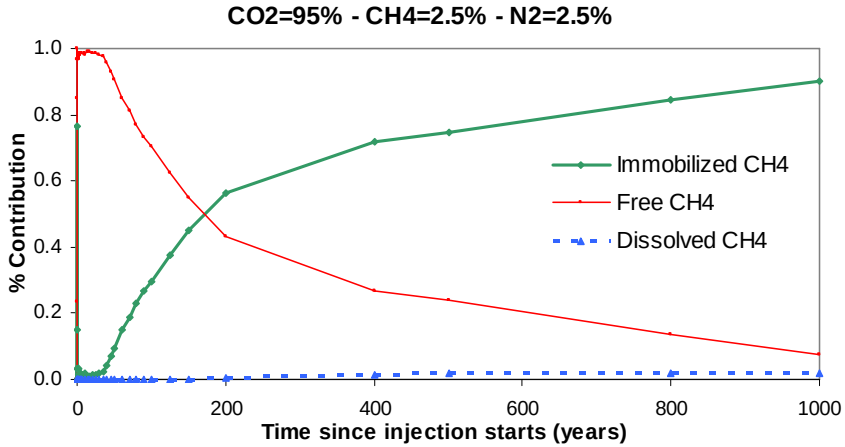

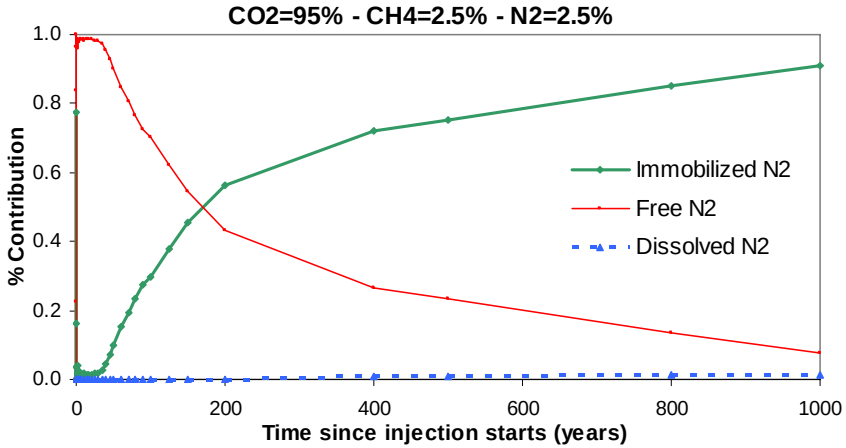

60. Case 26: Default PVT data 100-0-0 (CO2-CH4-N2) in volume

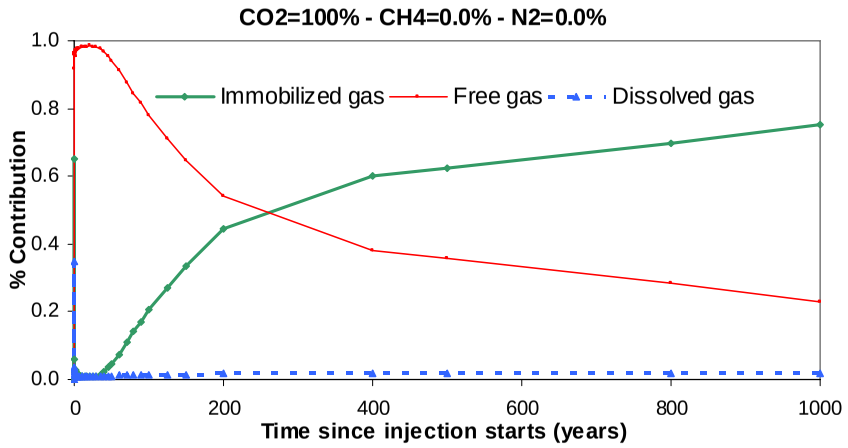

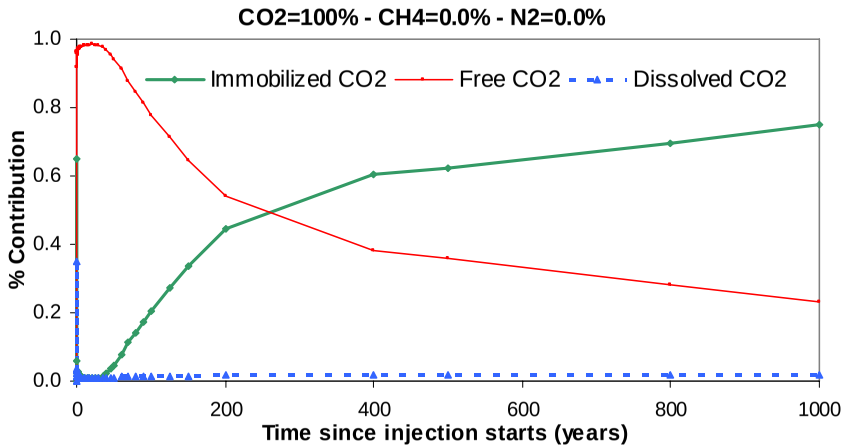

61. Case 27: Default PVT data 75-25-0 (CO_2-CH_4-N_2) in volume

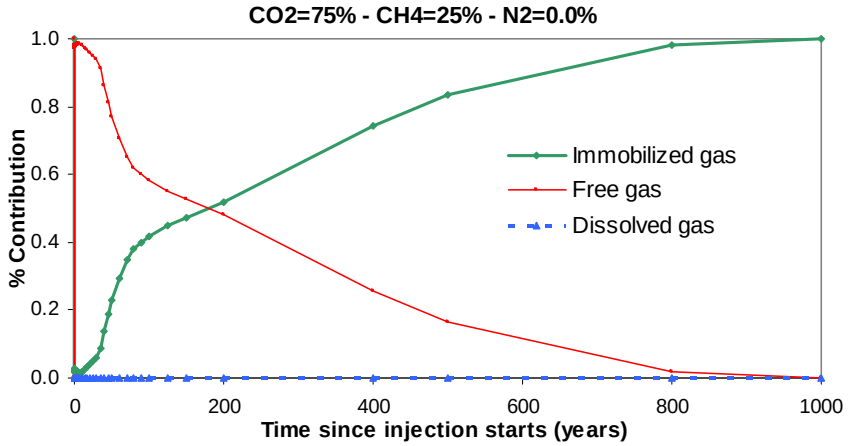

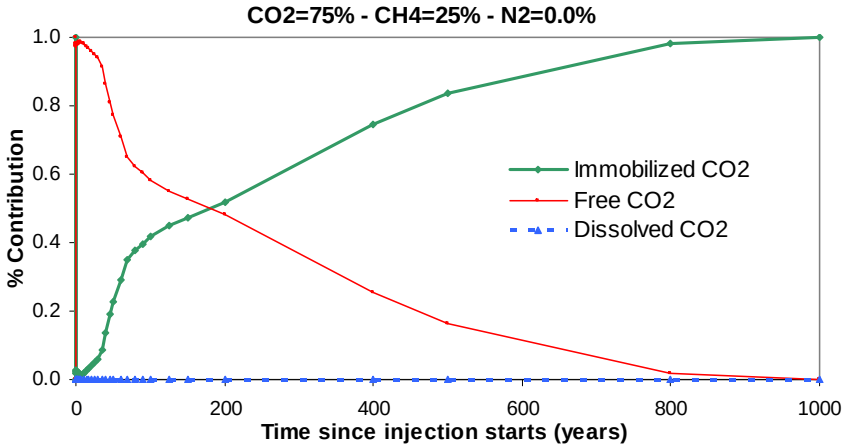

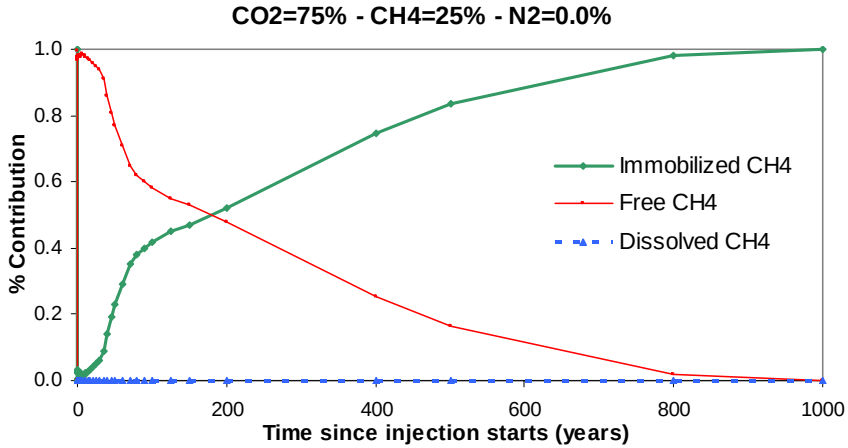

62. Case 28: Default PVT data 75-0-25 (CO_2-CH_4-N_2) in volume

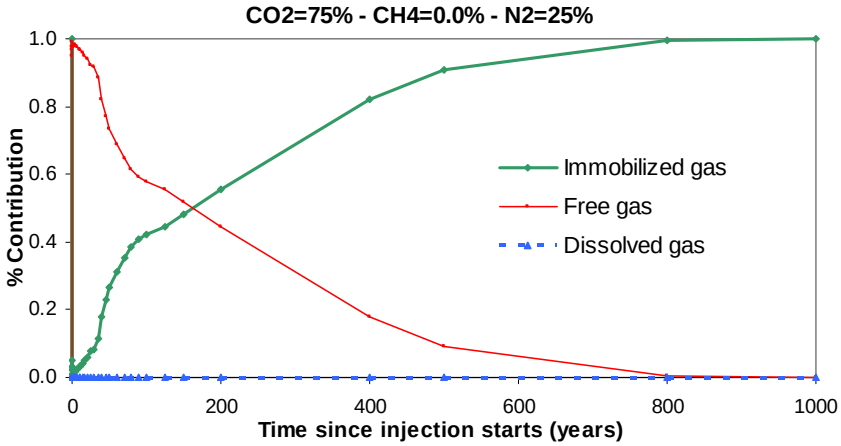

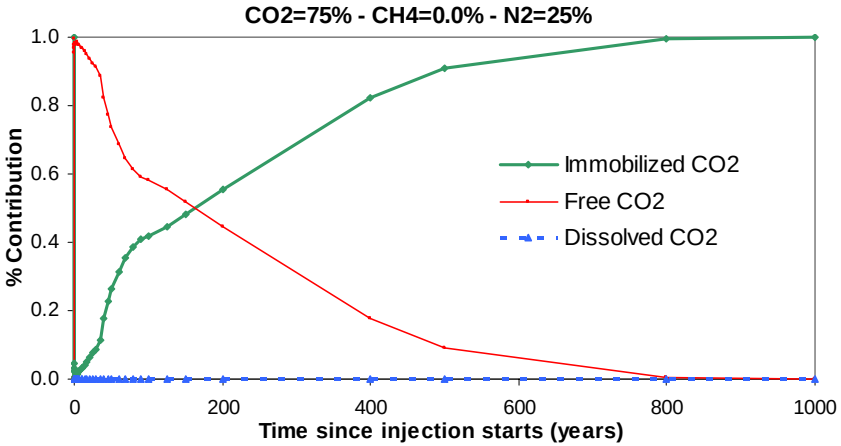

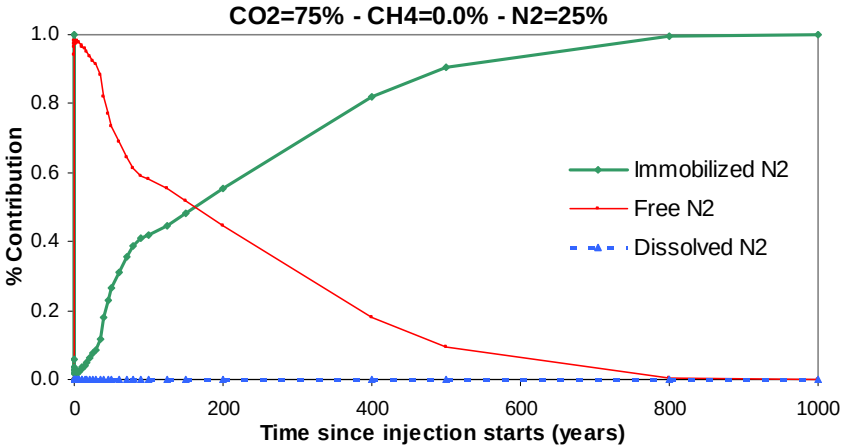

63. Case 29: Fixed pressure 100-0-0 (CO_2-CH_4-N_2) in volume

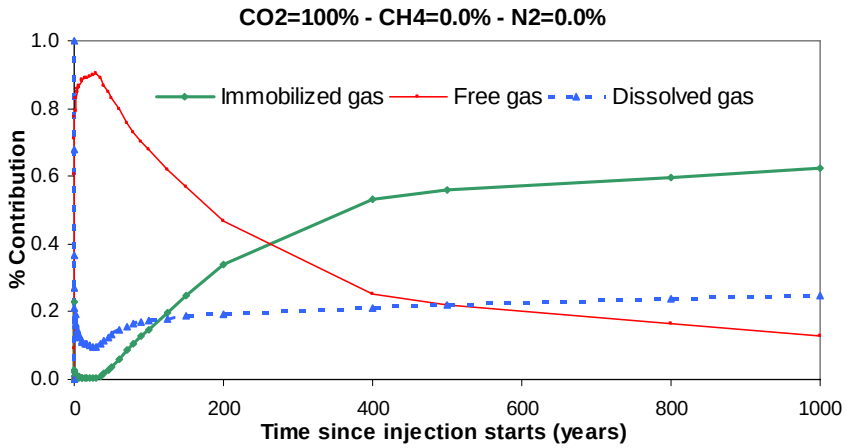

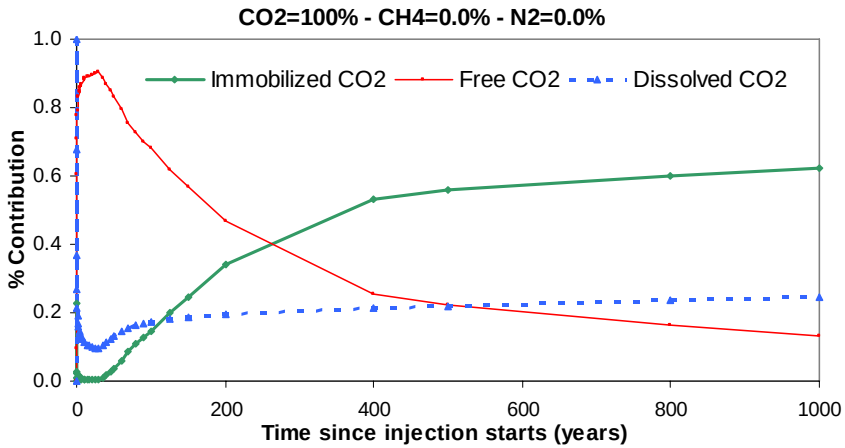

64. Case 30: Fixed pressure 75-25-0 (CO_2-CH_4-N_2) in volume

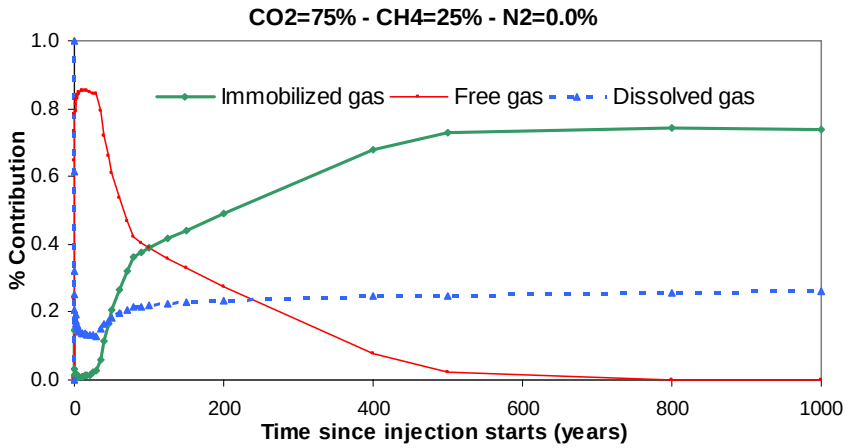

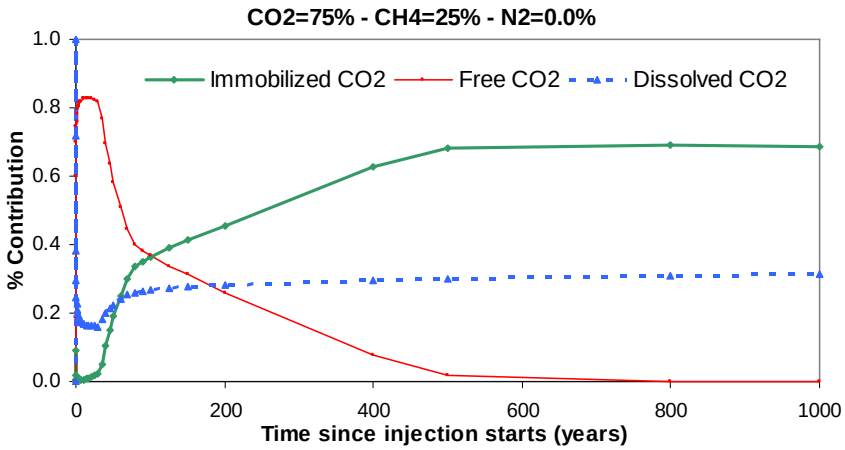

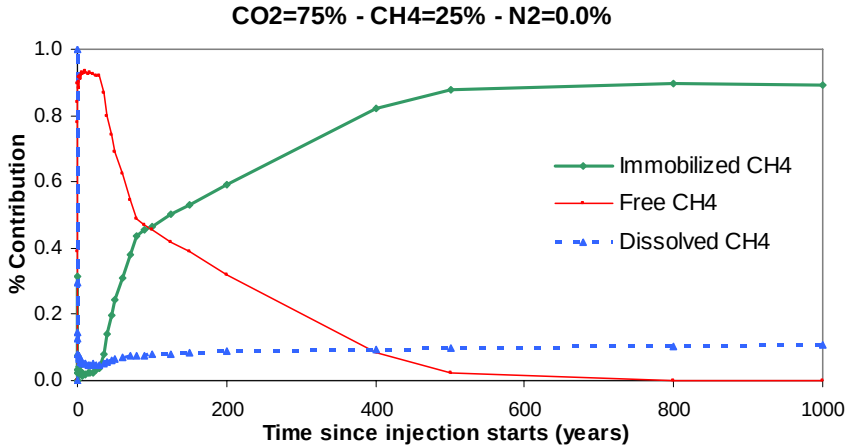

65. Case 31: Fixed pressure 75-0-25 (CO_2-CH_4-N_2) in volume

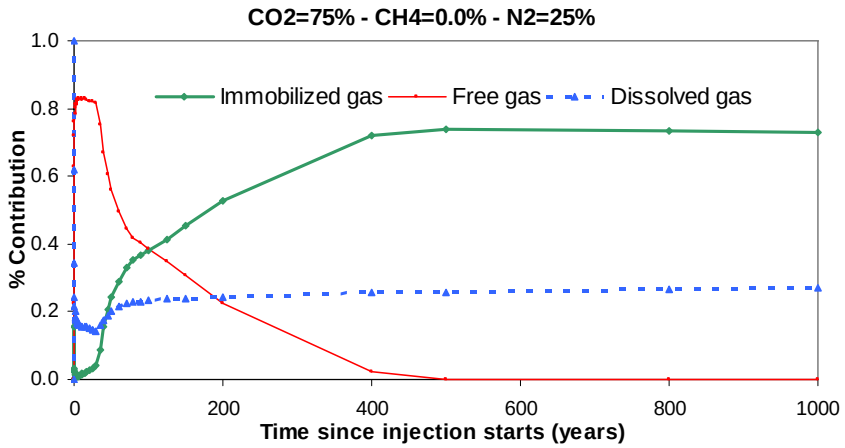

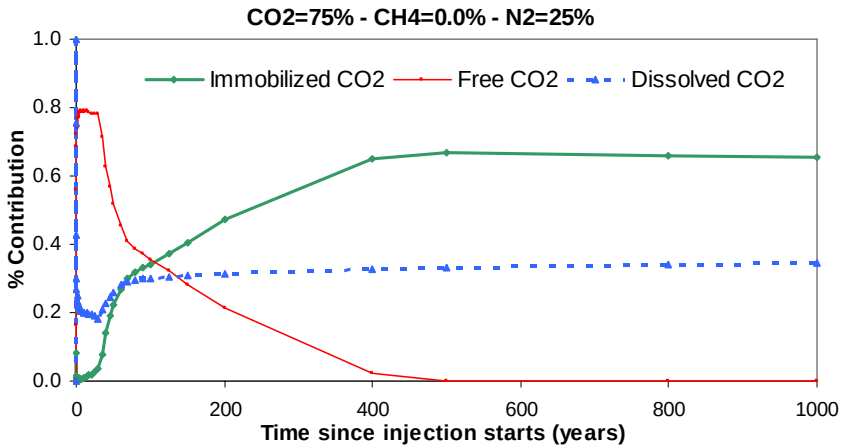

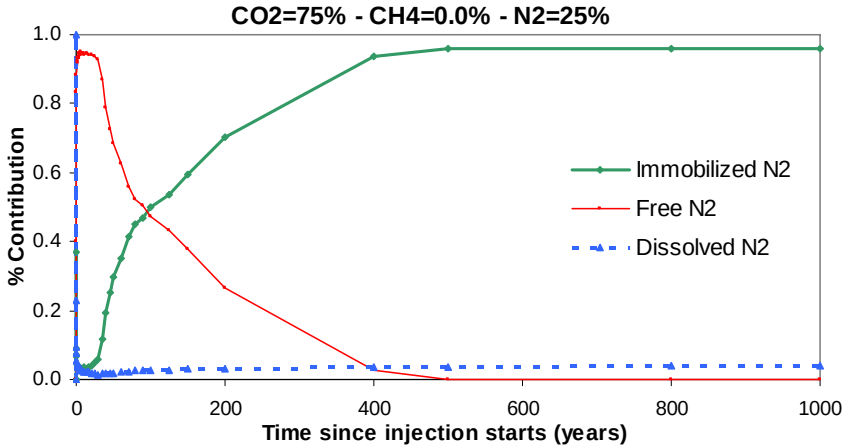

66. Case 39: Porosity = 0.2 with 95-2.5-2.5 (CO_2-CH_4-N_2) in volume

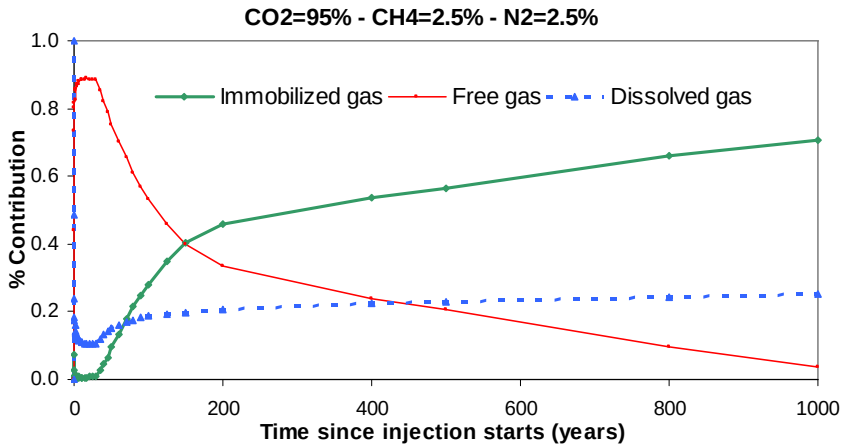

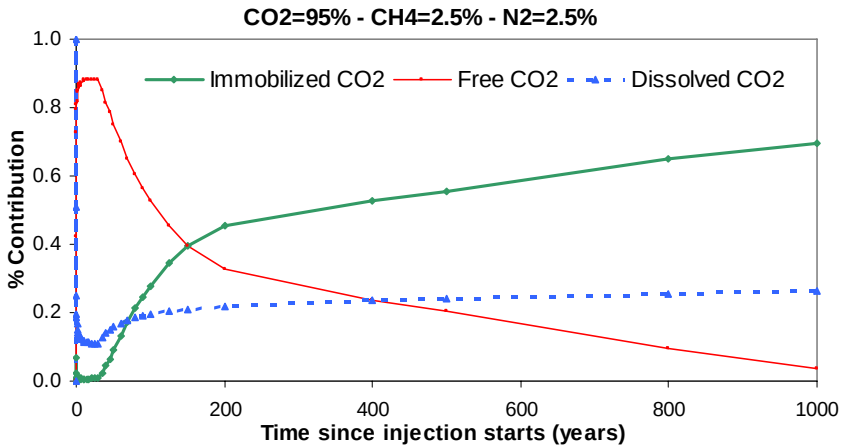

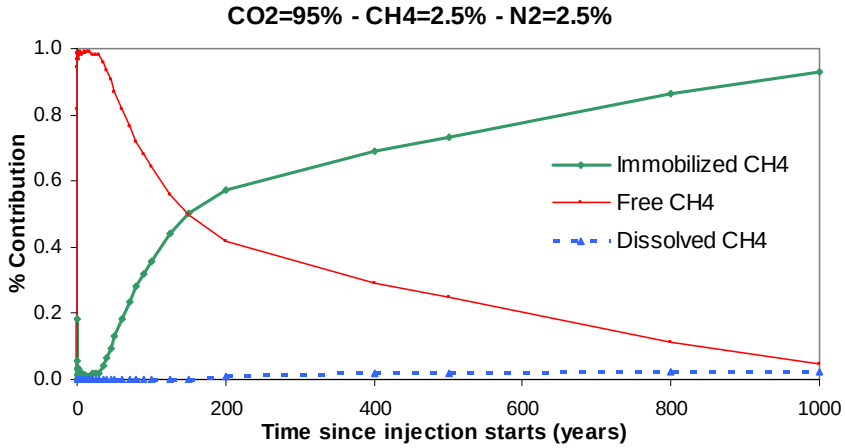

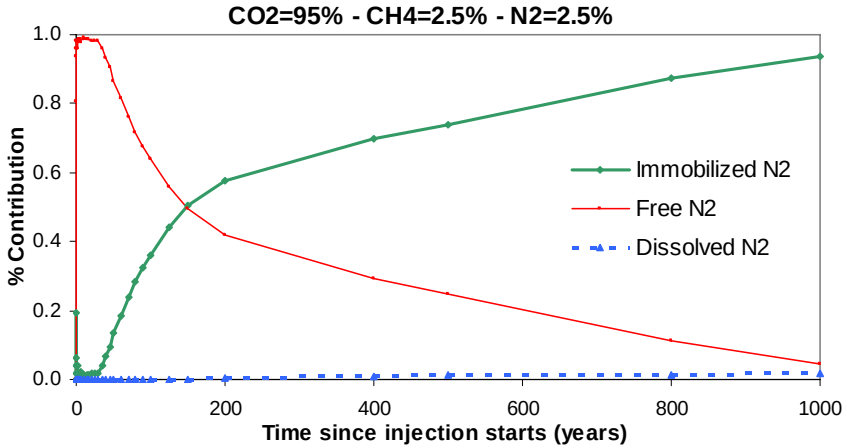

67. Case 40: Porosity = 0.3 with 95-2.5-2.5 (CO_2-CH_4-N_2) in volume

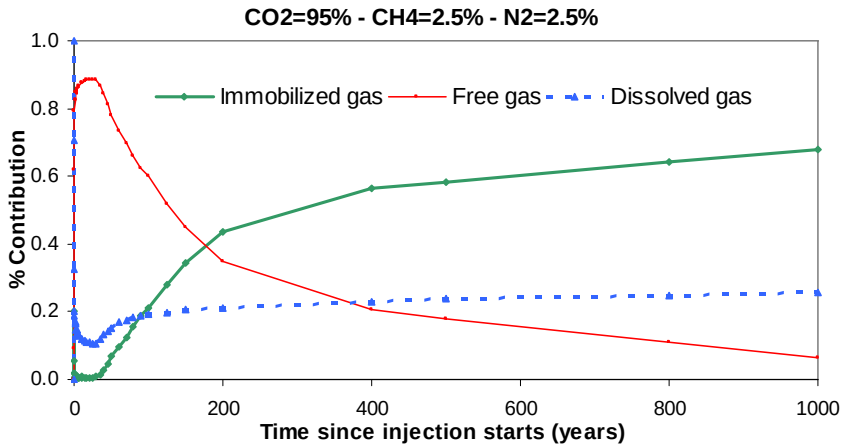

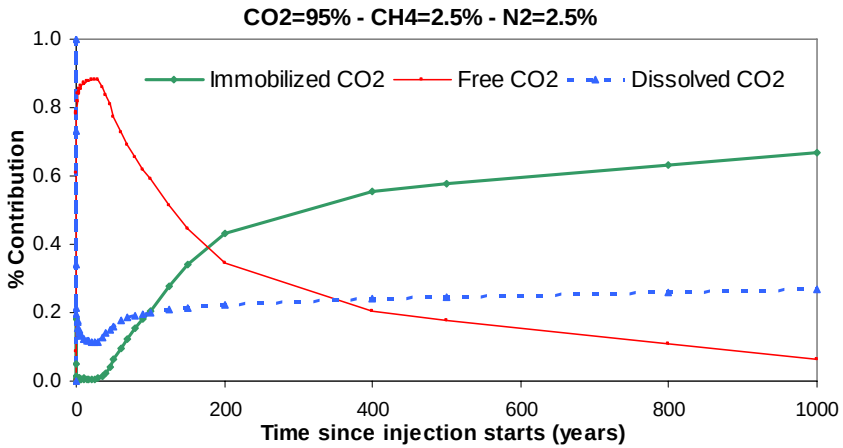

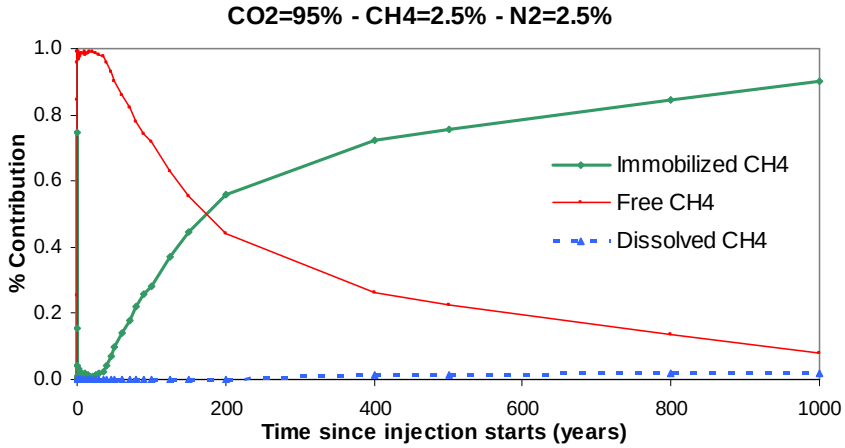

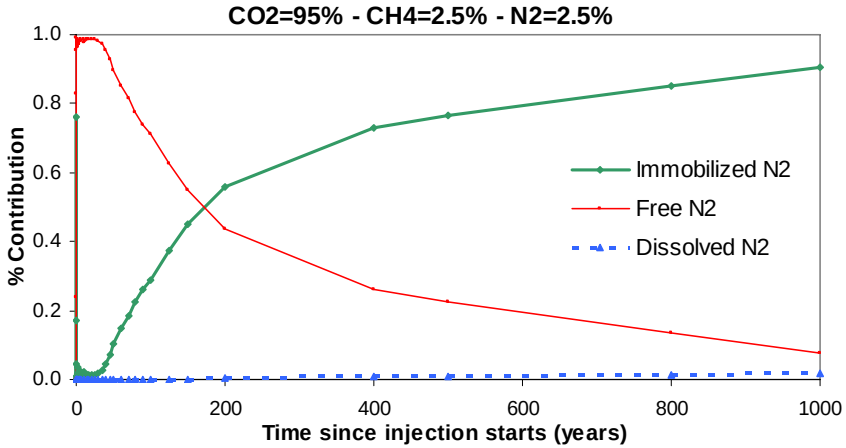

68. Case 41: capillary pressure included with 95-2.5-2.5 (CO_2-CH_4-N_2) in volume

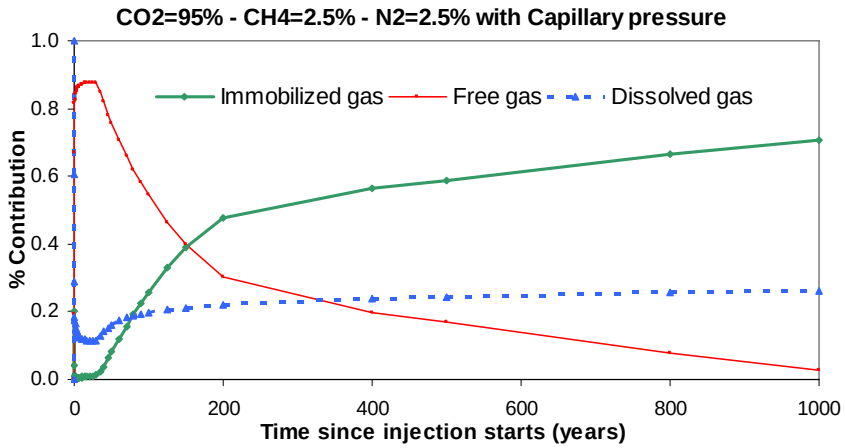

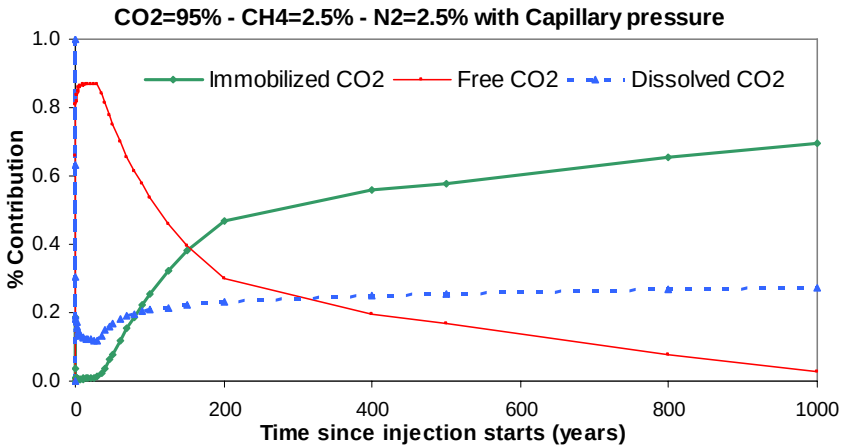

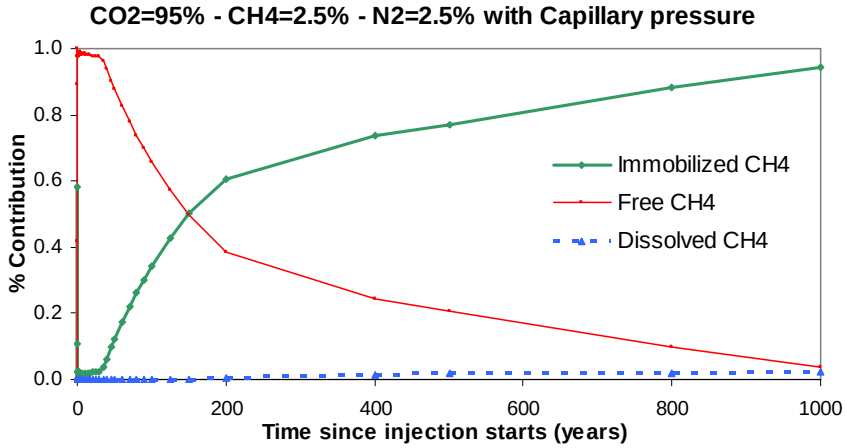

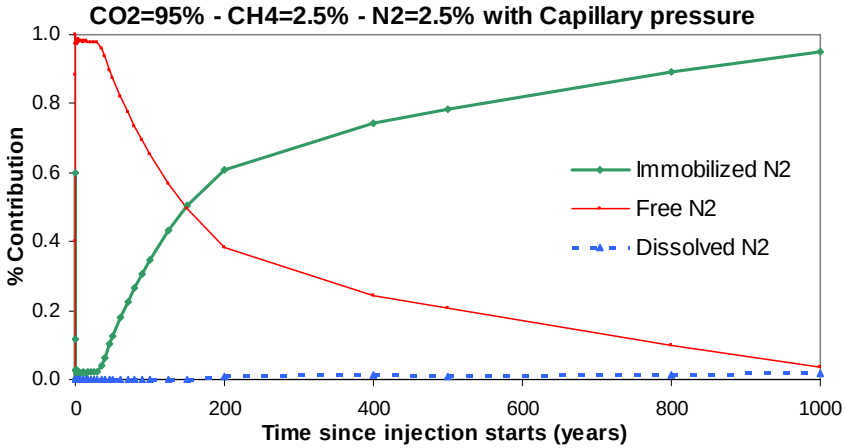

VIII. Appendix D: Figures from Gulf Coast Case

Case F1 100%-0%-0% (CO_2-CH_4-N_2), (Injection rate = 3.0×10^6 ft^3/day)

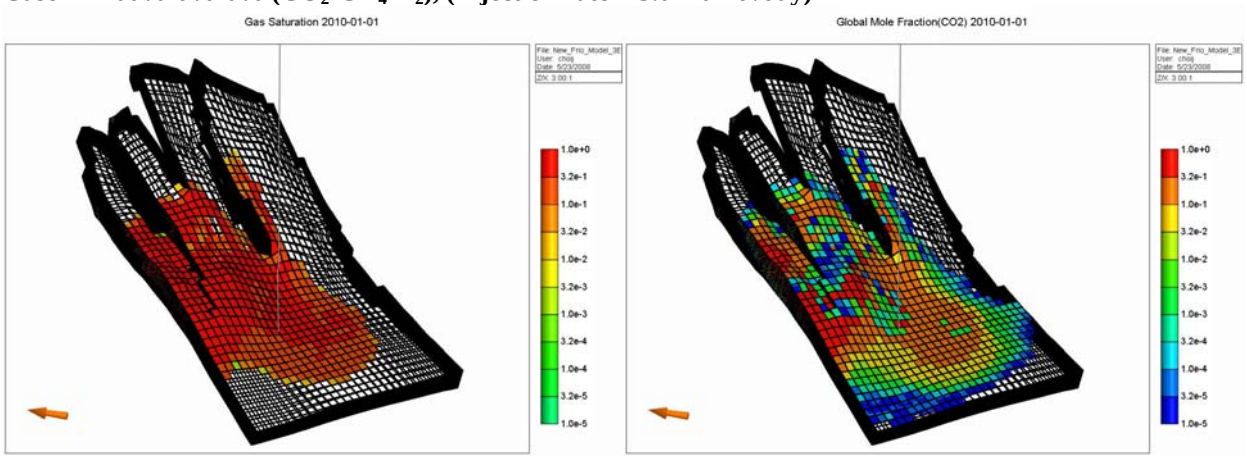

Gas saturation (10 yr) Global mole fraction (CO_2, 10 yr)

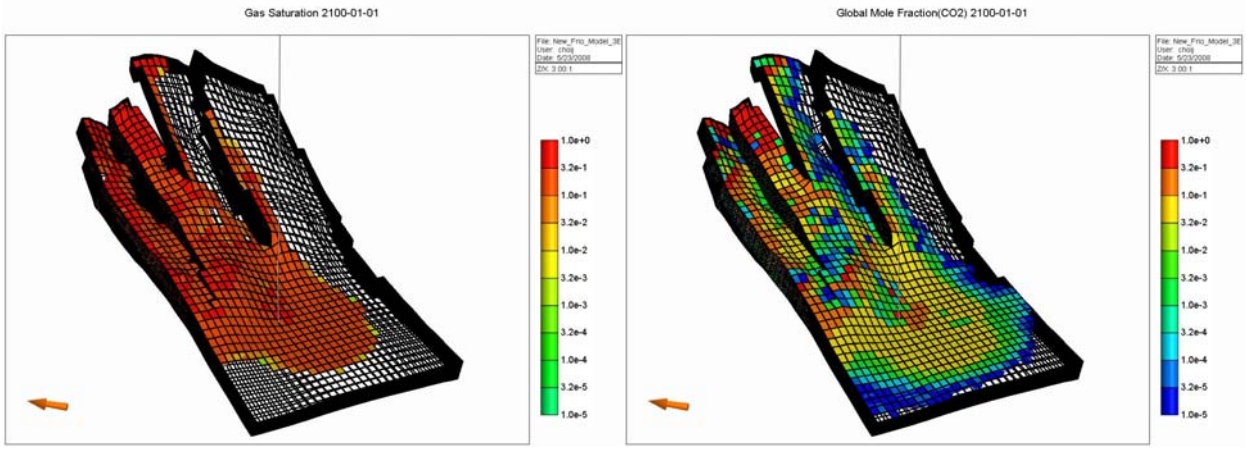

Gas saturation (100 yr) Global mole fraction (CO_2, 100 yr)

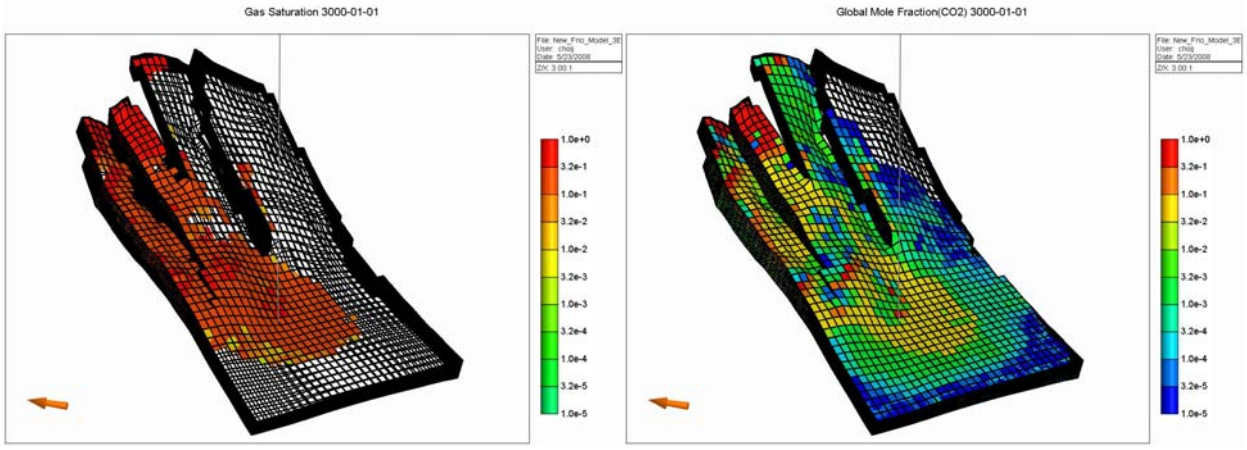

Gas saturation (1000 yr) Global mole fraction (CO2, 1,000 yr)

Figure 39. Illustration of gas saturation and CO_2 extent at selected times for 100% CO_2 Gulf Coast case.

Case F2 75%-25%-0% (CO_2-CH_4-N_2), (Injection rate = 3.0×10^6 ft^3/day)

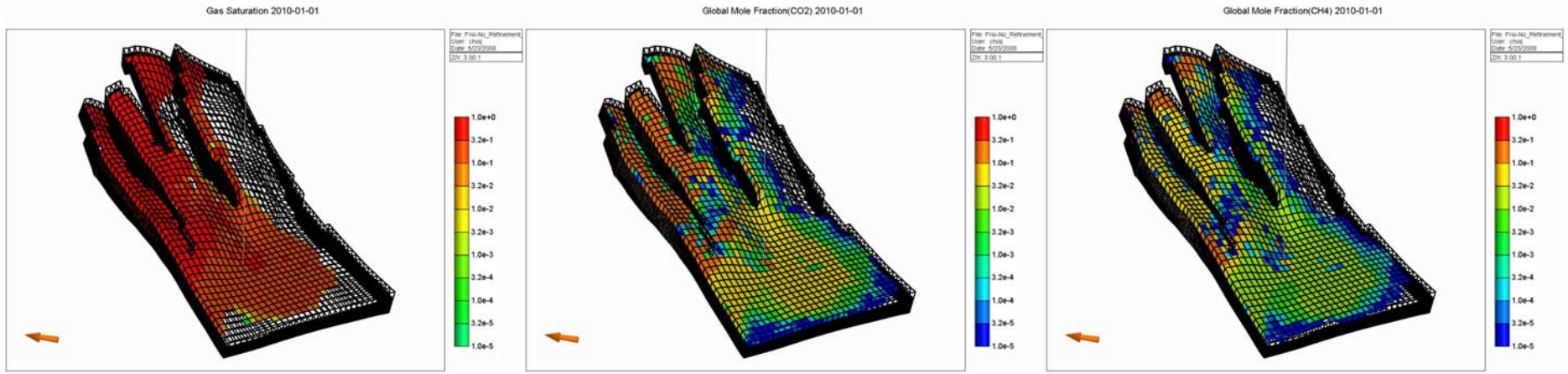

Gas saturation (10 yr) | Global mole fraction (CO_2, 10 yr) | Global mole fraction (CH_4, 10 yr)

Gas saturation (100 yr) | Global mole fraction (CO_2, 100 yr) | Global mole fraction (CH_4, 100 yr)

Figure 40. Illustration of gas saturation and CO_2 and CH_4 extent at selected times for 75% CO_2–25% CH_4 Gulf Coast case.

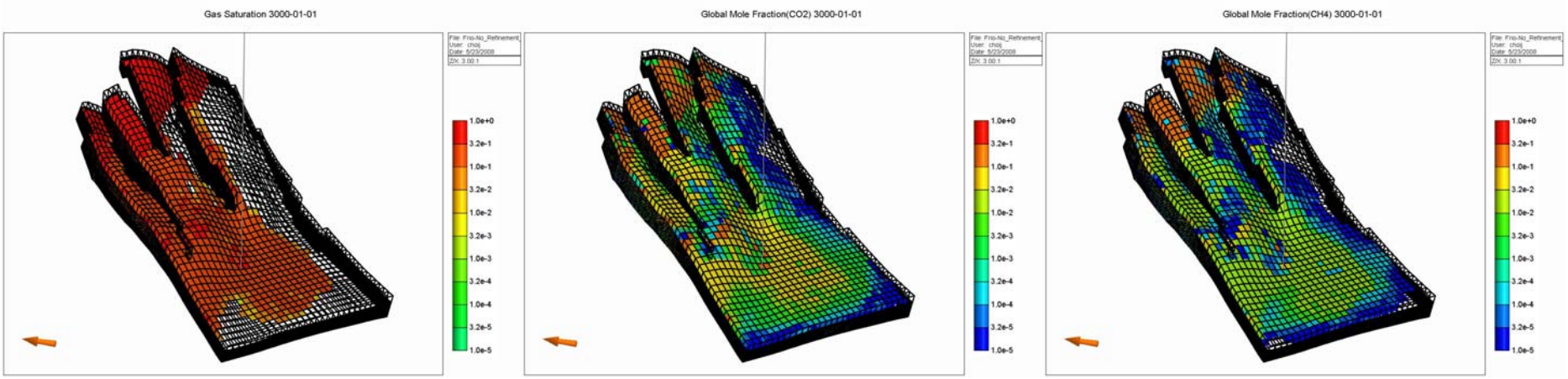

Gas saturation (1,000 yr) Global mole fraction (CO_2, 1,000 yr) Global mole fraction (CH_4, 1,000 yr)

Figure 40 (continued).

Case F3 75%-0%-25% (CO_2-CH_4-N_2), (Injection rate = 3.0×10^6 ft^3/day)

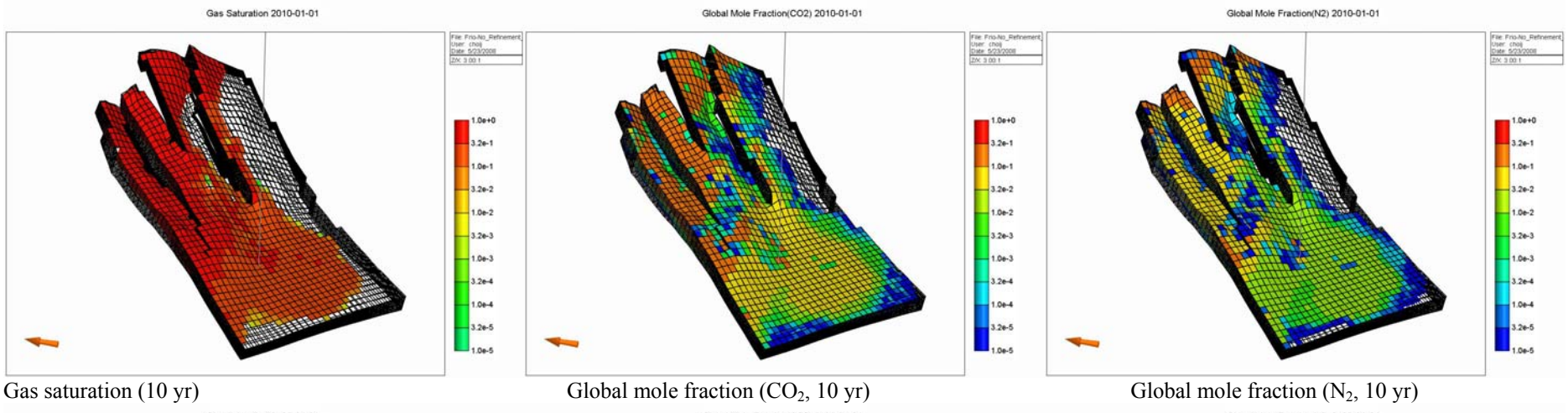

Gas saturation (10 yr) Global mole fraction (CO_2, 10 yr) Global mole fraction (N_2, 10 yr)

Gas saturation (100 yr) Global mole fraction (CO_2, 100 yr) Global mole fraction (N_2, 100 yr)

Figure 41. Illustration of gas saturation and CO_2 andN_2 extent at selected times for 75% CO_2–25% N_2 Gulf Coast case.

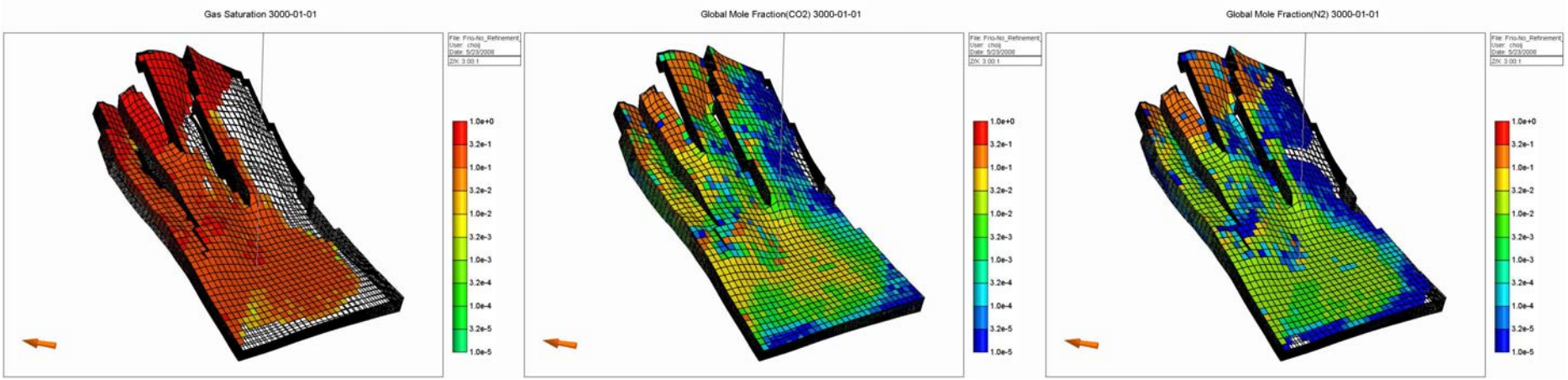

Gas saturation (1,000 yr) Global mole fraction (CO_2, 1,000 yr) Global mole fraction (N2, 1000 year)

Figure 41 (continued).

Case F1 100-0-0 (CO_2-CH_4-N_2) at 1,000 yr

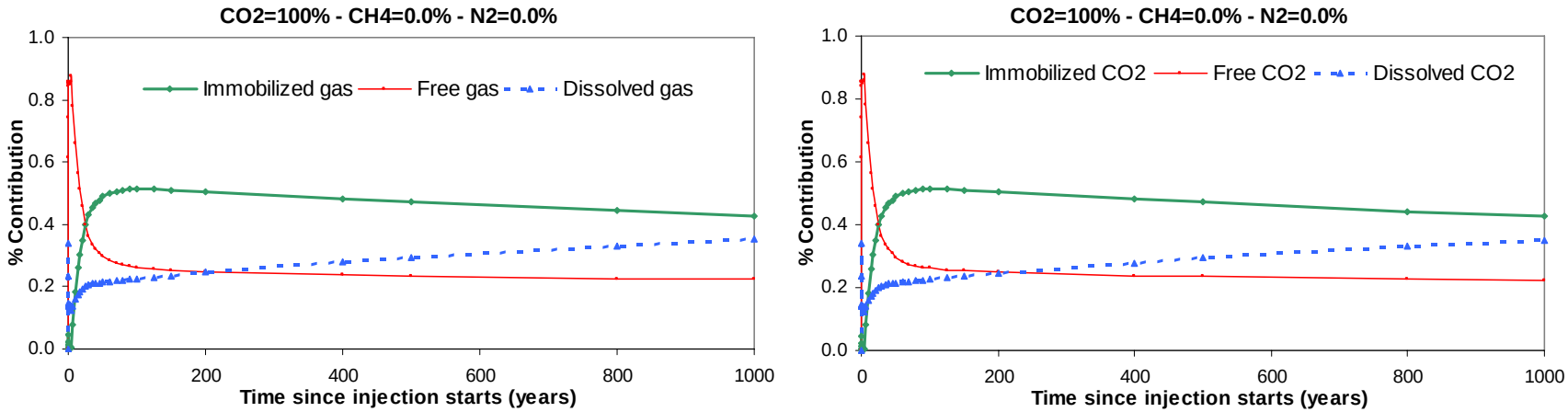

Figure 42. Phase distribution through time (1,000 yr) for the 100% CO_2 Gulf Coast case.

Case F1 100-0-0 (CO_2-CH_4-N_2) at 100 yr

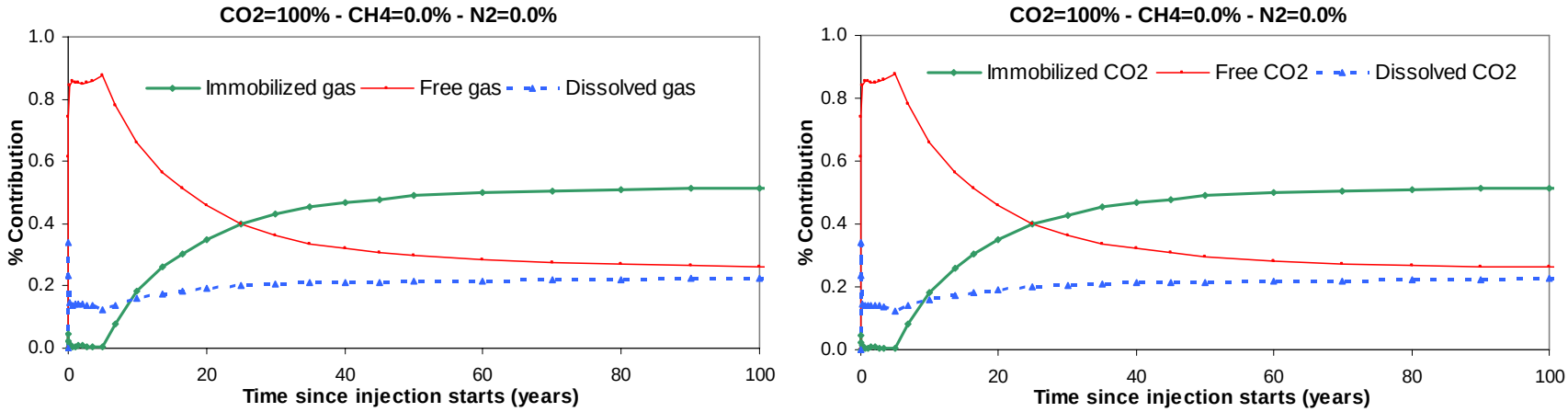

Figure 43. Phase distribution through time (100 yr) for the 100% CO_2 Gulf Coast case.

Case F2 75-25-0 (CO_2-CH_4-N_2) at 1,000 yr

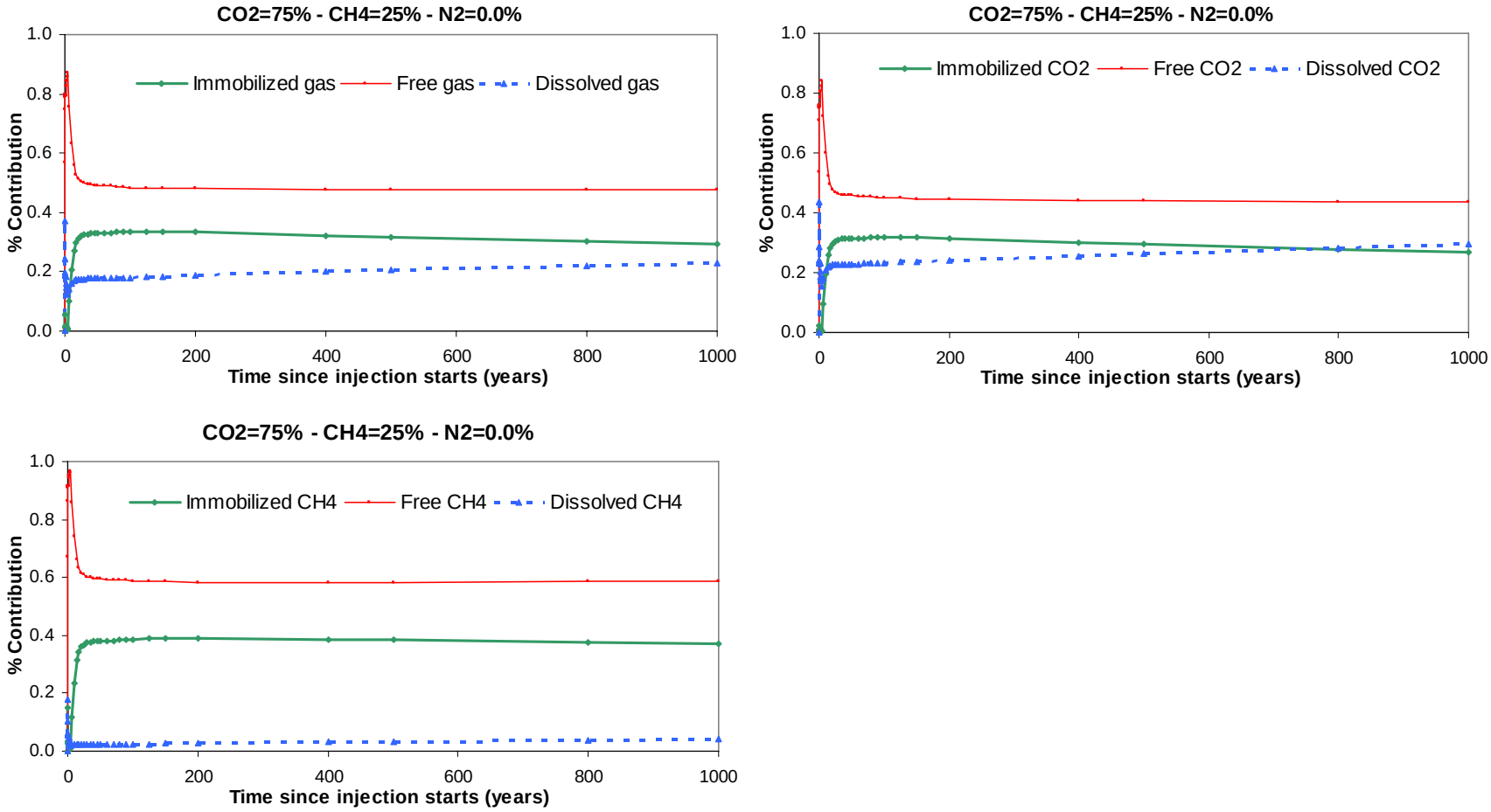

Figure 44. Phase distribution through time (1,000 yr) for the 75% CO_2–25% CH_4 Gulf Coast case.

Case F2 75-25-0 (CO_2-CH_4-N_2) at 100 yr

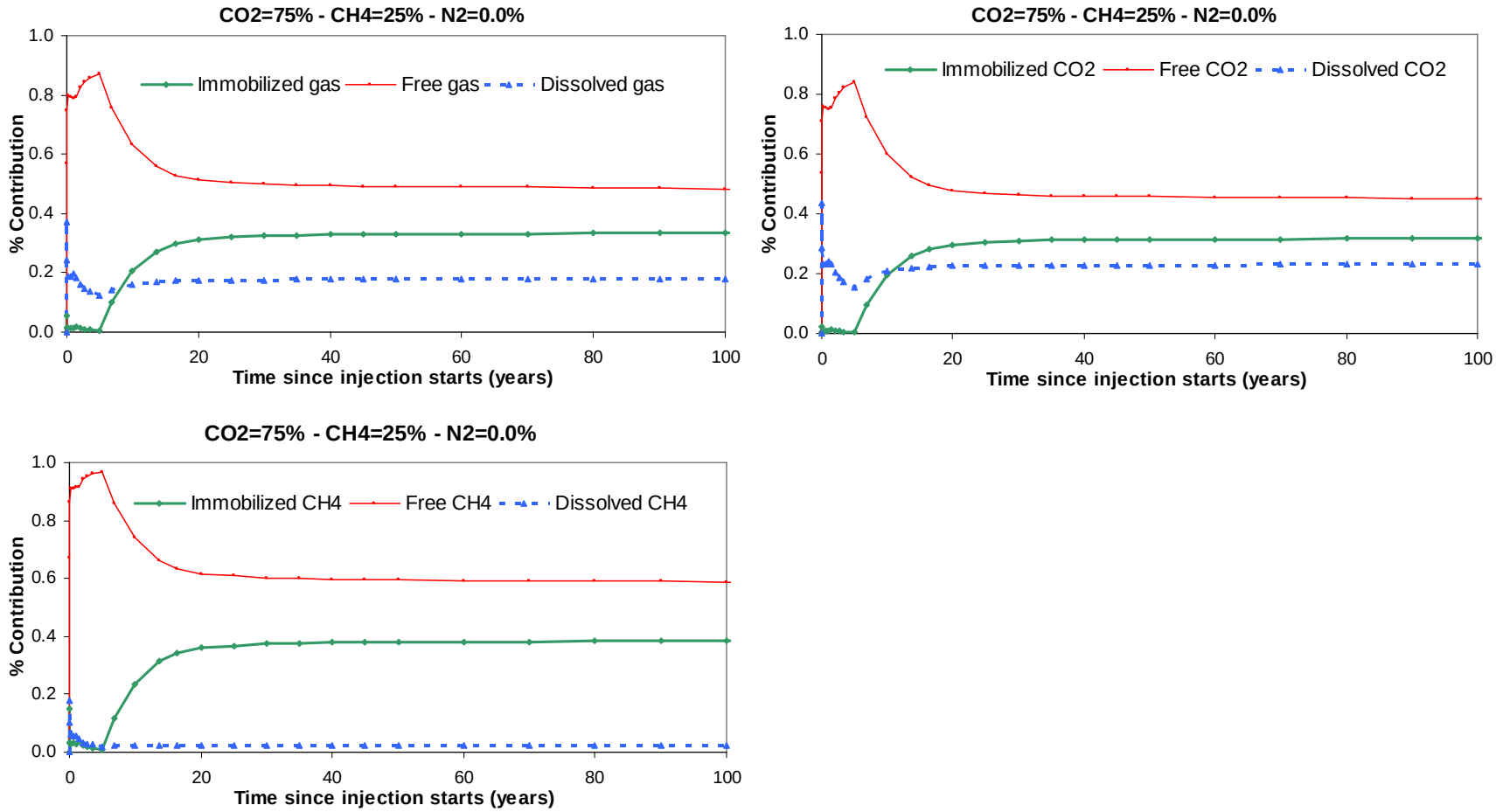

Figure 45. Phase distribution through time (100 yr) for the 75% CO_2–25% CH_4 Gulf Coast case.

Case F3 75-0-25 (CO_2-CH_4-N_2) at 1,000 yr

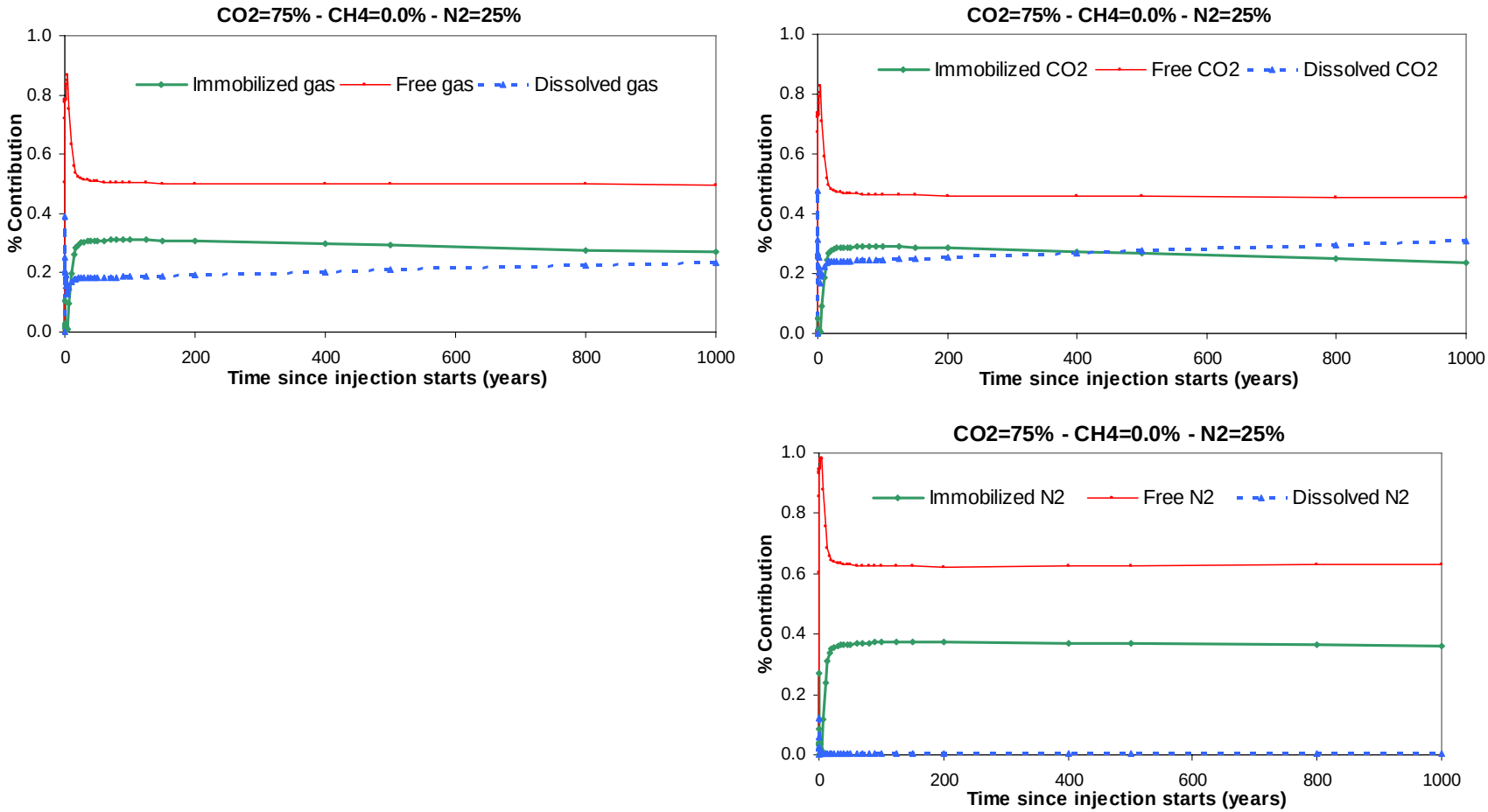

Figure 46. Phase distribution through time (1,000 yr) for the 75% CO_2–25% N_2 Gulf Coast case.

Case F3 75-0-25 (CO_2-CH_4-N_2) at 100 yr

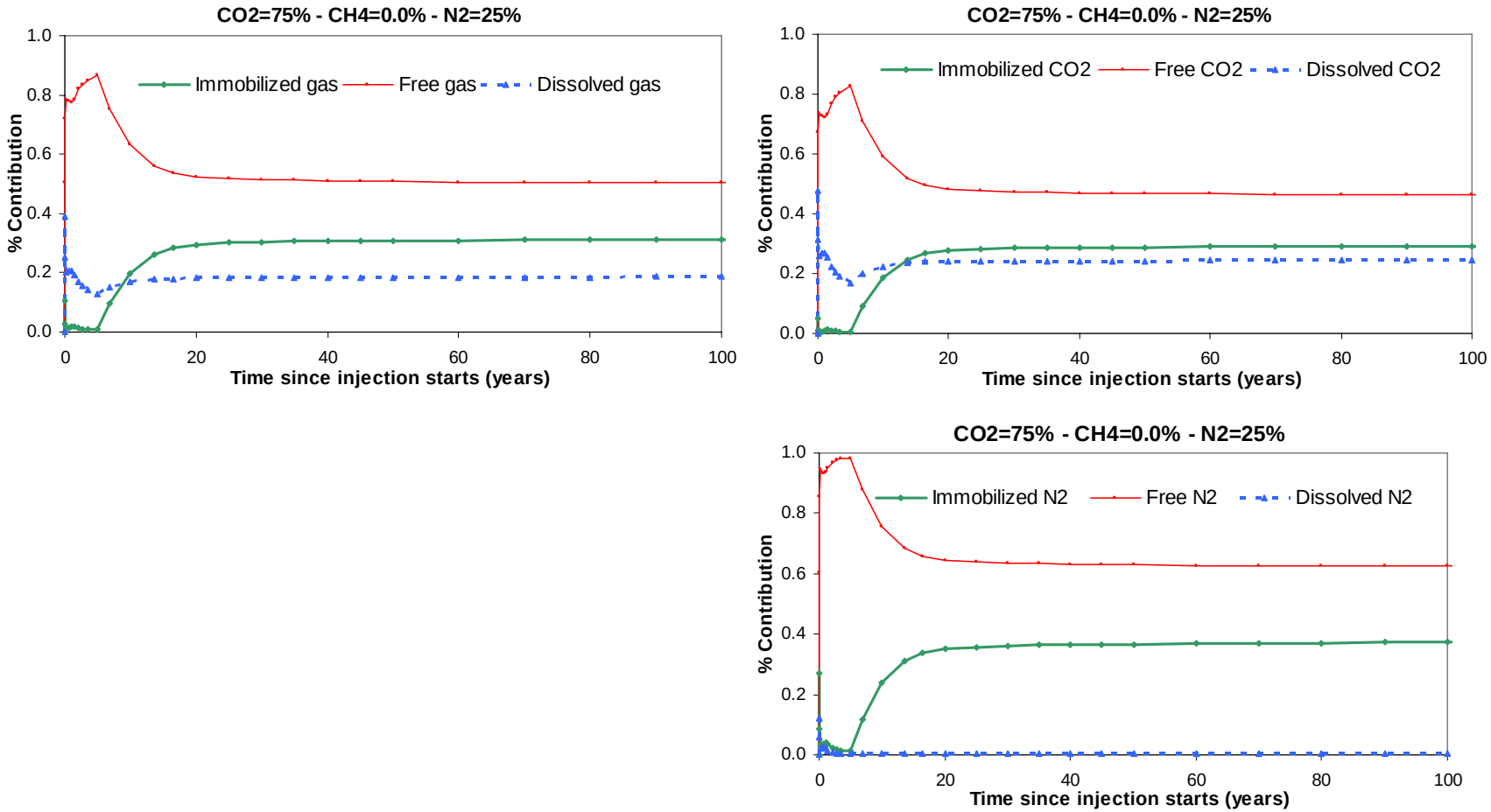

Figure 47. Phase distribution through time (100 yr) for the 75% CO_2–25% N_2 Gulf Coast case.

IX. Appendix E: Bibliography on Gas Solubility in Brines

A few selected journal articles, reports, and handbooks

Methane Solubility

Abraham, M., Andonian-Haftvan, J., Whiting, G. S., and Leo, A., 1994, The factors that influence the solubility of gases and vapours in water at 298 K, and a new method for its determination, *Journal of Chemical Society Perkin Transactions*, 2, 1777-1791.

Amirijafari, B., and Campbell, J. M., 1972, Solubility of gaseous hydrocarbon mixtures in water, *Society of Petroleum Engineers Journal*. 12(1), 21-7

Carroll, J. J. and Mather, A. E., 1997, A model for the solubility of light hydrocarbons in water and aqueous solutions of alkanolamines, *Chemical Engineering Science*, 52(4), 545-552.

Clever, H. L. and Young, C. L., 1987, *Solubility Data Series*, 27/28, Methane, Pergamon Press, Oxford.

Cramer, S. D., 1984, Solubility of methane in brines from 0 to 300 degr., *Ind. Eng. Chem. Process Des. Dev.*, 23, 533-538.

Culberson, O. L., and McKetta, J. J., Jr., 1951, The solubility of methane in water at pressures to 10 000 psia, *Petroleum Transactions, AIME*, 192, 223-226.

Duan, Zhenhao, and Mao, Shide, 2006, A thermodynamic model for calculating methane solubility, density and gas phase composition of methane-bearing aqueous fluids from 273 to 523 K and from 1 to 2000 bar, *Geochimica et Cosmochimica Acta*, 70(13), 3369-3386

Duan, Z., Moeller, N., and Weare, J. H., An equation of state for the CH4-CO2-H20 system: 1. Pure Systems from 0 to 100 degr. and 0 to 800 bar, *Geochimica et Cosmochimica Acta*, 56, 2605-2617.

Kordas, A., Magoulas, K., Stamataki, S., and Tassios, D., 1995, Methane-hydrocarbon interaction parameters correlation for the Peng-Robinson and the T-Mpr equation of state, *Fluid Phase Equilibria*, 112, 33-44.

Lekvam, K., and Raj Bishnoi, P., 1997, Dissolution of methane in water at low temperatures and intermediate pressures, *Fluid Phase Equilibria*, 131, 297-309.

O'Sullivan, T. D., and Smith, N. O., 1970, The solubility and partial molar volume of nitrogen and methane in water and in aqueous sodium chloride: from 50 to 125 degr. and 100 to 600 Atm, *The Journal of Physical Chemistry*, 74(7), 1460-1466.

Perry, R. H. and Green, D., 1984, Perry's Chemical Engineer's Handbook, 6th ed., McGraw-Hill International Editions.

Sachs, W., 1998, The diffusional transport of methane in liquid water: method and result of experimental investigation at elevated pressure, *Journal of Petroleum and Science Engineering*, 21, 153-164.

Sander, R., 1999, Compilation of Henry's law constants for inorganic and organic species of potential importance in environmental chemistry, Version 3, Internet module last accessed June 2008 http://www.mpch-mainz.mpg.de/~sander/res/henry.html

Soereide, I., and Whitson, C. H., 1992, Peng-Robinson predictions for hydrocarbons, CO_2, N_2, and H_2S with pure water and NaCl brine, *Fluid Phase Equilibria*, 77, 217-240.

Wang, Y., Han, B., Yan, H., and Liu, R., 1995, solubility of CH_4 in the mixed solvent t-butyl alcohol and water, *Thermochimica Acta*, 253, 327-334.

Nitrogen Solubility

Alvarez, J., Crovetto, R., and Fernandez-Prini, R., 1988, The dissolution of N_2 and of H_2 in water from room temperature to 640 K, Ber. Bunsenges. *Physical Chemistry*, 92, 935-940.

Perez, R. J., and Heidemann, R. A., 2006, Coupling an equation of state and Henry's Law to model the phase equilibria of gases and brines: Examples in the N_2–H_2O–NaCl system, *Journal of Geochemical Exploration*, 89, 331-334.

O'Sullivan, T. D., Smith, N., and Nagy, B., 1966, Solubility of natural gases in aqueous salt solutions-III Nitrogen in aqueous NaCl at high pressures, *Geochimica Cosmochimica Acta*, 30, 617-619.

O'Sullivan, T., and Smith, N., 1970, The solubility and partial molar volume of nitrogen and methane in water and aqueous sodium chloride from 50 to 125 C and 100 to 600 atm, *The Journal of Physical Chemistry*, 74 (7), 1460-1466.

Wiebe, R., and Gaddy, V. L., 1935, The solubility of a mixture of hydrogen and nitrogen in water at 25 degrees in the pressure range 50 to 1000 atmospheres, *Journal of the American Chemical Society*, 57, 1487-1488.

Carbon Dioxide Solubility

Addics, J., Owren, G., and Tangvik, K., 2001, Solubility of carbon dioxide and methane in aqueous alkanolamine solutions, International Gas Research Conference, Amsterdam, November.

Duan, Z., Moeller, N., and Weare, J. H., An equation of state for the CH_4-CO_2-H_2O system: 1. Pure Systems from 0 to 100 degr. and 0 to 800 bar, *Geochimica et Cosmochimica Acta*, 56, 2605-2617.

Rumpf, B., Nicolaisen, H., Ocal, C., and Maurer, G., 1994, Solubility of carbon dioxide in aqueous solutions of sodium chloride, Experimental results and correlation, *Journal of Solution Chemistry*, 23(3).

Soereide, I.; Whitson, C. H., 1992, Peng-Robinson predictions for hydrocarbons, CO_2, N_2, and H_2S with pure water and NaCl brine, *Fluid Phase Equilibria*, 77, 217-240.

X. Appendix F: Listing of Files Contained in the Attached DVDs

This write-up describes the content of the attached DVDs. The following folders are included in the two DVDs. Folders from 'Case01_CO2-CH4-N2(95-5-0)_volume' to 'Case41_Consider_Capillary Pressure' are for generic models. Gulf Coast Case_XXXXXX folders contain Gulf Coast Case models. Each directory has the same structure as describe in the latter part of this appendix.

1) DVD1

Case01_CO2-CH4-N2(95-5-0)_volume
Case02_CO2-CH4-N2(95-0-5)_volume
Case03_CO2-CH4-N2(95-2.5-2.5)_volume
Case04_CO2-CH4-N2(90-10-0)_volume
Case05_CO2-CH4-N2(90-0-10)_volume
Case06_CO2-CH4-N2(90-5-5)_volume
Case07_CO2-CH4-N2(85-15-0)_volume
Case08_CO2-CH4-N2(85-0-15)_volume
Case09_CO2-CH4-N2(85-7.5-7.5)_volume
Case10_CO2-CH4-N2(80-20-0)_volume
Case11_CO2-CH4-N2(80-0-20)_volume
Case12_CO2-CH4-N2(80-10-10)_volume
Case13_CO2-CH4-N2(75-25-0)_volume
Case14_CO2-CH4-N2(75-0-25)_volume
Case15_CO2-CH4-N2(75-12.5-12.5)_volume
Case16_CO2-CH4-N2(100-0-0)_volume
Case17_CO2-CH4-N2(75-25-0)_mass
Case18_CO2-CH4-N2(75-0-25)_mass
Case19_CO2-CH4-N2(95-2.5-2.5)_volume_Dip=1
Case20_CO2-CH4-N2(95-2.5-2.5)_volume_Dip=5

2) DVD2

Case21_CO2-CH4-N2(95-2.5-2.5)_volume_perm_100md
Case22_CO2-CH4-N2(95-2.5-2.5)_volume_perm_600md
Case23_CO2-CH4-N2(95-2.5-2.5)_volume_Verti_perm_ratio_0.1
Case24_CO2-CH4-N2(95-2.5-2.5)_volume_Verti_perm_ratio_0.005
Case25_CO2-CH4-N2(95-2.5.-2.5)_volume_CPOR_5E-05
Case26_CO2-CH4-N2(100-0-0)_volume_No_user_component
Case27_CO2-CH4-N2(75-25-0)_volume_No_user_component
Case28_CO2-CH4-N2(75-0-25)_volume_No_user_component
Case29_CO2-CH4-N2(100-0-0)_volume_Fixed_pressure
Case30_CO2-CH4-N2(75-25-0)_volume_Fixed_pressure
Case31_CO2-CH4-N2(75-0-25)_volume_Fixed_pressure
Case39_ CO2-CH4-N2(95-2.5-2.5)_volume_Porosity=0.2
Case40_ CO2-CH4-N2(95-2.5-2.5)_volume_Porosity=0.3
Case41_CO2-CH4-N2(95-2.5-2.5)_Capillary Pressure

Gulf Coast Case_CO2-CH4-N2(100-0-0)_volume
Gulf Coast Case_CO2-CH4-N2(75-0-25)_volume
Gulf Coast Case_CO2-CH4-N2(75-25-0)_volume
Gulf Coast Case_CO2-CH4-N2(95-2.5-2.5)_volume

Naming rule for directories using examples

1) Case03_CO2-CH4-N2(95-2.5-2.5)_volume: 'CaseXX' represents the case number for generic case. 'CO2-CH4-N2(95-2.5-2.5)' describes the fraction of injection gas: in this case, the volumetric fraction of the injection gas is 95% CO_2, 2.5% CH_4, and 2.5% N_2. 'volume' means that the fraction of the injected gas is based on volume (i.e., mole).

2) Case17_CO2-CH4-N2(75-25-0)_mass: 'mass' means that the fraction of the injected gas is based on mass instead of volume.

3) Case19_CO2-CH4-N2(95-2.5-2.5)_volume_Dip=1: 'Dip=1' indicates that the dip of the reservoir is 1°. Otherwise, the value of the dip for other cases is 2°.

4) Case23_CO2-CH4-N2(95-2.5-2.5)_volume_Verti_perm_ratio_0.1: 'Verti_perm_ratio_0.1' represents that the ratio of vertical permeability to horizontal permeability is 0.1. Otherwise, the value of the ratio for other cases is 0.01.

5) Case25_CO2-CH4-N2(95-2.5-2.5)_ volume_CPOR_5E-05: 'CPOR_5E-05' indicates that the pressure dependence of formation porosity (i.e., rock compressibility, unit: 1/psi) is 5×10^{-5}. Otherwise, this value for other cases is 5×10^{-6}.

6) Case29_CO2-CH4-N2(100-0-0)_volume_Fixed_pressure: 'Fixed_pressure' means that injection pressure of the injection gas is fixed instead of the injection rate. Otherwise, the injection rate is fixed for other cases.

7) Case39_ CO2-CH4-N2(95-2.5-2.5)_volume_Porosity=0.2: 'Porosity=0.2' represents that the porosity of the reservoir is 0.2. Otherwise, the porosity for other cases is 0.25.

8) Case41_CO2-CH4-N2(95-2.5-2.5)_Capillary Pressure: 'Capillary Pressure' indicates that capillary pressure data is considered.

9)Gulf Coast Case_CO2-CH4-N2(100-0-0)_volume: 'Gulf Coast Case' indicates that the files in this directory is for Gulf Coast Case. 'CO2-CH4-N2(100-0-0)_volume' means that the mole (volume) fraction of the injected gas is 100% CO_2.

Description of files in each directory

Each directory contains an XXX.zip file. In the zip file, following files are included

1) XXX.dat: GEM input data file. It contains all information required to run the model.

2) XXX.out: GEM output file. Results of simulation are written in text format.

3) XXX.mrf: GEM results file. It contains simulation results.

4) XXX.irf: GEM SR2 index file. This file is used to open XXX.mrf file. The results of GEM simulation are accessible using softwares 'Results 3D' and 'Results Graph' in CMG package. 'Results 3D' shows the three dimensional grid results. 'Results Graph' provides all the graphs from the simulation. 'Results 3D' and 'Results Graph' open XXX.irf instead of obtaining data directly from XXX.mrf.

5) XXX.rst: GEM restart file. It is required for restarting the simulation.

6) XXX.xls: This Microsoft Excel file contains the results from the post-process to get the change of phase fraction of mobile gas with respect to time.

In addition to these files, the zip files for Gulf Coast Case models contain following files

7) XXX.inc: GEM inclusion file. These files contain data such as grid, permeability, porosity, rock array, initial condition of reservoir, and well operation. Basically, the data contained in these files can be included in the XXX.dat file (in such case, these XXX.inc files are not required). However, due to their size, these files are created and called in XXX.dat during simulation.